Faculty of Science and Engineering

WA School of Mines: Minerals, Energy and Chemical Engineering

Department of Petroleum Engineering

Numerical Simulation for the Reserve Estimation and Production Optimization from Tight Gas Reservoirs

Omar Falih Al-Fatlawi

This thesis is presented for the Degree of

Doctor of Philosophy

of

Curtin University

December 2018

DECLARATION OF ACADEMIC INTEGRITY

To the best of my knowledge and belief, this thesis contains no material previously published by any other person except where due acknowledgment has been made.

This thesis contains no material, which has been accepted for the award of any other degree or diploma in any university.

Name: Omar Falih Al-Fatlawi

Signature:

Date: 5/11/2018

COPYRIGHT

I warrant that I have obtained, where necessary, permission from the copyright owners to use any third-party copyright material reproduced in the thesis (e.g. questionnaires, artwork, unpublished letters), or to use any of my own published work (e.g. journal articles) in which the copyright is held by another party (e.g. publisher, co-author).

Name: Omar Falih Al-Fatlawi

Signature:

Date: 5/11/2018

DEDICATION

I would like to dedicate my thesis to my dear mother, for her encouragement, sincere wishes and her prayers

To my lovely wife Dhifaf and children Maryam and Jaafar who have supported me and believed that I would do it

To my brothers and all family members for their love and support

Acknowledgment

Abstract

With increasing trends in depletion of conventional gas resources, current interests have shifted more towards the development of efficient techniques, procedures and technologies for the exploitation and optimum development of unconventional resources from tight gas reservoirs (TGRs). However, owing to poor understanding of production and flow mechanisms from fractured wells in tight reservoirs, exploitation and development have been challenging. The key objectives of this thesis are to understand the current state of the science and technology associated with exploitation and development of tight gas research, and accordingly develop holistic approaches/techniques for the accurate prediction of reserves; and the optimization of the production performance of tight gas reservoirs considering a broader perspective from reserve estimation to development of tight gas fields through rigorous numerical reservoir simulations of a representative tight gas field in Australia. This is achieved by a number of simplified yet novel numerical tools associated with the identification of accurate compressibility gas factor methods/approaches covering a range of tight gas reservoir pressures and temperatures; modification of the existing material balance approach towards accurate estimation of the tight gas reserves; developing a new set of type curves for fractured vertical wells in TGRs for estimating gas reserve and other key parameters of wells and reservoir; developing a new technique to analysis pressure transient data through elliptical flow for fractured vertical wells in TGRs; suggesting a new method to estimate equivalent drainage area of fractured vertical wells; and optimization of infill drilling wells in TGR and optimization of vertical fractured and multistage fractured horizontal wells. Consequently, this thesis adds new insights into the exploitation and optimum development of tight gas fields through numerical simulation studies with an emphasis on addressing and mitigating various critical challenges associated with accurate prediction of many parameters encountered during the appraisal phase and/or early stages of the development of tight gas reservoirs.

Publications

Published and Accepted Papers:

1. **Al-Fatlawi, O.**, Hossain, M. M., & Osborne, J. (2017). Determination of best possible correlation for gas compressibility factor to accurately predict the initial gas reserves in gas-hydrocarbon reservoirs. International Journal of Hydrogen Energy, 42(40), 25492-25508.

2. **Al-Fatlawi, O.**, Mofazzal, M. H., Hicks, S., & Saeedi, A. (2016, November). Developed material balance approach for estimating gas initially in place and ultimate recovery for tight gas reservoirs. In *Abu Dhabi International Petroleum Exhibition & Conference*. Society of Petroleum Engineers.

3. **Al-Fatlawi, O.**, Roy, V., Aswin, R., Hossain, M. M., & Kabir, A. H. (2017, June). Optimization of Infill Drilling in Whicher Range Field in Australia. In SPE Kingdom of Saudi Arabia Annual Technical Symposium and Exhibition. Society of Petroleum Engineers.

4. **Al-Fatlawi, O.**, Hossain, M. M., & Saeedi, A. (2017, June). A New Practical Method for Predicting Equivalent Drainage Area of Well in Tight Gas Reservoirs. In SPE Europec featured at 79th EAGE Conference and Exhibition. Society of Petroleum Engineers.

5. Hossain, M. M., **Al-Fatlawi, O.**, Brown, D., & Ajeel, M. (2018, March). Numerical Approach for the Prediction of Formation and Hydraulic Fracture Properties Considering Elliptical Flow Regime in Tight Gas Reservoirs. In Offshore Technology Conference Asia. Offshore Technology Conference.

Manuscripts Submitted or in Preparation:

1. **Al-Fatlawi, O.**, Hossain, M. M., O., Patel, N., & Ajeel, M. Optimization of Multiple Hydraulically Fractured Horizontal Wells in Tight Gas Reservoirs. (to be **Submit**)

2. **Al-Fatlawi, O.**, Hossain, M. M. Recognition of most appropriate optimization technique to accurately optimize fracture half-length for vertical wells in tight gas-hydrocarbon reservoirs. (**to be Submit**)

Nomenclature

A Area of permeable barrier between blocks, ft^2

$A_{equ.}$ Equivalent drainage area, acre

A_p Planned equivalent drainage area, acre

b_{Dpss} dimensionless pseudo-steady-state parameter

B_g Gas formation volume factor, ft^3/scf

BY Best year production rate, Mscf/month

c_{gi} Gas compressibility at initial reservoir pressure, psia^{-1}

F_c Fracture conductivity, mD.ft

F_{cD} Dimensionless fracture conductivity

G_1 Gas initially in block.1, scf

G_2 Gas initially in block.2, scf

GIIP   Gas initially in place, scf

G_p Cumulative gas production, scf

G_{pT1-2} Cumulative gas flow rate from block.2 to block.1, scf

h reservoir thickness, ft

k Permeability, mD

k_f Fracture permeability, mD

K_{Lee} Empirical component of the gas viscosity equation (dimensionless)

M_a Apparent Molecular of gas mixture, mole

NPV Net present value, $.

N_f Number of fractures (dimensionless)

P Pressure, psia

$\bar{P}$ Average reservoir pressure, psia

P_D Dimensionless pressure

p_i Initial reservoir pressure, psia

P_p Normalized pseudo-pressure function

P_{pr} Pseudo-reduced pressure (dimensionless)

p_{wf} flowing bottomhole pressure, psia

q Gas flow rate, scf/day

q_{12} Instantaneous gas flow rate from block 2 to block 1, scf/day

q_D Dimensionless flow rate

q_{Dd} Dimensionless decline rate function

r_{eD} Dimensionless reservoir radius

r_e Reservoir radius, ft

RF_p Planned recovery factor, fraction

r_i Radius of investigation, ft

r_w Radius of wellbore, ft

S_w Water saturation (dimensionless)

S_{wir} Initial connate water saturation (dimensionless)

T Absolute temperature, K

t Time, days

t_{DA} Dimensionless time based on drainage area

t_{Dd} Dimensionless decline time function

t_{ca} Material balance pseudo-time function, days

T_{rec} Reciprocal of pseudo-reduced temperature (dimensionless)

w_f Fracture width, in

x_f Fracture half-length, ft

X_{Lee} Empirical component of the gas viscosity equation, mol/°K

Y_{HY} Reduced density term of the z factor equation (dimensionless)

Y_{Lee} Empirical component of the gas viscosity equation, mol/°K

Z	Gas compressibility factor.
$\emptyset$	Reservoir porosity (dimensionless)
μ_g	Gas viscosity, cP
ρ_g	Gas density, lb/ft^3
τ	Transmissibility of the thin permeable zone, mD.ft

List of Content

List of Figures

List of Tables

Chapter 1: Introduction

1.1   Background

1.1.1   Unconventional hydrocarbon reservoirs

Unconventional reservoirs are generally considered to have very low to ultra-low permeability, requiring special recovery operations outside of the conventional operating practices for commercial exploitation. These special techniques include reservoir stimulation (e.g., hydraulic fracturing), horizontal well or multistage fractured horizontal well. However, the definition of unconventional resources has undergone continuous updating due to rapid technological innovations and constant scientific research and development (R&D) to add new hydrocarbon reserves. These advancements in drilling technology has increased the potential of drilling ultra-deep hydrocarbon formations, and has made it possible to explore and exploit potential hydrocarbon resources in ultra-deep formations mostly classified as unconventional reservoirs also.

Various societies and organisations have published different classifications of unconventional resources. For instance, tight gas and oil, shale oil and gas, gas hydrates, and coalbed methane are classified as unconventional hydrocarbon resources by the Canadian Association of Petroleum Producers (CAPP) and the Society of Petroleum Engineers (SPE). Information Handling Services (HIS) considers shale oil, shale gas, tight oil shale, extra heavy oils, tight sands gas, coal gas, coal mine gas, syngas coal, and hydrates gas to be unconventional resources.

Chinese National Standards and China's oil and gas industry standards introduce six classification criteria and definitions of unconventional gas and oil resources: heavy oil, tight oil, tight gas, oil shale, coalbed methane and tar sand. The term heavy oil describes oils that have difficulty flowing through porous media and tar sand is defined as an oil with a viscosity greater than 10000 cP at the reservoir temperature. Tight oil suited to porous media with low permeability precludes wells that produce naturally at an economic flow rate (Hongjun et al., 2016).

U. Ahmed and Meehan (2016) suggest a definition of unconventional resources based on the categories of wells and the completions required. They classify conventional resources as reservoir fluids that can be produced at economic rates by vertical wells

and that do not require a hydraulic fracture length greater than 200-ft or as unfractured horizontal wells. Unconventional resources are those that cannot be produced at economic rates unless vertical wells with a long hydraulic fracture or horizontal wells with multiple hydraulic fractures are employed.

1.1.1.1 Unconventional gas resources

There has been a remarkable increase in gas demand over the last decade, even exceeding that of oil (Dmitrievsky, 2005; Dudley, 2013; Esfahani et al., 2015; Gerhard et al., 2005), due to its inherent advantage of low greenhouse emission. Natural gas has been playing a pivotal role in providing low carbon emission fuel to face the growing global energy demand (Zahid et al., 2007) and it is expected that it will represent about one-quarter of the total worldwide energy demand by 2035. Unconventional gas resources are predicted to provide more than a quarter of the entire worldwide gas production by 2035 (BP, 2017). As a matter of fact, the reserves of gas in unconventional reservoirs are significantly greater than in conventional reservoirs, as displayed in Figure 1.1 (Islam, 2014). However, the commercial gas production from unconventional reservoirs has a number of challenges to overcome.

Tight gas is generally considered to be gas extracted from very low or ultra-low permeable reservoirs and tight gas is predominantly dry natural gas. The US Federal Energy Regulatory Commission (FERC) introduced a specific political definition of tight gas reservoirs (TGRs) in order to regulate the number of wells that could obtain federal or local tax credits to produce gas from tight gas formations. That definition is formations with predicted permeability to gas flow of less than 0.1 mD (Stephen A Holditch and Lee, 2007; Smith et al., 2009).

Due to the continuous depletion of conventional resources and the paucity of newly discovered conventional reservoirs, the campaign for exploration and development of tight gas reservoirs has been increasing. Accordingly, it is expected that the gas and oil industry will go through three stages: production from conventional reservoirs, production from conventional and unconventional reservoirs, and then production from unconventional reservoirs (Chengzao, 2017), to meet the future energy challenges. Consequently, unconventional tight gas is expected to alleviate the conflict between supply and demand of gas (Yan et al., 2017). Unconventional gas reservoirs

globally produced 9.273×10^{11} m^3 in 2015, equating to 27% of total gas production (Hongjun et al., 2016).

Conventional Reservoirs

Tight gas, Coalbed methane, Shale

Gas hydrates and the poorest quality resources

Increasing need for advanced technology

Increasing need costs of production

Higher quality resources

Increasing volume of reserves
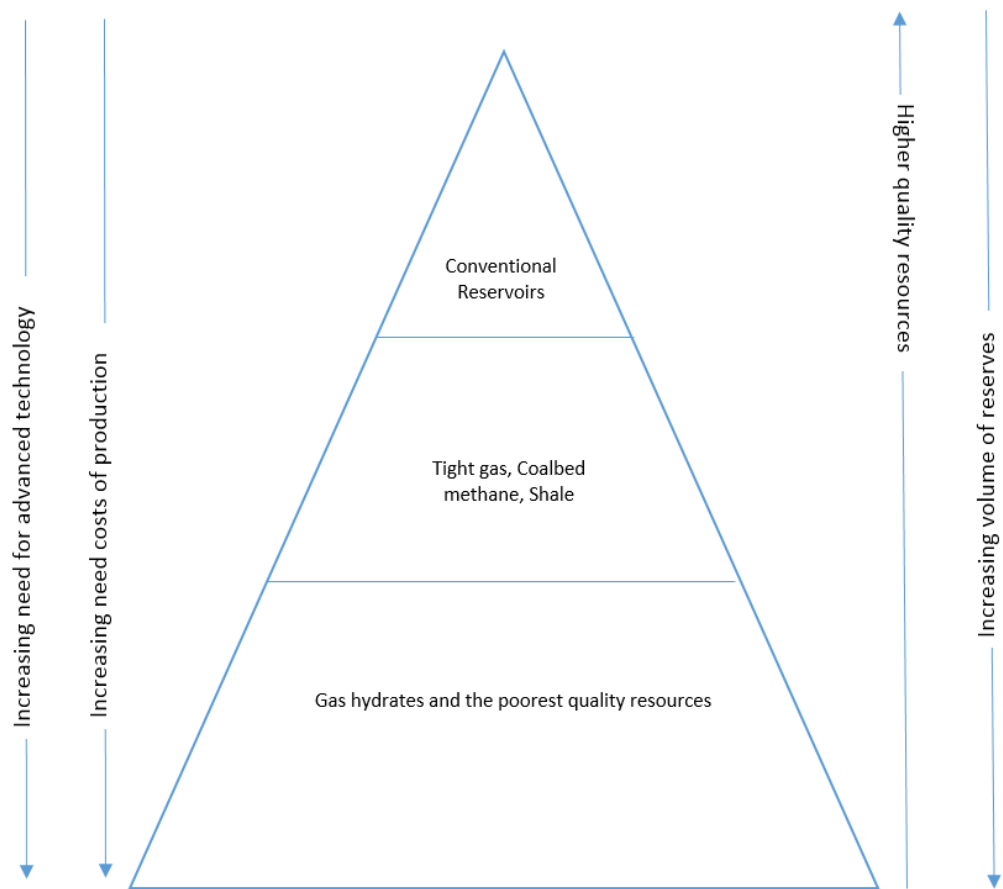
Figure 1.1 The resource triangle diagram

1.1.1.2 Distribution of worldwide unconventional gas resources

After sixteen decades of exploration, evaluation, and evolution, conventional hydrocarbon resources have already been thoroughly explored and analysed. But unconventional resources are yet to be fully researched, especially the global distribution of unconventional hydrocarbon resources.

Significant amounts of unconventional gas resources have been discovered globally and have been evaluated in around 360 basins (Hongjun et al., 2016). The distribution of worldwide unconventional gas resources are shown in Figure 1.2 (Rogner (1997). However, Dong et al. (2012) found that Rogner's estimation of gas resources was conservative because many unconventional gas reservoirs have been discovered around the world since the 1990's, therefore Rogner's appraisal was not evaluated

quantitatively. So, Dong et al. (2012) reviewed Rogner's estimation to propose a new estimate of worldwide gas initially in place of unconventional resources based on statistical correlations, as presented in Figure 1.3. Worldwide reserves of unconventional gas resources has been estimated at around 125,742 Tcf, of which 71981 Tcf is tight gas, 49709 Tcf is shale gas, and 4052 Tcf is coal bed methane (Dong et al., 2012; Stephen A Holditch, 2013).

Middle East and North Africa

24%
76%
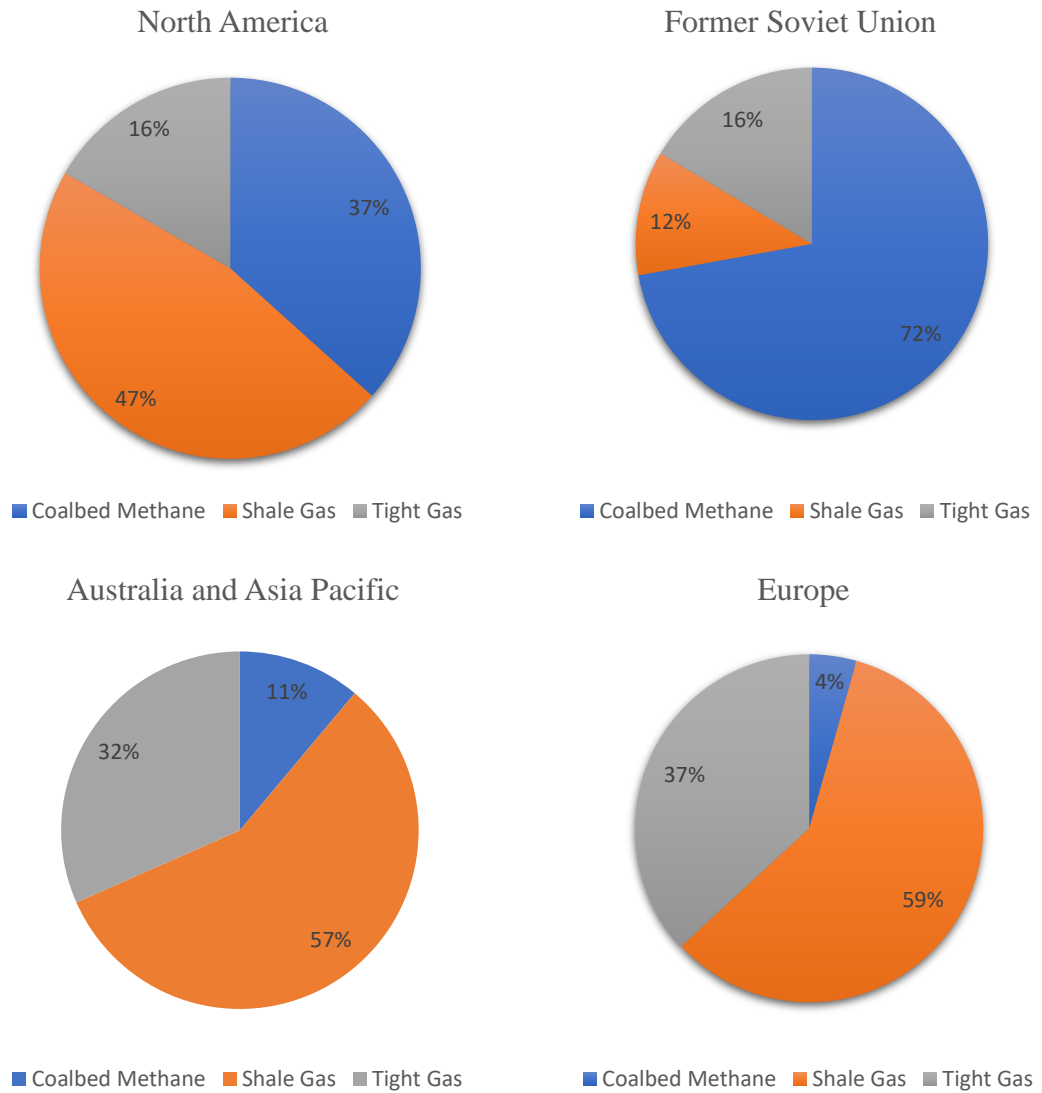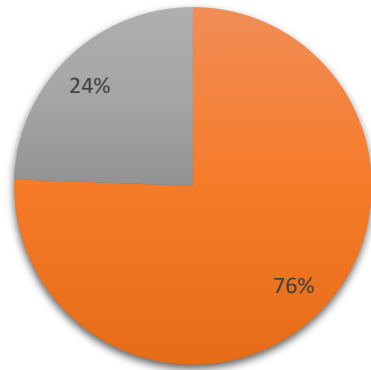
■ Coalbed Methane ■ Shale Gas ■ Tight Gas

Central Asia and China

7%
24%
69%
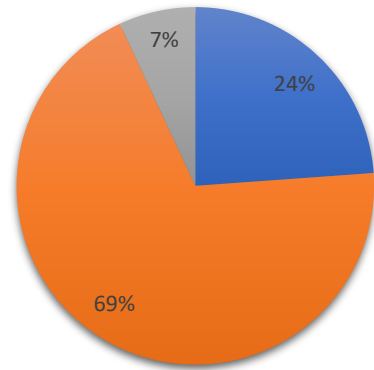
■ Coalbed Methane ■ Shale Gas ■ Tight Gas

Latin America

1%
38%
61%
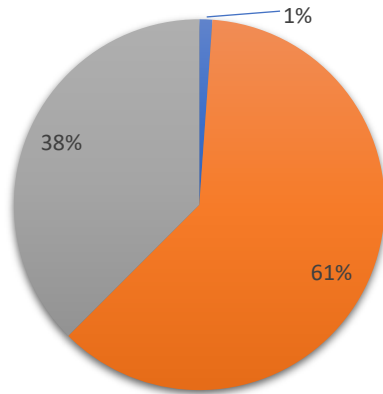
■ Coalbed Methane ■ Shale Gas ■ Tight Gas

Sub-Saharan Africa

4%
25%
71%
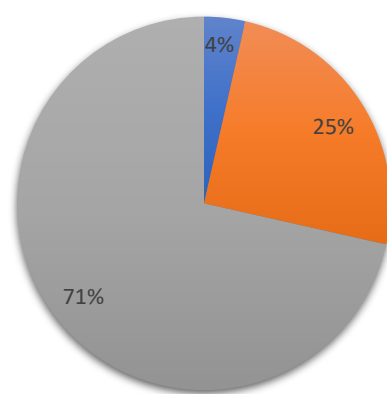
■ Coalbed Methane ■ Shale Gas ■ Tight Gas

Figure 1.2 Distribution of worldwide unconventional gas resources (after Rogner (1997))

North America

8.89%
32.24%
58.87%
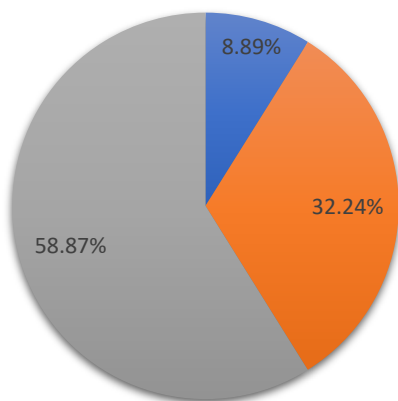
■ Coalbed Methane ■ Shale Gas ■ Tight Gas

Commonwealth of Independent States

1.89%
35.02%
63.08%
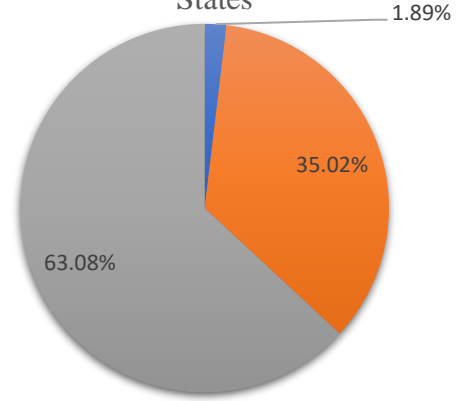
■ Coalbed Methane ■ Shale Gas ■ Tight Gas
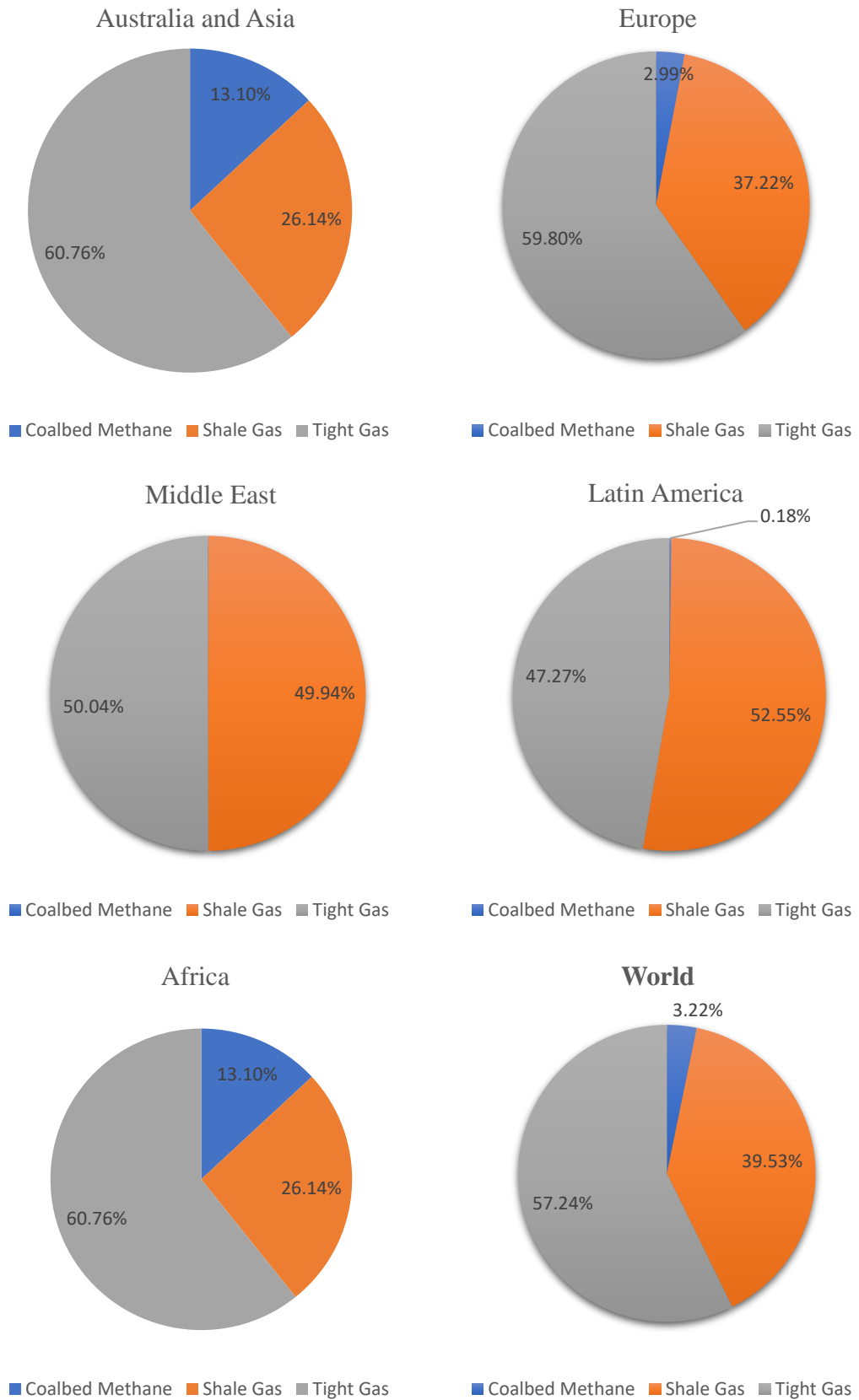
Figure 1.3 Global estimate of gas initially in place of unconventional gas resources (after Dong et al. (2012)

1.1.1.3 Importance of tight gas reservoirs (TGRs)

Tight gas reservoirs (TGRs), described earlier as formations having permeabilities less than or equal to 0.1 mD, are illustrated in Figure 1.4 (Rezaee, Saeedi, & Clennell, 2012) and require massive well stimulation processes for commercial extraction of gas. The typical pore sections of a conventional sandstone reservoir rock, as displayed in the left panel in Figure 1.4, are well connected and quite large, allowing relatively smooth flow of fluids through the porous medium. Conversely, the centre and, particularly, the right panel images show narrow pore spaces which appear to mainly be isolated from one another. The narrow pore channels significantly restrict the fluid flow through the formation. Hence these reservoirs need massive stimulation processes to generate economically feasible production rates.

The worldwide distribution of the three main unconventional gas resources: tight gas, shale gas and coalbed methane, are presented in Figure 1.2. Among these, tight gas represents a significant portion of the total global gas reserve (Figure 1.2). In addition, the tight gas reserve is widely distributed throughout the main petroleum basins worldwide (Dong et al., 2012; Stephen A Holditch, 2013; Rogner, 1997). The different industrial sectors are undergoing rapid development and expansion to meet the requirements of the predicted worldwide population growth. The current worldwide energy consumption is around 550 quads and the world population is at 7.4 billion. By 2030, these figures are predicted to reach up to 722 quads and 8.2 billion people, respectively (Abdullah, 2017; Aguilera et al., 2008).

As a result, tight gas resources are expected to play a vital role in meeting the increasing trend of global energy demand. However, optimum development of tight gas fields to achieve economically viable outcomes (i.e. economic production rates) is a rather challenging task requiring the fields of science, technology, and planning all working together (Pankaj and Kumar, 2010). With this aim, research efforts have worked quantitatively and qualitatively to develop scientific methods and techniques capable of adequately studying TGRs. Even in the conventional gas-rich areas in the Middle East, the assessment of TGR reservoir prospects have turned into a priority focus of energy companies (A. Aly et al., 2009; A. M. Aly et al., 2010; Forsyth et al., 2011). The research trends focusing on TGRs aim to evaluate, analyse and make production easier. Figure 1.5 shows the increasing number of research publications relating to TGRs over the last four decades, with a total of 8242

publications (Curtin University library catalogue database). The accelerating number of studies highlights the importance of tight gas reservoir research and development.
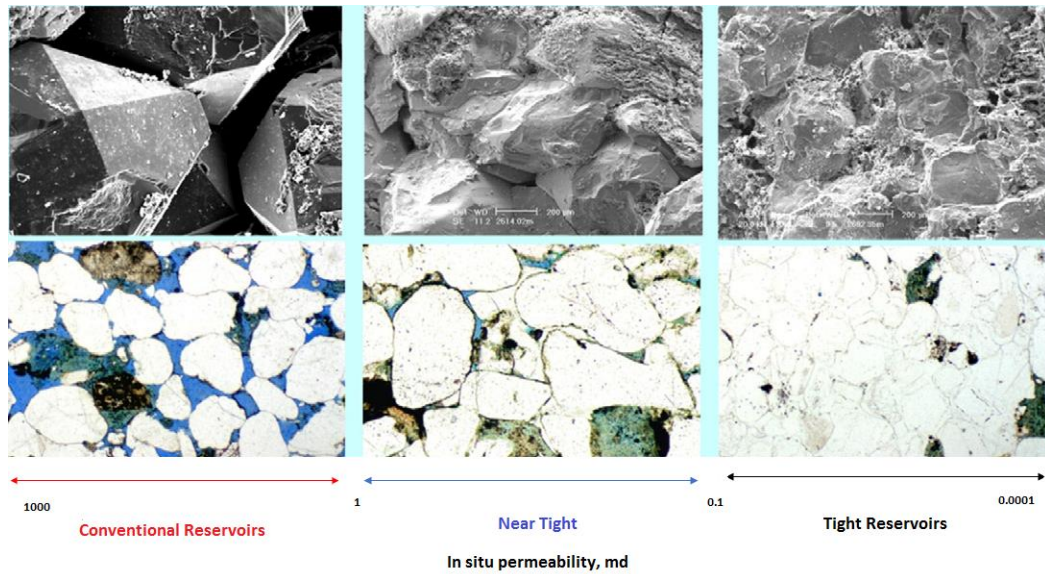
Figure 1.4 Conventional reservoirs, near tight and tight reservoir examples, based on in-situ permeability (Rezaee et al., 2012)
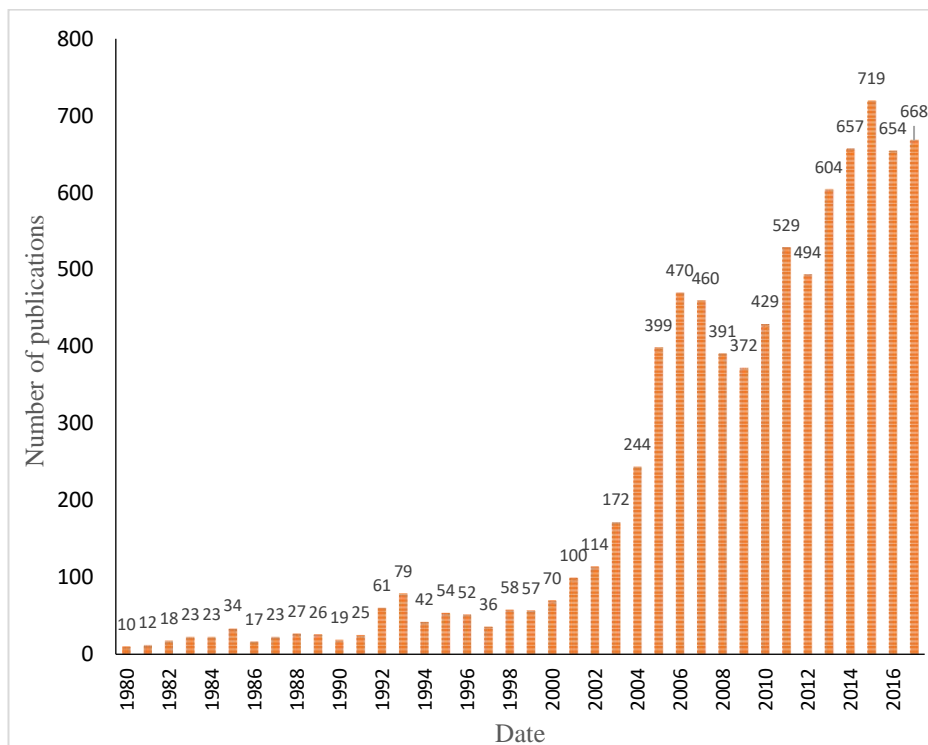
Figure 1.5 Number of publications on tight gas reservoirs between 1980 to 2017 (Curtin University library catalogue database)

The first field development to produce tight gas was achieved by advanced hydraulic fracturing in the San Juan Basin, Western United States, in the 1960's. In spite of this technology, the total production of tight gas only reached around one Tcf annually by 1970 in United States (US). After that, factors such as tax credits and technological advancements in well stimulation techniques, improving remedial and interventional operation processes contributed greatly to increasing tight gas production to around 2.5 Tcf annually (Jiang et al., 2015; Naik, 2003). This growing significance of tight gas is evidenced by US research teams registering more than 100,000 tight gas producing wells in 900 tight gas fields across 23 basins. Consequently, the total gas production reached approximately 6.2 Tcf in 2010 - equal to a quarter of the total natural gas production in the US that year, and the production of tight gas increased to a third of the gross natural gas production in the US by 2013 (International Energy Agency, 2013; Jiang et al., 2015).

1.1.1.4 Reserve estimation of tight gas reservoirs

Accurate estimation of reserves in any reservoir is critical for economic justification of potential development decisions. However, accurate estimation of TGRs is an extremely challenging proposition for reservoir engineers. Techniques such as material balance, type curves analysis, decline curve analysis, and the volumetric method, are successfully exercised for conventional reservoir estimation, but are not appropriate fits for unconventional reservoirs due to the inherent limitations in the underlying assumptions of these techniques (Stuart A Cox et al., 2002; West and Cochrane, 1995). Consequently, these conventional techniques lead to inaccurate estimation (Shoaib et al., 2015) with high levels of uncertainty (and technical risks). Therefore, the development of improved techniques for the accurate estimation of tight gas reservoirs and the minimization of uncertainty, become essential in overcoming such critical challenges.

The application of the conventional material balance equation for TGRs was noted as having a critical drawback due to its violation of two main assumptions. Firstly, notable pressure variation across TGR is present. Secondly, the volume of the drainage area changes with respect to production time (Al-Fatlawi et al., 2016; David A Payne, 1996; Tarek and Nathan, 2012). Similarly, the traditional techniques for decline curve analysis of tight gas reservoirs are mostly unable to construct adequate gas reserve estimates. The poor performance of traditional decline curve analysis occurs mainly

because the collected production data is existent during the transient flow period due to low formation permeability. Thus, the principal assumption of boundary-dominated flow (BDF) is violated (Jiménez et al., 2017; Kupchenko et al., 2008). Moreover, the conventional decline curve analysis assumes that all production controls will remain constant, but it is difficult to maintain the production controls in tight gas reservoirs for very long. Therefore, the exponential decline curve produces an underestimated gas reserve, and the hyperbolic decline curve results in an overestimated gas reserve. In the same way, the application of volumetric techniques leads to high levels of uncertainty in gas reserve estimation. Owing to estimations of the areal extent of reservoirs being inconclusive, the calculated porosity and saturation are likely to be overestimated and underestimated, respectively (Jimenez et al., 2017; Shoaib et al., 2015).

Production data analysis based on a type curve approach is considered to be a practical tool for estimating gas reserve, formation permeability, drainage area and the drainage radius of tight reservoirs (Chen and Teufel, 2000). Therefore, many investigators have worked to develop different forms of type curves for different kinds of gas reservoirs, including both conventional and unconventional. Many of the conventional type curve formats have led to unrealistic results because they are inconsistent with tight gas reservoirs. So, some investigators have focused on the development of type curves of TGRs under assumption, considering the high nonlinearity of gas behaviour with respect to pressure and low permeability formations causing long transition periods.

Finally, due to the inadequacy of conventional techniques to provide trustworthy estimations of tight gas reserves, this thesis developed two techniques - a compartmented material balance approach and a new set of type curves for hydraulic fractured vertical wells in TGRs. The developed method and proposed types curves are comprehensively discussed in Chapter 3. Furthermore, a new method was developed to estimate the equivalent drainage area of hydraulic fractured vertical wells in TGRs. The estimation of the drainage area and reserve may be employed as the basis for economic analysis to assist in development planning, property assessment, and loan securement. The method is comprehensively discussed in the authors paper titled "A new practical method for predicting equivalent drainage area of well in tight gas reservoirs" (Al-Fatlawi et al., 2017b), included in Chapter 3.

1.1.1.5 Pressure transient analysis in tight gas reservoirs

The pressure transient and/or well test analysis become standard procedures to estimate key reservoir properties and fracture parameters for hydraulically fractured tight gas wells, such as fracture conductivity, fracture half-length, skin, reservoir permeability, and reservoir drainage radius. However, well test analysis is rather complex for tight reservoirs compared to conventional reservoirs because the pressure transient takes an utterly long time to traverse from the well to the boundary due to low permeability. Consequently, multiple flow regimes such as linear, bi-linear, elliptical and radial, can prevail. The main flow regimes are generally categorised according to the time they may occur, and the sort of wellbore (e.g., horizontal or vertical) drilled into the formation; and the type of well completion (e.g., fractured or unfractured). In order to correctly estimate reservoir properties, particularly associated with the boundary effect from pressure transient analysis (PTA), it is essential to recognize the flow regimes correctly. For illustration, the radial flow regimes in the case of a vertical well are characterised by a horizontal radial flow direction, which may exist in the period before the pressure pulse has reached the boundary of the reservoir. These different flow regimes and hydraulic fracturing systems require different analysis techniques to capture their effects, in order to correctly predict the reservoir and fracture parameters.

The flow regimes in hydraulic fractured TGRs are complex, mainly because of the large hydraulic fractures near the wellbore, combined with low matrix permeability and reservoir heterogeneity; and consequently, the interpretation of well tests or pressure transient data using the classical approaches typically used for conventional reservoirs can produce erroneous results with high levels of uncertainty. In addition, the time required to achieve radial flow regimes for such tight reservoirs, a key condition in classical approaches, is impractically long and not feasible from both the economic and practical operation viewpoint. Therefore, amendments to these inherent causes and operating limitations of the well test technique are required in order to analyse linear or elliptical flow regimes for predicting the actual drainage area to accurately estimate the reservoir and fracture properties. These aspects are comprehensively studied, and a simplified numerical approach is developed as a part of this PhD thesis work. The developed model is used on the reservoir and fracture parameters based upon well test or production data from hydraulic fractured vertical

wells in TGR, considering the elliptical flow regime. The model is validated based upon a rigorous numerical simulation and sensitivity studies using Australian tight gas field data for various scenarios. The detailed model, including validations, sensitivity studies, and findings, is comprehensively discussed in the authors paper entitled "Numerical Approach for the Prediction of Formation and Hydraulic Fracture Properties Considering Elliptical Flow Regime in Tight Gas Reservoirs" (M. M. Hossain et al., 2018), included in Chapter 3.

1.1.1.6 Production optimization of tight gas reservoirs

Production optimization of TGRs is one of the most critical challenges in the gas industry. Whilst the potential reserves of tight gas represent a significant portion of the global hydrocarbon reserve, economic development of tight gas reservoirs essentially requires reservoir stimulation. The hydraulic fracture stimulation and horizontal well with multistage hydraulic fracturing technology appear to be the most viable techniques for the development of such TGRs. However, difficulties are encountered for optimum development, which includes optimization of well planning, the number of wells, well completion approaches, various hydraulic fracture parameters such as fracture geometry, number of hydraulic fractures in a horizontal well, etc. It is also quite challenging to employ or find an optimization technique that is simple yet provides accurate estimates, and is readily available for the routine industry work environment. Such difficulties impose a high level of uncertainty about development planning of tight gas reservoirs, and significantly affects the financial and technical assessment of any development plan.

1.2   Research objectives and significance

The main objective of this thesis is to construct models and methods to improve and simplify reserve estimation, production performance and pressure analysis, and to optimize production forecasting of TGRs. While tight gas has become a valuable energy resource for energy companies, appropriate reserve estimations and production optimization are essential and inherent to progress the role of tight gas. Natural gas is considered one of the predominant primary sources of energy and as playing a critical role in meeting the global energy demand into the foreseeable future. Customers have been motivated and encouraged to consider natural gas a prime energy resource for environmental, economic, and abundance reasons. The environmental motivation to

consider natural gas as a primary source of energy is the fact that burning natural gas provides a substantial amount of energy with fewer emissions than from other fossil-based resources such as oil and coal. Also, emissions from the combustion of natural gas are much cleaner compared to other fossil-based fuels (Shah, 2017). There are positive economic incentives for the use of natural gas, expressed through stable worldwide growth rates of consumption and production compared to the unsteady growth rates of consumption and production of oil and coal. There has been a clear decline in the projected future of oil and coal, as shown in Figure 1.6 and Figure 1.7 (BP, 2018). In addition, the 2018 Annual Energy Outlook with projections to 2050 considered that natural gas accounts for the largest share of total U.S. energy production, as shown in Figure 1.8 (EIA, 2018). The last driver of natural gas being a prime energy source is the abundance of the reserve in both conventional and unconventional reservoirs. The U.S. Energy Information Administration (EIA) confirmed that natural gas production is expected to continue rising because of the huge size of these reserves (EIA, 2018). Figure 1.9 and Figure 1.10 show the abundance of natural gas reserves within various world regions (BP, 2018).

Scientific research and innovation would be key in the optimum development of unconventional gas fields for exploration and production of natural gas and would be important from estimation of the reserve to the optimization of the production plan. In this regard, this thesis focuses on the advancement of techniques for optimum development of unconventional tight gas reservoirs through improvement and advancing the understanding of associated approaches, starting from the reserve estimation through to production optimization of TGRs. The key objectives of this thesis are to understand the current state of the science and technology associated with exploitation and development of tight gas research, and accordingly to develop holistic approaches/techniques for the accurate prediction of reserves. The optimization of the production performance of TGRs will be viewed in a broader perspective, from reserve estimation to development of tight gas fields by using rigorous numerical reservoir simulation of a representative tight gas field in Australia.
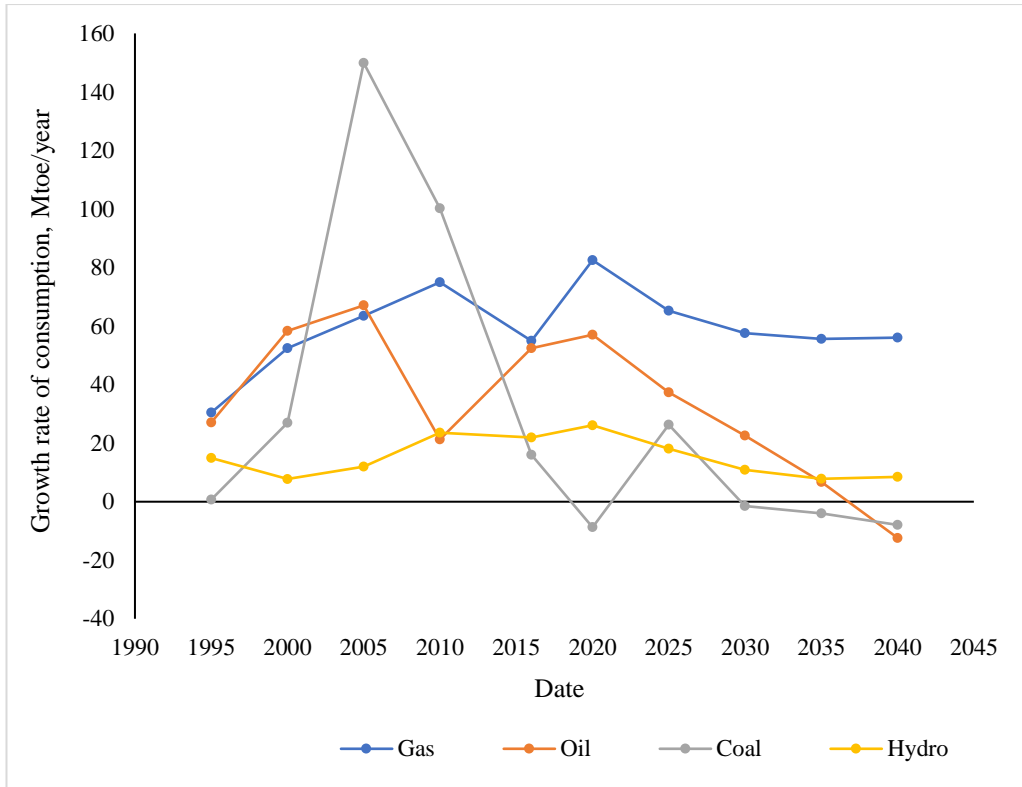
Figure 1.6 The growth rates of worldwide natural gas consumption
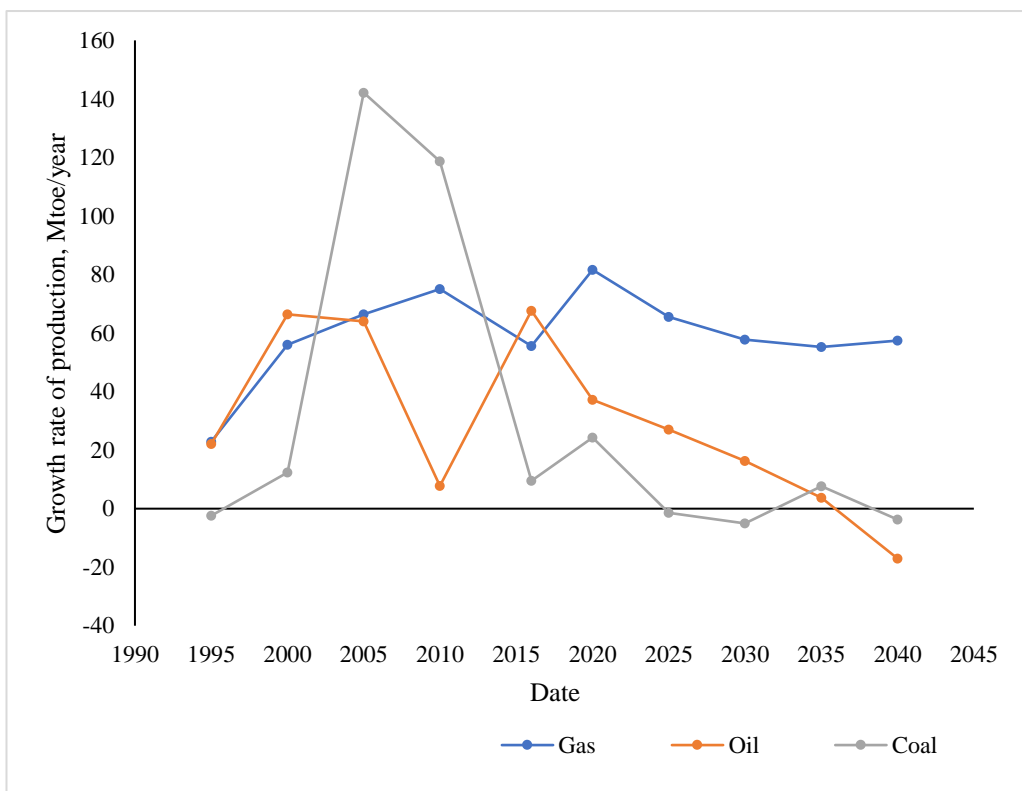
Figure 1.7 The growth rates of worldwide natural gas production
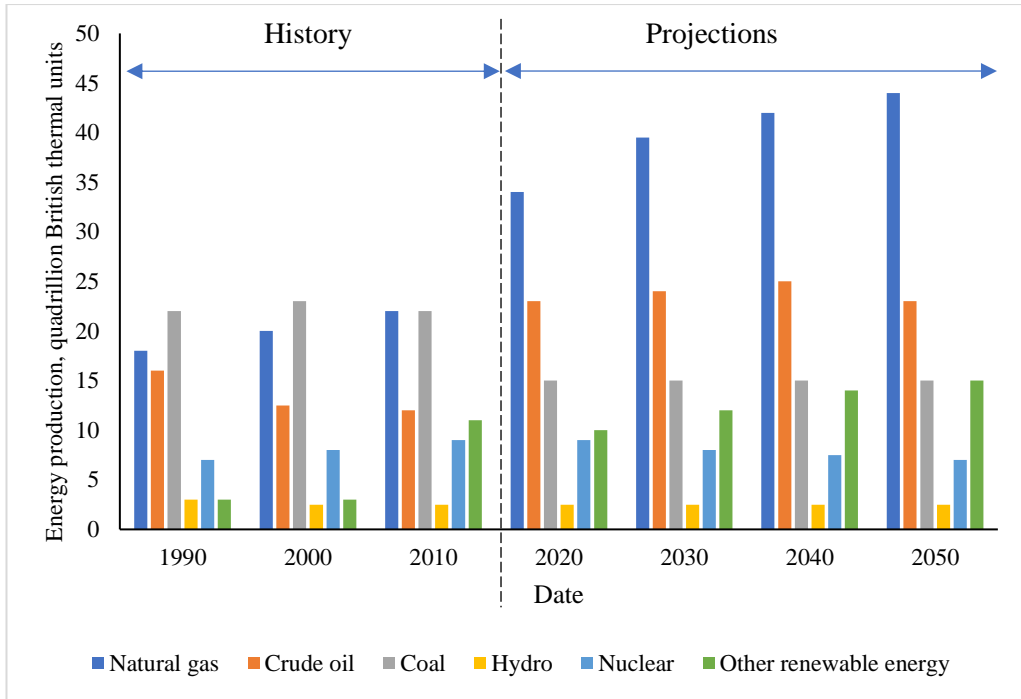
Figure 1.8 The sources of U.S. energy production
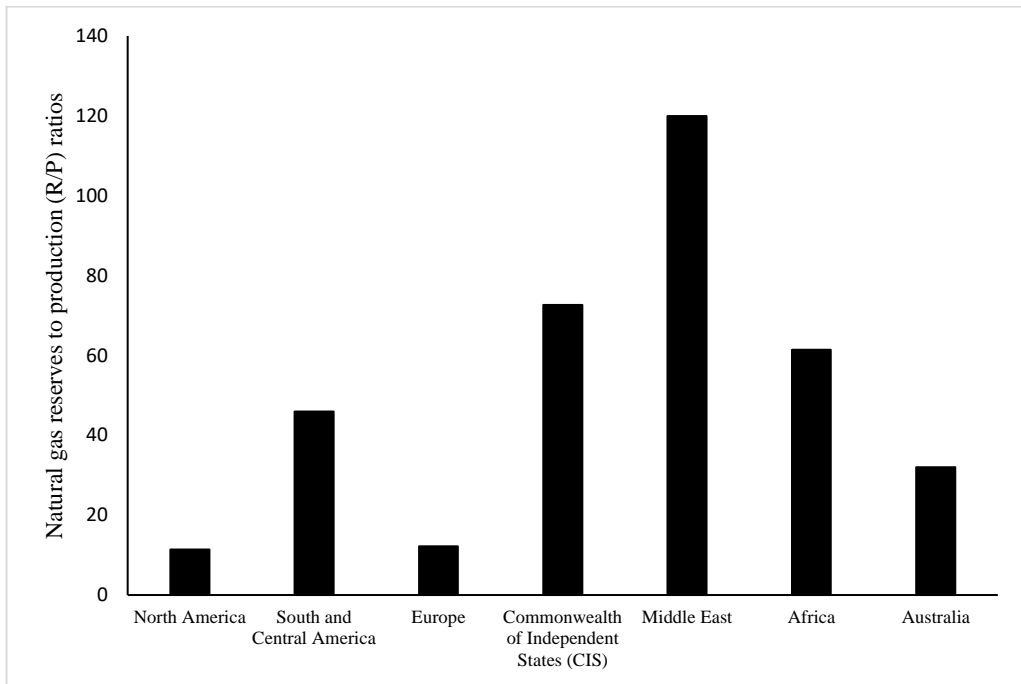
Figure 1.9 Natural gas reserves to production (R/P) ratios at the end of 2017 by region
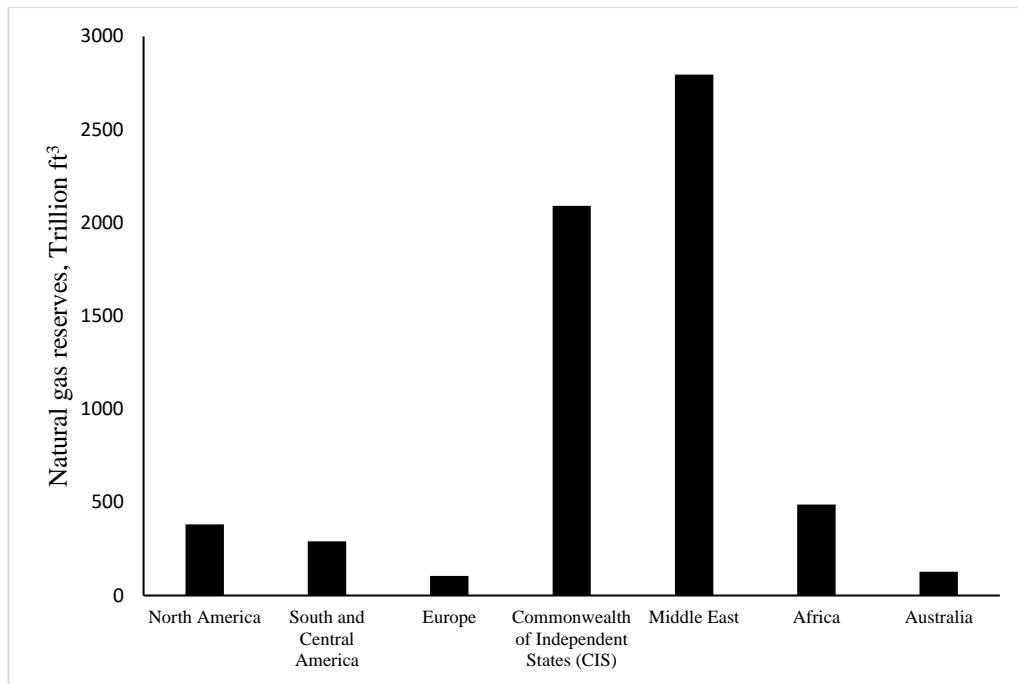
Figure 1.10 Natural gas reserves at the end of 2017 by region

1.3   Outline of the thesis

The estimation of gas properties is considered to be playing a vital role in almost every section of oil and gas industries (Elsharkawy, 2002; Esfahani et al., 2015; X. Wang and Economides, 2013). For instance, performing estimation of gas initially in place (GIIP), ultimate recovery (UR) of gas from a gas-hydrocarbon reservoir, and analysis of gas well test data, substantially depend on how accurately the gas compressibility factor known as the Z-factor is calculated (Chamkalani et al., 2013; Shen et al., 2014).

The Z-factor is employed to transform the volume of ideal gas to the volume of real gas and modifies the behaviour of gas from a perfect trend to the real trend (Mokhatab et al., 2015; Travis et al., 2013). Consequently, the Z-factor is a principal consideration in petroleum engineering computation (Chamkalani et al., 2013; Jianyi et al., 2002; Kamari et al., 2013; Obuba et al., 2013) and can be either estimated by laboratory tests or using mathematical relationships. Although the laboratory tests should lead to more accurate estimation of the Z-factor than the mathematical relationships, expensive laboratory facilities are required, which may not be feasible, especially throughout the lifespan of gas production processes (Al Marri and Kabir, 2015; Chamkalani et al., 2013). As a result, laboratory tests are not appropriately fit for routine industry analysis. In addition, laboratory tests require accurate samples of gas which are not

always easily accessible. Therefore, the industry relies more so on mathematical relationships or empirical correlations than the experimental work to estimate the Z-factor, which poses the challenging question of which correlation to use for the calculation of the Z-factor among the numerous correlations available (Wu et al., 2012).

The range of correlations has have various intensities and deficiencies in terms of the accuracy of the estimated Z-factor (Fayazi et al., 2014). The suitability of a correlation depends on the associated gas compositions, such as the relative distribution of hydrocarbon and non-hydrocarbon components which vary from region to region (Cellek and Pınarbaşı, 2017; Zhou et al., 2006). Based upon the correlations developed, the range of pressures and temperatures need to be considered also. Frequently, gas compositions are unknown and temperature and pressure vary beyond the valid range. As these Z-factor correlations were formulated more than 75 years ago, no unique correlation can be adequately used for all reservoirs at any temperature or pressure, because each correlation was tuned to a particular range of pressures, temperatures, and chemical compositions. Therefore, determining the best possible Z-factor correlation remains challenging. An incorrect determination of a Z-factor correlation can lead to significant error, which in turn results in underestimates or overestimates of many other gas properties and gas initially in place (GIIP), which ultimately affects the recovery of gas.

As a part of this thesis, a method has been proposed and a VBA interface-based Excel program has been developed employing that proposed method. The method is based upon various widely practiced Z-factor correlations ranging from simple explicit empirical equations to those derived from Equations of State (EOS). These correlations were used to calculate the Z-factor at different pressures and temperatures, and the results were then compared with the Virial Equation of State recommended in Report Number 8 of the American Gas Association (AGA8) and Z-factor data obtained from laboratory experiments. The developed program generates the data in the form of four lookup tables for a range of pressures, temperatures and gas compositions, based on sensitivity studies. The tables highlight the best possible correlations to be used to calculate the Z-factor for a certain gas system within certain pressure and temperature ranges. The lookup tables may also be used to benchmark and determine the most accurate correlation for certain pressure (isobar) and temperature (isotherm)

conditions. Each table covers a group of real natural gas systems having a range of compositions with varied fractions of non-hydrocarbon components. The details of the developed method are comprehensively discussed in the author's paper, entitled "Determination of best possible correlation for gas compressibility factor to accurately predict the initial gas reserves in gas-hydrocarbon reservoirs" (Al-Fatlawi, Hossain and Osborne, 2017) included in Appendix (A).

The developed program and lookup tables are used to estimate the initial gas reserves or gas initially in place for the Whicher Range tight gas field, to justify the potential application of the proposed method, and to develop lookup tables as a simple tool for use in real field cases. The developed computational tool and lookup tables suggested in this thesis are useful to improve the efficiency of all techniques of gas reserve estimation such as reservoir simulation, material balance equation or decline curve analysis, as all of these techniques require Z-factor correlation. This thesis also presents insightful discussions about the limitations of various correlations widely used by the industry for routine analysis, which are elaborated in the authors' paper (Al-Fatlawi, Hossain and Osborne, 2017).

The material balance method is one of the most conventional approaches to estimating gas reserves, but it cannot deliver an accurate reserve estimation of TGRs because low permeability violates the main assumptions of the method. However, four published papers: David A Payne (1996), Hagoort and Hoogstra (1999), Engler (2000), and Kuppe et al. (2000) only addressed material balance techniques. So, a new approach for estimating gas reserves and ultimate recovery has been developed in this study.

Analysis of production data of TGRs is considered one of the most important research areas in unconventional gas resources. Production data could be continuously collected relatively inexpensively without needing to shut-in the well. The analysis of production data is used to estimate reservoir and well parameters. In addition, the type curve approach not only requires limited data, but could also be achieved without commercial simulators, making it a handy, fast, and cheap tool to evaluate TGRs and hydraulic fractured vertical reservoirs. On these grounds, some researchers created type curves of hydraulic fractured vertical wells in TGRs. Figure 1.11 shows the historical frequency of important research in this topic (Agarwal et al., 1998; Araya and Ozkan, 2002; Thomas Alwin Blasingame et al., 2007; Chen and Teufel, 2000; D. Cox et al., 1996; Fetkovich, 1980; Palacio and Blasingame, 1993; Pratikno et al., 2003;

M. Soliman et al., 1984; Wattenbarger et al., 1998; Xu et al., 2013). However, these type curves appeared to be oversimplified, often providing erroneous results and misleading interpretations of results. In this view, this study advances the approach by introducing a new set of type curves to analyse production data of hydraulic fractured vertical wells in TGRs. The development of a new set of type curves formulated based on a new statistical correlation is described in Chapter 3.
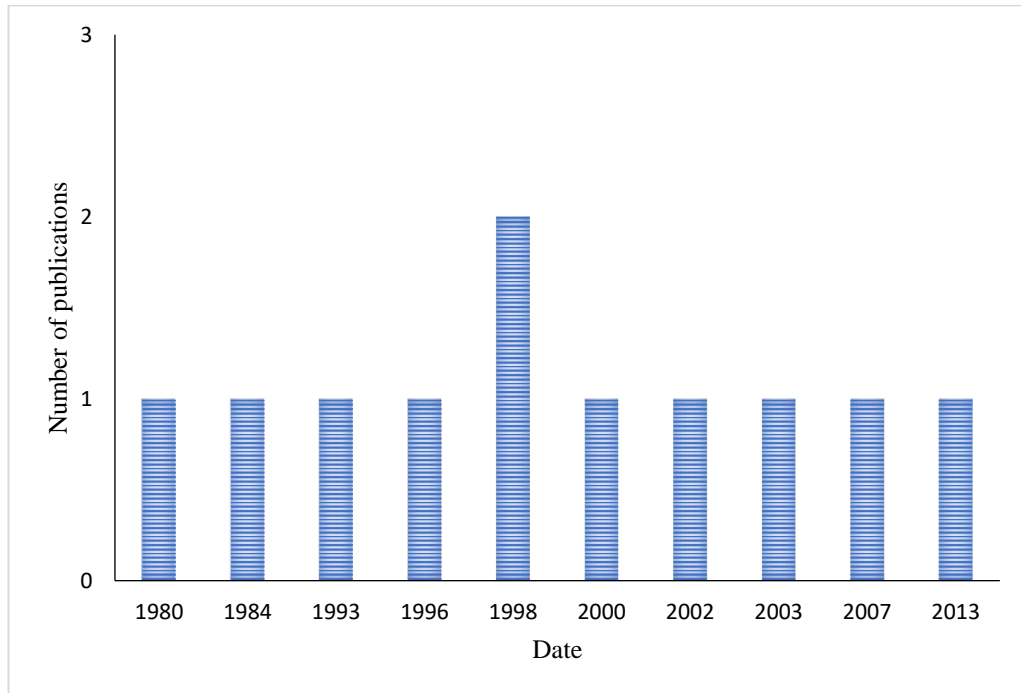
Figure 1.11 The number of publications on type curves of hydraulic fractured vertical wells in TGRs (Curtin University library catalogue database)

The economic evaluation of tight gas production is a challenging task because of the prevailing uncertainties associated with key reservoir properties, such as the size of the drainage area. One of the essential parameters required in the economic evaluation of the production from TGRs is the equivalent drainage area of the well, which relates to the actual volume of gas produced or withdrawn from the reservoir at a certain moment that changes with time. However, it is difficult to predict this equivalent drainage area of well in a tight gas reservoir as it's growing takes many years to reach the impermeable physical boundary of the reservoir. A literature review revealed only five published papers that deal with estimation of drainage areas of fractured wells in TGRs, as shown in Figure 1.12 (Alzate et al., 2001; Stuart Alan Cox et al., 2005; Du, 2008; El-Banbi and Wattenbarger, 1997; Escobar et al., 2007). Accordingly, the number of published papers is inadequate to fill this gap in knowledge. Therefore, in

this study a simplified method has been developed to calculate the equivalent drainage area of a hydraulic fractured vertical well in TGR, requiring a small dataset by combining the material balance equation and decline curve analysis.
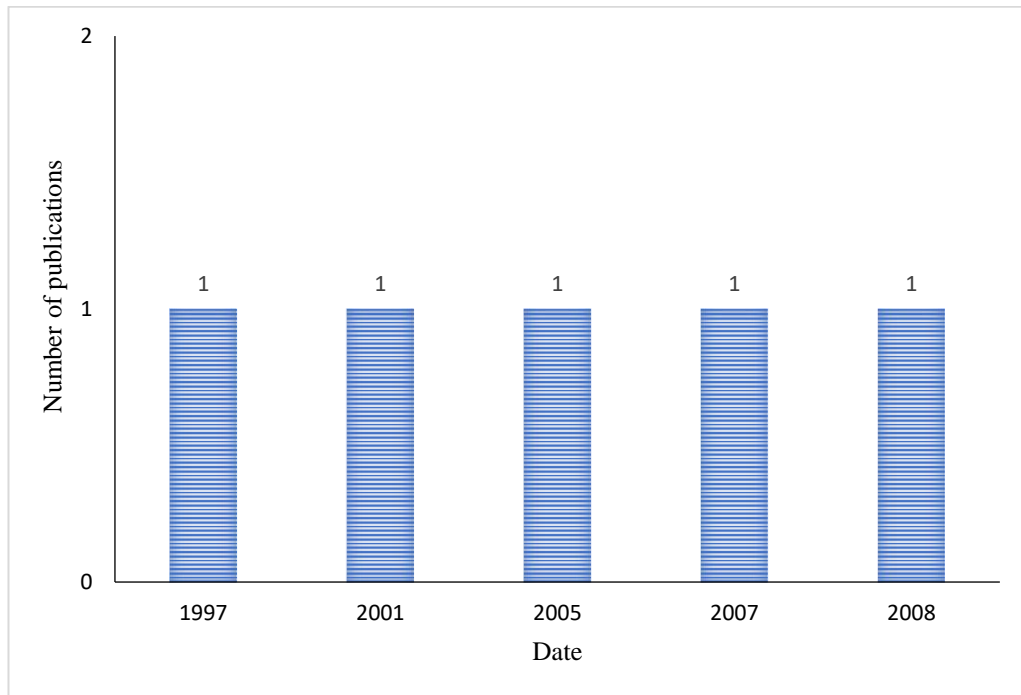
Figure 1.12 The number of publications on estimation of drainage areas of fractured wells in TGRs (Curtin University library catalogue database)

Well test analysis plays an important role in constructing successful field development plans because it provides data on formation permeability, hydraulic fracture half-length and initial reservoir pressure. In spite of this, pressure data analysis of fractured wells in TGRs is complicated because the low permeability of tight formations and the required time of the build-up test is prolonged and impractical. Consequently, the conventional techniques of analysis rarely succeed. In addition, incorrect estimation of the initial pressure of a reservoir highly affect the reservoir simulation results, production data analysis and field development planning (Ilk et al., 2010). However, the number of publications addressing pressure transient analysis of hydraulic fractured vertical wells in TGRs is inadequate in light of the importance of this practical problem, as shown in Figure 1.13 (Badazhkov et al., 2008; H. Bahrami et al., 2012a; Thomas Alwin Blasingame et al., 2007; Borges and Jamiolahmady, 2009; Branagan and Cotner, 1982; Cheng et al., 2009a; Gochnour and Slater, 1977; S. A. Holditch et al., 1983; Ilk et al., 2010; Jahabani and Aguilera, 2009; Kazemi, 1982; Pankaj and Kumar, 2010). Therefore, Chapter 4 proposes filling this gap of knowledge

by providing a simplified numerical approach to calculate the hydraulic fractures and reservoir parameters based upon well test data collected from hydraulic fractured vertical wells in tight gas reservoirs in terms of an elliptical flow regime.
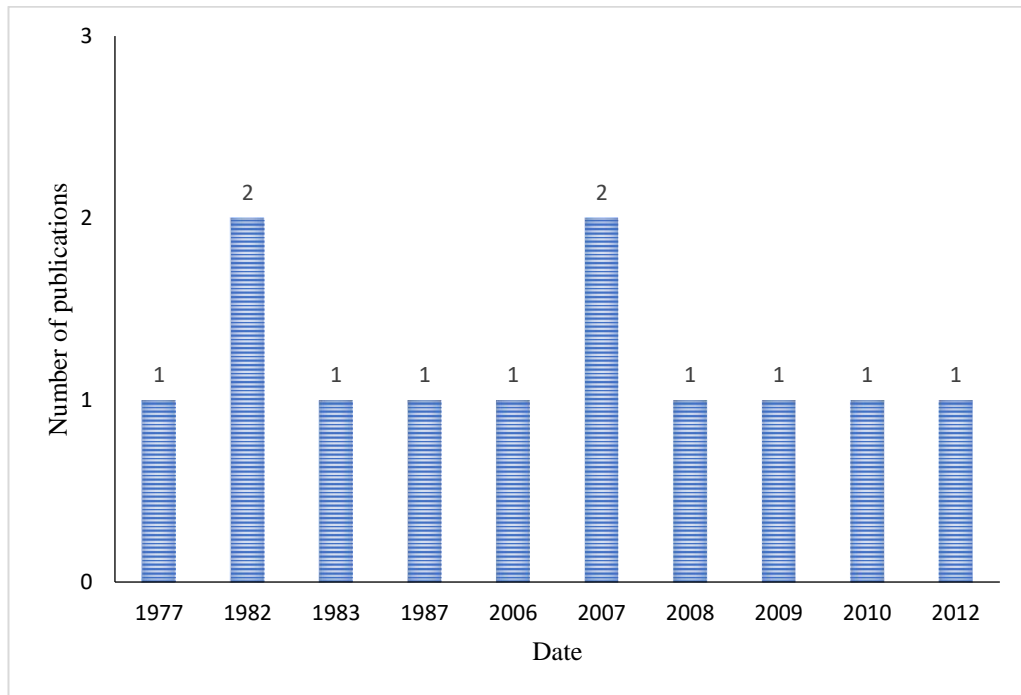
Figure 1.13 The number of publications on pressure transient analysis of fractured vertical wells in TGRs (Curtin University library catalogue database)

Hydraulic fracturing is a well stimulation technique aiming to improve the well productivity by creating highly permeable fracture in the formation near the well. The hydraulic fracture is achieved by injected a fracturing fluid into the formation to fracture reservoir rock and thus raise the flow of reservoir fluids. The hydraulic fracturing has been successfully practiced since 1947, and employed extensively in TGRs since the 1970's, and has been further integrated with horizontal wells. Optimization of a hydraulic fracturing design can be achieved using optimization techniques to evaluate a series of cases (e.g., single well or multi-well) and converge on a solution. Each different optimization technique can provide varying results and efficiency, therefore the improved accuracy and time saved through utilizing the most suitable technique can provide benefits in a reservoir simulation study. The optimization of the geometry of hydraulic fractures is performed using optimization techniques included in direct search methods and derivative approaches. The direct search methods, such as genetic algorithms, are generally very slow, requiring huge computation facilities and memory, which restricts the search and convergence

21

capacity of the algorithms. Within the literature, there are many researches into optimal hydraulic fracture design using different techniques. To the author's knowledge, however, there has been very little research into comparing and selecting the most applicable optimization technique for a hydraulic fracturing reservoir simulation model. To bridge this gap in knowledge, Chapter 5 tests the ability of optimization techniques to find the optimum fracture half-length of vertical wells in TGRs to define the accuracy, and the required memory and time for each method. This study provides practical guidance to determine the most suitable optimization technique requiring the shortest simulation time, the smallest memory size and most acceptable accuracy. The formulated guidance facilitates the selection of an optimization technique for a range of permeabilities and for both single and multi-wells, without needing a high level of optimization experience. In this respect, an extensive study was carried out to better understand the various optimization techniques currently practiced by the industry, based on a comprehensive literature review and analysis of simulation studies of tight gas reservoirs, with a view to establishing a simplified, practical yet accurate tool for optimization of hydraulic fractured parameters. The studies are comprehensively discussed in Chapter 5. Accordingly, the new optimization technique is developed and described in Chapter 6 and the conclusions and recommendations are provided in Chapter 7.

Chapter 2: Literature Review

2.1   Reserve estimation techniques

2.1.1   Volumetric technique

The volumetric technique is one of the most straightforward methods to estimate gas initially in place (*GIIP*) because the main principle is simple, requires limited data and does not need dynamic reservoir data such as flowing bottom hole pressures or production flow rates (Satter and Iqbal, 2015). The essential data for applying the volumetric method are structural and stratigraphic cross-sectional maps, well logs, core tests, fluid sample analysis, and well tests. The contour maps and well logs are employed to calculate the bulk volume, the porosity measurements lead to converting the bulk volume to pore volume, the resistivity logs define the water saturation in the pores to estimate the gas volume at reservoir conditions, and the fluid sample analysis and pressure-volume-temperature correlations calculate the gas formation volume factor that converts *GIIP* from initial reservoir conditions to standard conditions. The volumetric equation can be applied at any stage of depletion of a reservoir. Before production data is available, volumetric estimations can be made to calculate *GIIP* (Tarek and Nathan, 2012). Volumetric calculations can also be used throughout the production period of a well in comparison to material balance approaches. The volumetric estimate can be expressed simply by Equation 2.1.

$$G = \frac{43560 \, A \, h \, \emptyset \, (1 - S_{wi})}{B_{gi}} \qquad\qquad 2.1$$

Where:

G is gas in place, scf.

$\emptyset$ is reservoir porosity, fraction.

h is reservoir thickness, ft.

A is area of reservoir, acres.

S_{wi} is water saturation, fraction.

B_{gi} is gas formation volume factor at the initial reservoir pressure, ft^3/scf.

The gas formation volume factor can be computed by Equation 2.2

$$B_g = Z \frac{T}{P} \frac{P_{sc}}{T_{sc}}$$
2.2

Where:

Z is the compressibility factor of gas.

P_{sc} is pressure at standard conditions, psia.

T_{sc} is temperature at standard conditions, °F.

The gas compressibility factor can be computed based on the experimental tests or the correlations. Although the experimental tests ought to lead to a more accurate estimation of the gas compressibility factor than the correlations, it demands expensive experimental equipment that may be infeasible, especially over the full lifespan of a gas production reservoir (Mohammed Saleh Al-Jawad and Hassan, 2012; Al Marri and Kabir, 2015; Chamkalani et al., 2013). Therefore, the industry depends on empirical correlations rather than laboratory tests to compute the gas compressibility factor, which raises the challenging question of which correlation to employ with numerous correlations presented (Wu et al., 2012) and each having various strengths and weaknesses regarding their accuracy in estimating the gas compressibility factor (Fayazi et al., 2014). The precision of these correlations depends on the compositions of gas samples, temperatures and pressures. Thus, inappropriate selection of correlations can develop unreliable results with high degrees of uncertainty, and mislead the estimation of gas initially in place (Al-Fatlawi et al., 2017a). A novel method in this respect has been developed as a part of this PhD research to accurately estimate gas initially in place in reservoirs through determination of the most appropriate correlations, which can precisely compute the gas compressibility factor and other Pressure-Volume-Temperature properties for an extensive range of gas compositions, pressures, and temperatures. The developed model, including case studies, is comprehensively discussed in the author's peer reviewed paper titled "Determination of best possible correlation for gas compressibility factor to accurately predict the initial gas reserves in gas-hydrocarbon reservoirs" (Al-Fatlawi et al., 2017a) included in Appendix (A).

2.1.2 Material balance technique

The material balance equation (MBE), shown in Equation 2.3, has been an important tool for reservoir engineering for the estimation of gas reserves, and interpretation and prediction of reservoir performance (Hagoort, 1988).

$$\frac{p}{z} = \frac{p_i}{z_i}\left(1 - \frac{G_p}{G}\right)$$

2.3

For conventional reservoirs, this material balance equation 2.3 is considered a key tool to estimate the reserve of gas reservoir (W. J. Lee and Wattenbarger, 1996). A linear relationship appears between the average reservoir pressure/gas compressibility factor (p/Z-factor) and the cumulative produced gas (G_p). Furthermore, (p/Z-factor) versus G_p plots is frequently used as a simple, straightforward and practical method of estimating gas initially in place (*GIIP*) because it is independent on well and reservoir configurations, rock properties, or flow rates (Tarek and Nathan, 2012). This material balance equation is based upon three main assumptions: the reservoir is at a constant temperature, all portions of the reservoir have the same fluid properties and pressure, and the reservoir is considered to be a constant volume tank (Tarek and Nathan, 2012). Contrarily, the linear relationship between the pressure/gas compressibility factor and the accumulative gas production does not exist because of low permeability, which violates two assumptions of the gas material balance equations: (i) significant pressure drop across the reservoir is existent; and (ii) the volume of the reservoir is not constant over production time because the drainage area expands for a long time, which could be many years (Al-Fatlawi et al., 2016). In addition, the material balance equation plots are impractical in TGRs because build-up requires impractically prolonged shut-in times to estimate an accurate average reservoir pressure. For example, standard shut-in times of 48, 72 or 150 hours (typically considered) are not enough to reach the boundary of the drainage area in vertical wells centred in a reservoir of 574 acres, so the estimated pressure from the build-up test is less than the real average reservoir pressure, as shown in Figure 2.1. The shut-in periods prior to pressure measurements affect the accuracy of the material balance equation, in that whenever the shut-in time prior to pressure measurements increases, the estimation of the average reservoir pressure improves, as explained in Figure 2.1. Table 2.1 displays the calculated GIIP based on the conventional approach of the material balance equation (CMBE) that

provides underestimates of gas initially in place at different shut-in periods prior to pressure measurements with significant error percentages, as shown in Table 2.1. Equation 2.4 is used to calculate the absolute percentage error (APE) of the estimated *GIIP* based on the conventional approach of the material balance in comparison with the calculated gas initially in place based on a reservoir simulation model of a TGR.

Thus, the plot of (*p/Z*-factor) versus G_p provides an underestimated ultimate recovery factor and gas initially in place in TGRs (McLaughlin and Gouge, 2006). Accordingly, the material balance equation could be ineffective or fail to apply in TGRs (Stephen A Holditch, 2006). Therefore, the conventional material balance equation should be developed to be satisfactory for application in TGRs.
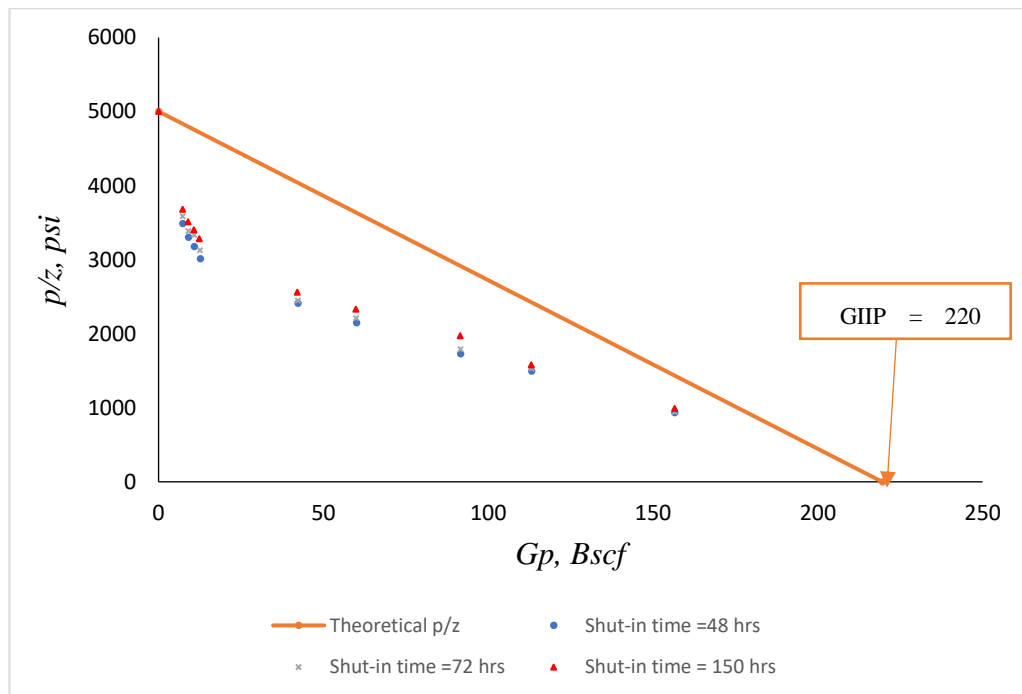
Figure 2.1 Conventional approach of gas material balance equation

$$APE = \left| \frac{GIIP_{RS} - GIIP_{CMBE}}{GIIP_{RS}} \right| \times 100\% \qquad 2.4$$

Where:

GIIP $_{RS}$: calculated gas initially in place based on reservoir simulation.

GIIP $_{CMBE}$: calculated gas initially in place based on the conventional approach of material balance equation.

Table 2.1 Error in calculation of *GIIP* from the conventional material balance equation at different shut-in times

Shut-in time, hr	GIIP $_{CMBE}$, Bscf	APE, %
48	30	86
72	32	85
150	34	85

A number of studies have focussed on solutions to the material balance equation for TGRs, based on the compartmented reservoir approach that states that the reservoir is divided into compartments with each pair of compartments in contact over a permeable barrier (Lord and Collins, 1991). David A Payne (1996) proposed that a compartmented reservoir approach would better reflect the true behaviour of a tight gas reservoir. Also, it could be used to predict GIIP accurately compare to the p/z plot method which, based on a tank model, could lead to greater than 100% error in estimating ultimate recovery factor and gas initially in place. Payne's model implemented an explicit calculation of the system of MBEs corresponding to the tank model in the form of compartments. This method showed that TGRs exhibit non-linear pressure decline, which was proven when it accurately represented the pressure behaviour of a Waterton gas field in Canada. Payne's method is employed to compute the cross flow between the compartments using the pressure squared approach with the assumption of ideal gas behaviour. The key advantage of Payne's method is that it can be completed simply in a spreadsheet program to demonstrate the suitability of the compartmented reservoir approach for estimating pressure behaviour in a tight gas reservoir, GIIP and UR factor. Hagoort and Hoogstra (1999) built a model based on Payne's work and employed an implicit iteration technique to solve the set of material balance equations in a compartmented tight gas reservoir. They employed the real gas law to characterise the behaviour of real gases, and solve the equation using the Newton Rapson method. Their method is reported to be robust, and rigorously accounts for the pressure dependency of the gas properties, so it can converge at a solution in a reasonable number of iterations. However, the Newton-Raphson iteration scheme is difficult to implement in a spreadsheet-based programming language due to the requirement of the derivative for the partial differential equation, which defines the material balance equation. Also, a poor initial guess for the iteration could result in the

algorithm failing to converge at a solution for the system of equations, often providing erroneous results and consequently misleading the interpretation.

Kuppe et al. (2000) presented a productivity index weighted p/z plot for the application of multi-layered, commingled TGRs, which could be used for forecasting the gas initially in place of individual layers. Although this method was demonstrated to be successful in their case, it does not implement a compartmented reservoir approach. It also has the disadvantage of only suitable for use in conditions with no allowable crossflow between the layers, such as during extended shut-in periods, and where the permeability difference between the individual layers does not exceed an order of magnitude (Kuppe et al., 2000).

Engler (2000) devised a method of using shut-in pressure data for TGRs to evaluate the trends could be used to estimate GIIP. This method was successful in obtaining better GIIP estimates for three sample fields. However, it also recommended the use of decline curve analysis and reservoir simulation to verify the results and does not implement a compartmented reservoir approach. The main drawback of this method is that it has only been proven on three fields and may not be representative of TGRs outside of these examples. It also has the drawback of requiring verification by decline curve analysis, which does not rely on any physical properties of the reservoir.

After reviewing the key literature relevant to employing the material balance equation for estimating the ultimate recovery factor and gas initially in place in TGRs, it is evident that there is potential to improve the performance and accuracy of the material balance equation in TGRs with the aim of making it simpler, faster and more explicit than the existing published methods. In addition, most published methods are based on the derivative of the material balance equation, which is not written in explicit form. Accordingly, a simplified computational tool is developed as a part of this PhD thesis, comprehensively presented in the author's paper titled "Developed material balance approach for estimating gas initially in place and ultimate recovery for tight gas reservoirs" (Al-Fatlawi et al., 2016), and elaborated in Chapter 3. This tool can calculate a better estimation of GIIP and UR factor for a tight gas reservoir by simulating the physical conditions of the reservoir, and can simply and quickly determine whether expensive and time-consuming reservoir simulation is worthwhile.

2.1.3 Decline curve analysis

Decline curve analysis (DCA) is widely applied for evaluating the existing situation of the reservoir and predicting the future reservoir performance (Bahadori et al., 2007; Kamari et al., 2017; Khanamiri, 2010; Poston and Poe, 2008; Shirman, 1999). The simplest definition of decline curve analysis is fitting a decline equation to a historical production decline and assuming this fitted decline trend into the future decline trend. The fitted equation is used to estimate the reserve based on performance prediction (Poston and Poe, 2008).

The strengths of decline curve analysis depend on the availability of production data, and it requires short run-time and is a low cost. In addition, decline curve analysis is easy to program and simple to operate with a spreadsheet, avoiding the need for a commercial simulator. On the other hand, there are many deficiencies of the DCA. Firstly, the variations of the production conditions alter the future production trend, changing the estimated gas reserve. Secondly, the prediction of future performance is inconclusive of multilayered or fractured reservoirs because of the effects of cross-flow. Thirdly, forecasting of production trends of tight reservoirs is difficult because most of the production life occurs prior to the BDF period.

Arps (1945) suggest the first methodical approach for oil and gas production data analysis. Arps' decline curve is a formulation that relates the production rate with time and includes two parameters. The decline rate is defined as the fractional change in natural logarithm of the flow rate with respect to time, while the decline exponent is defined as the time-rate change of the inverse decline rate. Arps (1945) created three models of the production rate decline: exponential decline with a decline exponent equalling zero, hyperbolic decline with a decline exponent greater than zero and less than 1, and harmonic decline with a decline exponent equalling 1. The exponential decline is the most widely used model because it is easy to determine the parameter of the decline function and it provides a conservative estimation of future decline trend. The hyperbolic decline is more representative of the production trend of real wells, but the determination of the parameters is difficult because it requires trial and error procedures.

Due its simplicity, the Arp's decline curve has been very popular and widely used in the industry since its inception during the 1950s (Towler and Bansal, 1993). It appears

as a hand tool requiring very minimal data (Kupchenko et al., 2008). However, the main weakness of Arps' decline curve model is that it was derived mathematically without a strong physical basis (Hagoort, 2003; Towler and Bansal, 1993). As a result, Arps' model cannot provide accurate results of TGRs because of the main assumption - the existence of the BDF period - and is not an appropriate fit for TGRs (Mattar and Moghadam, 2009; Okouma Mangha et al., 2012). Arps' decline curve was found to have erroneous estimation, exceeding 100%, of gas reserves in tight reservoirs during transient flow period, which represents most of the production history. The underestimated value of the b-exponent is the main reason this erroneous estimation is generated, where the b-exponent, ranging from 0 to 1, represents the flow conditions at the boundary-dominated flow while the actual flow conditions are mostly in the transient flow period (Rushing et al., 2007). Thus, implementation of conventional techniques of decline curve analysis for unconventional reservoirs has proven to be inaccurate because of the complicated nature of flow behaviour over reservoir and between the reservoir and the wells. However, many researchers have explained that Arps' decline curves can be adjusted to unconventional reservoirs, as exhibited in Table 2.2.

Table 2.2 The most commonly used production decline curves

The reference	The contribution
• Spivey (1986) • Long and Davis (1988) • Towler and Bansal (1993) • Jikich and Popa (2000)	These researchers suggested approaches to optimize the three parameters of the hyperbolic decline curve based on regression analysis.
Maley (1985)	The paper mentioned that the decline exponent of Arps' equation could be greater than 1, especially for tight gas wells and during linear flow period. A limit of the superbolic or hyperbolic decline curve to an exponential decline curve was suggested at a certain decline rate or a specific time to avoid forecasting of excessively long well life.

Robertson (1988)	A modified formula of hyperbolic decline was suggested in which the conventional hyperbolic decline was divided into two sections: the first section conforming to the conventional hyperbolic decline and the second section fitting to the exponential decline curve. The suggested formula was introduced to avoid that the outputs of the hyperbolic decline but may be too optimistic.
Rushing et al. (2007)	The authors studied the applicability of Arps' decline curve analysis for TGRs. They identified that its incorrect usage causes significant error in TGRs during transient flow period and transitional period between the end of transient and the beginning of BDF periods. Moreover, a decline exponent greater than one is found during the above two flow periods, while a decline exponent range between 0.5 and 1 is found during BDF period.
Kupchenko et al. (2008)	The tight gas production statuses during linear flow, pseudo-radial flow (transient), transitional flow from transient to BDF periods were investigated. The researchers found a relationship between the decline exponent and pressure derivative at each of the above flow periods as follows: decline exponent (b) equals 2, ≤ 0.5, and $2 < b < 20$ for linear flow, boundary-dominated flow, and pseudo-radial flow, respectively. Finally, the suggested method could forecast the production decline trend of the whole life of a TGR based on the original form of Arps' relationship.
• D Ilk et al. (2008) • Dilhan Ilk et al. (2008)	The authors provided a new method for calculating the loss-ratio and a derivative of the loss-ratio by taking the inverse of the loss-ratio parameter. The continuous evaluation of the inverse of the loss-ratio parameter exhibited a power-law behaviour for early time data. A

	straight line characterised this power-law trend on a log-log plot which is valid for wells in TGRs. As a result, the power-law exponential rate decline relation is introduced as a tool to analyse production data of TGRs.
Valko (2009)	The authors formulated the stretched exponential decline model to characterise the decline trend of real production data of wells in unconventional reservoirs.
Mattar and Moghadam (2009)	The research focused firstly, investigated the power law exponential decline for different cases of TGRs, examined through the transient and BDF periods, especially for linear and radial transient flow. Secondly, the power law exponential decline was adjusted to match to analytical reservoir models. Thirdly, the decline exponent was assigned as 0 to -0.13 during the transient period, and 0.5 during the BDF.
Bahadori (2012)	The research introduced a technique to estimate the optimum values of Arps' decline curve exponent and initial decline rate based on a Vandermonde matrix. To accomplish this, the author applied a simulator to fit a set of coefficients of the equation to develop a simplified method to analyse the past production performance for gas wells and reservoir to forecast the future production performance. The method put forward by Bahadori (2012) showed good agreement with the data collected from T. Ahmed (2006) and Gentry (1972); suggesting an efficient production predictive method based on decline curves.
Mahadik et al. (2012)	The study suggested an approach to analyse production of fractured wells in TGRs using numerical simulation. The rate derivative was used to compute optimum parameters of production decline models. They found that exponential decline was a better fit for late-time

	production data, while hyperbolic decline was more suited to early-time production data. The suggested approach was examined to forecast the reserve and future production trend of a tight gas reservoir in Western Australia. The examination showed an acceptable match with the results of reservoir simulation models.

2.1.4 Type curve matching

A key job of reservoir engineers is to employ production and pressure history in order to perform: reserve estimates, production forecasting, reservoir and well characterisations and field development planning. Type curve analysis of production data is a method aiming to achieve the best match between the actual historical production rate versus time, and the theoretical model. The axes of the theoretical model are represented graphically in dimensionless variables that can be formulated by multiplying a certain variable such as flow rate by a combination of coefficients with opposite dimensions, but the selection of the combination depends on the kind of problem to be solved (Tarek and Nathan, 2012). The dimensionless type curves format can be employed to estimate reserve in contacted drainage area during transient period or the total gas in place during boundary-dominated flow period (Stotts et al., 2007). This gas reserve forecasting can be estimated based on the history of production data without the requirement for a full set of well and reservoir data, long process time and commercial simulator.

Overall, many researchers worked to create and develop sets of type curves over the last few decades. Table 2.3 presents the most commonly used type curves determined by the literature review.

Table 2.3 The most commonly used type curves

The reference	The contribution
Fetkovich (1980)	The author created type curves based on an integration of solutions of analytical flow equations with decline curve equations suggested by Arps. Fetkovich's type curves covered the transient and BDF periods for wells

	producing at constant flowing bottomhole pressure. The main benefit of this method is that it is valid for transient flow periods or in a BDF period. The main drawback of this method is it ignores the change of gas properties with respect to pressure and temperature.
Fraim and Wattenbarger (1987)	This paper aimed to improve Fetkovich's decline curves for gas wells by suggesting a normalised time calculated from the compressibility and viscosity at the average reservoir pressure. At a BDF, the relationship between the rate of decline and normalized time for a gas reservoir producing at constant wellbore pressure was linear.
McCray (1990)	A new time function was proposed to convert the production history including variable pressure drop or flow rate performance into an equivalent production history at a constant bottomhole pressure. The research was later developed to an equivalent constant rate analysis approach by T. A. Blasingame et al. (1991).
Palacio and Blasingame (1993)	A new set of type curves were developed by introducing two new variables called pseudo-pressure normalised production and the material balance pseudotime. The suggested parameters contributed to considering variable flowing bottomhole pressure and variation of gas properties with respect to pressure and temperature.
Agarwal et al. (1998)	A new combination of rate-time, rate-cumulative, and cumulative-time production decline type curves were developed based on material balance pseudo-time, pseudo-pressure normalised production and dimensionless parameters in well test analysis. This set of production decline curves is valid for application in analysing well production data from radial and fractured vertical gas and oil wells to estimate gas

	reserve, formation permeability and fracture half-length.
Chen and Teufel (2000)	A set of Fetkovich's type curves was developed to analyse production data, including the missing flow regimes in Fetkovich's work that were near-linear up to a pure-linear flow. The suggested set was appropriate for tight gas wells because of the often-observed linear flow regime.
Pratikno et al. (2003)	The authors developed a type curve of a fractured vertical well by introducing a parameter called pseudo-steady constant "b_{Dpss}" for a certain case of dimensionless fracture conductivity F_{cD} and dimensionless radius r_{eD}, and formulated a correlation for calculating b_{Dpss} for a range of F_{cD} and r_{eD}. r_{eD} was considered a function of reservoir radius "r_e" and fracture half-length "x_f", which may have been valid for conventional reservoirs, or a reservoir with moderate permeability when the pressure pulse may have reached the reservoir boundary within a reasonable time.

2.2 Predicting equivalent drainage area of well in tight gas reservoirs

The prediction of the drainage area of fractured wells in TGRs represents a critical step to develop production plans. The drainage area of fractured wells in TGRs expands with time during the transient period and consequently, it is much smaller than the physical drainage area over the transient flow period in the case of a TGR due to the low permeability. Therefore, the production forecasting based on physical drainage area (as generally considered for conventional reservoirs) can result in not only substantial errors in valuation but can also misguide the decision-making process. Relating to the prediction of drainage areas of fractured wells in TGRs, the previous work published in the literature and the developed work contained in this thesis are also explained in detail in the authors paper titled "A New Practical Method for Predicting Equivalent Drainage Area of Well in Tight Gas Reservoirs" (Al-Fatlawi et al., 2017b) and is further elaborated in Chapter 3.

2.3 Analysis of pressure data of hydraulic fractured vertical wells in tight gas reservoirs

Accurately estimating the parameters of hydraulic fractured wells and tight gas formations is one of the key challenges service companies and producing companies face (M. Soliman et al., 1984). The analysis of well testing data is complicated because of the low permeability of tight formations and the high level of heterogeneity. The low permeability impedes the transfer of pressure pulse from the well to the reservoir boundary (Jahabani and Aguilera, 2009). Thus, the build-up period required to analyse the pressure data of hydraulic fractured wells (especially vertical wells) in TGRs is time-consuming and wasteful of money and other resources. As a result, the conventional methods of PTA are not adequate in achieving conclusive outcomes and are often inconclusive, and typically are very poor for TGRs (Borges and Jamiolahmady, 2009; Garcia et al., 2006; Gochnour and Slater, 1977). Consequently, such inadequate and inconclusive analysis of TGRs can lead to erroneous reservoir evaluation, further resulting in indecisive and risky field development planning. The other difficulty faced by well test engineers is the identification of different flow regimes during the production life of hydraulic fractured wells in TGRs. These flow regimes are determined by the complex geometry of the hydraulic fractured wells and the low permeability of the tight reservoirs (Neal and Mian, 1989), with the hydraulic fractures significantly altering reservoir flow patterns (Meehan, 1989). The five typical flow regimes are fracture linear flow, bilinear flow, formation linear flow, elliptical flow, and pseudoradial flow (Cinco-Ley and Samaniego-V, 1981; Hale and Evers, 1981; Kucuk and Brigham, 1979; Thompson, 1981). Accurate identification of these flow regimes, and changes throughout the production period, are essential for better interpretation of pressure transient or well test data, and a sound understanding of the reservoir characteristics and changes in well drainage area over the production period are important, especially to predict formation and hydraulic fracture properties. Another kind of well test called Diagnostic Fracture Injection Test (DFIT) also is used to determine the hydraulic fractures and reservoir properties. DFIT is performed by injecting a volume of fluid into the reservoir to create a hydraulic fracture. After the accomplishment of the injection period, the pressure is observed for hours or days. The collected pressure data are employed to calculate the desired parameters of hydraulic fractures and reservoir (Barree et al., 2015). However, the work focuses on the

analysis of build-up test because recent well test analysis results of tight gas formations, transient build-up analysis is found to be mostly acceptable technique used for the determination of the properties of hydraulic fractures in tight formation (N. Bahrami, 2013; Dahroug, 2015). In this PhD work, these aspects are extensively studied, and accordingly, a numerical approach was developed to predict formation and hydraulic fracture properties considering the elliptical flow regime in TGRs, and has been published in a paper titled "Numerical approach for the prediction of formation and hydraulic fracture properties considering elliptical flow regime in tight gas reservoirs" (M. M. Hossain et al., 2018), included in Chapter 3.

2.4 Optimization and forecasting of production from tight gas reservoirs

2.4.1 Optimization of infill drilling

Historically, one of the most challenging steps to establish a successful development plan for a tight gas reservoir has been finding appropriate answers for essential questions such as: What is the spacing between the wells? How many wells should be drilled? What is the optimum flow rate? So, location selection of the wells is important to enhance the field performance throughout its production period. Recently, many studies related to the development of the optimization technique for infill drilling were reported in the literature, highlighting the importance of well placement (Luo and Kelkar, 2010).

When it comes to the question of how to increase the recovery of hydrocarbons from a field, optimization of infill drilling in both conventional and unconventional reservoirs is highly effective (Cheng et al., 2006; Cipolla and Wood, 1996; Satter et al., 2008). However, this is a very challenging, especially in the case of unconventional reservoirs such as TGRs, because of their low permeability and high level of geological heterogeneities, requiring larger numbers of wells to be drilled. Apart from that, real field data is often limited for TGRs. Although full reservoir simulation may be the most acceptable method to accurately determine the infill drilling potential in a reservoir, it is often complicated because of the shortage of accurate data, the expense and the time consumed. Therefore, an alternative approach is desirable and has been an area of interest for scholars and energy operators since the 1990s, with several techniques proposed to determine an optimum infill-drilling plan.

One of the first of these techniques was the empirical infill-drilling forecast model introduced by French et al. (1991) to investigate infill drilling performance in Clearfork and San Andreas formations. Their prediction appeared to be an adequate match to the real reservoir data. McCain et al. (1993) introduced a statistical technique to evaluate the potential of infill drilling in a TGR. Their technique divides the reservoir into sections and then compares the wells performance to select areas requiring advanced analysis. Consequently McCain et al. (1993) made specific conclusions about the infill potential of those areas. Although their technique is quick and profitable comparison with a full reservoir simulation, McCain et al. (1993) utilized a log interpretation in their technique to attain the accuracy of thickness computations. The well placement in TGRs assessed by Cipolla and Wood (1996) was based upon a statistical analysis technique in which they considered one-layered, single-well reservoir simulation model to study the infill drilling potentials of Ozona gas field in Texas. Their technique involves the employment of 51 arbitrarily selected wells out of 1500 wells to determine the ultimate gas recovery and drainage area. The purpose for sampling only 51 wells was due to mainly the difficulties in performing the analysis of 1500 wells in the field comprehensively. These wells were considered to simulate the global distribution of the whole field. The best 12 months production data of the 51 wells were compared with that of the entire 1500 wells. The results obtained from this study indicated possibility to adding an additional 400 Bcf of gas into the existing reserve by developing the Ozona field with 40-acre spacing. Consequently, 1125 potential locations with 80-acre spacing were identified for infill drilling program. The statistical method was later modified by Voneiff and Cipolla (1996), who proposed it as Moving Window Method (MWM) or technique. The MWM requires only the well location, initial production rate and rate history data (flow rate) to appraise the infill drilling potentials of the field. A fast approach developed by Guan et al. (Linhua Guan, 2004; L Guan and Du, 2004) was appeared to be an extension of the MWM, which includes a model formulated from pseudo steady state equation and MBE. The approach uses a model developed from 4D linear regression and is used to evaluate the performance of infill candidates. This approach can evaluate the infill drilling potential for a group of wells compared to individual infill well potential (L Guan et al., 2004). The approach appears to work well with lesser dependencies (since it is dependent on production data and well location only)

and provides with fast determination. However, the accuracy of the approach depends on the level of heterogeneity in the reservoir.

Gao and McVay (2004) introduced a rapid inversion technique for infill-drilling candidate selection. This simulation-based regression approach employs an automatic algorithm for infill candidate selection to locate prospective infill wells. The problem with this method is that it fixes the values of all reservoir properties, except permeability, as initial values.

Teufel et al. (2004) developed the Infill Well Locator Calculator (IWLC) as a tool to aid operators determine infill-drilling locations in TGRs. While IWLC is a simplified approach to assess infill potential in TGRs, While IWLC is a simplified approach to assess infill drilling potential in TGRs, some uncertainty in the assessment may be expected because ignoring heterogeneity within the test area.

Cheng et al. (2009b) developed a systematic methodology to design infill drilling plan in TGRs. The methodology consisted of two stages. The first is a sequential inversion algorithm for quick history matching providing spatial distribution of pore volume, permeability and remaining gas in place. The second stage is a successive selection approach for infill candidate spots. The author validated the applicability of the methodology using field and mechanistic cases.

Turkarslan et al. (2010) developed an approach to determine the optimum well spacing and quantify reserves uncertainty in heterogeneous TGRs by integrating a reservoir model with a Bayesian decision model for accounting the risk facing operators. This model incorporates uncertainties in reservoir properties to forecast infill production in unconventional gas reservoirs, but it overestimates those uncertainties, which reveals an inaccurate production prediction.

Luo and Kelkar (2010) evaluated the infill drilling potential on the basis only production history data and determined the incremental versus acceleration potential for infill well in a TGR using a statistical approach. This approach was formulated based on the evaluation of the current wells by plotting the production data in a particular way so that data can be linearly extrapolated to predict the estimated ultimate recovery (EUR) per each well in TGRs at the abandonment time. This abandonment time was determined based on the producing life of wells in TGRs, which mostly occurs in the transient flow period. Luo and Kelkar (2010) derived this relationship for

bilinear and linear flow regimes that commonly occur in hydraulically fractured wells in TGRs.

The decline curve analysis (DCA) combined with volumetric approach to estimate in-place hydrocarbon volume appeared to be a widely practiced approach in the industry. In this approach, first the DCA is considered for forecasting the EUR. Then the required number of wells and their spacing to drain the hydrocarbon reservoir are determined by utilising the predicted EUR per well and the total hydrocarbon in place (Q. Huang et al., 2016). This approach mainly depends on the availability of production history data and appears to be relatively easy to use. However, the DCA is practically curve fitting approach which has many limitations and weaknesses, which may result very doubtful and misleading outcome (Gaskari et al., 2007; McCain et al., 1993).

Other methods, such as the evolutionary strategies, implement the concept of Darwinian natural evolution to determine optimal well locations. This technique fundamentally searches for mixing the variables of the solution candidates towards maximization of the objective function. The technique begins with the systematisation of the variables and the creation of chromosomes (Emerick et al., 2009). The created chromosomes in the initial population are then assessed to determine its performance (termed as fitness) in their domain (reservoir) (Bittencourt and Horne, 1997). The operation of the assessment of population individuals is usually attained by comparing with the objective function. In particular to TGRs optimization, the cumulative production or the net present value (*NPV*) within a specified period of time are considered to objective function (Montes et al., 2001; Nasrabadi et al., 2012). Subsequently, the selection operation carries out in which individuals are assessed and graded to recognize the individuals having the maximum probability of reproduction. A new generation of individuals (offspring) with two various operations (termed as crossover and mutation) are produced in the reproduction operation by the parent chromosomes.

The initial best-fit parents are allowed to exchange genes in the crossover operator (Mori and Tseng, 1997). The mutation results a random alteration of the value of the gene, which ensures the natural evolution operation carried out by adding new genetic data (Rajakumar and George, 2012). Although the interest in well placement optimization using methods, such as evolutionary strategies has been growing, the experience in field scale application of these methods are very limited due to primarily

the expenses especially associated with time and computational power (Montes et al., 2001). Considering the limitations and constraints of each of the existing models for optimum placement of infill drilling discussed above, a simple yet robust method of optimum well placement that can successfully determine the optimum number of wells for maximum recovery from tight gas reservoirs, is desirable, especially in cases of limited data. In this respect, an infill drilling optimization method is developed in this study. The method is developed by combining the numerical reservoir simulation modelling with the Moving Window Method (MWM). An optimum infill-drilling plan for Whicher Range (WR) Tight-gas Field in Western Australia was proposed employing the developed model. The accuracy and effectiveness of the developed optimum plan was justified based on comparative studies using a standard reservoir simulation model. It is demonstrated that the proposed plan can effectively forecast the optimum number of wells, and production rate of each well, which is similar to the results obtained from standard reservoir simulation studies. The proposed approach requires less data and is found to be much simpler and faster compared to standard reservoir simulation. The model, including validation and sensitivity studies, is comprehensively discussed in the authors' paper published in SPE titled "Optimization of Infill Drilling in Whicher Range Field in Australia" (Al-Fatlawi et al., 2017c), and is further elaborated in Chapter 4.

2.4.2 Optimization of hydraulic fracturing

Optimization is conducted to find the ideal or "best case" outcome for a scenario, and can be achieved through utilising appropriate optimization algorithms towards maximisation or minimisation of the objective function. The objective function is defined by single or multiple decision variables that to be optimized by minimising or maximising this function. The decision variables are referred to the variables that are adjusted towards minimisation or maximisation of objective function, and achievement of optimum solution. The decision variables are limited by mathematical inequalities termed as constraints or controlling factors that determine the domains of the decision variables.

Basically, the development of the optimum well planning and completion strategies are the cornerstone of the development of the production plan of a tight gas field. Well productivity in a tight gas reservoir is substantially connected to the contact flow area

between the reservoir and the well (M. Y. Soliman et al., 2008). This fact imposes that hydraulic fracturing for vertical or horizontal wells should be applied to create an adequate flow area to reach economic productivity. Therefore, the hydraulic fracturing technique is the key stimulation technology to develop TGRs (M. Hossain et al., 2000; M. M. Hossain and Rahman, 2008; David A. Payne and Cormack, 1989; Veatch, 1983)

2.4.2.1. Parametric study based on sensitivity analysis for hydraulic fracturing

The parametric study based optimisation techniques involves in finding the minimum or maximum of the objective function from the trend of the objective function, obtained from the sensitivity analysis of the decision variables. However, an optimization analysis of hydraulic fractured vertical wells in three different TGRs were conducted by Stephen A Holditch et al. (1978) using a model developed using the Gringarten et al. (1974) well performance equations; and the Geertsma and De Klerk (1969) KGD fracture model. Their study revealed that long hydraulic fractures combined with small well spacing, were required to optimize production from the TGRs with permeabilities less than 0.01 mD. In contrary, the optimum production may be achieved from larger well spacing with shorter fracture lengths for the gas reservoirs having permeability around 0.1mD and above (Stephen A Holditch et al. (1978). However, increasing the fracture length or decreasing the well spacing does not appear to be a favourable option. This because their study reveals that the incremental production potential or gain did not show enough merit to justify additional expenses to implement this option.

The hydraulic fracture optimization for fractured horizontal wells in TGRs studied by Guo and Evans (1993) used inflow performance models derived by combining the material balance equations. The model is derived in combination of the material balance for both aquifer-drive and volumetric depletion gas reservoirs accounting the multiphase flow, and non-Darcy effects through the fractures. Based on their study they demonstrated that the optimum production for a given TGR project's investment can be achievable by fractured horizontal wells. Instead of drilling extra wells, creating more fracturing stages along the length of a horizontal well for certain fracture geometry was found to be appropriate for optimizing production performance towards maximizing the *NPV* (Guo and Evans, 1993).

Abass et al. (2009) carried out sensitivity studies for the optimization of transverse hydraulic fracture spacing along the wellbore axis using a reservoir model. The study

considered a simple homogenous synthetic reservoir model having permeabilities of 0.1 and 0.01 mD, representative to a typical tight gas reservoir. The reservoir model was assumed to be intersected with a 5000 ft horizontal well in which the number of transverse fractures along the length of horizontal well was considered as the decision variable. This simple study demonstrated that five transverse fractures appeared to be adequate enough to maximise the cumulative gas production (as the objective function) when the reservoir permeability is 0.1 mD. Whereas at least 15 to 20 transverse fractures were required to achieve the optimum gas production for the same model when the permeability of 0.01 mD was considered.

Han et al. (2013) conducted optimization study for fractured horizontal wells considering a composite tight gas reservoir model consisting of an inner dual porosity/dual permeability region closed to a horizontal wellbore, and an outer region single porosity model. The reservoir model considered Darcy's law characterize fluid flow through reservoir matrix, and non-Darcy effects through the fracture resulted from high velocity of gas. The model was simulated to study the sensitivity of fracture conductivity, natural fracture density, and, hydraulic fracture length on an objective function defined by cumulative gas production for a given timeframe. It was observed in their study that, though the gas production increases with increasing the fracture length, the production increasing trend is influenced fractures conductivity. For instance, the increasing trend of production tends to slow down at a fracture half-length of 350 ft for low fracture conductivity, whereas the production continues to increase for higher fracture conductivity. The existence of natural fracture, and natural fracture density also affect the optimisation of fracture properties. Han et al. (2013) demonstrated interesting results from their optimization study for several cases of a hydraulically and naturally fractured reservoirs with several assumptions on the reservoir properties which require a more detailed study when used to a real reservoir system.

The analysis of Han et al. (2013) greatly differed by the work of as the later authors group considered analytical model developed based on KGD fracture model (Geertsma and De Klerk, 1969), which is better applicable for fractures with greater height than length. Consequently the model proposed by Stephen A Holditch et al. (1978) is potentially limited by the plane strain assumption used in the KGD solution (MM Rahman and Rahman, 2010). The methodology proposed by Han et al. (2013) was

based on numerical simulation employing a dual permeability/dual porosity model, which accounted for the non-Darcy flow across the fracture network, though the calculated hydraulic fracture system using this method is constrained to constant width planar fractures only.

Moreover, the optimization technique followed in above discussed works are primarily based upon the sensitivities studies. These kinds of approaches are limited to assessing only a single decision variable objective function, and thus are less useful for multivariable objective functions. The systematic and sophisticated approaches are desirable as such approach may facilitate to deal with more complex and multi-objective functions.

Finally, from the literature discussed in this section, many optimization methods were employed to optimize the hydraulic fracturing of horizontal and vertical wells in TGRs. Based on this comprehensive review, it is hard to find a single optimization approach or method that can be used as common approach to optimize the hydraulic fracturing process in tight gas reservoirs. Further, most of the published work focused on using the genetic algorithm that converges extremely slowly to global optimum values. Although, the genetic algorithm may successfully reach the optimum solution for complex and nonlinear functions, it's extremely slow processing speed requires high power computing facilities, and it is very often not fit for routine industry analysis, especially in the case of tight project deadlines. As a part of this study, different optimization algorithms are rigorously tested through sensitivity studies performed by a commercial numerical simulator using a real field case to understand the level of complexity of each optimization algorithm, in order to justify the need for further development of a simplified optimization technique. Accordingly, a simple yet robust optimization technique for the optimization of hydraulic fracturing of horizontal wells in low permeability reservoirs is developed. The sensitivity studies and developed optimization model are comprehensively discussed in Chapters 5 and 6.

Chapter 3: Reserve Estimation and Production Rate Data Analysis, and Prediction of Fracture Half-Length and Reservoir Permeability for Tight Gas Reservoirs*

Gas reserve estimation, and rate and pressure data analysis are vital steps on which many crucial decisions about the potential development and production feasibility of a gas field depend. The techniques and/or tools typically considered for reserve estimation include: Volumetric, Material Balance (MB), Decline Curve Analysis (DCA) and Type Curve Analysis (TCA). These methods are made to estimate the reserves and to assess and forecast the recovery of the reserves, based on assumptions aligning with the specific conditions and characteristics appropriate for conventional reservoirs. All these methods seldom cover the characteristics and conditions that prevail in tight gas reservoirs (TGRs); for instance, formation permeability is extremely low, reservoirs are highly heterogeneous, and pressure response is far more complicated than in conventional gas reservoirs. While the conventional material balance equation is developed with assumptions for the application in a reservoir with a constant drainage area and boundary-dominated flow, the drainage area in TGRs changes over the productive lifespan, mostly during the transient flow period. Therefore, the estimation of reserves and determining the well and reservoir properties of TGRs is a challenging undertaking for reservoir engineers. With this in mind, this PhD focuses on the advancement of the abovementioned existing techniques which are discussed further in this chapter. This chapter also includes discussion on: a numerical technique developed to solve the material balance equation (MBE) using the concept of the multi-tank; a compartmented reservoir model for the estimation of gas initially in place (*GIIP*) and the ultimate recovery (*UR*) factor for TGRs; a new set of type curves formulated for different dimensionless fracture conductivities of TGRs to estimate gas reserve, reservoir permeability, drainage area, and fracture half-length of hydraulic fractured vertical wells; a new technique proposed for predicting the equivalent drainage area of a fractured well in TGR; and a numerical approach developed for the estimation of the reservoir and fracture parameters based upon well test data from hydraulic fractured vertical wells in TGRs considering an elliptical flow regime. All of the abovementioned developed techniques in this chapter are adopted to require limited and available data and to simplify their application.

* Some of content given in this chapter are based on the material published in authors' papers:
Paper 2: Al-Fatlawi et al., 2016
Paper 4: Al-Fatlawi et al., 2017b
Paper 5: M. M. Hossain et al., 2018

3.1 Estimation of gas reserve using material balance equation for tight gas reservoirs

The gas material balance equation (MBE) has been widely utilized as a practical and simple tool to estimate gas initially in place (*GIIP*) and the ultimate recovery (*UR*) factor of a gas reservoir. The classical form of the equation is developed by considering the reservoir as a simple tank model, in which the relationship between the pressure/gas compressibility factor (*p/z*) and cumulative gas production (*G_p*) generally appears to be linear. This linear plot is usually extrapolated to estimate *GIIP* at zero pressure, and a UR factor for a given abandonment pressure. While this assumption is reasonable to some extent for conventional reservoirs, it may incur significant error when applied for unconventional tight gas reservoirs. This study focuses on developing a simple numerical method to solve the MBE using the concept of a multi-tank, compartmented reservoir model which are reported to better represent the behaviour of TGRs. A simple and practical computational tool is developed by solving the numerical model using the False Position iterative method. The tool is applied to calculate *GIIP* and the *UR* factor for an Australian tight gas field after validation of the tool based on history matching. This section will discuss the details of the developed model, model validation and application of the model in a tight gas field, including feasibility studies and analysis of results. The results of the feasibility studies demonstrated that the developed tool can be used for a more accurate estimation of *GIIP* and the *UR* factor.

3.1.1 Compartmented model

The compartmental reservoir concept involves dividing a reservoir into a number of smaller compartments. Compartmentalising a TGR allows the engineer to simulate depletion of the reservoir while also maintaining the assumption of tank-like behaviour in each compartment and the substantial pressure gradient condition of a TGR. For the base case analysed in this research, the compartmented model consists of two blocks separated by a permeable boundary as presented in Figure 3.1.
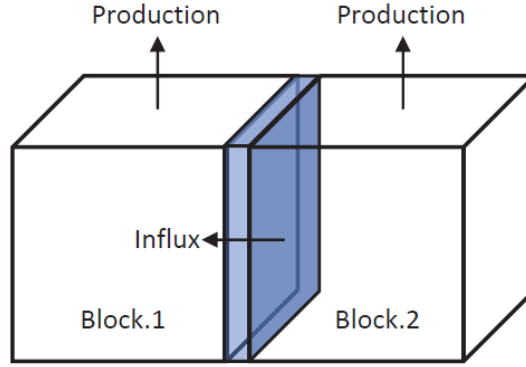
Figure 3.1 Compartmented reservoir model schematic (Al-Fatlawi et al., 2016)

The fluid and rock properties of two blocks are considered to be identical, with the only differences being the block size and the production rates from one or both of the blocks. The compartmented model can be used to predict the behaviour of either dry or wet gas using the specific gravity of the gas and the pseudo-critical temperature and pseudo-critical pressure. Production from either of the blocks will result in a pressure reduction from the initial equilibrium pressure. If a pressure differential is observed between the two blocks due to this production, fluid will flow between them via a very thin permeable zone. The time step size could also be reduced to improve the accuracy of the calculation. However, at some point the model and time step size should be limited to make the computation faster and more efficient in order to implement it as intended with a first pass to decide whether further time and monetary investment in reservoir simulation studies would be worthwhile. The flow through the permeable zone is assumed to be linear and is governed by Darcy's law (Hagoort and Hoogstra, 1999).

3.1.2 Mathematical modelling of compartmental model

The two reservoir compartments are defined by two pressure dependent material balance equations considered to be interdependent due to the linkage by the cumulative influx term (G_{pT1-2}) and are expressed by Equations 3.1 and 3.2.

$$F_{MB,1} = p_1 - \frac{z_1 p_{1i}}{z_{1i}} \left(1 - \frac{G_{p1} + G_{pT1-2}}{G_1} \right) \tag{3.1}$$

$$F_{MB,2} = p_2 - \frac{z_2 p_{2i}}{z_{2i}} \left(1 - \frac{G_{p2} + G_{pT1-2}}{G_2} \right) \tag{3.2}$$

47

Equations 3.1 and 3.2 can be rewritten for the calculation of p_1 and p_2 using False Position iterative method as:

$$P_1{}^{n+1} = \frac{P_{1u}{}^n \, F(P_{1l}{}^n) - P_{1l} \, F(P_{1u}{}^n)}{F(P_{1l}{}^n) - F(P_{1u}{}^n)} \qquad 3.3$$

$$P_2{}^{n+1} = \frac{P_{2u}{}^n \, F(P_{2l}{}^n) - P_{2l}{}^n \, F(P_{2u}{}^n)}{F(P_{2l}{}^n) - F(P_{2u}{}^n)} \qquad 3.4$$

It should be noted that the convention adopted is the cumulative influx term $G_{pT1\text{-}2}$ which is considered to be positive when gas flows from compartment No.2 into compartment No.1. The cumulative influx term is calculated by integrating the instantaneous influx rate with respect to time, and is given by:

$$G_{p12} = \int_0^t q_{12} dt \qquad 3.5$$

The instantaneous influx term, q_{12} in Equation 3.5, has been calculated by implementing the Darcy equation, using real pressures and the harmonic mean of the viscosity and formation volume factor for the two compartments, as given in Equation 3.6. This allows for the pressure dependency of the gas properties in compartment one and two to be accounted for in the instantaneous influx term.

$$q_{12} = \frac{kA/w}{\mu_g B_g} (p_2 - p_1) \qquad 3.6$$

The kA/w term in Equation 3.6 describes the transmissibility term for the thin permeable zone separating the two compartments, and can be incorporated as follows:

$$q_{12} = \frac{\tau}{\mu_g B_g} (p_2 - p_1) \qquad 3.7$$

The harmonic average is applied to calculate the average of gas viscosity and the gas formation volume factor. The gas viscosity (μ_g) is calculated using Lee et al.'s semi-empirical equation (Equation 3.8) (A. L. Lee et al., 1966) with ρ_g in lb/ft^3 and T in °R:

$$\mu_g = 10^{-4} K_{Lee} exp\left[X_{Lee}\left(\frac{\rho_g}{62.4}\right)^{Y_{Lee}}\right]$$

3.8

Where,

$$K_{Lee} = \frac{(9.4 + 0.02M_a)T^{1.5}}{209 + 19M_a + T}$$

3.9

$$X_{Lee} = 3.5 + \frac{986}{T} + 0.01M_a$$

3.10

$$Y_{Lee} = 2.4 - 0.2X_{Lee}$$

3.11

The real gas density in Equation 3.8 is calculated by,

$$\rho_g = \frac{pM_a}{zRT}$$

3.12

Where the Z-factor is calculated using an appropriate correlation depending on reservoir pressure, temperature and gas composition following the approaches discussed in the author's paper (Al-Fatlawi et al., 2017a) included in Appendix A.

The formation volume factor (B_g) is calculated directly using Equation 3.13,

$$B_g = \left(\frac{p_{sc}}{T_{sc}}\right)\left(\frac{zT}{p}\right)$$

3.13

Note that the terms 'compartment' and 'block' are interchangeably used. The 'block' in the subsequent section should be understood as a compartment.

3.1.3 Solution approach

The developed procedure is based on an iterative numerical technique. The solution process begins by constructing two initial p/z verses G_p plots that are based upon the calculation of *GIIP* of the two bocks using the volumetric method. After that, the

production starts directly from Block 1 by a producing well, and indirectly from Block 2 which communicates with Block 1 by a permeable barrier, so the communication factor defining the gas is transmissibility between the blocks, calculated using the average of the length, permeability, and cross-sectional area of the two blocks. The following iterative steps can be used to solve the MBEs for compartmented tight gas reservoirs.

Step 1: The calculation of cumulative gas production:

Cumulative gas production can be calculated by dividing the production history into small time intervals.

Step 2: The calculation of the gas flow rate between the two blocks:

The gas flow rate between the two blocks is calculated using Equation 3.7. The pressure of each block requires iterative calculation. In this study the False Position iterative technique is considered due to its simplicity and robustness. If the two initial values of the pressure of each block are respectively, upper pressure, P_u^n and lower pressure P_l^n, the corresponding new pressure values for Block 1 and Block 2 can be calculated using Equations 3.1 to 3.4.

Step 3: The calculation of pressure in each block:

If the old pressure is P^n, and new is P^{n+1} in each block then

$|P^{n+1} - P^n| \geq$ AAPE, where the allowable absolute percentage of error (AAPE) is 1 psi, The old P_u^n and P_l^n should be replaced until achieving the convergence (i.e., $|P^{n+1} - P^n| \leq$ AAPE) according to the following rules:

If $P_u^n \times P^{n+1} < 0$, Then $P_l^{n+1} = P^{n+1}$

If $P_l^n \times P^{n+1} < 0$, Then $P_u^{n+1} = P^{n+1}$

Steps 1 through 3 can be repeated for new time intervals until the end of the production history and then the predicted simulation can be run, based on good history matching. The prediction is achieved to estimate the *GIIP* and UR factor.

The real gas pressure, volume and temperature (PVT) data such as the Z-factor, μ_g and B_g can be computed with an equation of state or reliable correlations following the approaches discussed in the author's paper (Al-Fatlawi et al., 2017a) included in Appendix A.

3.1.4 Feasibility of the conventional material balance equation for tight gas reservoirs

As mentioned earlier, the accuracy of the estimation of *GIIP* for TGRs using conventional MBE could be unreliable because of the low permeability of TGRs, which violates the assumptions of a constant drainage area, and because of the relatively small pressure variation along the reservoir. To justify the extent to which these assumptions are violated, a vertical well reservoir simulation model is considered to perform sensitivity of the reservoir's permeability. The model considers a vertical well at the centre of a homogeneous reservoir. The reservoir model (with specifications listed in Table 3.1) was run for eight different permeability values ranging from 0.01 to 100 mD and the 2D pressure distribution in the reservoir for different levels of permeability are shown in the Figure 3.2 (a) to (h) to estimate *GIIP* in each case using the standard numerical reservoir simulator, Rubis. The other data used in the simulation are presented in Table 3.1.

Table 3.1 Data of the reservoir simulation model

Area of reservoir, ft^2	25×10^6 (5000 x 5000)
Thickness, ft	100
Porosity, %	10
Reservoir Pressure, psi	5000
Reservoir Temperature, ^{o}F	200
Gas specific gravity	0.7

The 2D pressure distribution presented in Figure 3.2(a) to Figure 3.2(h) display how the pressure distribution from the well to the boundary is affected by permeability. The pressure pulse quickly reaches the boundary in a high permeability reservoir, as shown in Figure 3.2(a) to Figure 3.2(e), and consequently, the variation in pressure appears to be insignificant, resulting in a larger drainage area in the case of highly permeable conventional reservoirs (in this case $k = 10 - 100$ mD). However, a significant pressure difference along the distance between the well and the boundary can be observed in the case of very low permeable reservoirs, as shown in Figure 3.2(f) to Figure 3.2(h), and consequently the drainage area is observed to be much smaller for low permeable reservoirs (in this case, $k = 0.0 - 1$ mD). This simple sensitivity analysis confirms that

the conventional MBE is not an appropriate fit and is unfeasible for TGRs in estimating *GIIP* and the *UR* factor.

Figure 3.3 shows that the absolute error percentage calculated using Equation 3.14 is significantly higher when the reservoir permeability is very low (i.e. in case of TGR). The error level is low when the permeability is higher, and the absolute error percentage is almost constant when the permeability is more than 10 mD. This simple error analysis warrants that the conventional MBE could incur significant error when the reservoir permeability is low. In other words, conventional MBE should not be used for predicting *GIIP* and the *UR* factor for TGRs.

$$Absoluate\ error = \left| \frac{GIIP_{RS} - GIIP_{MBE}}{GIIP_{RS}} \right| \times 100\% \qquad\qquad 3.14$$

where,

GIIP$_{RS}$	Gas initially in place calculated using reservoir simulation.
GIIP$_{MBE}$	Gas initially in place calculated using conventional MBE.

A spreadsheet-based computation tool has been developed, employing the mathematical model and the methodology described in earlier sections. The tool was used to solve the system of MBEs of compartmental reservoirs. The tank model considered in reservoir simulation studies, described in Table 3.1, is simulated to predict the cumulative gas production at the same tight gas reservoir conditions. The simulation results are then compared with the results from the developed spreadsheet-based computational tool in order to justify the accuracy of the developed tool. In the simulation model, the TGR is divided into two identical blocks with a well located in the centre of Block 1.

The computation tool is designed, not only to analyse the performance of the compartmented model, but also to collect all the user inputs. The initial conditions for the procedure are then assigned by passing input values to functions where possible. Cumulative influx, instantaneous influx, Z-factor, real gas density, gas viscosity, formation volume factor and hydrocarbon pore volume are calculated using corresponding functions with values passed into it. This removes the possibility of inadvertently altering key variables which are repeatedly used in different formulations. The time step is set up by running a Do While loop set to run a maximum number of times. The False Position iteration scheme is also set up using a Do While loop inside the time step loop which calculates the pressures using Equations 3.3 and

3.4 for cumulative influx over a time step. The loop iterates until the calculated pressure converges to within a tolerance input by the user. The loop exits when the convergence criteria are met, or if pressure in one of the compartments is calculated to fall below zero. This then exits to the time step loop in order to calculate an updated cumulative influx and cumulative production to increment the time step and to output the calculated values to the spreadsheet for plotting. The program outputs the calculated data into a table which is used to populate two different graphs - the p/z versus the cumulative production graph and the instantaneous influx and cumulative influx versus cumulative production. The program also provides the number of iterations required to obtain solution for the user for assessment.
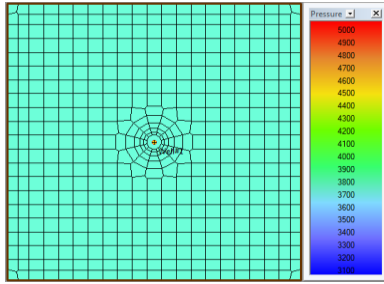
Figure 2(a): 2D pressure distribution for reservoir of 100 md permeability
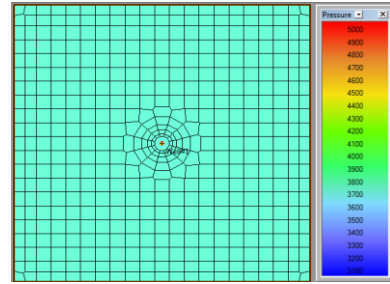
Figure 2(b): 2D pressure distribution for reservoir of 75 md permeability
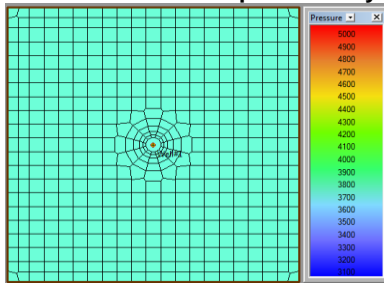
Figure 2(c): 2D pressure distribution for reservoir of 50 md permeability
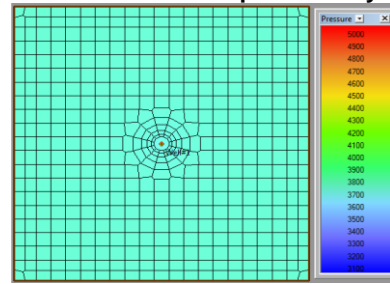
Figure 2(d): 2D pressure distribution for reservoir of 25 md permeability
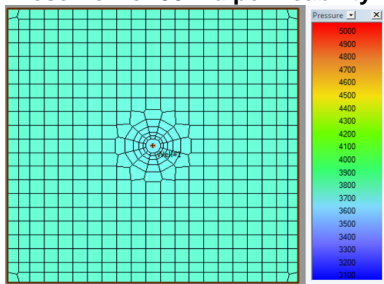
Figure 2(e): 2D pressure distribution for reservoir of 10 md permeability
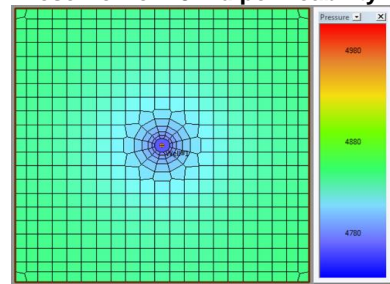
Figure 2(f): 2D pressure distribution for reservoir of 1 md permeability
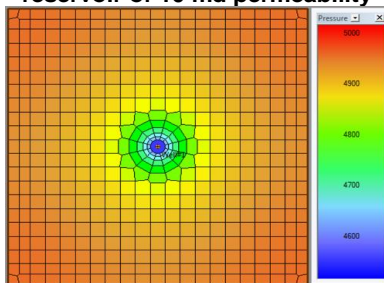
Figure 2(g): 2D pressure distribution for reservoir of 0.1 md permeability
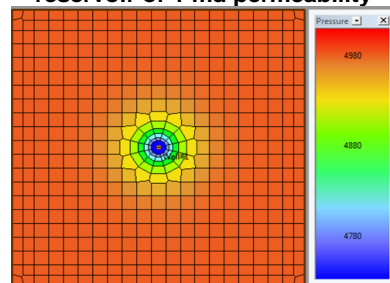
Figure 2(h): 2D pressure distribution for reservoir of 0.01 md permeability

Figure 3.2 2D pressure distribution for different levels of permeability (Al-Fatlawi et al., 2016)
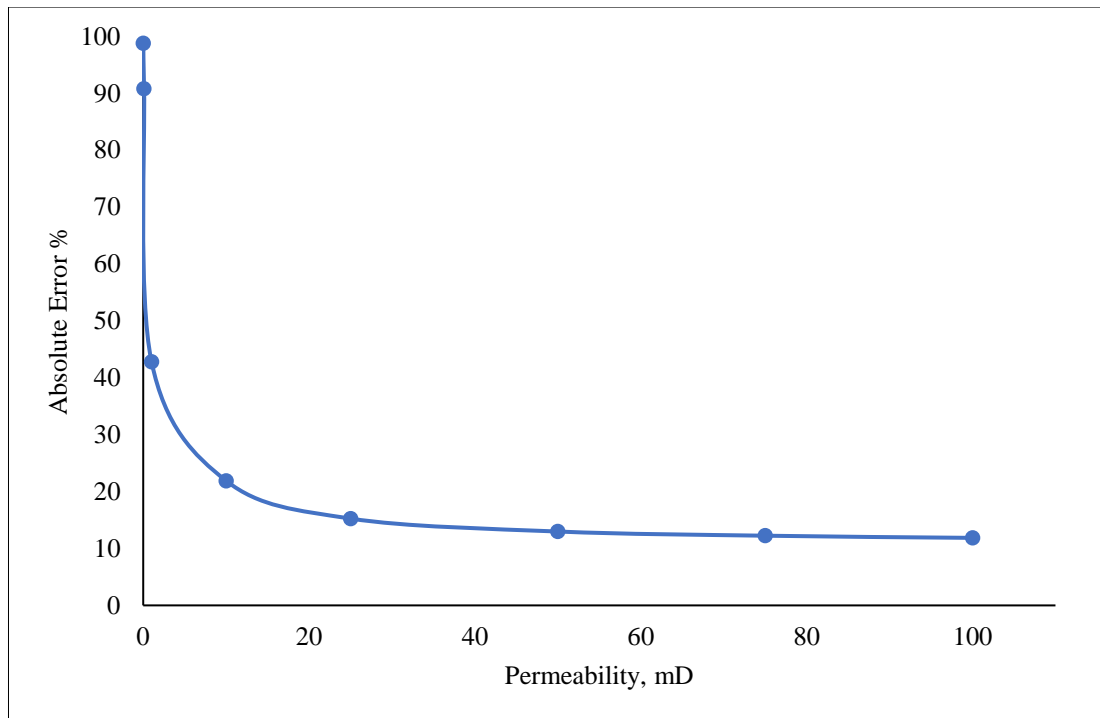
Figure 3.3 The relationship between AAPE (i.e. the accuracy of MBE) as a function of permeability of the reservoir (Al-Fatlawi et al., 2016)

3.1.5 Feasibility and Sensitivity of the compartmented model through comparative study with reservoir simulation

Accurate field estimation of transmissibility between the blocks is difficult, but may be fitted using MBE (Q.-H. Huang et al., 2015). The transmissibility is a function of the permeability of the reservoir, and consequently the transmissibility of TGRs is less than that of conventional gas reservoirs. The developed tool is used for multiple simulation cases to justify the ability and accuracy of applying the MBE in compartmental TGRs.

For a comparative study, the developed program and reservoir simulation runs multiple cases for range of transmissibility between 0-200 mD-ft. The transmissibility between the two blocks is assumed to be zero mD-ft (i.e. τ=0) in the case of the first simulation which is run to history match the pressure data of the production well located in Block 1. The zero transmissibility reflects the extremely tight reservoir in which there is no fluid flow communication between Block 1 and Block 2. In this case, the well produces from Block 1 only, and there is no contribution from Block 2. History data used for the validation is taken from a representative TGR. Good agreement between the reservoir simulation results and the history data is observed, as shown in Figure

3.4. The absolute error percentage (APE) between the *GIIP* (calculated using the proposed method) and the *GIIP* of Block 1 (calculated using reservoir simulation) is found to be insignificant (0.24 %), and warrants the validity the proposed method. After history matching, the simulations using the proposed computation tool and the Rubis standard reservoir simulator are repeated for various transmissibility results, which are presented in Figure 3.5.

It can be observed from Figure 3.5 that when the transmissibility is 1 mD-ft, the predicted *GIIP* of the block containing the production well appears to be higher compared to that of $\tau = 0$ mD-ft. This is because Block 2 contributes additional gas to the production well in Block 1 when $\tau > 0$ mD-ft, which is observed in this case to be 5% of the total production of $\tau = 1$ mD-ft. A similar increase trend can be observed in the cumulative G_p when transmissibility increases. In other words, increasing the transmissibility between the blocks increases the cumulative gas production due to an increase in fluid communication between the blocks. The absolute error percentage of the UR factor (i.e. G_p/G at zero abandonment pressure) calculated from the developed model and the reservoir simulation model for transmissibility factors of 0, 1, 10 and 200 are respectively, 12.70, 7.54, 7.40 and 1.34 percent. It is noteworthy that the error level increases with decreasing transmissibility, which may be due to the effect of low permeability.

Figure 3.6 shows the effect of the instantaneous flow rate (influx) from the non-producing block to the producing block as a function of cumulative gas production for different transmissibility factors. It can be observed that the higher the transmissibility the higher the influx between the blocks. For high transmissibility, especially when $\tau = 100 \sim 200$ mD-ft (in this case), the influx between the blocks increases rapidly to reach the maximum rate, indicating the reservoir pressure wave has reached the boundary resulting in a pseudo-steady state condition; and the reservoir behaves like a conventional reservoir. This is due to the fact that the higher transmissibility is a representation of conventional high permeability reservoirs for which the conventional MBE is applicable. However, the variation in the influx of cumulative gas production for low transmissibility factors (1 ~10 mD-ft), is nonlinear in nature and is deemed typical of low permeability TGRs. Evidently the TGR with low transmissibility demonstrates a slow growth of influx or instantaneous flow rate between the blocks, and consequently the MBE results in an inaccurate estimate of *GIIP* and/or UR factor,

when it is employed in the early stage of the production life of the reservoir. Therefore, the extension of p/z using the proposed compartmented reservoir approach provides more accurate estimation of *GIIP* for each producing block in a TGR.

It is also worth mentioning that the False Position iteration scheme is found to be very fast, taking less than 15 seconds to run each simulation. The developed computation tool is found to be a robust, simple and efficient technique, readily useable by inexperienced frontline engineers in a routine industry environment.
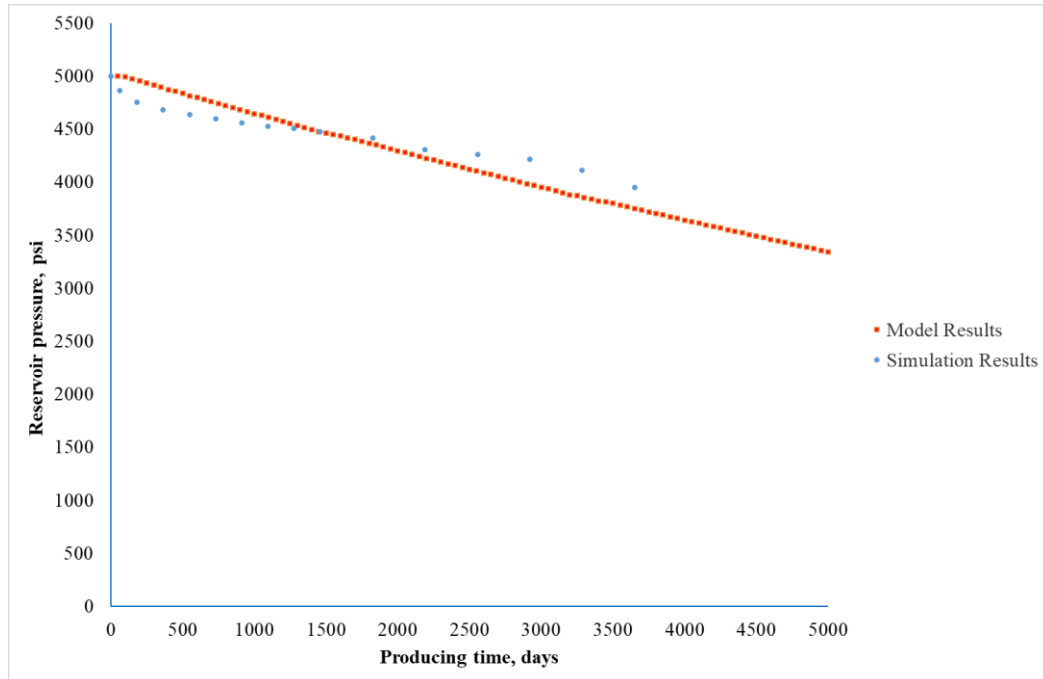
Figure 3.4 History matching of the pressure decline versus producing time of a reservoir simulation model by the developed model (Al-Fatlawi et al., 2016)
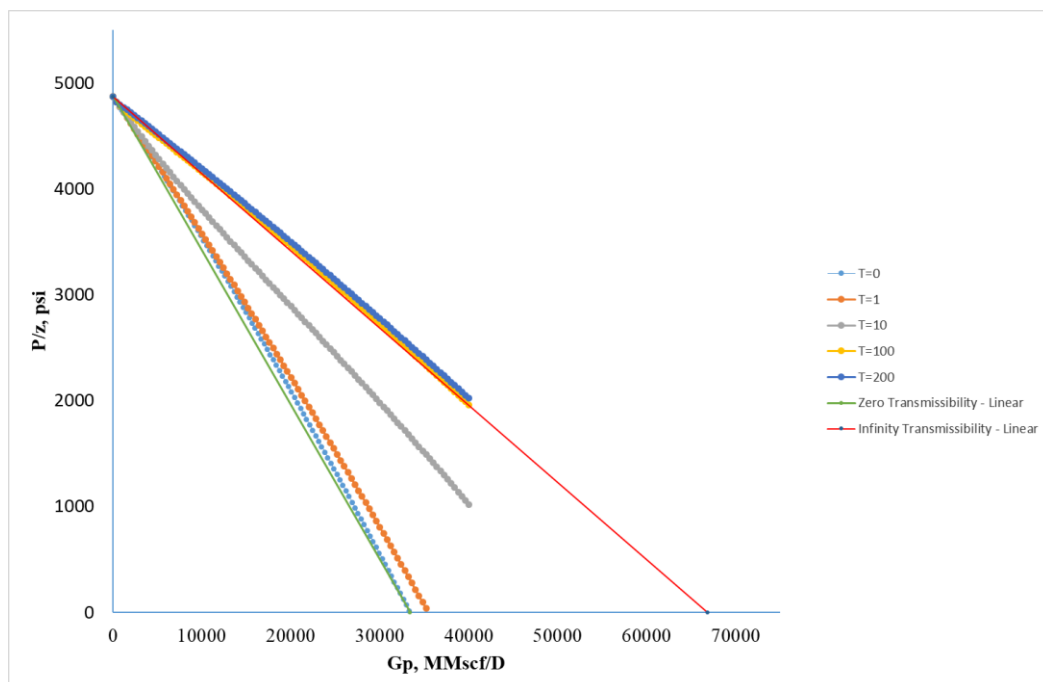
Figure 3.5 The sensitivity of transmissibility effect on the p/z vs. Gp relations of a compartmental reservoir (Al-Fatlawi et al., 2016)
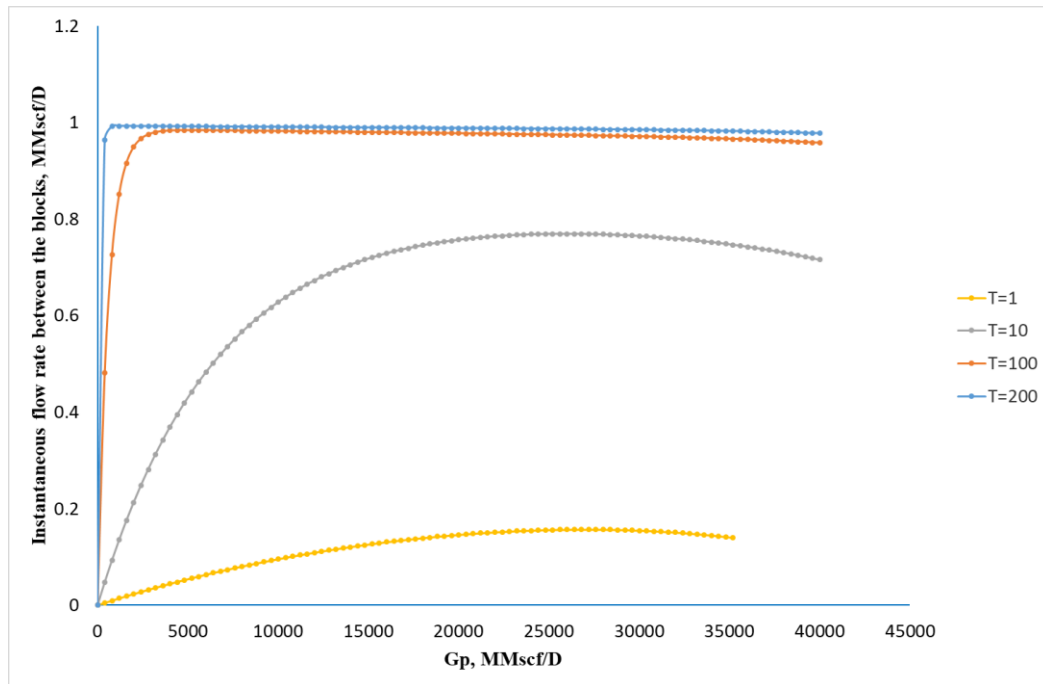
Figure 3.6 The sensitivity of the transmissibility effect on instantaneous flow rate between the blocks of a compartmented reservoir (Al-Fatlawi et al., 2016)

The application of the material balance equation based on the tank model is found to be an inaccurate tool to estimate *GIIP* and *UR* factors for TGRs due to its underlying assumptions which are mainly applicable for conventional gas reservoirs. An alternate form of MBEs is developed, derived from the compartmental reservoir concepts. A spreadsheet-based simple computational tool is developed employing the developed model in which the implicit nature of the system of MBEs is solved using False Position iterative approach. The standard reservoir simulation, history matching and feasibility study results demonstrated that the developed tool provide estimation of *GIIP* and *UR* factors of TGRs with higher levels of accuracy. The tool is found to be robust and simple; and appropriate for use as a first pass to determine whether further expensive and time-consuming reservoir simulation tasks are feasible and/or worthwhile.

3.2 Analysis of Production Data for Fractured Wells in Tight Gas Reservoirs

The pressure transient in a tight gas reservoir usually propagates very slowly from the wells to the reservoir boundary due to the low permeability of its formation. Consequently, the transition flow period may take from a few years to more than a

decade to reach the BDF regime. The conventional decline curve analysis (DCA) is established for boundary dominated flow. The use of DCA for these transient flow periods can lead to developing misleading and erroneous results in estimation of actual reserves. The type curve matching approach is found to be a more useful tool, not only to estimate reserves in tight gas reservoirs, but also to estimate parameters associated with reservoir and well completion parameters, for instance reservoir permeability and fracture half-length in the case of fractured wells. Various forms of type curves found in the literature are used to estimate gas reserves, ultimate recovery factors and other parameters such as fracture half-length and reservoir permeability. Although the Fetkovich's type curves is one of the most popular and widely used type curves for estimating parameters for conventional reservoirs, its use appears to be challenging for TGRs. This work adopts a statistical correlation, which is developed for the 'pseudo-steady constant' as a function of dimensionless drainage radius. This section provides comprehensive discussion on a new set of type curves for different dimensionless fracture conductivities. The proposed set of type curves is developed based on the Fetkovich type curve and the adopted statistical correlation for the 'pseudo-steady constant'. The developed type curves are then used to analyse the production data of real TGRs. The proposed type curves appear to be a handy and straightforward method, not requiring a full reservoir or well dataset, and can be used to perform production data analysis using even a simple spreadsheet-based program to calculate the reservoir permeability, fracture half-length, gas in place and drainage area.

The correlation and the developed type curves are validated based on the analysis of a real TGR model using reservoir simulation. The results show high agreement with the results obtained from commercial reservoir simulation and the measured data, which warrants that the proposed approach can be used as a practical tool and replace the need for an expensive commercial simulator. This section provides discussion on the development of the proposed type curves including validation of the model, and case studies.

3.2.1 Methodology for proposed type curves

The mentioned Fetkovich type curves and the statistical correlation proposed by Pratikno et al. (2003) are given in Equation 3.15. Table 3.2 presents the value of all constant coefficients considered in Equation 3.15.

$$b_{Dpss} = \ln(r_{eD}) - 0.049298 + 0.43464\ r_{eD}^{-2} + \frac{a_1 + a_2u + a_3u^2 + a_4u^3 + a_5u^4}{1 + b_1u + b_2u^2 + b_3u^3 + b_4u^4} \qquad 3.15$$

where,

$$r_{eD} = {}^{r_e}\!/_{x_f}$$
$$u = \ln(F_{CD})$$

Table 3.2 Values of all constant coefficients used in Equation 3.15

Coefficients	Value
a_1	0.936268
a_2	-1.00489
a_3	0.319733
a_4	-0.0423532
a_5	0.00221799
b_1	-0.385539
b_2	-0.0698865
b_3	-0.0484653
b_4	-0.00813558

The dimensionless pseudo-steady-state parameter (b_{Dpss}) is a constant for a well model or configuration and is independent of time or pressure, but is dependent on the dimensionless fracture conductivity, F_{cD}, and dimensionless radius, r_{eD}.

Equation 3.15 is a statistical correlation based on dependent variables, F_{cD} and r_{eD} which can be determined using Equations 3.16 and 3.17, respectively.

$$F_{CD} = \frac{k_f\ w_f}{k\ x_f} \qquad 3.16$$

$$r_{eD} = \frac{r_e}{x_f} \qquad 3.17$$

The parameter b_{Dpss} is modified in this study by redefining the dimensionless radius, r_{eD}, in which the radius of investigation, r_i, is considered in place of the reservoir radius, r_e. To build the correlation, a reservoir simulation model has been constructed. The simulation model is considered a circular reservoir with a hydraulic fractured vertical well, placed at the centre of the reservoir. Thirty-five simulation cases have been designed to generate the required data to build the correlation. Table 3.3 presents the data list considered for the reservoir model and well constraints.

Table 3.3 The properties of the reservoir model

Property	Value
Reservoir radius, *ft*	2978
Pay zone thickness, *ft*	100
Porosity, *%*	10
Initial reservoir pressure, *psi*	6500
Reservoir fluid	Gas
Minimum bottom hole flowing pressure, *psi*	1000
Net to gross ratio	1
Permeability, *mD*	0.01-1
Fracture half-length, *ft*	25-1500

The 35 simulation scenarios are achieved to cover the following range of dimensionless reservoir radius and dimensionless fracture conductivity as shown below:

r_{eD}: 2, 3, 5, 10, 25, 50, 100.

F_{cD}: 1, 5, 10, 50, 100.

Based on the results of the above reservoir simulation scenarios, p_D and t_{DA} are calculated.

Using the pressure and time obtained from simulation scenarios, the pseudo-steady constant, b_{Dpss} is calculated using Equation 3.18.

$$b_{Dpss} = p_D - 2\pi t_{DA} \qquad\qquad 3.18$$

Figure 3.7 to Figure 3.11 show the calculated p_D versus t_{DA} employed to determine b_{Dpss} using Equation 3.18. Table 3.4 presents the calculated b_{Dpss} for all 35 reservoir scenarios.
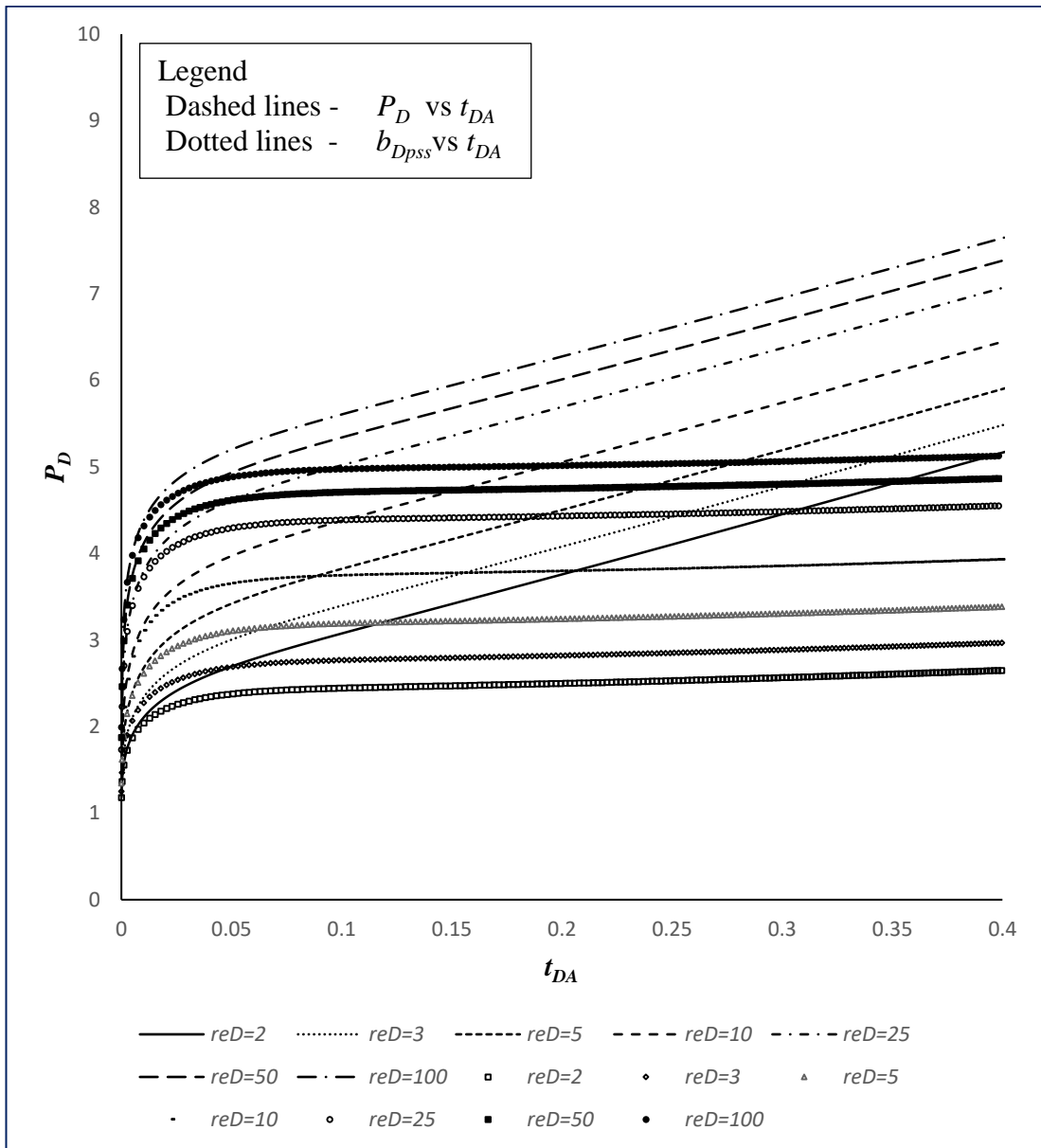
Figure 3.7 P_D and b_{Dpss} versus t_{DA} for a vertical well with a dimensionless fracture conductivity of 1
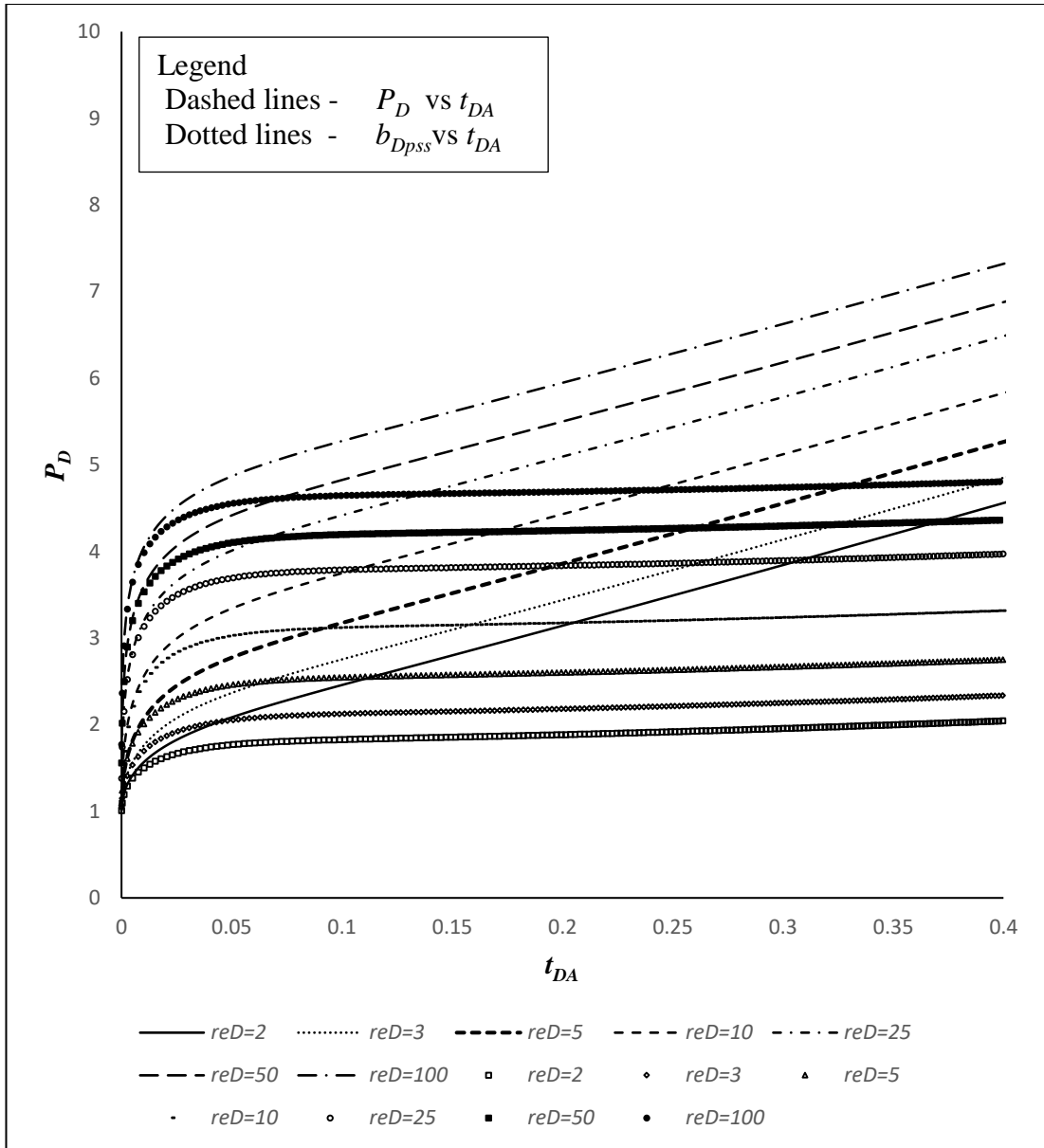
Figure 3.8 P_D and b_{Dpss} versus t_{DA} for a vertical well with a dimensionless fracture conductivity of 5
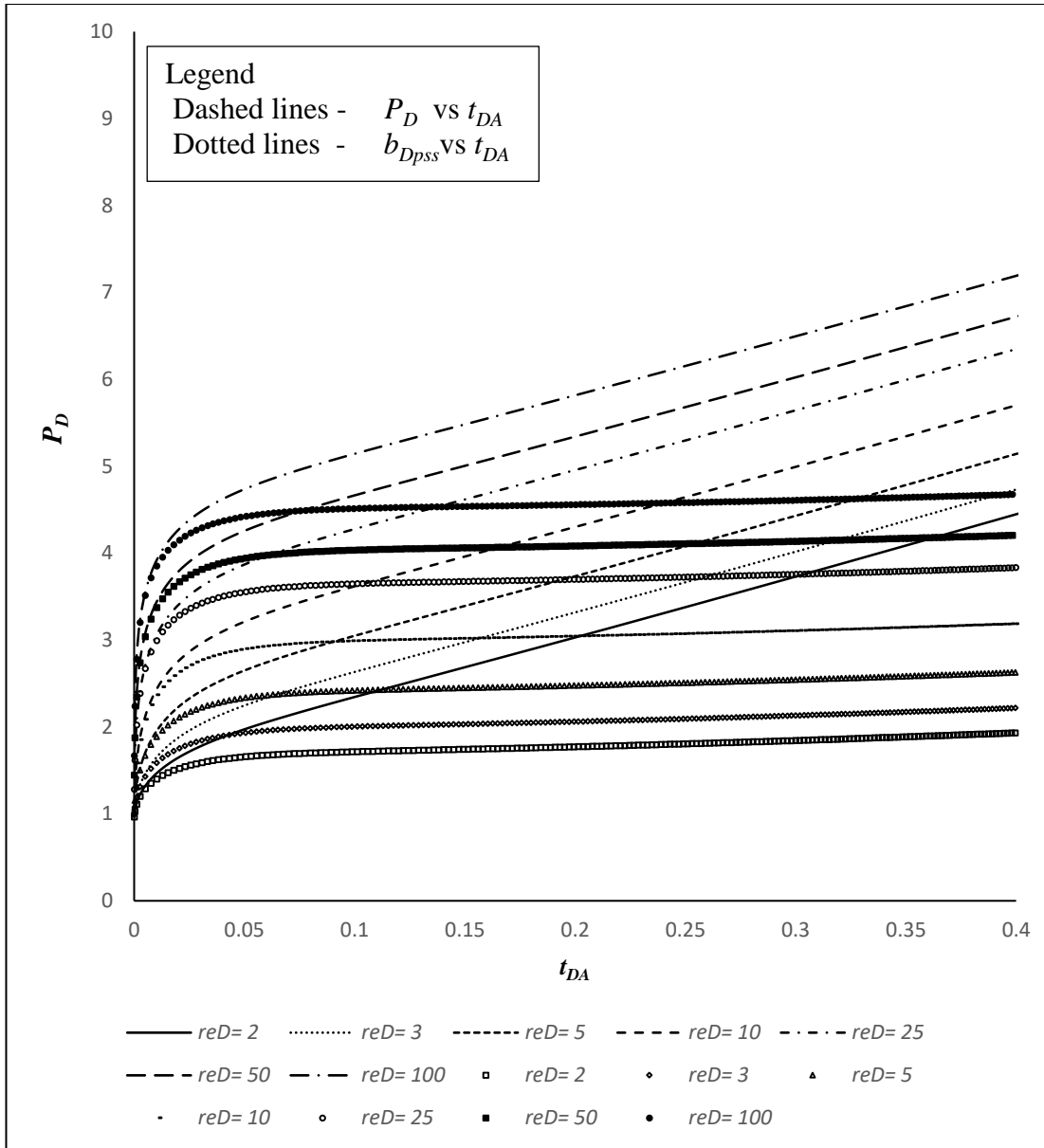
Figure 3.9 P_D and b_{Dpss} versus t_{DA} for a vertical well with a dimensionless fracture conductivity of 10
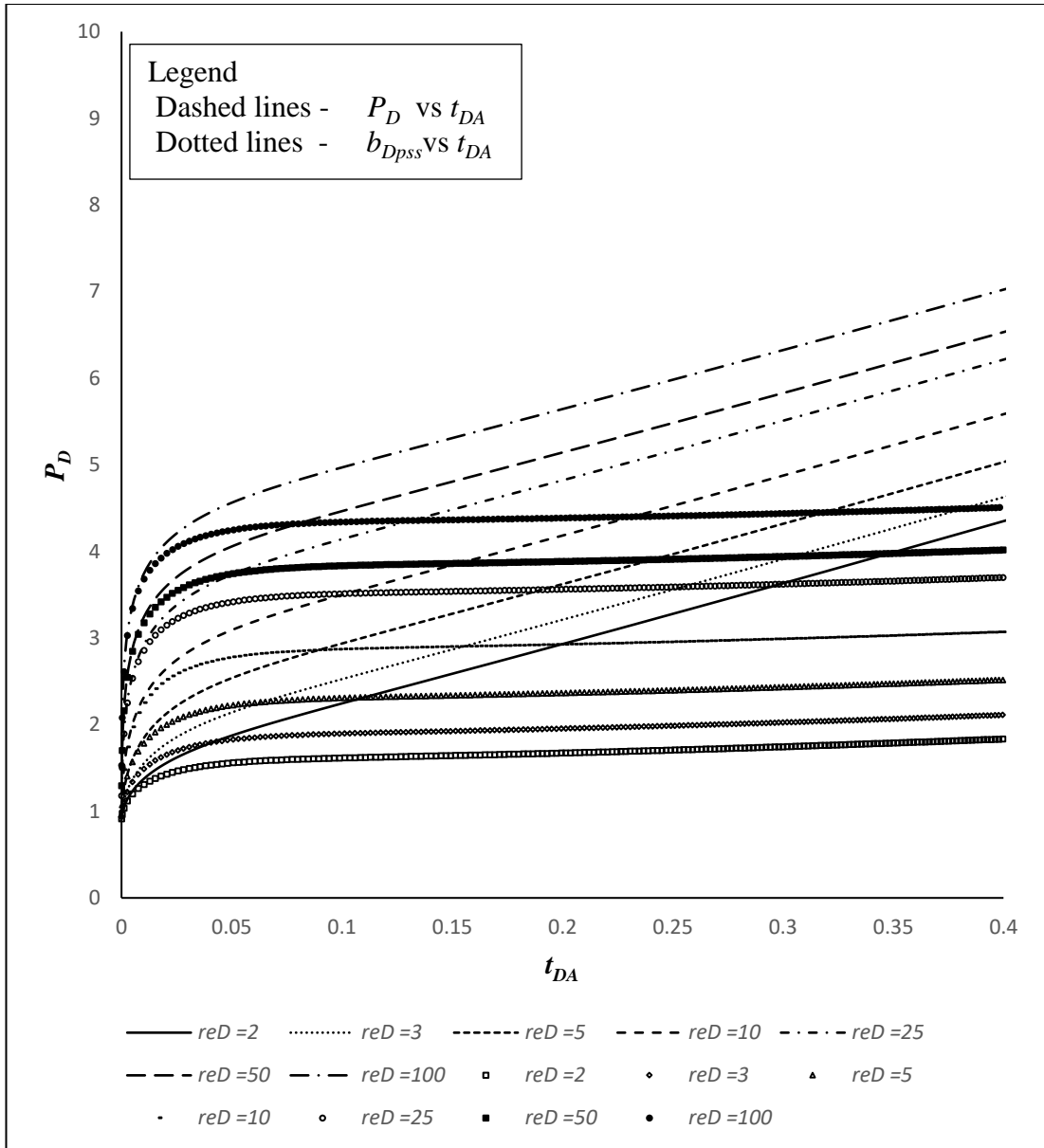
Figure 3.10 P_D and b_{Dpss} versus t_{DA} for a vertical well with a dimensionless fracture conductivity of 50
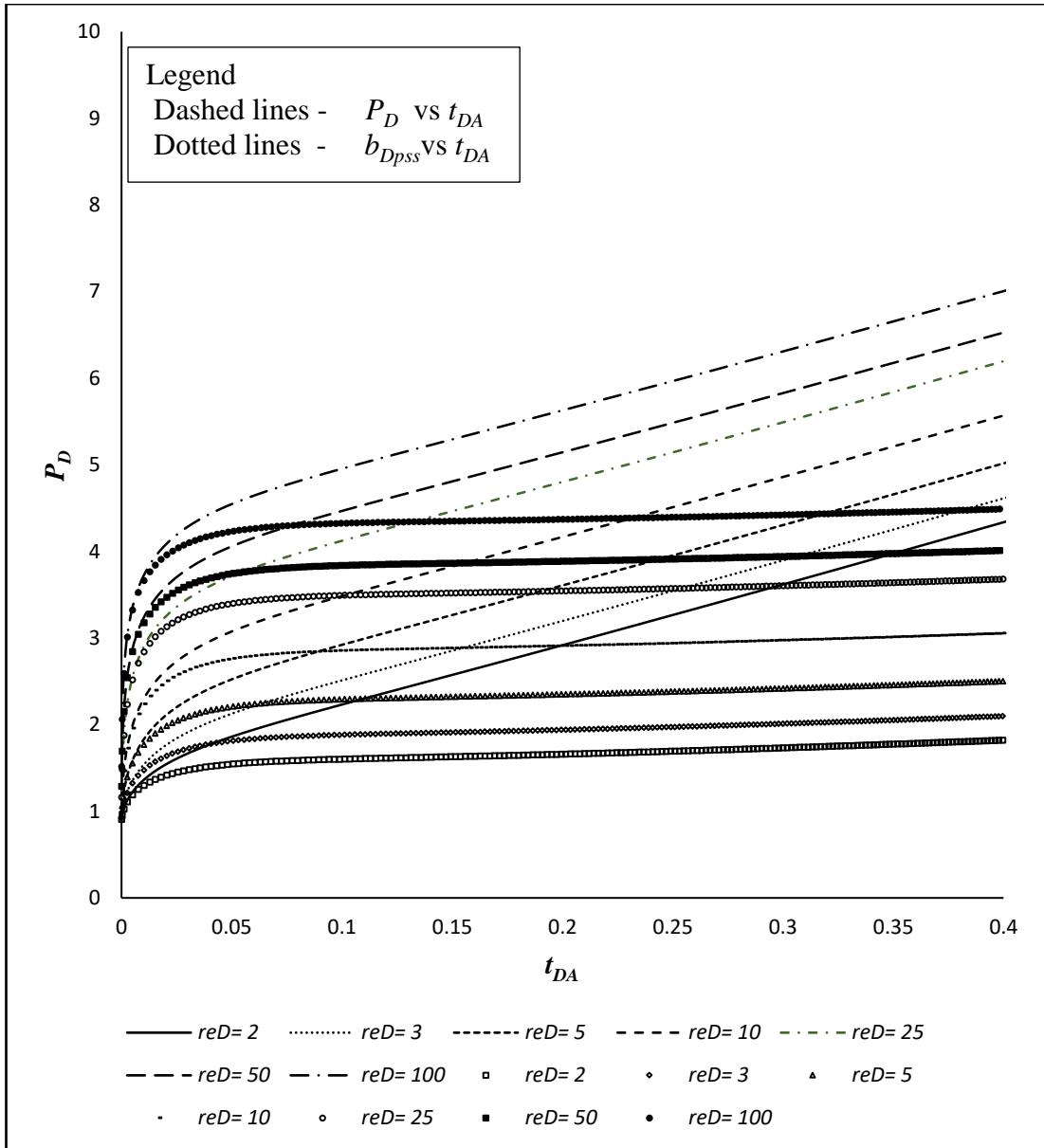
Figure 3.11 P_D and b_{Dpss} versus t_{DA} for a vertical well with a dimensionless fracture conductivity of 100

Table 3.4 The dimensionless pseudo-steady-state parameter calculated at different r_{eD} and F_{CD} values for a vertical fractured well with a finite conductivity in a bounded reservoir

		r_{eD}						
		2	3	5	10	25	50	100
F_{CD}	1	2.6	2.93	3.35	3.89	4.52	5	5.1
	5	2	2.29	2.71	3.28	3.93	4.49	4.77
	10	1.89	2.17	2.586	3.147	3.795	4.34	4.64
	50	1.79	2.07	2.48	3.03	3.66	4	4.47
	100	1.78	2.05	2.46	3.015	3.642	3.976	4.458

The pseudo-steady constant is a function of dimensionless fracture conductivity, F_{CD}, and dimensionless reservoir radius, r_{eD}, which is the function of the radius of the investigation, r_i, and the fracture half-length, x_f, redefined and expressed by Equation 3.19.

$$r_{eD} = \frac{r_i}{x_f} \qquad\qquad 3.19$$

The calculated values of b_{Dpss} corresponding with F_{CD} and r_{eD} are provided as input variables for the statistical model based on the regression analysis to develop a new correlation of b_{Dpss} as a function of r_{eD} and F_{CD}, expressed by Equation 3.20. Table 3.5 presents the values of the constant coefficients of the suggested correlation of b_{Dpss}.

$$b_{Dpss} = a_1 \, r_{eD}{}^{a_2} + a_3 \, \ln(r_{eD}) + a_4 + \frac{a_5 + a_6 \, \ln(F_{CD}) + a_7 \, [\ln(F_{CD})]^2 + a_8 \, [\ln(F_{CD})]^3}{1 + + a_9 \, \ln(F_{CD}) + a_{10} \, [\ln(F_{CD})]^2 + a_{11} \, [\ln(F_{CD})]^3} \qquad 3.20$$

Table 3.5 The value of constant coefficients of the suggested correlation of b_{Dpss} (Equation 3.20)

Constant	value
a_1	0.055625
a_2	1.56E-11
a_3	0.740375
a_4	0.46239
a_5	1.598604
a_6	1.041522
a_7	0.969009
a_8	0.901807
a_9	0.094247
a_{10}	1.133946
a_{11}	1.327048

A set of equations is suggested as an input to the statistical model, and the confidence level is observed. The equation which confirms a minimum level of difference between the b_{Dpss}, calculated by equation and the b_{Dpss}, calculated by the suggested correlation,

is considered a better correlation. The generated correlation is in good agreement with the reservoir simulation results, where the new correlation has an absolute average error (APE) of 1.67%, an average relative error (ARE) of 0.006, the sum of the relative error squares (SRE) equalling 0.024 and the sum of the squares of errors (SSE) equalling 0.418. Equations 3.21 to 3.24 are employed to calculate the above error criteria to prove the accuracy of the suggested correlation statistically.

$$APE = \sum \left[\left| \frac{b_{Dpss_{equation}} - b_{Dpss_{correlation}}}{b_{Dpss_{equation}}} \right| \times 100 \right] \qquad 3.21$$

$$ARE = \sum_{i=1}^{N} \left[\left(\frac{b_{Dpss_{equation}} - b_{Dpss_{correlation}}}{b_{Dpss_{equation}}} \right)_i \right] / N \qquad 3.22$$

$$SRE = \sum_{i=1}^{N} \left[\left(\frac{b_{Dpss_{equation}} - b_{Dpss_{correlation}}}{b_{Dpss_{equation}}} \right)_i^2 \right] / N \qquad 3.23$$

$$SSE = \sum_{i=1}^{N} \left(b_{Dpss_{equation}} - b_{Dpss_{correlation}} \right)^2 \qquad 3.24$$

The generated correlation is observed to be a good approximation for b_{Dpss} for of r_{eD} values ranging from 2 to 100 and F_{CD} ranging from 1 to 100.

3.2.2 Generation of type curve using proposed correlation

The final step in this chapter is to generate a simple set of type curves based on the Fetkovich format for different dimensionless fracture conductivities, by varying the dimensionless reservoir radius and dimensionless fracture conductivity.

The following ranges of the cases are covered by the suggested set of type curves in this chapter:

r_{eD}: 2, 3, 5, 10, 25, 50, 100.
F_{cD}: 1, 5, 10, 50, 100.

The above cases are simulated with the generated reservoir models employing the proposed correlation. The main idea here is to record the bottom-hole pressures and flow rates versus time which would be used as an input to the traditional equations to generate type curves. The recorded bottom-hole flowing pressures and flow rates are given as an input to Equations 3.19, 3.20, 3.25, 3.26, 3.27 and 3.28 to generate the set of type curves.

$$q_D = \frac{1424\,q\,T}{kh(\Delta m(p))} \qquad\qquad 3.25$$

$$t_{DA} = 0.00633\frac{kt}{\emptyset(\mu c_t)_i A} \qquad\qquad 3.26$$

$$t_{Dd} = \frac{2\pi t_{DA}}{b_{Dpss}} \qquad\qquad 3.27$$

$$q_{Dd} = q_D b_{Dpss} \qquad\qquad 3.28$$

Where:

q_D: Dimensionless flow rate.

t_{DA}: Dimensionless time.

q_{Dd}: Dimensionless decline rate function.

t_{Dd}: Dimensionless decline time function.

The resultant data obtained from the above calculations are plotted as a conventional form of q_{Dd} and t_{Dd} to obtain the format of Fetkovich's type curves for different dimensionless fracture conductivities, F_{cD} and dimensionless reservoir radius, r_{eD}, tuned according to the developed correlation of b_{Dpss}, as shown in Figure 3.12 to Figure 3.16.
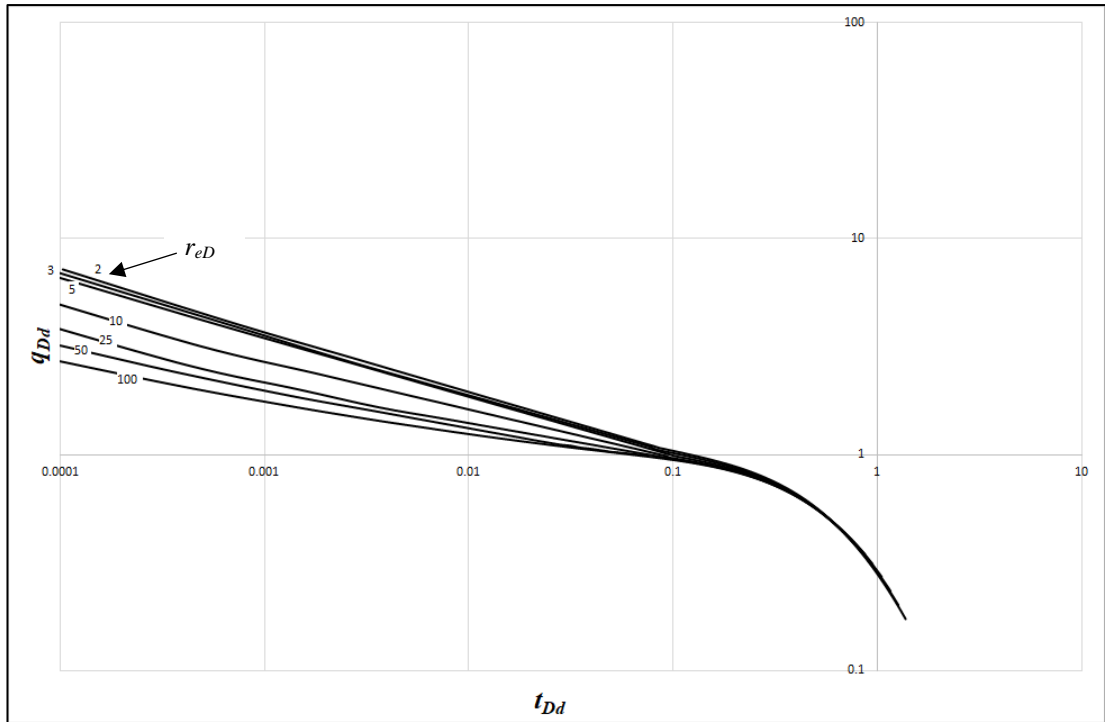
Figure 3.12 Decline type curve - dimensionless decline rate function versus dimensionless decline time function for a fractured vertical well with F_{CD}=1, for different r_{eD} (2, 5, 10, 25, 50, 100)
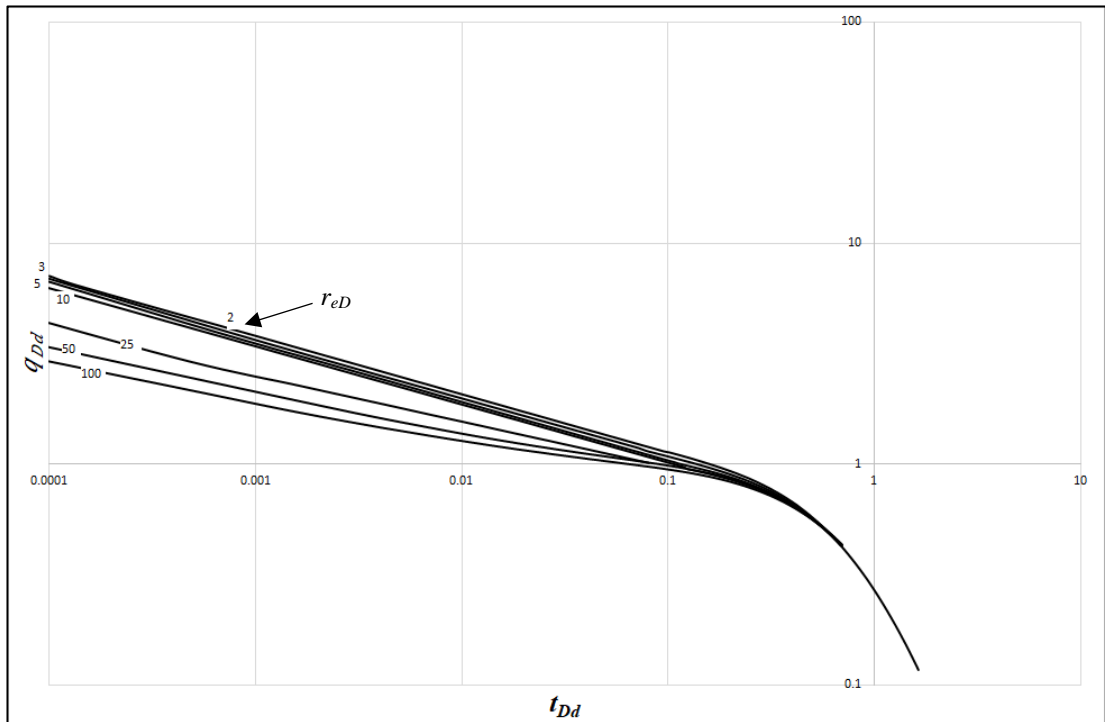
Figure 3.13 Decline type curve - dimensionless decline rate function versus dimensionless decline time function for a fractured vertical well with F_{CD} =5, for different r_{eD} (2, 5, 10, 25, 50, 100)
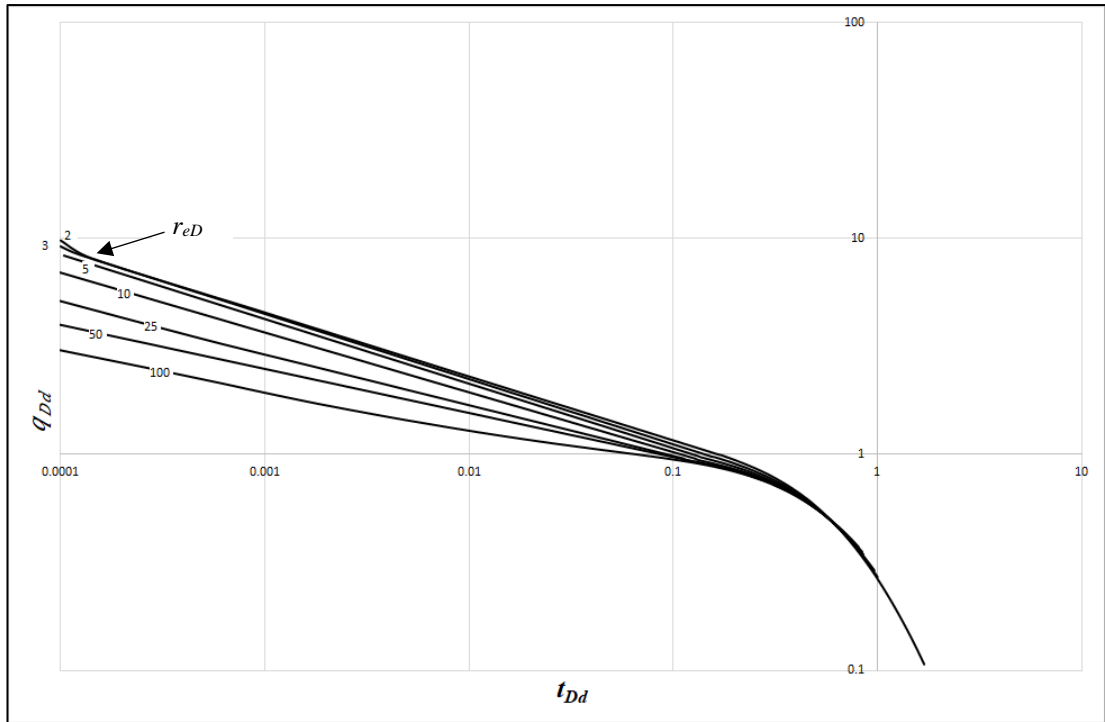
Figure 3.14 Decline type curve - dimensionless decline rate function versus dimensionless decline time function for a fractured vertical well with F_{CD} =10, for different r_{eD} (2, 5, 10, 25, 50, 100)
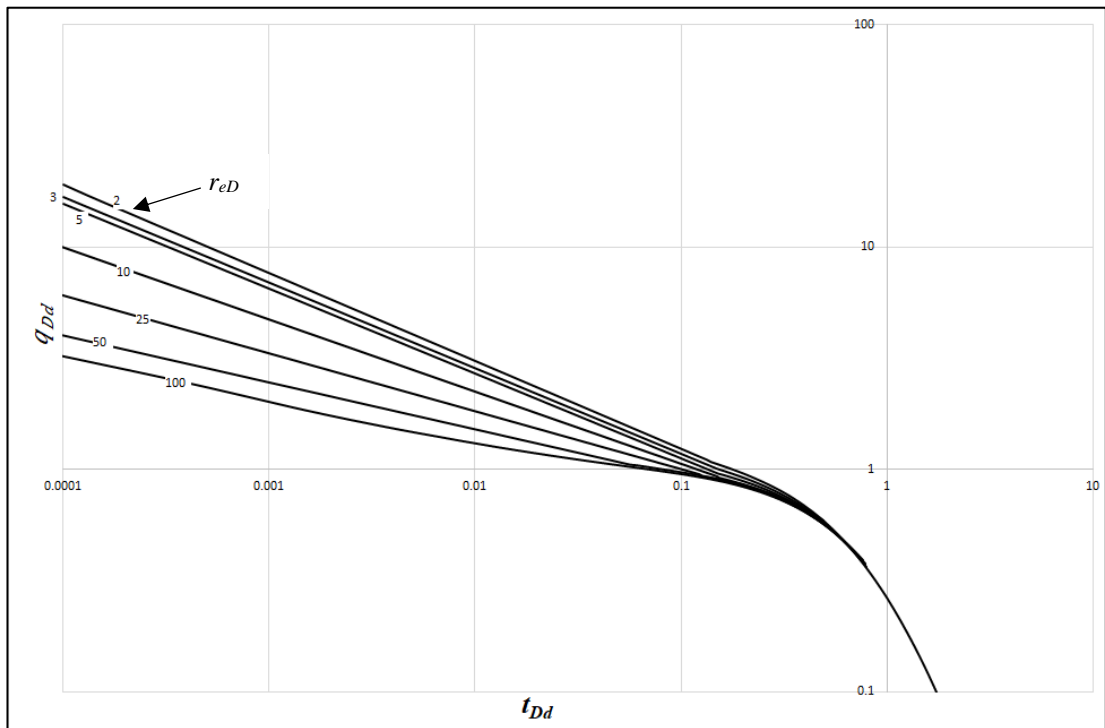
Figure 3.15 Decline type curve - dimensionless decline rate function versus dimensionless decline time function for a fractured vertical well with F_{CD} =50, for different r_{eD} (2, 5, 10, 25, 50, 100)

71
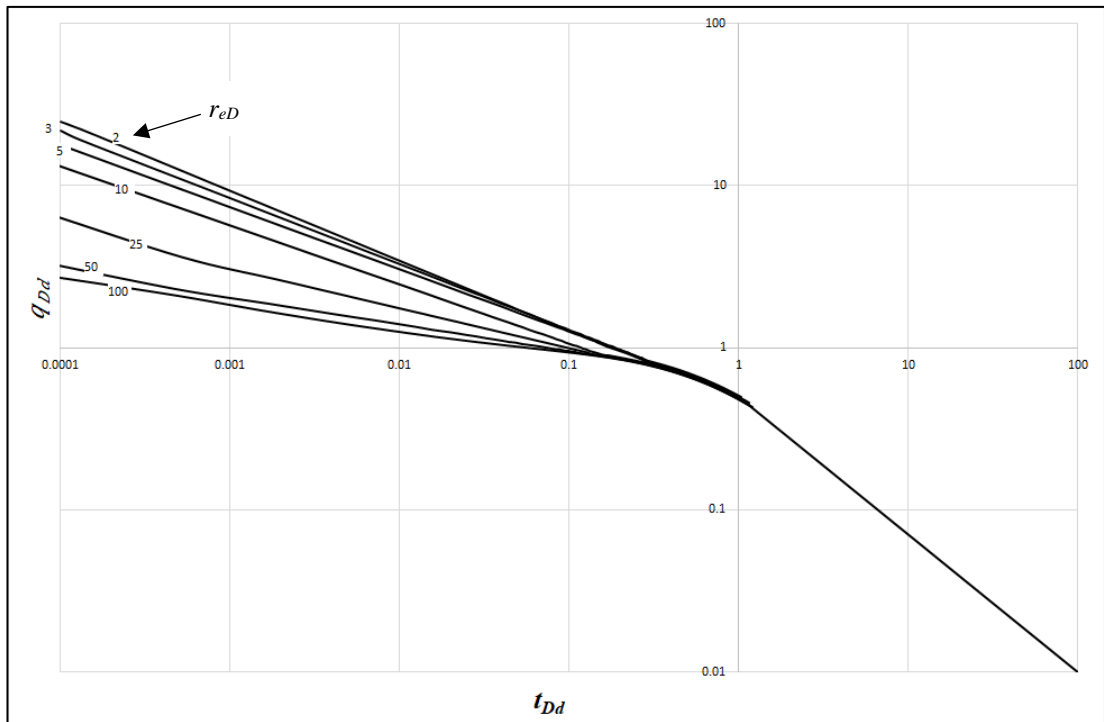
Figure 3.16 Decline type curve - dimensionless decline rate function versus dimensionless decline time function for a fractured vertical well with $F_{CD} = 100$, for different r_{eD} (2, 5, 10, 25, 50, 100)

3.2.3 Validation of the correlation

The obtained correlation for the pseudo-steady state, b_{Dpss}, and the developed set of type curves are validated using production data of two field examples from Australian tight gas fields. This production data pertains to wells in real TGRs. The basic data of the two field examples used to calculate parameters such as gas in place (G), drainage area, equivalent drainage radius, permeability to gas and fracture half-length are provided in Table 3.6. Moreover, Table 3.6 includes the gas in place calculated by reservoir simulation and the fracture half-length estimated from fracturing job reports. The equations used to calculate these parameters are given by Equations 3.29 to 3.31.

Table 3.6 The basic and the measured data of two field cases used to verify the suggested correlation for b_{Dpss}

Property	Case.1	Case.2
Pay zone thickness, *ft*	112	250
Porosity (avg.), *fraction*	0.15	0.11
Initial reservoir pressure, *psia*	6500	7100

Reservoir fluid	Gas	Gas
Permeability (avg.), *mD*	0.05	0.041
Initial flow rate, *Mscf/D*	2600	14350
Water saturation, *fraction*	0.22	0.2
Production period, *month*	22	24
Gas in place, *Bscf*	32	120
Drainage area, *acres*	158	345
Fracture half-length, *ft*	60	1090

$$G = \frac{1}{c_{gi}} \frac{(t_{ca})_{MP}}{(t_{Dd})_{MP}} \frac{(q/\Delta P_p)_{MP}}{(q_{Dd})_{MP}}$$

3.29

$$A = \frac{GB_{gi}}{\emptyset h(1 - S_{wir})}$$

3.30

$$k_g = 141.2 \frac{B_{gi}\mu_{gi}}{h} b_{Dpss} (\frac{(q_g/\Delta P_p)_{MP}}{(q_{Dd})_{MP}})$$

3.31

To perform type curve matching, pseudo-pressure drop normalized rate function ($\frac{q}{\Delta P_p}$) is plotted against material balance pseudo-time function (t_{ca}). The equations to calculate the pseudo-pressure drop normalized rate function, normalized pseudo-pressure function and material balance pseudo-time function (t_{ca}) are given by Equations 3.32 to 3.34, respectively:

$$\frac{q}{\Delta P_p} = \frac{q}{\left[P_{p_i} - P_{p_{wf}}\right]}$$

3.32

$$P_p = \frac{\mu_i z_i}{p_i} \int_{p_{base}}^{p} \frac{p}{\mu z} dp$$

3.33

$$t_{ca} = \frac{\mu_i \, c_{gi}}{q \, (t)} \int_0^t \frac{q(t_{ca})}{\mu(\bar{p}) \, c_g(\bar{p})} \, dt \qquad\qquad 3.34$$

The pseudo-pressure drop normalized rate function $(\frac{q}{\Delta P_p})$ is calculated for those two tight gas field cases including hydraulic fractured wells. $(\frac{q}{\Delta P_p})$, calculated using Equations 3.32 and 3.33, is plotted on a logarithmic scale against the material balance pseudo-time function (t_{ca}), shown in Figure 3.17 and Figure 3.18.
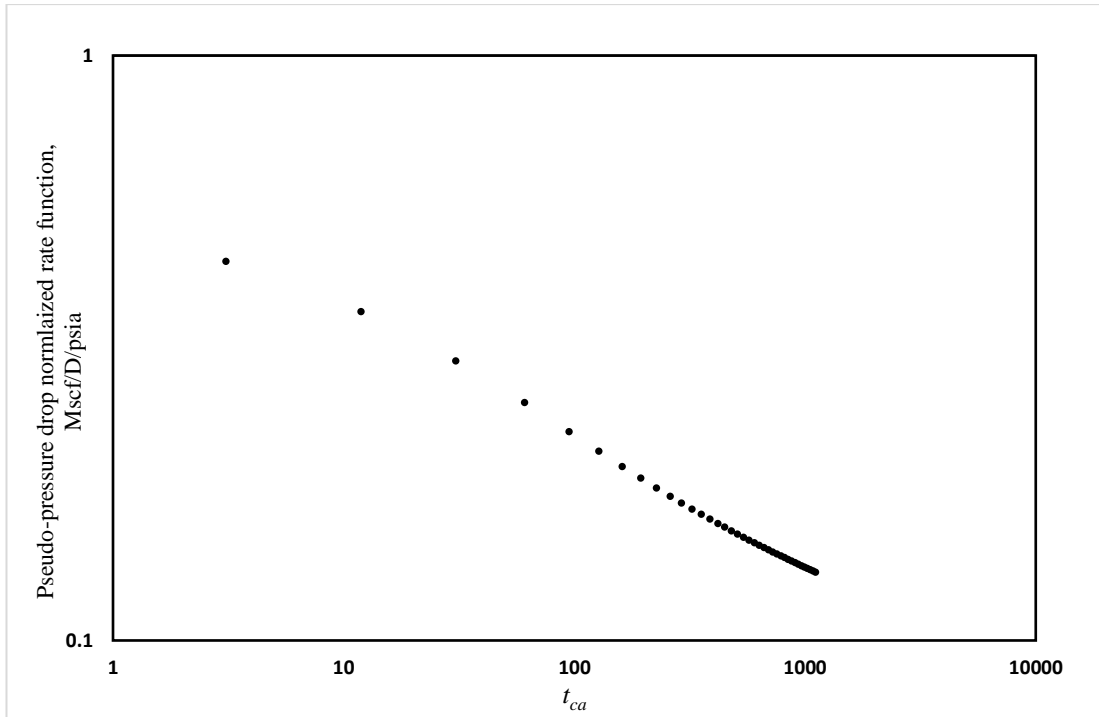
Figure 3.17 Log-Log plot of pseudo-pressure drop normalized rate function $(\frac{q}{\Delta P_p})$ versus material balance pseudo-time function, t_{ca} for Case 1
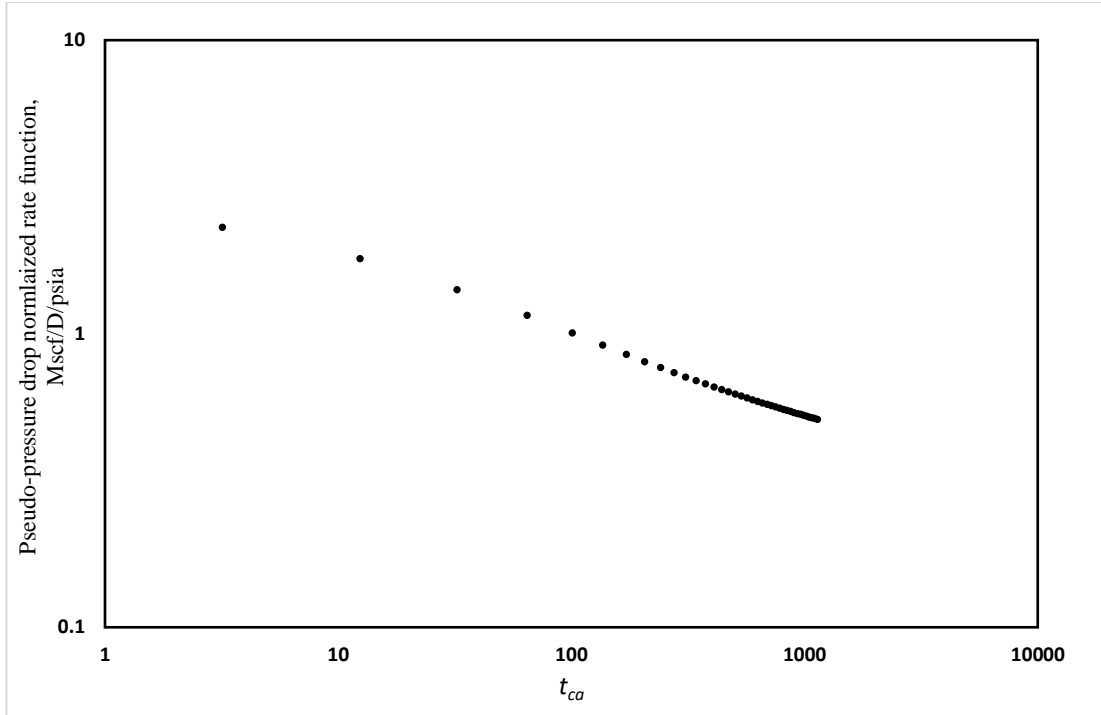
Figure 3.18 Log-Log plot of pseudo-pressure drop normalized rate function ($\frac{q}{\Delta P_p}$) versus material balance pseudo-time function, t_{ca} for Case 2

The plot of the calculated pseudo-pressure drop normalized rate function with respect to material balance pseudo-time function for Case 1 and Case 2 are overlapped with the developed set of type curve analysis for hydraulically fractured vertical wells to obtain a certain match point for each case. The extracted data at the match point for Case 1 and Case 2 are listed in Table 3.7. The selection of a suitable type curve chart for each case is based on the value of F_{CD}. For each field case, the type curve matching has been tuned between $\left(\frac{q}{\Delta P_p}\right)$ vs t_{ca} and dimensionless decline rate (q_{Dd}) and dimensionless decline time (t_{Dd}).

Table 3.7 The data extracted at the match point for each of Case.1 and Case.2

Match point coordinate	Case.1	Case.2
F_{CD}	100	10
q_{Dd}	1	1
t_{Dd}	1	1
r_{eD}	25	2
$q/\Delta P(p)$, Mscf/D/psi	0.11	0.4
t_{ca}, day	18000	20000

Based on the type curve matching, Table 3.8 displays the gas in place, drainage area, reservoir permeability and fracture half-length, all calculated using Equations 3.19, 3.20, 3.29, 3.30, and 3.31.

Table 3.8 The results type curve matching for Case 1 and Case 2

Case No.	G, Bscf	A, acres	k, mD	x_f, ft
1	30.5	160.4	0.0504	59.66
2	123.3	360.2	0.0397	1117

Table 3.9 shows the absolute error percentage (AEP) of the calculated values in Table 3.8 compared to the field data.

Table 3.9 Absolute error percentage (AEP) of the results of type curve matching for Case 1 and Case 2

Case No.	AEP, %			
	G, Bscf	A, acres	k, mD	x_f, ft
1	4.69	1.52	0.8	0.57
2	2.75	4.41	3.17	2.48

The absolute error percentages shown in Table 3.9 explain the good matching between the calculated results from the developed set of type curves and the field data, because all absolute error percentages are less than 5%. The absolute error percentages detail how the new correlation of b_{Dpss} and the developed set of type curves have a high level of confidence in applicability to field conditions to estimate reservoir permeability, fracture half-length, gas in place and drainage area because of the slight difference between the calculated and measured well and reservoir parameters. Furthermore, a detailed approach is provided for the analysis of the production data from a TGR over 22 to 24 months, which is not considered a long production period compared to the entire production life of a reservoir that can reach up to 30 years (Al-Fatlawi et al., 2017b; H. Bahrami et al., 2012a; Maley, 1985). Therefore, this method could contribute to analysing production data and developing future field development plans.

A new correlation to calculate the pseudo-steady constant is derived and successfully validated. The study is further extended by the generations of type curves based on the proposed correlation which can be used as a simple and convenient tool to analyse production performance of fractured wells in a TGR. The method is straightforward and simple enough to be very useful in routine industry tasks, especially for frontline engineers.

A new technique based on the proposed correlation of the pseudo-steady constant and the developed set of type curves is formulated and proposed to analyse the production data of fractured vertical wells in TGRs. This technique is applied to a real tight gas field with six months of production. It is observed that the proposed technique provides outcomes similar to reservoir data with a high level of accuracy.

Example cases are presented to demonstrate the application process/methodology involved to employ the technique in a representative field case.

3.3 Equivalent drainage area of well in tight gas reservoirs

The accurate estimation of the well drainage area is a crucial requirement because drainage area values lead to developing the infill drilling plan, considered a substantial key to economically evaluating the reservoir. Specifically, estimation of the drainage area of a TGR well is considered an essential parameter to determine the productive ability of the well and the infill drilling planning. Moreover, the estimation of gas in-place volume associated with each well is an important key to any reservoir-management development (Ismadi et al., 2012), in spite of the challenges in calculating the drainage area of wells in TGRs because of the low formation permeability (Satter and Iqbal, 2015). There are only a few papers regarding the estimation of well drainage area in TGRs (Stuart Alan Cox et al., 2005).

In this section of the thesis, a practical method for predicting the equivalent drainage area of a fractured well in a TGR is proposed. This method is based upon combining gas material balance equations and decline curve analysis. The developed method is validated against reservoir simulation results, which demonstrate that the proposed method is accurate enough to predict the equivalent drainage area and may be considered a practical tool for production forecasting for TGRs. Sensitivity analyses are carried out to investigate various factors, such as porosity, permeability, and fracture half-length on equivalent drainage area for fractured vertical well in TGRs.

Based on the sensitivity study, it is observed that the fracture half-length and porosity have a strong impact on the equivalent drainage area, and propagation of equivalent drainage area with time.

3.3.1 Drainage area concept

'Drainage area' has been defined in a number of ways. The simplest definition is using the area of connected permeable formation bounded by physical boundaries and depleted by a well located inside the area to obtain an economic recovery factor (Khan et al., 2011). However, there is still uncertainty and confusion about the exact meaning and definition of 'drainage area' (Pouladi et al., 2017). Therefore, the definitions and methods to estimate the drainage area outlined in the literature are discussed below.

Technically, two broad definitions classify the 'drainage area', as a result of this classification all the methods for calculating the drainage area are working according to it. Firstly, the physical drainage area is limited by impermeable physical boundaries meaning the drainage area remains constant and does not change with time (Yesiltepe, 2015). Secondly, the effective drainage area is defined based upon the travelling distance of pressure waves from production activities, meaning the effective drainage area enlarges during the transient period, and as a result the effective drainage area is smaller than the physical drainage area over the transient flow period. One of the significant difficulties of estimating the drainage area is the ambiguous concept of the radius of investigation that has no standard definition in the petroleum industry literature (Kuchuk, 2009). Regarding TGRs, the effective drainage area is probably smaller than the physical drainage area because the low permeability delays the movement of the pressure pulse through the formation.

Some researchers introduced "pressure mapping" as a simple tool to estimate the drainage area. The pressure mapping method uses the reservoir simulation models for calculating the reservoir pressure to draw pressure streamlines that show the route of fluid towards the well, and then the plotting of those fluid routes characterizes the drainage area (Anderson, 1991; Hurst, 1987).

Samaniego et al. (1997) connected the drainage area to the drainage radius by sonic velocity based on the distance between them during a specific period. They assumed that pressure drop due to production at a well is transferred radially at sonic pressure. To calculate the drainage area, Samaniego et al. (1997) formulated a synergistic approach by combining the geological, seismic, well log, petrophysical and reservoir

pressure analysis data. Alzate et al. (2001) proposed a systematic simulation study of a fractured vertical well in a TGR to describe the evolution of drainage shape and size over time, and numerically determined the shape and size of a drainage area for a specified iso-pressure line as the function of dimensionless fracture conductivity and fracture half-length. Alzate et al. (2001) concluded that the primary factor controlling the shape and size of a drainage area is fracture half-length. Escobar et al. (2007) combined seismic and production analysis, and geostatistical and reservoir simulation modelling to describe the drainage area for an anisotropic low permeability gas reservoir. Stuart Alan Cox et al. (2005) introduced a new conception to estimate the drainage area by connecting the effective drainage area and the recovery factor. They suggested a theoretical method to estimate the drainage area through the formulation of a relationship between rock properties, reservoir geometry, and fracture properties. Du (2008) suggested a new methodology to calculate the drainage area based on the integration of pressure transient analysis and pressure-rate deconvolution. Most of these approaches are relatively complicated and require large datasets, making them inappropriate for application in real field cases. With this view, this study aims to develop a simple method which can accurately predict the equivalent drainage area of wells in TGRs with limited data.

3.3.2 Prediction of equivalent drainage area of well in tight gas reservoirs

In this study, a simplified method is proposed to estimate the equivalent drainage area through employing the material balance technique and decline curve analysis. The study also presents the relationship between cumulative gas production and average reservoir pressure based on the material balance equation (MBE), as well as gas flow rate and time based on the decline curve analysis (DCA). It is assumed that the reservoir production mechanism is volumetric without external support (i.e. natural water drive) and the fluid is a dry natural gas and the reservoir temperature is constant. The method is developed based on the concepts of the gas material balance and decline curve analysis (DCA) in the following five steps:

Step 1: The first step involves constructing a relationship between the average reservoir pressure/gas compressibility factor (p/z) as a function of cumulative gas production (G_p) based on the gas material balance equation (Figure 3.19 (a)) using production data (e.g. rate, time, and pressure from well tests). In the event actual production data is not available, the reservoir simulation models can be run to generate

these production and pressure data. These data can then be extrapolated (when real production is available) or generated by reservoir simulation up to the end of the current production time (t_p), and can be extrapolated to complete the material balance relationship as shown in Figure 3.19 (a).

Step 2: After calculating the average reservoir pressure at an assumed future time, t_f from the (p/z vs G_p) plot, the corresponding drainage area equivalent to cumulative gas production $(G_p)_f$ can be calculated using the volumetric equation (Equation 3.35).

$$A_{equ.} = \frac{(G_p)_f \, (B_g)_f}{\emptyset \; h}$$ 3.35

Where, subscript f represents any future time.

Step 3: The planned equivalent drainage area is then calculated by multiplying the equivalent drainage area as calculated in Step 3 by the predetermined or planned recovery factor using Equation 3.36. The recovery factor is generally set by the operator or the owner of the reservoir as per the future plan or as expected.

$$A_p = A_{equ.} \, (RF)_p$$ 3.36

Where, $(RF)_p$ is the planned or expected recovery factor.

Step 4: The relationship between the equivalent drainage area and the production time can be constructed based on the static material balance ($G_p \; vs. \bar{P}/z$) as shown in Figure 3.19 (a) and the DCA, as shown in Figure 3.19 (b), following the DCA model proposed by Mahadik et al. (2012).

Step 5: For prediction purposes, the equivalent drainage area ($A_{equ.}$) and planned equivalent drainage area (A_p) at an assumed future time ($t_{f.}$) can be determined based on the cumulative gas production $(G_p)_f$ is calculated at t_f using the decline curve analysis shown in Figure 3.19 (b) and the average reservoir pressure $(\bar{P})_f$ at the $(G_p)_f$ using the material balance technique shown in Figure 3.19 (a), and then applying Steps 3 and 4.
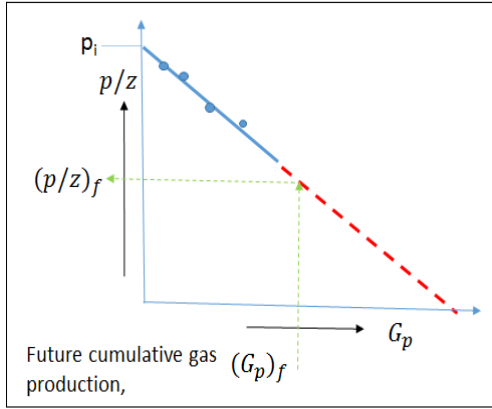
Figure 3.19(a): Based on material balance
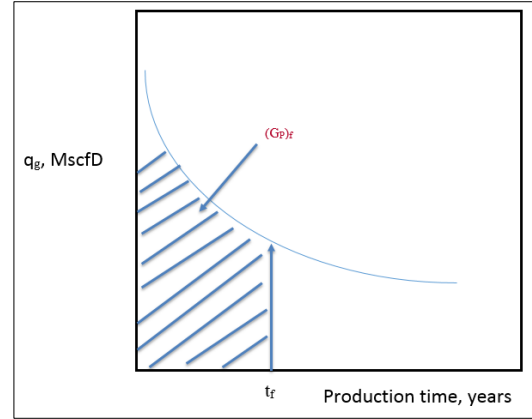
Figure 3.19(b): Based on Decline Curve Analysis

Figure 3.19 Schematic showing the process of proposed method

Among the many DCA models, the model proposed by Mahadik et al. (2012) is found to be simple but accurate enough to analyse production data for production forecasting of TGRs. Mahadik et al. (2012) decline curve introduces the rate derivative technique expressed in Equation 3.37:

$$\bar{q}_D = \frac{-1}{[d(ln(q_D))]/dt}$$ 3.37

Where the dimensionless rate (q_D) defined as:

$$q_D = \frac{q_t}{q_i}$$ 3.38

Where:

q_g Gas flow rate, Mscf/day
q_i Initial flow rate, Mscf/day

The rate derivative technique is employed to reduce the uncertainties associated with determination of optimum values of the decline exponent, *b*, and the initial decline constant, D_i, in the production decline model.

For the hyperbolic decline model, Equations 3.39 and 3.40, respectively, can be used to calculate the dimensionless production rate and the rate derivative as a function of the decline constant and time (Mahadik et al., 2012).

$$q_D = \frac{1}{[1 + b \, D_i \, t]^{\frac{1}{b}}}$$

$$\bar{q}_D = b \times t + \frac{1}{D_i}$$

Equation 3.40 shows that a linear plot of the rate derivative versus time results in a linear relationship with a slope of b and the intercept of the reciprocal of the initial decline constant $(\frac{1}{D_i})$. Using the plot and fitting a straight line on the rate derivative data can deliver the most accurate value for b for production forecast applications.

3.3.3 Reservoir simulation models

Since actual field production and pressure data is not available, this study considers many reservoir simulation models designed using the Kappa reservoir simulator Rubis to generate the production and pressure data for a typical TGR and to validate the results of the developed method. Table 3.10 shows the parameters considered in the reservoir simulation models. For all reservoir simulation models, the top of the reservoir is considered at a depth of 13000 ft with the initial reservoir pressure and temperature of 5000 psia and 200 °F, respectively, and a wellhead pressure of 400 psia. All reservoir models have a closed outer boundary and with sealed top and bottom boundaries. The specific gravity of dry gas is considered to be 0.7. The well is assumed to be a fully penetrating hydraulic fractured vertical well centred in the reservoir consisting of single layer.

The reservoir simulation model is used for two primary purposes: (a) to collect the required data for subsequent flow and shut-in periods to construct the relationship of the material balance technique; (b) to calculate the production and the recovery factor for a 30-year production period. Simulation data are then employed to calculate the equivalent drainage area for comparing with the equivalent drainage area calculated using the developed method.

Figure 3.20 and Figure 3.21 present the simulation models at the initial conditions for square and circular reservoirs, respectively, while Figure 3.22 and Figure 3.23 show

the simulation models after ten years of production for square and circular reservoirs, respectively.

Table 3.10 Specification of the reservoir simulation models

Model No.	Dimensions, ft	Shape	$\varnothing$, %	k, mD	x_f, ft
1	$10000 \times 10000 \times 100$	square	10	0.01, 0.05, or 0.1	100, 200 or 500
2	$10000 \times 10000 \times 100$	circular	10	0.01, 0.05, or 0.1	100, 200 or 500
3	$10000 \times 10000 \times 100$	square	15	0.01, 0.05, or 0.1	100, 200 or 500
4	$10000 \times 10000 \times 100$	circular	15	0.01, 0.05, or 0.1	100, 200 or 500
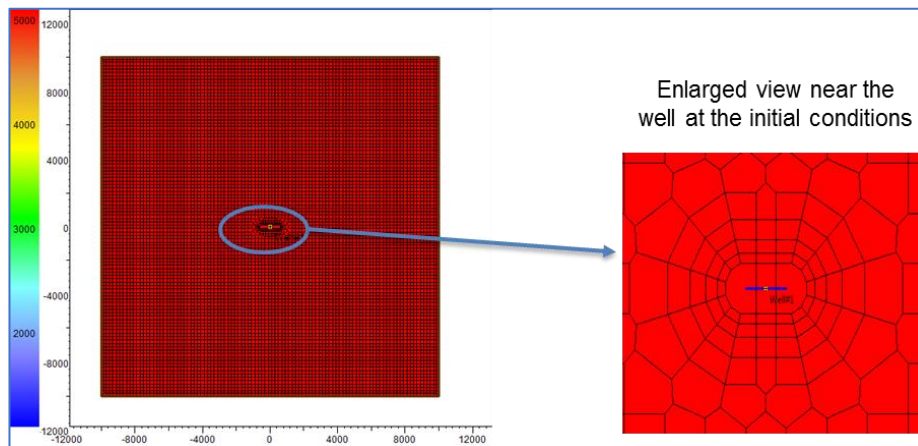
Figure 3.20 The simulation model for a square reservoir at initial conditions
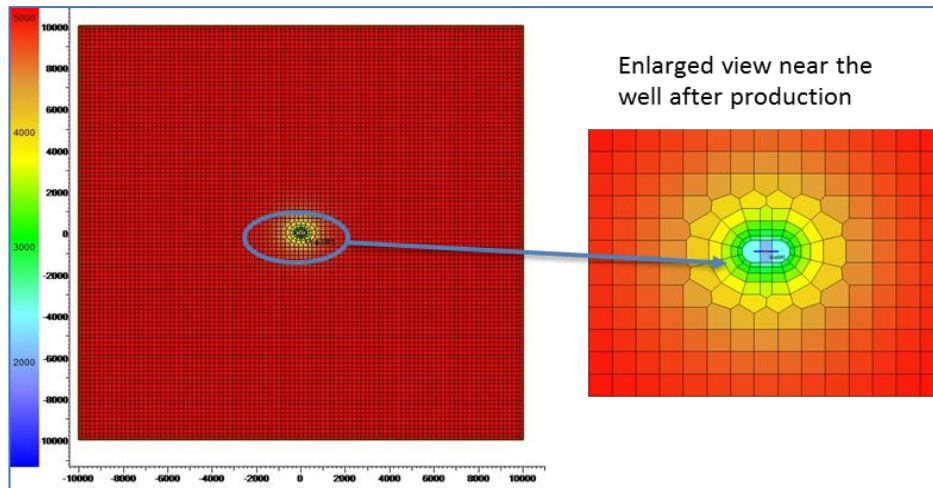
Figure 3.21 The simulation model for a square reservoir after production
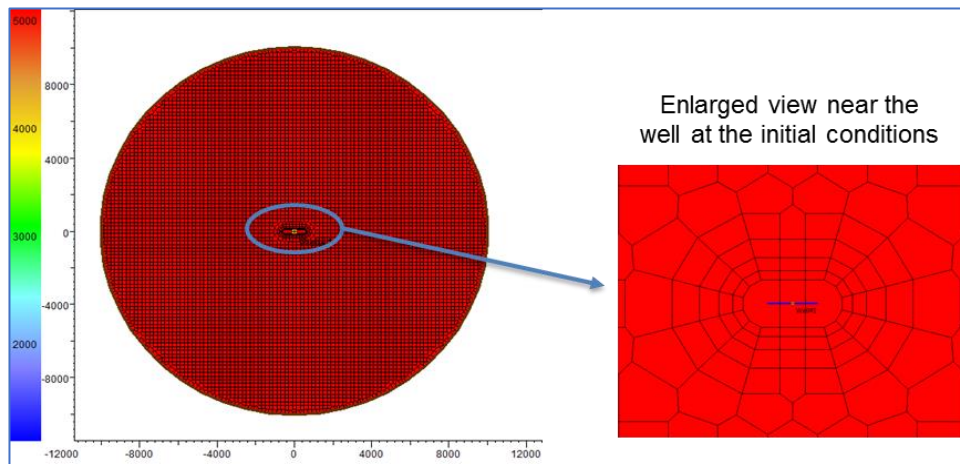
Figure 3.22 The simulation model for a circular reservoir at initial conditions
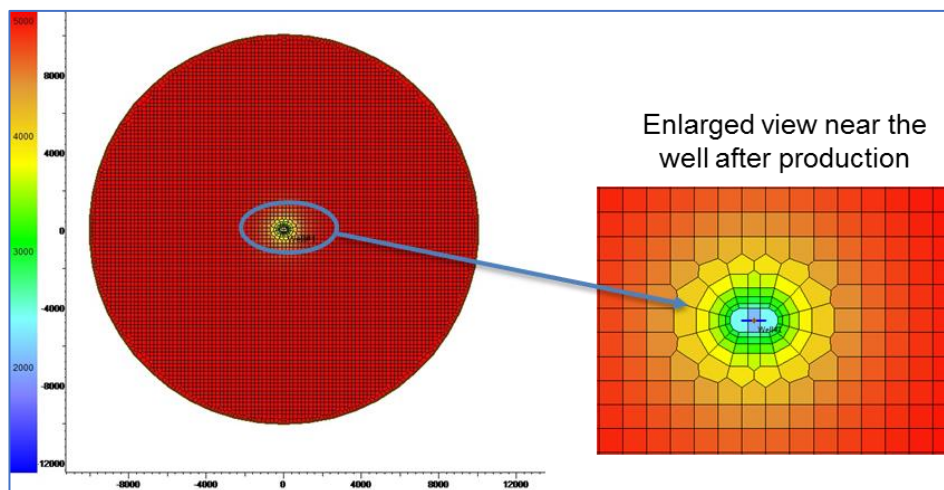
Figure 3.23 The simulation model for circular reservoir after production

3.3.4 Validation of the developed method

To validate the developed method, the planned equivalent drainage area is calculated twice based on the developed method and reservoir simulation. Table 3.11 shows the absolute error percentage of the planned equivalent drainage area calculated using the two techniques. Table 3.11 indicates the high accuracy of the developed method to estimate the planned equivalent drainage area for a fractured vertical well in a TGR with permeability ranging from 0.01 mD to 0.1 mD. The calculated absolute error percentage increases when the permeability decreases, which is believed to be because of the low permeability on the accuracy of the material balance technique.

Table 3.11 Absolute error percentage of the of planned equivalent drainage area

		Reservoir permeability, mD		
		0.1	**0.05**	**0.01**
Fracture half-length, ft	**100**	6.89	7.2	9.7
	200	4.37	5.83	8.37
	500	3.18	4.3	6.2

3.3.5 Effect of fracture length on the equivalent drainage area

Figure 3.24 and Figure 3.25 show the effect of the fracture half-length on the planned equivalent drainage area for reservoir permeability ranging from 0.01 to 0.1 mD, and the planned recovery factor of 80%, while Figure 3.26 and Figure 3.27 show the same effect under a planned recovery factor of 90% for a square and circular reservoir, respectively. The planned equivalent drainage area increases with increasing fracture length and permeability. This trend is considered to be reasonable as increasing permeability and/or fracture length increases the transmissibility, which in principle controls the propagation of the pressure pulse, and consequently increases the planned equivalent drainage area.
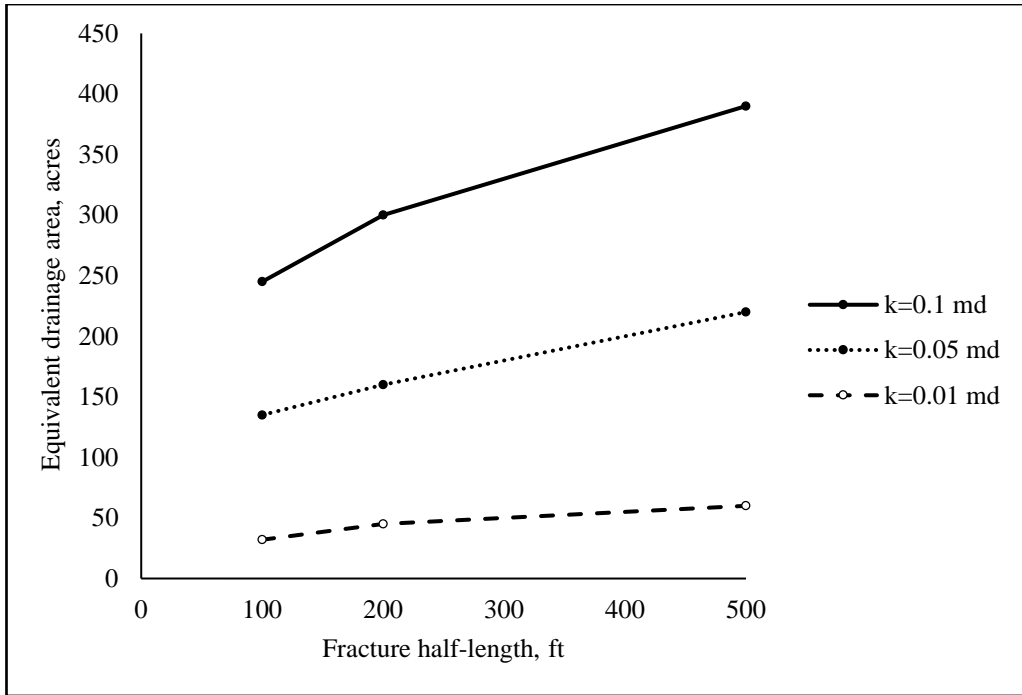
Figure 3.24 The effect of fracture half-length on the planned equivalent drainage area (square reservoir)
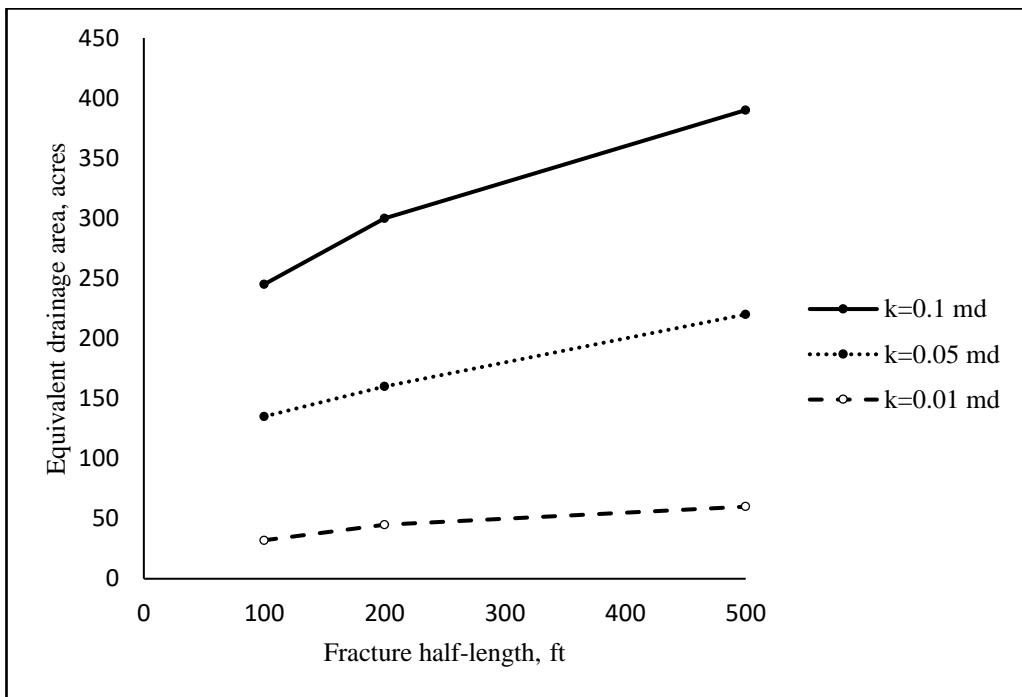
Figure 3.25 The effect of fracture half-length on the planned equivalent drainage area (circular reservoir)
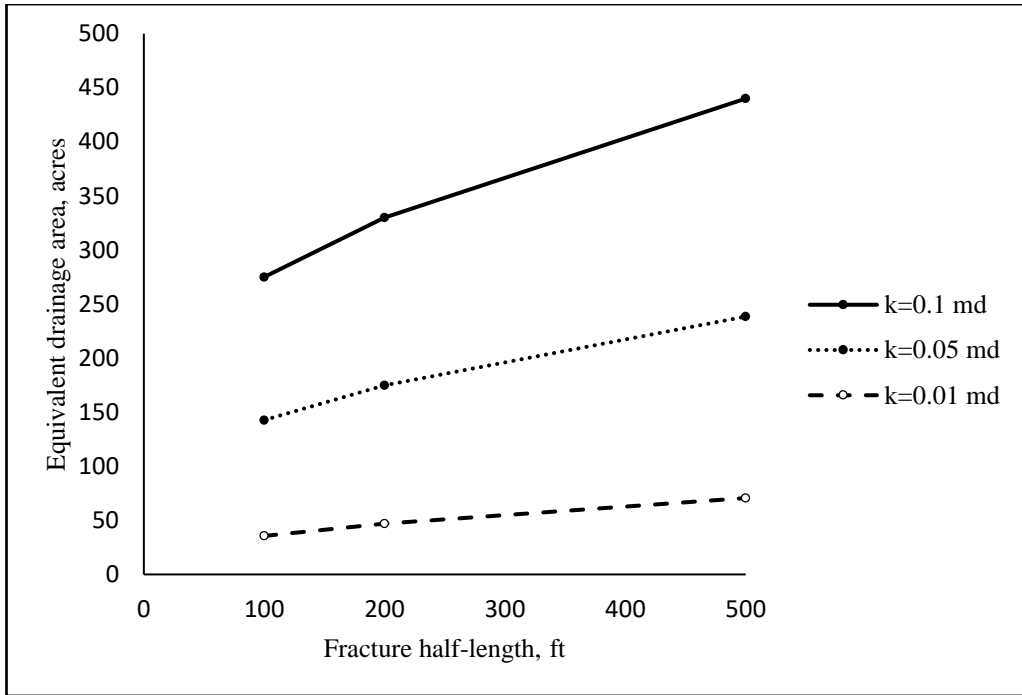
Figure 3.26 The effect of fracture half-length on the planned equivalent drainage area (square reservoir)
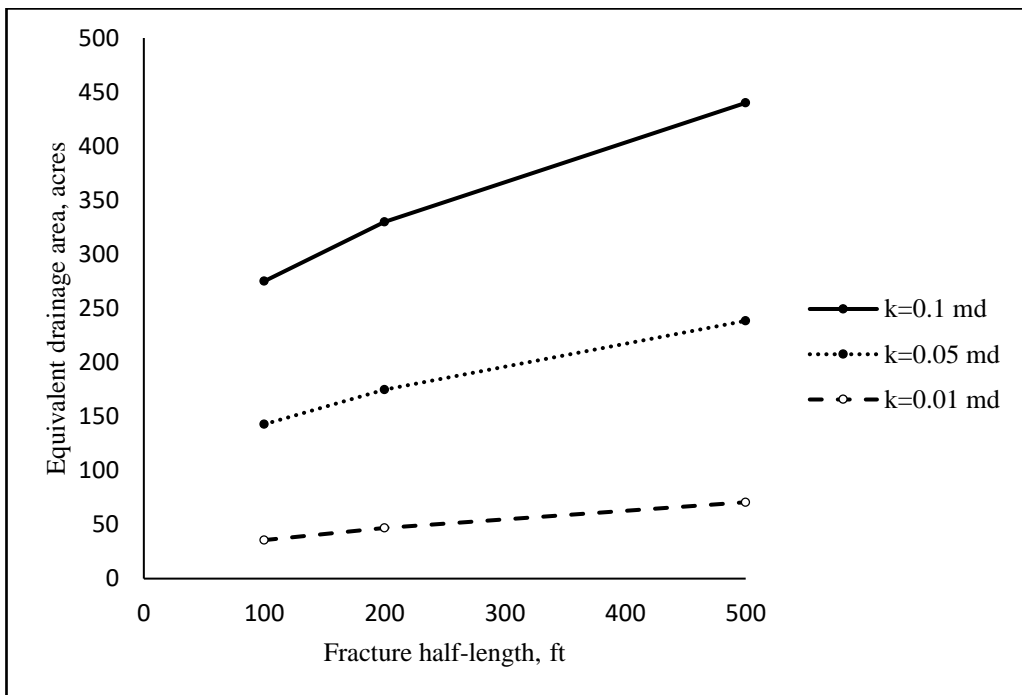
Figure 3.27 The effect of fracture half-length on the planned equivalent drainage area (circular reservoir)

3.3.6 Effect of reservoir shape on the equivalent drainage area

Reservoir models No.1 and No.2 have been employed to identify the sensitivity of the reservoir shape on the planned equivalent drainage area. Figure 3.28 shows that no

significant differences are observed between the planned equivalent drainage areas for the fractured vertical well centred in square reservoir and a circular reservoir under different permeability. However, the planned equivalent drainage area of the well in the circular reservoir is slightly greater than in the square reservoir. The low impact of the shape of reservoir on the planned equivalent drainage area is a result of the low permeability, and the two reservoirs have almost the same size.
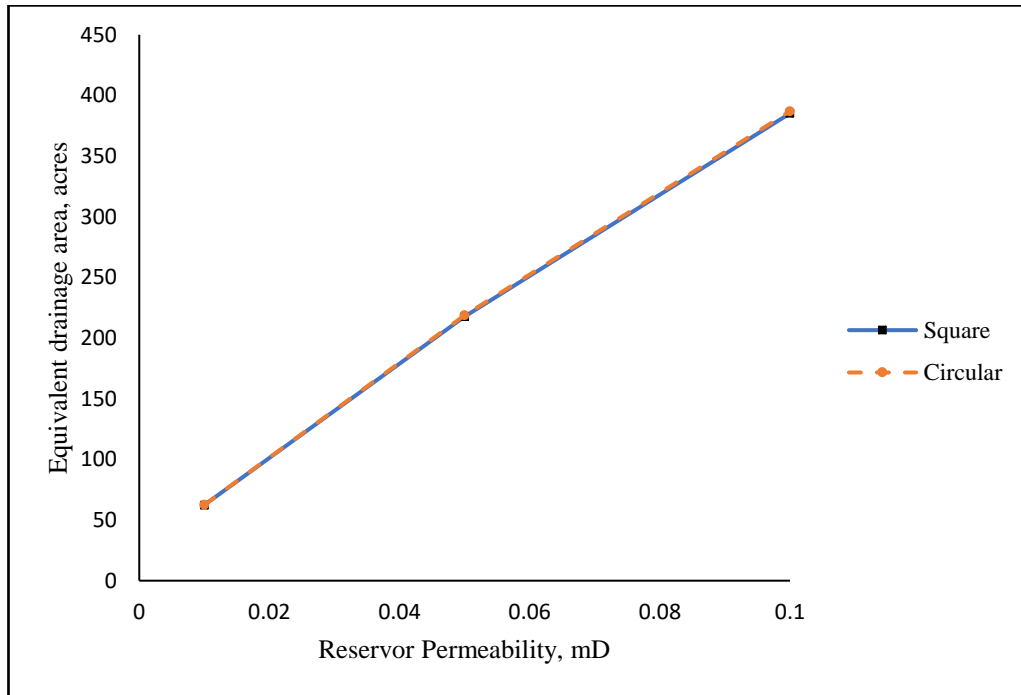
Figure 3.28 The effect of reservoir shape on the planned equivalent drainage area (fracture half-length = 500 ft)

3.3.7 Effect of porosity on the equivalent drainage area

The sensitivity of the porosity on the planned equivalent drainage area is analysed for a square reservoir and is presented in Figure 3.29 to Figure 3.31. From these figures, it can be observed that porosity has a strong impact on the planned equivalent drainage area. The planned equivalent drainage area decreases with the porosity, meaning the higher the porosity, the lower the drainage radius. The difference between the calculated planned equivalent drainage area for porosity of 10% and 15% increases with increasing reservoir permeability and fracture half-length. This sensitivity analysis has been carried out using reservoir simulation models No.1, No.2, No.3 and No.4.
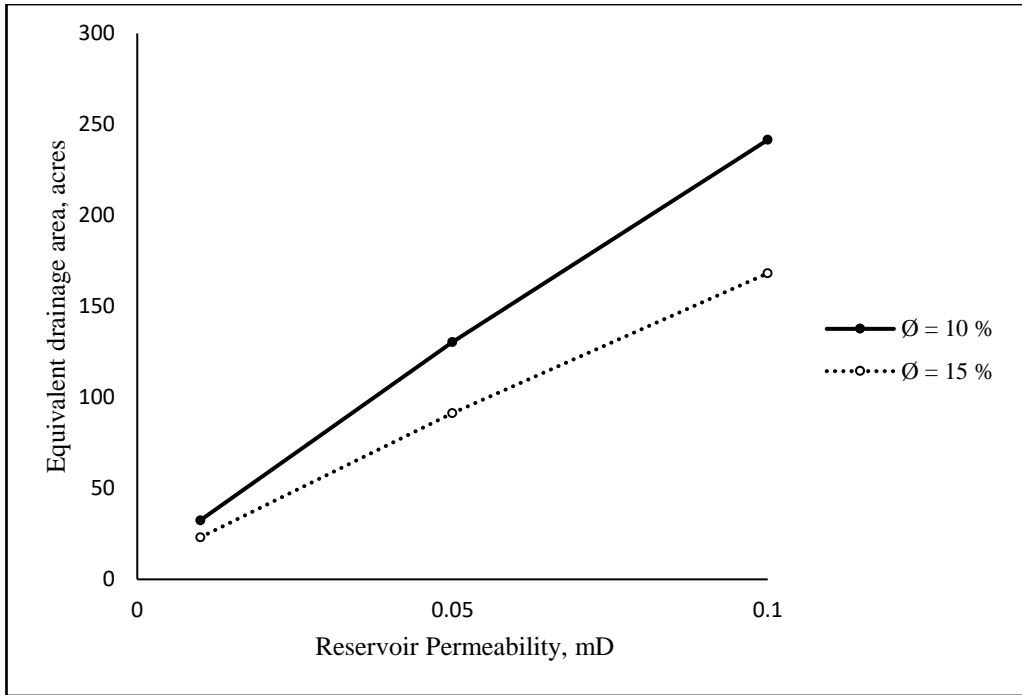
Figure 3.29 The effect of porosity on the planned equivalent drainage area (fracture half-length = 100 ft)
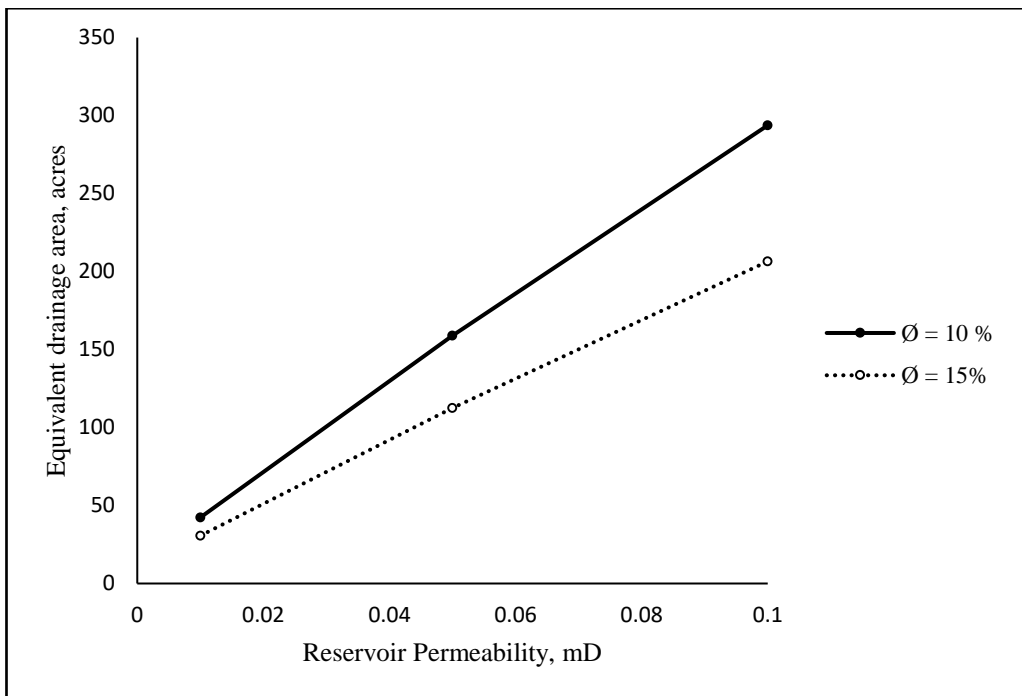
Figure 3.30 The effect of porosity on the planned equivalent drainage area (fracture half-length = 200 ft)
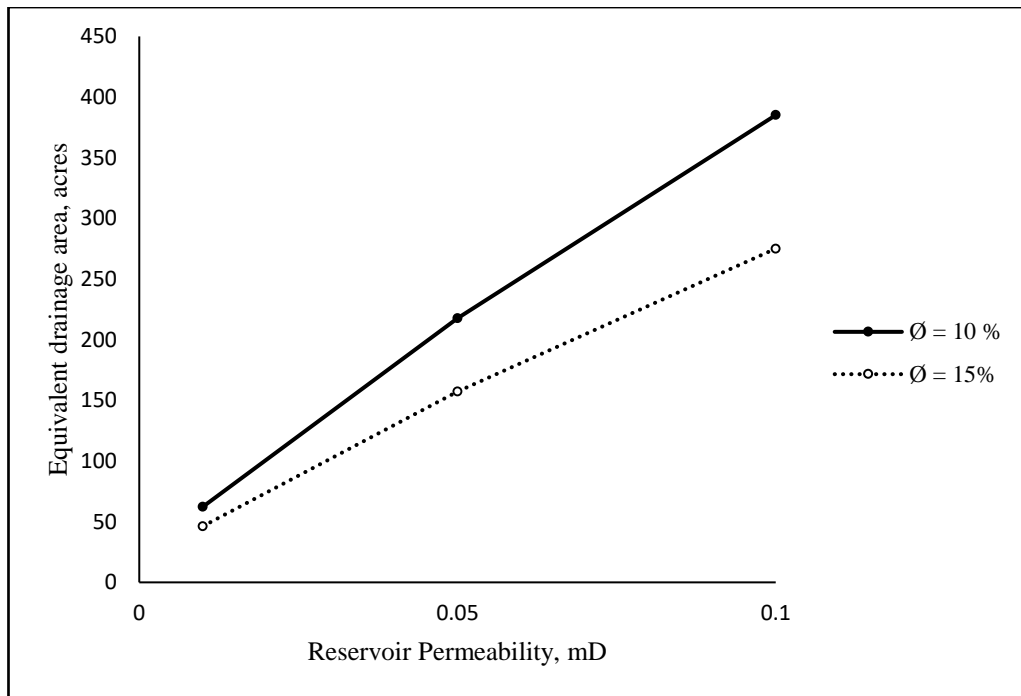
Figure 3.31 The effect of porosity on the planned equivalent drainage area (fracture half-length = 500 ft)

3.3.8 Propagation of equivalent drainage area

It is confirmed that planned equivalent drainage area extends over time because of the production. The propagation of the planned equivalent drainage area as a function of production time for different fracture half-lengths is shown in Figure 3.32 and Figure 3.33. These figures present two indicators: the first is the growing rate of the planned equivalent drainage area with production time in the reservoir of 0.1 mD permeability, which is greater than the reservoir of 0.01 mD permeability; and the second indicator is the growing rate of the planned equivalent drainage area with production time for the fracture half-length of 500 ft, which is greater than that for a fracture half-length of 100 ft. Both indicators are a result of the transmissibility which increases with the increase in permeability and fracture half-length, and consequently the higher transmissibility the greater the production. The prediction of the propagation of the planned equivalent drainage area starts from 10 years because the earlier data is employed to construct the material balance relationship and the decline curve which is basis of the developed method.
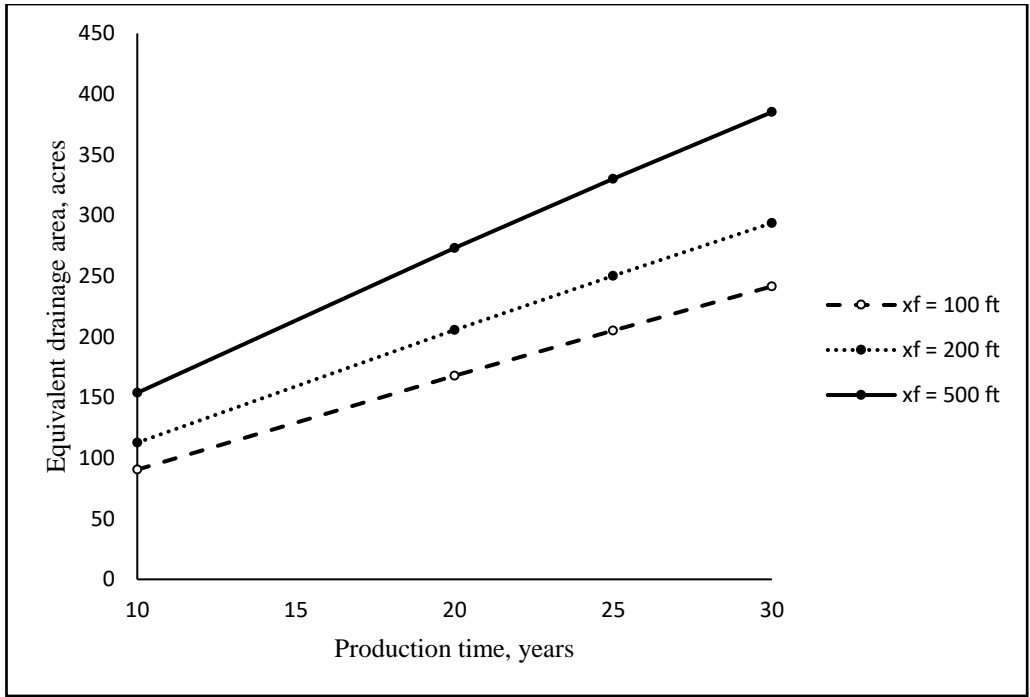
Figure 3.32 Propagation of planned equivalent drainage area (k=0.1 mD)
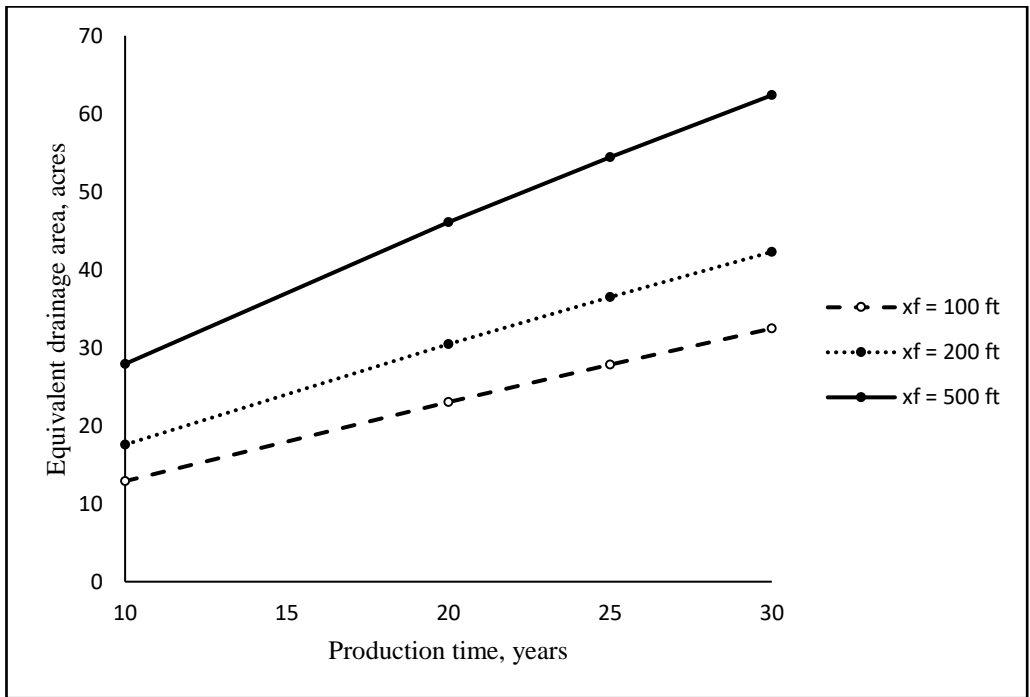
Figure 3.33 Propagation of planned equivalent drainage area (k=0.01 mD)

A simplified method of predicting the equivalent drainage area proposed in this study is derived based on the combined gas material balance and decline curve analysis for TGR. The model is validated using a reservoir simulation model for a typical TGR with permeability ranging from 0.01 to 0.1 mD in the case of a fractured vertical well

with fracture half-length ranging from 100 to 500 ft. Validation results have demonstrated that the proposed method is accurate enough to predict the equivalent drainage area for fractured vertical well in a TGR.

A sensitivity study is carried out to investigate the effect of various parameters which are porosity, permeability and fracture length on the planned equivalent drainage area. Sensitivity results have demonstrated that the fracture half-length and the porosity have a strong impact on the planned equivalent drainage area. On the other hand, the reservoir shape has a minor impact on the planned equivalent drainage area.

Propagation of the planned equivalent drainage area as a function of production time is significantly affected by the fracture half-length and reservoir permeability.

In conclusion, the suggested method is simple; and may be considered a practical tool to forecast growing of the equivalent drainage area for fractured vertical well in a TGR with respect to production time.

3.4 Prediction of hydraulic fracture properties

While hydraulic fractured wells in TRGs have been proven to be most viable option of the economic recovery of gas, the interpretation of pressure transient or well test data from these wells for accurate estimation of important reservoir and fracture properties (e.g. fracture length, fracture conductivity, skin and reservoir permeability) is rather complicated because of the multiple flow profiles/regimes. These flow regimes are complex due to the large hydraulic fractures near the wellbore, the low matrix permeability and the reservoir heterogeneity. Consequently, the interpretation of well test or pressure transient data using the classical approaches typically used for conventional reservoirs can produce incorrect results with high levels of uncertainty. In addition, the time required to achieve radial flow regimes for such tight reservoirs, a key condition of these classical approaches, is impractically long and not feasible in the context of both the economic and practical operations. These inherent causes and operating limitations require amendment of the well test technique to analyse linear or elliptical flow regimes to accurately estimate the reservoir and fracture properties.

This section comprehensively discussed the simplified numerical approach developed in this work for the prediction of the reservoir and fracture parameters based on well test data from hydraulic fractured vertical wells in TGRs, considering an elliptical flow regime. Emphases was placed on the development of a simple, efficient and accurate computation tool to supplement the need for commercial simulators, yet can estimate reservoir and fracture properties with high levels of accuracy, especially in the cases when limited pressure transient data is available.

3.4.1 Pressure transient analysis in tight gas reservoirs

The crucial step for accurate development of a TGR begins with the identification of the dominant reservoir flow regime (Stotts et al., 2007). Fracture size and length are critical parameters required to accurately evaluate the production performance of a TGR, as these parameters dictate the production rate and determine the rate at which drainage volumes expand. Although pressure derivative (H. Bahrami et al., 2012a), type curves (Thomas Alwin Blasingame et al., 2007), and analytical models (Badazhkov et al., 2008) were employed to analyse many production datasets recorded in low permeability fields in order to calculate the reservoir properties and hydraulic fractures parameters, the pressure transient analysis (PTA) in hydraulic fractured wells

is crucially important to evaluate the period of each flow regime, and to predict the performance of the wells (W. J. Lee and Wattenbarger, 1996).

Five flow regimes can potentially exist over the lifetime of a fractured well in a TGR: fracture linear flow, bilinear flow, formation linear flow, elliptical flow and pseudo-radial flow (W. J. Lee and Wattenbarger, 1996). Pressure transient analysis in hydraulic fractured TGRs has previously been based on bilinear, linear and pseudo-radial time periods, but this requires analysis of all three regimes for accurate analysis of reservoir and fracture properties. The most accurate permeability predictions are developed from the pseudo-radial flow period, but can take several years (if at all) for this flow regime to develop depending on the reservoir permeability. This results in adverse economic impacts due to long down times. For instance, the 2D pressure distributions for different permeabilities obtained from reservoir simulation studies for unfractured wells studied by Al-Fatlawi et al. (2016) are displayed in Figure 3.2. This figure illustrates how the pressure pulse transfers rapidly to the boundary when formation permeability is greater than 0.1 mD (Figure 3.2(a-d)), whereas it takes a long time to traverse through formations with a permeability less than 0.1 mD (Figure 3.2(e-f)). This demonstrates that the movement of the pressure pulse through tight porous media can cause different flow regimes to develop throughout the well's lifespan.

Reservoir and fracture properties also have a significant influence on the drainage pattern of tight gas wells. For example, Figure 3.34 highlights how reservoir permeability and fracture lengths can influence the pressure response in TGRs and extend the drainage area. Linear flow equations are more restrictive in such case than elliptical flow equations because linear flow equations alone cannot model radial effects late in a well's life.

Elliptical flow combines both radial and linear flow analysis techniques into a single model (Cheng et al., 2007). This flow is commonly considered at the transitional flow period, which occurs between the end of linear flow period and the beginning of radial flow period (W. J. Lee and Wattenbarger, 1996). Due to the low permeability in TGRs, the elliptical flow period typically begins early, and exists for a long period, which arguably makes it the best regime to estimate reservoir properties and fracture parameters. As demonstrated in Figure 3.34, the elliptical flow still occurs after ten years for a hydraulic fractured vertical well with permeabilities between 0.001-0.01

mD. To capture such a long period, acquisition of a large amount of rate and pressure data is necessary, and consequently, the pressure transient analysis techniques used to predict the reservoir and fracture parameters are required to deal with the effect of such varying pressure responses on flow regimes and drainage boundary. Hence the understanding of the elliptical flow period and the impact of reservoir and fracture properties on well performance is critical for accurate prediction of future reservoir performance and optimisation of the recovery process. However, a wide range of new reservoir parameters need to be considered to analyse tight gas reservoirs, including:

- Low reservoir permeability resulting in extensive transient periods.
- Permeability of hydraulic fractured regions and the rest of the formation (i.e. dual permeability behaviour), and other reservoir heterogeneities causing large pressure differentials.
- Stress dependent permeability due to the compressible fracture volumes, especially ultra-tight to shale.

Analytical models are commonly used for the determination of reservoir and fracture parameters, but limited models exist that consider elliptical flow in TGRs. Badazhkov et al. (2008) proposed an algorithm based on an analytical model and the current study was conducted based on Badazhkov et al. (2008) model, elaborated on in next section.

t_p, years / k, mD	1	5	10
0.01	$x_f = 500$ ft		
	$x_f = 700$ ft		
0.1	$x_f = 500$ ft		
	$x_f = 700$ ft		
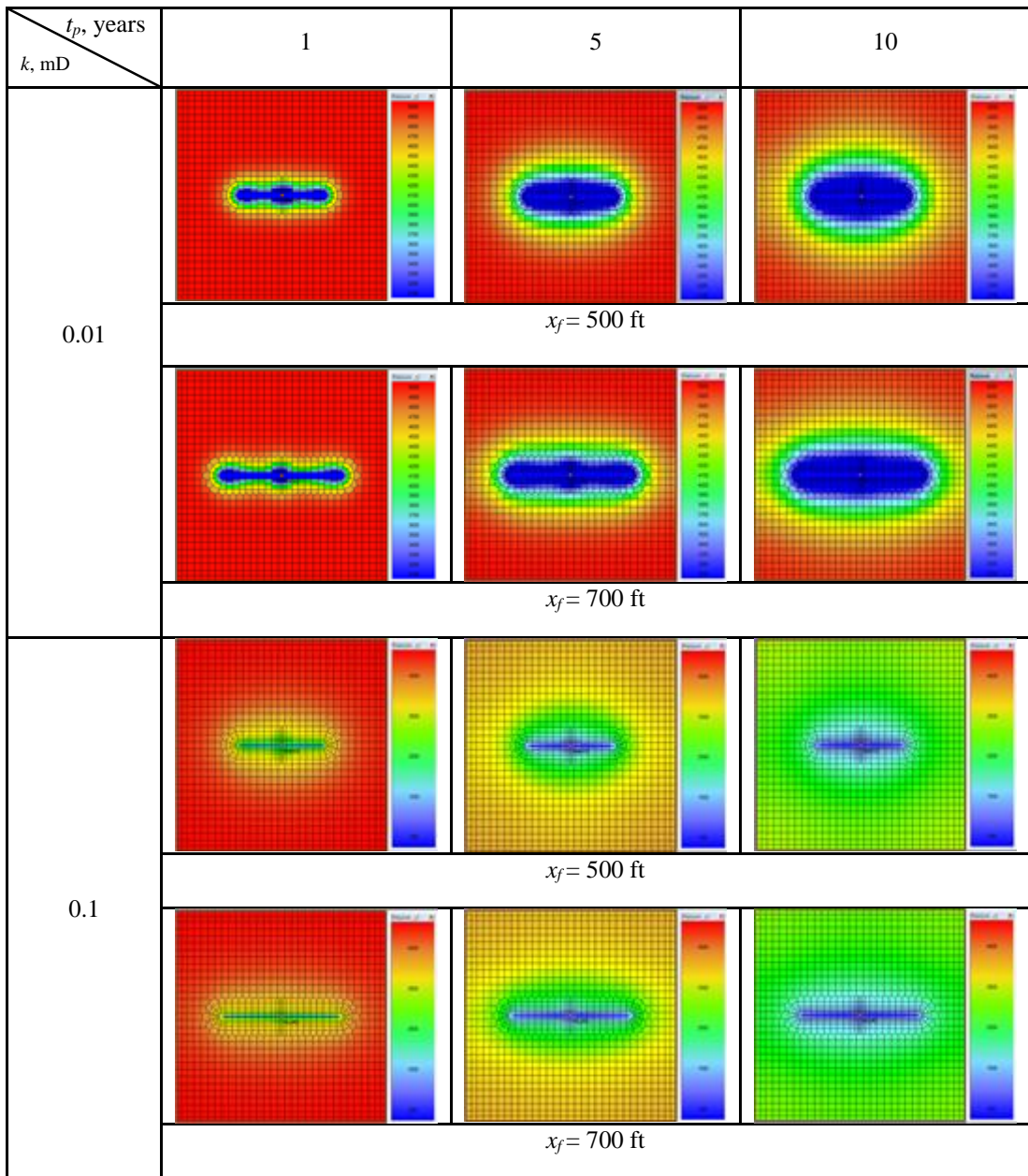
Figure 3.34 Pressure distributions for different reservoir and fracture properties over time for a tight gas well

3.4.2   Analytical model for elliptical flow regime

The elliptical flow equation considered by Badazhkov et al. (2008) stems from the basic gas flow equation in a porous medium in the presence of fractures with infinite conductivity. They further simplified the equation by neglecting gravity effects and assuming that the flow through the fracture system was laminar. By incorporating boundary conditions for an elliptical model into the real gas diffusivity equation, the classical diffusivity equation is transformed into the forms shown in Equation 3.41

(Badazhkov et al., 2008), and is considered the fundamental basis of the current study. A detailed derivation of Equation 3.41 can be found in Badazhkov et al. (2008).

$$\frac{\partial^2 \Psi}{\partial u^2} + \frac{\partial^2 \Psi}{\partial v^2} = \frac{\varphi \mu c (x_f)^2}{k} (\sinh^2 u + \sin^2 v) \frac{\partial \Psi}{\partial t} \qquad 3.41$$

Where Ψ is real gas pseudo-pressure function, and u, and v are arbitrary curve-linear axes, which can be transformed into Cartesian coordinate as: $x = \sinh v \sin u$ and $y = \cosh v \cos u$. The boundary conditions considered are given in Equations 3.42 and 3.43 (Badazhkov et al., 2008):

$$\Psi = \Psi_{X_f} \ at -x_f < x < -x_f, y = 0 \qquad 3.42$$

$$\Psi = \Psi_e \ at \ A^2 - B^2 = x_f^2 \qquad 3.43$$

Where A and B in Equations 3.42 and 3.43 are the major and minor axes of the ellipse of the elliptical flow region, respectively, which physically represent the reservoir drainage lengths/radii in the x and y directions, respectively. In the subsequent section, A and B will be termed as drainage. The dimensionless terms of time and pressure are considered by incorporating the rate equation with the above diffusivity equations (Equations 3.42 and 3.43), making it possible to determine the drainage area as a function of time. For this unsteady state scenario, the radius of drainage is assumed to expand over time, but the flow is assumed to be fixed for each drainage area.

The dimensionless time and pressure variables are considered as the time required to achieve stabilisation within the drainage area and can be expressed by Equations 3.44 and 3.45:

$$t_D = \frac{kt}{\mu c \emptyset B^2} \qquad 3.44$$

$$p_D = \frac{\pi T_{sc} kh (\Psi_e - \Psi_{X_f})}{p_{sc} T Q_{sc}} \qquad 3.45$$

Where,

T_{sc} Temperature at standard condition, °F
p_{sc} Pressure at standard condition, psia
Q_{sc} Flow rate at standard condition, Mscd/day
h Reservoir thickness, ft
μ Gas viscosity, cP

The dimensionless time correlating to a stabilized flow regime resembling radial flow within a drainage area can be approximated as $t_D = 0.38$ (Jones, 1963). Using this value of dimensionless time (Equation 3.44) and combining it with the dimensionless term of pressure (Equation 3.45), the major and minor drainage radii (A) and (B) can be expressed as:

$$A = \sqrt{B^2 + x_f^2} \qquad\qquad 3.46$$

$$B = 0.02634 \sqrt{\frac{kt}{\varphi \mu c}} \qquad\qquad 3.47$$

Variables of A and B are used to describe the elliptical area within which the pseudo-steady state flow can be assumed. From the relationships developed in the derivation of this analytical equation, a diagnostic plot of deference of pseudo-pressure drop ($\Delta\Psi$) versus $\ln(A + B)$ will produce a straight line during the elliptical flow period. The slope of this plot yields formation permeability, while the intercept yields fracture half length. With permeability and fracture half-length unknown, initially, an iterative process is required. Badazhkov et al. (2008) developed an algorithm in order to allow convergence of the results. Details of the iterative scheme can be found in this chapter.

When considering finite conductivity fractures, the additional pressure loss in the fracture also requires consideration. In the finite conductivity fracture scenario, the extra pressure drop in the fracture between the fracture tips is non-elliptical, which impacts the pressure and flow between the reservoirs and wellbore (Cheng et al., 2007). Dimensionless fracture conductivity is introduced by Badazhkov et al. (2008) in terms of the ratio of fracture half-length (x_f) to the effective wellbore radius (r_{we}), and is expressed as a function of dimensionless fracture conductivity given in Equation 3.48:

$$R = \frac{x_f}{x_{fe}} = \frac{\pi}{2F_{cD}} + 1 \qquad\qquad 3.48$$

This ratio is used to update the definition of elliptical region variables, A and B as given by Equations 3.49 and 3.50, respectively:

$$A' = \sqrt{B'^2 + x_f^2} \qquad\qquad 3.49$$

$$B' = R \times B \qquad\qquad 3.50$$

Where A' and B' represent updated or modified major and minor axes of the elliptical model in order to account for the impact of fracture conductivity on the propagation of pressure drop, and are required to be solved iteratively. Again, elliptical flow data will show a straight line of $\Delta\Psi$ *versus* $\ln(A' + B')$. For a finite conductivity fracture, the algorithm introduced by Badazhkov et al. (2008) is considered a bilinear flow regime period, and is solved graphically. A plot of pseudo-pressure drop ($\Delta\Psi$) versus $t^{0.25}$ (to characterize bilinear flow) is used for the determination of fracture conductivity. In order to identify the start and end of the elliptical flow from the production data, this method used a slope of 0.36 of a straight line on a log-log pseudo-pressure drop derivative plot. This slope 0.36 is considered from a study completed by Chacon et al. (2004) and is applied to horizontal and vertical fractured wells.

3.4.3 Numerical technique

As described, the algorithm and solution approach presented by Badazhkov et al. (2008) are predominantly a graphical approach. In the current study, a numerical iterative technique is developed to estimate reservoir and fracture properties. The technique assumed the inverse relationship of $\ln(A+B)$ versus the pseudo-pressure drop $\Delta\Psi$ to be linear during the elliptical flow period for the infinite conductivity fracture scenarios, accordingly expressed by Equation 3.51:

$$\ln(A + B) = a\,\Delta\Psi + c \qquad\qquad 3.51$$

Where:

$\Delta\Psi$ Pseudo-pressure difference, psi²/cP.

Where a and c are respectively, slope and intercept of plot of $\ln(A + B)\ vs\ \Delta\Psi$ (i.e. when $\ln(A + B)$ is plotted on y-axis and $\Delta\Psi$ on x-axis), given by Equations 3.52 and 3.53:

$$a = \frac{kh}{1422Q_{SC}(T + 460)}$$ (3.52)

$$c = \ln x_f$$ (3.53)

Combining Equations 3.51 to 3.53 yields:

$$\ln(A + B) = \frac{kh}{1422Q_{SC}(T + 460)} \times \Delta\Psi + \ln x_f$$ (3.54)

Adding Equation 3.46 for variable A into Equation 3.54 yields:

$$\ln\left(\sqrt{B^2 + x_f^2} + B\right) = \frac{kh}{1422Q_{SC}(T + 460)} \times \Delta\Psi + \ln x_f$$ (3.55)

Adding Equation 3.47 for variable B into Equation 3.55 yields the required relationships containing all required variables in the form of $y = ax + c$

$$\ln\left[\sqrt{\left(0.02634\sqrt{\frac{kt}{\varphi\mu c}}\right)^2 + x_f^2} + 0.02634\sqrt{\frac{kt}{\varphi\mu c}}\right]$$
$$= \left[\frac{kh}{1422Q_{SC}(T + 460)}\right]\Delta\Psi + \ln x_f$$ (3.56)

Where,

$$y = \ln\left[\sqrt{\left(0.02634\sqrt{\frac{kt}{\varphi\mu c}}\right)^2 + x_f^2} + 0.02634\sqrt{\frac{kt}{\varphi\mu c}}\right] = \ln[A + B]$$ (3.57)

$$x = \Delta\Psi \qquad\qquad\qquad 3.58$$

Equation 3.56 can be considered a governing analytical equation which accounts the flow in elliptical flow regimes, and can be solved numerically using a robust iterative approach to estimate the reservoir permeability and fracture properties (e.g. half-length, fracture conductivity). Simple Excel based programming or any other computation programming tools like MATLAB or FORTRAN can be used to develop the computation tool employing the developed technique. In this study, the equation is solved using a successive substitution iterative process. The following algorithm is developed in this study to solve Equation 3.56 numerically. This algorithm is used as the basis to develop a computation tool in MATLAB and Excel-VBA.

1. Assume initial permeability value (k).

2. Calculate B using Equation 3.47.

3. If fracture half-length prediction is poorly known, assume that: $A = € \times B$, where $€>1.0$, and the value of $€$ controls the number of iterations and convergences. Since drainage is considered to be elliptical, ($A>B$), and based on many computation cycles, it is observed that $€ = 1.5$ provides a fast convergence with a reasonable number of iterations. If an estimation for fracture half-length is known, calculate A using Equation 3.46. The y-axis values (Equation 3.57) can now be calculated. Only the y-axis, the values corresponding to elliptical flow are required.

4. Calculate x-axis values (Equation 3.58). This is simply the value of pseudo-pressure drop ($\Delta\Psi$) for all data in the elliptical flow regime period.

5. Apply the least square regression method, as outlined below, to elliptical flow data points to find the slope (a) and intercept (b) of Equation 3.56.

6. From the value of slope (a) calculated using the method of least squares, calculate k using Equation 3.52.

7. From the value of intercept (c), calculate x_f using Equation 3.53.

8. Calculate error tolerance for permeability, $\epsilon_k = \frac{|k_{calculated} - k_{assumed}|}{|k_{calculate}|}$. if $\epsilon_k >$ 0.001 then the procedure from step 2 with updated value of $k_{assumed} = k_{calculated}$ until obtaining the convergence of $\epsilon_k \leq 0.001$.

9. Similarly, calculate error tolerance for x_f, $\frac{|x_{f\,calculated} - x_{f\,assumed}|}{|x_{f\,calculate}|}$. If $\epsilon_x > 0.001$ then use the procedure from step 2 with an updated value of $x_{f\,assumed} = x_{f\,calculated}$ until obtaining the convergence of $\epsilon_x \leq 0.001$.

10. The reservoir permeability and fracture length can be calculated numerically following steps 1 to 9 once the condition of error tolerance is met.

Since the following steps do not require graphical analysis at each iteration, a computational tool can be easily developed using Excel-VBA programming or MATLAB/FORTRAN to carry out the calculation until the final conditions are met.

Regression analysis using least squares method

The least squares regression method is commonly used to estimate the value of parameters of slope and intercept for a set of data (Abdi, 2007). This method can find a line that best fits a set of data points. The steps required to apply the method of least squares are:

1. Record all data for x-axis values (pseudo-pressure drop) and y-axis values $\ln(A + B)$.

2. Find the average of all x-axis data points using $\bar{X} = \frac{\sum_{i=1}^{n} x_i}{n}$, where n is the number of x values

3. Find the average of all y-axis data points using $\bar{Y} = \frac{\sum_{i=1}^{n} y_i}{n}$, where n is the number of y values

4. Calculate $x_i - \bar{X}$ for all data points of X. Calculate $y_i - \bar{Y}$ for all data points of Y.

5. Multiply $x_i - \bar{X}$ with $y_i - \bar{Y}$ for all data points, i.e. $(x_i - \bar{X}) \times (y_i - \bar{Y})$

6. Find the square of $X - \bar{X}$ for all data points, $(x_i - \bar{X})^2$

7. Find the summation of all data points from step 5, $\sum_{i=1}^{n}(x_i - \bar{X}) \times (y_i - \bar{Y})$

8. Find the summation of all data points from step 6, $\sum_{i=1}^{n}(x_i - \bar{X})^2$

9. Determine the slope of the line by using the value found in step 7 and divide it by the value found in step 8, $slope = m = \frac{\sum_{i=1}^{n}(x_i - \bar{X}) \times (y_i - \bar{Y})}{\sum_{i=1}^{n}(x_i - \bar{X})^2}$

10. Determine the intercept of the line using $intercept = \bar{Y} - (m \times \bar{X})$

Applying the method of least square regression will provide the best approximation of straight line properties for a given linear data set (Abdi, 2007). This is required for the accurate determination of slope and intercept numerically to implement the proposed algorithm as explained earlier.

3.4.4 Analysis of the production data, and hydraulic fractured parameters

The proposed numerical approach was applied to analyse the transient pressure data for a hydraulic fractured vertical well from a representative tight gas field in Australia. The data was also analysed using the algorithm proposed by Badazhkov et al. (2008), and a widely acceptable industry standard commercial simulator KAPPA – SAPHIR. The purpose of this case study using three different approaches is to validate and justify the capabilities of the proposed simplified numerical technique. The predicted results from these three different approaches are presented in this section.

3.4.4.1 Prediction using commercial simulator KAPPA-SAPHIR

Results in this section investigate pressure transient data collected from a hydraulic fractured vertical well in a representative tight gas field in Australia. The pressure build-up data attained from well testing is investigated using pressure transient analysis to understand the log-log pressure derivative response of the well, and to estimate reservoir permeability, fracture half-length, and fracture conductivity using the KAPPA-SAPHIR simulator. The pressure and rate data obtained from DST over a period of 49 days, including the history matching profile, is shown in Figure 3.35. The inputs for KAPPA-SAPHIR are presented in Table 3.12. The analytical models considered in the simulator are to match the field data are shown in Table 3.13 and the predicted reservoir parameters are presented in Table 3.14.

The derivative plot is presented in Figure 3.36 in order to understand and analyse the well and reservoir characteristics including the flow regimes. The following observation can be made from this diagnostic plot:

- The wellbore storage effect appeared within 0.1-1 hours (point 1)
- The bi-linear flow (1/4 slope) or linear flow (1/2 slope) regimes as seen within 1-3 hours (point 2) appear to be masked wellbore storage due to low permeability

- The further wellbore storage effect (skin factor) in a fractured well may be clearly indicated within 3-11 hours (point 3)

- The pressure response far from the wellbore as characterized from 11-100 hours (point 4) indicates that the reservoir is still in a transient flow period and shows an approximate ½ slope, possibly demonstrating linear flow regimes in the formation.

- No boundary or infinite active reservoir flow (IARF) response is apparent beyond approximately 100 hours (point 5, within the range approximately 100-193 hrs), which appeared to be reflective of elliptical flow regimes.

This model can be used to develop an estimate of parameter values, but by no means should it be considered reliable in the prediction of reservoir and fracture properties. Only in conventional reservoirs can diagnostic log-log pseudo-pressure derivative plots be reliably used for the prediction of reservoir parameters. In this scenario, radial flow is not developed, making the model match parameter values inaccurate. A strong history match between the models compared to the actual pressure data has been found. A strong correlation is seen in the final build-up period. This confirms the log-log plot model match used to estimate values in Table 3.14.
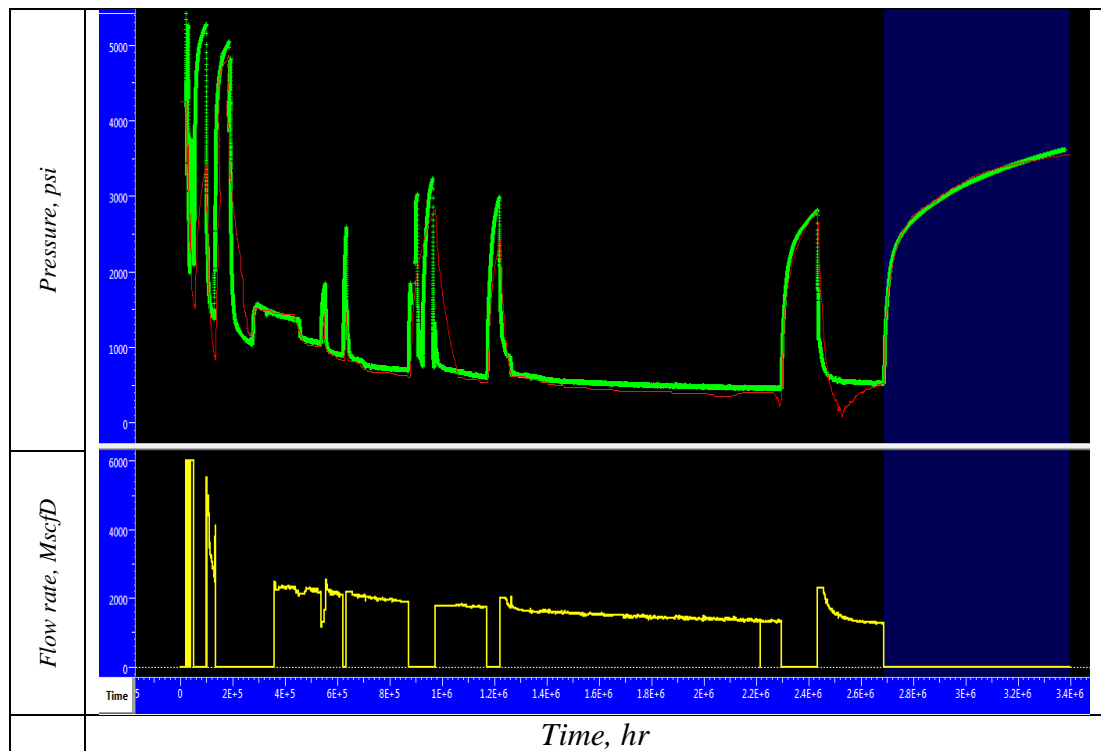
Figure 3.35 Pressure and rate data for a representative tight gas field in Australia. Pressure data shows a strong history match, whereas rate data shows a reasonably good match, especially in the final drawdown and build-up cycle.
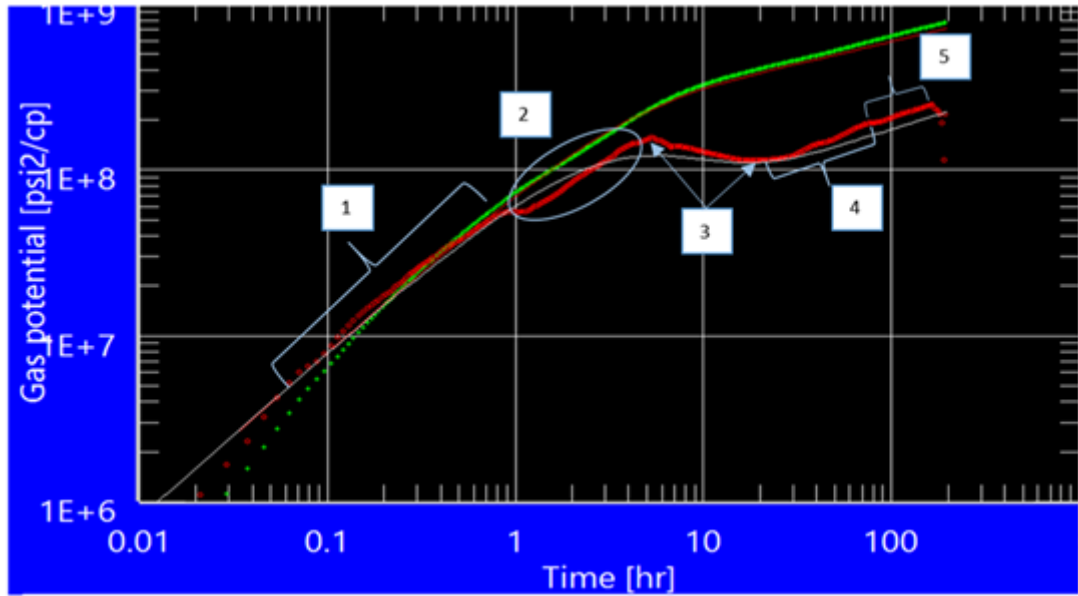
Figure 3.36 Pseudo-pressure function vs. time derivative plot generated by KAPPA-SAPHIR for a hydraulic fractured vertical well in a representative tight gas field in Australia.

Table 3.12 Model Inputs for Pressure Transient Analysis in KAPPA-SAPHIR

Parameter	Value
Well radius (r_w)	0.2 ft
Pay zone (h)	46 ft
Porosity (φ)	0.12
Analysis type	Standard
Reservoir temperature (T)	220 °F
Reservoir pressure (P_i)	5800 psi
Pressure range	14.7 – 6000 psi
Formation compressibility (c_t)	3×10^6 psi^{-1}
Water saturation (S_w)	40%
Test period, day	50

Table 3.13 Model considered to match field data

Model	
Wellbore model	Constant Wellbore Storage
Well model	Fracture – Infinite Conductivity
Reservoir model	Homogenous
Boundary model	Infinite

105

Table 3.14 Predicted parameters using KAPPA-SAPHIR Analysis

Parameter	Value
Initial pressure (P_i), psia	5621
Wellbore storage co-efficient (C), bb1/psi	0.165
Fracture half-length (x_f), ft	302
Reservoir permeability (k), mD	0.011
Permeability thickness (kh), mD.ft	0.512
Frracture conductivity (F_c), mD.ft	49989

3.4.4.2 Prediction using analytical method using Badazhkov et al. (2008) model

An iterative Excel program was developed employing the procedure described by Badazhkov et al. (2008) for both infinite fracture conductivity for the same field using the same input data presented in Table 3.12. The pseudo-pressure derivative curve shown in Figure 3.36 indicates that the elliptical flow appears to start at approximately 100 hours and continues to the end of the production data analysis at 193 hours into the shut-in period. The parameter values of fracture half-length and reservoir permeability predicted by KAPPA-SAPHIR may be used as a good initial guess for application of the algorithm proposed by Badazhkov et al. (2008), so fast convergence can be achieved. A flowchart describing the process carried out to develop the Excel spreadsheet program is illustrated in Figure 3.37.

| Enter initial values for k and x_f into excel. | → | Enter other reservoir input data such as Φ, μ, c_t, Q_{SC}, T and h | → | Import time and pseudo-pressure data from Saphir analysis into excel. | → | Calculate variables A and B for every time using input values. |

| From the slope of trend-line calculate k. | ← | Display trend-line equation on the plot for the elliptical straight line region. | ← | Plot pseudo-pressure versus ln(A+B). | ← | Create a column to calculate ln(A+B) for all time values. |

| From the x-intercept of the trend-line, calculate x_f. | → | Put newly calculated k and x_f into new excel cells. | → | Repeat process using same input data, with only k and x_f changing. | → | Repeat above steps until convergence of k and x_f. |

Figure 3.37 Flow chart of Analytical Method - Infinite Conductivity Analysis

The analysis is carried out for an infinite conductivity fracture with initial value of $k = 0.01 mD \ and \ x_f = 300ft$. The other data in Table 3.12 are used to calculate A and B using Equations 3.46 and 3.47. Figure 3.38 is a plot of the pseudo-pressure drop $\Delta\Psi$ (psi^2/cP) versus ln(A+B) using the initial values of fracture half-length and permeability. This plot shows a straight-line period for elliptical flow. Permeability is calculated from the slope using Equation 3.52. Fracture half-length is estimated from the intercept of the straight line using Equation 3.53. The new values of fracture half-length and permeability are determined as 217 ft and 0.045 mD, respectively.

ln(A+B) is then updated, and the process is repeated for the new k and x_f values, until achieving the convergence. This takes six iterations, as shown in Table 3.15. The convergence criteria used is 0.0001mD for permeability (difference between the assumed and the calculated values) and 1 ft for fracture half-length (difference between the assumed and the calculated values). Figure 3.39 shows the pseudo-pressure drop versus ln(A+B) plot for the final iteration. The final values of permeability and fracture half-length are 0.0583 mD and 321.7 ft, respectively. It is worth mentioning that a plot of pseudo-pressure drop versus ln(A+B) is required for each iteration, which is the

most inconvenient part of this approach, and consequently makes this technique practically unreasonable.
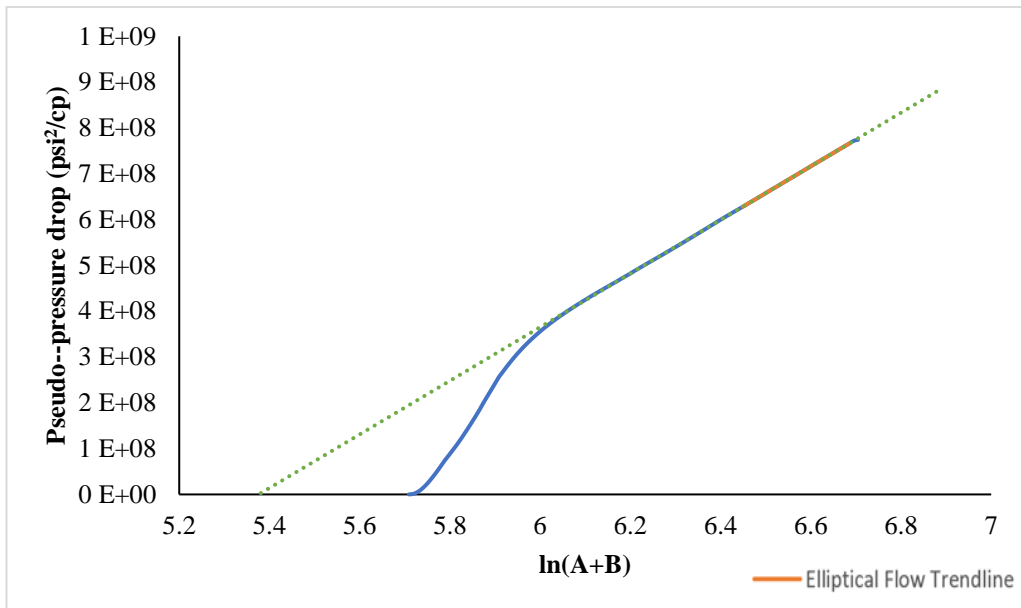
Figure 3.38 Infinite conductivity - Linear relationship of pseudo-pressure drop vs. *ln(A+B)* 1st iteration, k=0.01mD, x_f=300 ft.
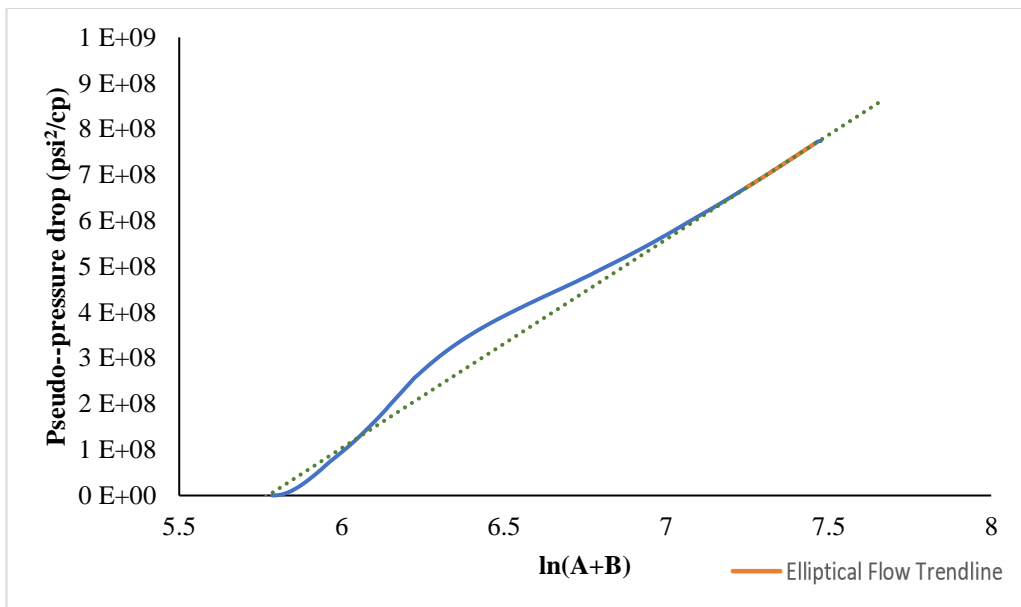
Figure 3.39 Infinite conductivity - Linear relationship of pseudo-pressure drop vs. ln(A+B). Final iteration

Table 3.15 Iteration for Infinite Conductivity case using initial values of k=0.01mD and x_f=300 ft

Results for each iteration – Infinite conductivity		
Iteration	$k\ (mD)$	$x_f\ (ft)$
Initial value	0.01	300
1	0.0454	216.2
2	0.0603	263.8
3	0.0600	307.8
4	0.0588	320.1
5	0.0584	321.9
6	0.0583	321.7

For comparison, the process was repeated for an infinite case, where initial permeability and fracture half-length values were considered to be far from actual values. This process is to investigate the convergence speed of this method. Assuming initial $k = 0.001mD$ and $x_f = 1000ft$, it takes just 10 iterations for convergence, as shown in Table 3.16, which appears reasonable in this case. However, it is implied that the number of iterations would increase as long the difference between the initial guess and the actual solution increases.

Table 3.16 Iteration for Infinite Conductivity case using initial values of k=0.001mD and x_f=1000 ft

Results for each iteration – Infinite conductivity		
Iteration	$k\ (mD)$	$x_f\ (ft)$
Initial value	0.001	1000
1	0.00617	933.1
2	0.0160	783.6
3	0.0283	589.1
4	0.0419	419.5
5	0.0529	332.6
6	0.0575	315.2
7	0.0584	317.8
8	0.0584	320.3
9	0.0584	321.2
10	0.0584	321.6

3.4.4.3 Prediction based upon proposed numerical approach

The proposed numerical technique is also applied for the same field with same data assuming an infinite conductivity fracture scenario. An important consideration for the application of this proposed technique is to ensure that only elliptical flow data values are entered into the developed computer program. From the analytical method proposed by Badazhkov et al. (2008) described earlier, it is known that the linear portion of the pseudo-pressure, $\Delta\Psi$ versus $\ln(A+B)$ plot, correlates to the elliptical flow data, indicated by the orange elliptical flow trend line in Figure 3.39. Before entering the required value of $\ln(A+B)$ and pseudo-pressure data into the program, an initial plot of pseudo-pressure $\Delta\Psi$ versus $\ln(A+B)$ using initial guess values of k=0.01 mD and x_f $_{=}$300 ft may provide a strong indication of the elliptical flow data points, as seen in Figure 3.38. All data points on the linear portion of this graph should be considered in the developed program. However, from Figure 3.39, the final iteration using the proposed method appears to be a much shorter straight line elliptical flow period than in Figure 3.38, indicating less data in elliptical flow than initially observed. Care should be taken when applying data to the developed program to ensure the data is the elliptical flow data. The final permeability and fracture half-length values for the field case can be more accurately estimated using the developed program with four iterations. Values of permeability and fracture half-length obtained using the proposed method are compared with the two other techniques and are presented in Table 3.17. In addition, the average permeability of the core samples at the reservoir conditions is about 0.05 md, so the reservoir permeability calculated using the proposed numerical technique is close to the measured core permeability. Based on these findings, the proposed numerical technique is validated by comparing its findings with the method proposed by Badazhkov et al. (2008) and the core tests.

Table 3.17 Comparison of Numerical, Analytical and Conventional Method Results for the Field Case

The method	Permeability, k (mD)	Fracture half-length, x_f (ft)
Proposed numerical technique	0.059	312
Method proposed by Badazhkov et al. (2008)	0.058	322
Commercial simulator - SHAPHIR	0.011	302

As can be seen in Table 3.17, the proposed numerical approach demonstrates a close agreement (almost same) with the method proposed by Badazhkov et al. (2008) to estimate both permeability and fracture length, while the difference appears to be about 3% compared to the estimation of fracture length using the commercial simulator, which suggests that the proposed numerical approach can be reliably applied in predicting formation permeability and fracture half-length for a hydraulic fractured vertical well.

The model matching by the commercial simulator, especially KAPP-SAPHIR is subjective and is particularly challenging to analyse data for fractured wells in TGRs, as it is hard to identify pseudo-radial flow and it is often very judgmental. In addition, model matching in the commercial simulator and conventional diagnostic derivative plots rely mainly on the pseudo-radial flow periods to accurately predict reservoir properties, especially permeability. The model matched by SAPHIR would likely use data from the linear or elliptical flow region and apply radial flow equations to these early time periods, resulting in erroneous estimations of parameters. The absence of pseudo-radial flow in the production data evaluation for this field case may be a feasible reason for the discrepancy between permeability predicted by the SAPHIR model (0.011mD) and the permeability predicted by the analytical and proposed numerical techniques (0.058/0.059mD). Since the numerical technique proposed in this study produces a unique value using comprehensive model accounting elliptical flow regimes, the predicted reservoir permeability is likely to be more accurate and closer to 0.059 mD in reality.

Comparing the fracture half-lengths recorded in Table 3.17, the proposed numerical technique produces a fracture half-length of 312 ft, just 3% variation compared to the result obtained from SAPHIR. The model matched by SAPHIR provides a rough estimate for the fracture half-length. However, the proposed numerical method is considered a more precise value, due to its development from the elliptical flow equation. This close correlation provides confidence that the predicted fracture half-length is within in the range of 312 to 322ft and is more representative. This may be because the SAPHIR model may use early time periods on the derivative plot, such as linear flow, to more reliably predict fracture half-length. However, conventional analysis is poor in estimating permeability when pseudo-radial flow is not present.

Accuracy of the predicted value and the number of iterations required to converge a solution point using the method by Badazhkov et al. (2008) depends on how close the initial guess of permeability and fracture half-length are to the real answer. Final answer to the convergence point also depends on initial guess. For example, using initial guess values of 0.01mD and 300 ft for permeability and fracture half-length respectively, it takes six iterations to reach convergence as shown in Table 3.15, whereas using initial values of 0.001mD and 1000ft takes 10 iterations, as shown in Table 3.16. However, the predicted values of k and x_f in both cases are not exactly the same (although they are approximate). In addition, this method requires a plot of pseudo-pressure drop versus $\ln(A+B)$ for each iteration. Such issues are not observed in the proposed technique which is independent of initial guesses and demonstrates fast convergence. For example, the predicted permeability (0.059 mD) and fracture half-length (312 ft) are always the same regardless of the value of initial guesses. The developed program even shows speedy convergence with initial guesses of 0.0001mD and 10000ft for permeability and fracture half-length, respectively, and results in the same estimation. In other words, the proposed new numerical technique is found to successfully overcome any issues related to iteration convergence from poor initial guesses and time consuming repetitive graphical iterations.

A new numerical technique to estimate reservoir permeability and fracture parameters based on pressure transient data collected from a hydraulic fractured well in a tight gas reservoir are proposed. The technique proposed is based upon the analytical model initially presented by Badazhkov et al. (2008) considering elliptical flow regimes. The proposed technique is applied to a representative tight gas field in Australia. The case

study results demonstrate that the technique is simple, robust and capable of reliably predicting the formation permeability and fracture half-length for infinite-conductivity fractures in tight gas reservoirs. This case study also warrants that:

- The proposed technique may be considered a good alternative tool for the commercial simulators to analyse the elliptical flow period of hydraulic fractured vertical wells in TGRs.

- The practical applicability of the proposed numerical method is validated using a field case. Application to a real field example focused on the hydraulically fractured vertical well provides accurate estimations of fracture half-length and formation permeability for well test data.

- The results produced via the proposed numerical technique and method proposed by Badazhkov et al. (2008) in the field case provide a robust comparison to the conventional derivative log-log plot analysis carried out in Saphir. The newly calculated value of permeability varies only slightly with that obtained from SAPHIR.

The proposed numerical iterative technique is expected to be easily applied to a wide range of tight gas fields with varying properties and will eliminate the need for manual graphical analysis at each iteration step, thereby reducing computation processing time significantly, and increasing the speed of the process while producing equally reliable results that reduce uncertainty.

Chapter 4: Infill-Drilling Potential and optimization in Tight Gas Reservoirs*

Because of the heterogeneous nature and low permeability of tight gas reservoirs (TGRs), a number of wells are required to be drilled to ensure the economic production rate and to maximize the ultimate recovery. Cumulative gas recovery per well in a TGR is generally restricted due to the low reservoir permeability resulting in low flow rates and low recovery efficiencies compared to wells in conventional high permeability reservoirs. The recovery efficiency can be maximized by using optimal drilling completion techniques, and decreasing the costs of drilling, completion and stimulation. Infill drilling is a standout amongst the most widely recognized and powerful strategies for maximizing recovery by reducing the well spacing and increasing the sweep efficiency. However, it is a challenge to determine the optimum number of wells and their accurate locations to ensure minimum interference between wells and acceleration of the recovery factor from the field. Detailed reservoir modelling is the most trusted method to determine the location of the infill wells, but it is time consuming, expensive and in some cases not very manageable in routine industry task environments. A fast yet cost effective method is naturally desirable. Over the last few decades, researchers have come up with techniques like the Moving Window Method (MWM), rapid inversion, and Infill Well Locator Calculator (IWLC), to optimise infill drilling. This chapter provides comprehensive discussion on the development of an optimum infill-drilling plan for Whicher Range (WR) Tight-gas Field in Western Australia based on reservoir simulation modelling combined with the Moving Window Method. The accuracy and effectiveness of the developed optimum infill drilling plan are justified through comparative studies using a standard reservoir simulation model that demonstrates that the proposed plan can effectively predict the optimum number of wells including the production rate of each well similar to those obtained from standard reservoir simulation studies. It is also inferred that reservoir simulation combined with MWM requires less data, and is much simpler and faster compared to standard reservoir simulation. It also worth noting that the content of this chapter is based on the authors paper, "Optimization of Infill Drilling in Whicher Range Field in Australia" (Al-Fatlawi et al., 2017c).

114

4.1 Infill drilling

Infill drilling can be referred to as simply adding new wells in a field after the initial field development plan to increase the recovery factor from the reservoir. The reservoir heterogeneity and the layer continuity affect the well conductivity, so adding more wells can decrease the well spacing, resulting in improving the well conductivity (L Guan and Du, 2004) and thus improve the recovery factor. Since adding new wells contributes to maximizing the recovery factor by increasing the production from incremental reserves by adding new wells and accelerate reserves produced from existing wells (Luo and Kelkar, 2010), it is considered a critical factor to optimize the production from any gas reservoirs, especially TGRs. Therefore, the infill drilling process should be controlled by applying an optimization technique rather than random addition. With the increasing importance of TGRs as an adequate future energy source, the importance of applying infill drilling in TGRs has received significant attention by the industry. Consequently, many TGR investors have become more interested in developing infill drilling techniques. Although, infill drilling is a complex challenge for reservoir engineers because of the number of variables, such as rock properties, well spacing, number of wells drill, and completion options, an important factor that needs to be taken into consideration is determination of the optimum number of infill drilling that will maximize the ultimate recovery of gas.

4.2 Fundamentals of Moving Window Method (MWM)

The Moving Window Method (MWM), also referred to as the Mosaic technique, is employed in this work with reservoir simulation modelling. In this method, a window is considered to move from one well to another well to analyse the infill potential inside each window. MWM compares the production data of old wells to new wells, and thus, specific conclusions can be drawn about well interference, extent of depletion, areas of undrained acreage and effect of changing the well spacing. The method is illustrated in Figure 4.1.
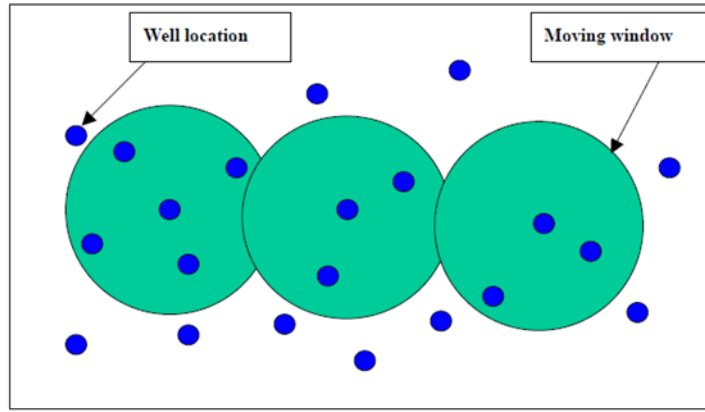
Figure 4.1 Illustration of Moving Window Method, showing the movement of the window across the test area (L Guan and Du, 2004)

Compared to the previous versions of the MWM, this method adopts a highly rigorous model-based approach within each moving window. The model is fundamentally based on a pseudo-steady state flow equation and material balance equation. The model is simplified by assuming that the reservoir properties are homogeneous in each moving domain. Equation 4.1 illustrates the reservoir model was used in this technique (Derivation of this equation is clearly explained, (Linhua Guan, 2004)).

$$ln\ q = ln(kh) + C_1 + ln(p_i - p_{wf} - C_2 \frac{G_p}{A}) - ln(ln(\sqrt{A}) + C_3) \qquad 4.1$$

Where:

C_1 Intermediate result in the reservoir model of moving window technology

C_2 Intermediate result in the reservoir model of moving window technology

C_3 Intermediate result in the reservoir model of moving window technology

The above equation was simplified using the parameters best year production rate (*BY*) and virgin best year (*VBY*) as proxies for production rate and *kh*, respectively. In the method developed by Linhua Guan (2004), the area of Voronoi polygon around each well was taken as a proxy for drainage area, *A*. In this chapter, the transient drainage area was calculated after a 5-year production period, which was used directly without any proxies. The modified 4D linear regression equation thus obtained is shown in Equation 4.2.

$$BY\ =\ f\ (VBY, Gp/A, A) \qquad 4.2$$

BY is the best year production rate, an average production rate in 12 consecutive months, which can be calculated from the cumulative production for the best 12 consecutive months divided by 12, q_{gi}. Figure 4.2 illustrates how *BY* is calculated.

VBY is virgin best year, the best year rate of a well at virgin conditions i.e., depletion effects removed.

A is the transient drainage area around each well based on x, y well locations.

G_p /*A* is cumulative production divided by drainage area.

Equation 4.1 can also be written in a generalized form as shown in Equation 4.3.

$$y = a_o + a_1 x_1 + a_2 x_2 + a_3 x_3 \qquad\qquad 4.3$$

Where,

a_o, a_1, a_2 and a_3 are constants in the above equation. The variables y, x_1, x_2, and x_3 can be calculated using Equations (4.4-4.7).

$$y = \ln(BY) \qquad\qquad 4.4$$

$$x_1 = \ln(VBY) \qquad\qquad 4.5$$

$$x_2 = \ln(G_p/A) \qquad\qquad 4.6$$

$$x_3 = \ln(\ln(\sqrt{A})) \qquad\qquad 4.7$$
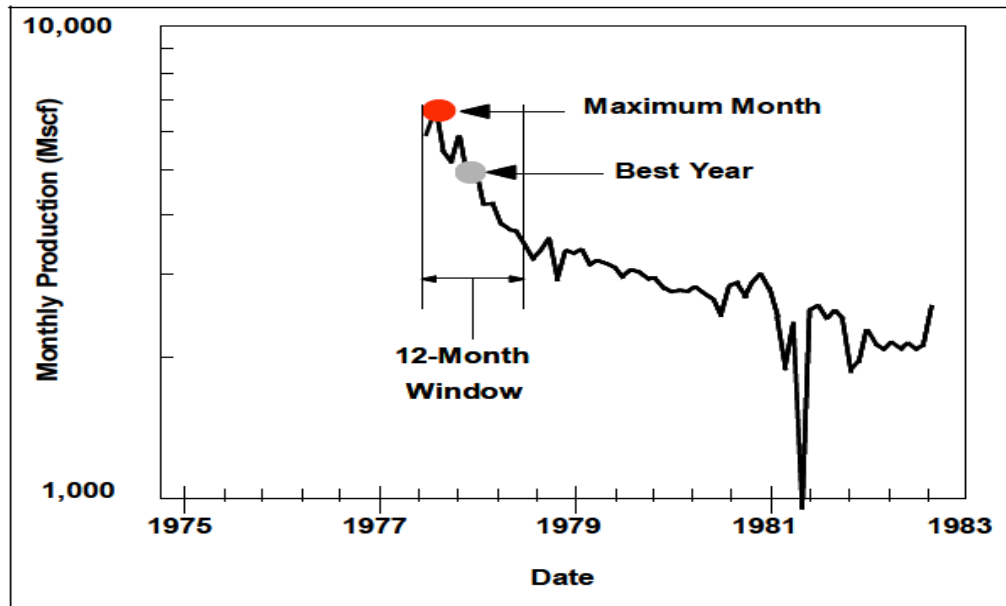
Figure 4.2 Illustration of how BY can be calculated (Guan, 2004)

4.3   Steps to perform the Moving Window Analysis technique

There are three steps to perform this technique, explained below.

1. Data collection – For each well, i, in the field, five quantities have to be defined, namely, best year production (q_{gi}), cumulative gas production (G_{pi}), drainage area (A_i), area of circular window centred around each well (W_i) and the time between initial field production and initial well production (t_{0i}).

   a) *BY*, i.e. best year production rate (q_g) is calculated by finding the cumulative production in the best 12 consecutive months, and then dividing it by 12. This can be obtained by observing the production data from the simulator.

   b) Cumulative production (G_p) is the cumulative production of each well during the observed production period of five years.

   c) Time interval between the date of first field production and that of each well (t_o).

   d) Transient drainage area (*A*) calculated using the transient drainage area as given by Equations 4.8 and 4.9 (Stuart Alan Cox et al., 2005). Transient drainage area was considered because within the 5 years period, the pressure regime was considered to remain transient for TGRs.

$$\text{Transient drainage radius, } r_t = \sqrt{\left(\frac{k_g t}{377\, \emptyset \mu_g c_t}\right)} \qquad 4.8$$

$$\text{Transient radial drainage area, } A = \pi\, r_i^2 \qquad 4.9$$

According to L Guan et al. (2004), optimum window size varies normally between 4 to 40 km^2 (1,000 to 10,000 acres), and typically contains 5 to 20 wells.

2. Determination of virgin best year (*VBY*) – 2D regression is performed within each window, W_i, to find the *VBY* rate of the well in its centre. For this, a linear model, $q_g = a_i t_0 + b_i$, using t_{0i} and q_{gi} values of each well within that window, is used. The intercept of the model, b_i, gives the *VBY* rate, $q_{gi,dap}$. $q_{gi,dap}$ represents the best year rate at virgin conditions before the reservoir pressure starts to decline after production starts. This linear model represents the relationship between time and production with appreciable accuracy according to (Voneiff and Cipolla, 1996). This operation is performed using the Statistical Package for the Social Sciences (SPSS) from IBM Corporation.

3. Formulation of 4D linear regression equation – A 4D regression is performed inside each window, W_i, by regressing the values of $q_{gi,dap}$, G_{pi} and *A* for each well inside the window. Once the regression coefficients are determined, the 4D linear equations can be formulated for each window. This regression is based on Equation 4.3. If the number of wells within a particular window is less than five, a regional regression will be used.

4. Predicting the *BY* rates of infill wells – Once the 4D equations are developed, $BY(q_g)$ of a new well, i, inside W_i can be determined by inserting the corresponding values of the variables into the 4D equation formulated for that window.

4.4 Development of the optimum infill drilling plan

The following steps were followed in order to develop the optimum infill-drilling plan, designed specifically for the Whicher Range (WR) tight-gas field:

1. Develop 3D dynamic reservoir model.
2. Perform history matching of 3D simulation model for WR reservoir.

3. Determine the locations of the initial set of infill wells and simulate them using the reservoir model (Stage-1).

4. Apply the MWM and develop the 4D regression equation for each window, *W*.

5. Create the second set of infill wells and predict the corresponding *BY* rates using MWM (Stage-2).

4.4.1 Development of 3D reservoir model

The development of a 3D reservoir model, is a crucial part of this work, especially for an underdeveloped field, because it is the only source of obtaining the required data from an underdeveloped field like Whicher Range. Unlike other tight gas reservoirs with 1000's of wells, WR field has only five wells of data, which made it a feasible task to analyse the core, log and production data from the wells, to construct a detailed model. The commercial reservoir simulator RUBIS, a module of software ECRIN suite (ver. 4.30.08) from KAPPA Engineering was used to create the simulation model.

The model was built in two steps. Step 1 involved the development of a petrophysical model and Step 2 involved the development of the dynamic reservoir model using the data collected in Step 1. Once the model was created, it was history-matched.

4.4.2 Determination of the locations and the simulation of the initial set of wells (stage-1)

The main objective of this stage is to identify appropriate locations of new wells based on certain expected production rates of wells for a given minimum surface pressure, and expected production rates for a certain period of time (say 30 years) through reservoir simulation. In this particular study of the WR tight gas field, fractured vertical wells were considered.

In order to identify the locations of the new wells in the WR tight gas field, the reservoir model was thoroughly analysed based on the cut-offs shown in Table 4.1. The reservoir properties such as porosity, permeability and water saturation in each layer were analysed based on the cut-offs, by studying the property maps and cross-section maps of various locations in the field. Once the locations of new wells were identified, the wells were simulated for a period of 30 years (typical lifespan of a tight-gas reservoir) to assess if they were productive with a minimum surface rate of 900 Mscf/d and expected surface pressure of 200 psi. Based on the simulation, all unproductive wells were relocated or removed.

Table 4.1 Cut-offs used to select the location for drilling Stage-1 wells

Parameter	Cut-off
Porosity, %	> 6
Water saturation, Fraction	< 0.45
Permeability, mD	> 0.03
Minimum surface rate at 200 psi minimum surface pressure, Mscf/d	900

Another factor considered while locating the wells, was that in order to apply the MWM in the next step, 5 to 20 wells are required within each window. However, as mentioned earlier, the WR field has only five wells of which only two have a short production history. Therefore, the new wells were located in such a way that they may satisfy this condition also.

4.4.2.1. Determination of optimum flow rates

All the selected wells described earlier were simulated for a period of 30 years to find the maximum production rate achievable from these wells. Table 4.2 shows the model parameters for selected Stage-1 wells.

The maximum achievable initial production rate for each well was determined while maintaining a minimum surface pressure of 200 psi. For this, each well was manually optimised through a trial and error process, by varying the flow rates systematically, until the maximum rate the well could provide was attained.

Once the maximum rates were determined, the entire reservoir, including the selected Stage-1 wells, was simulated for 30 years to understand the sweep efficiency of the wells. In addition, after observing, it was understood that there were many undrained areas in the reservoir. Hence a Stage-2 drilling plan was suggested which uses the MWM instead of the dynamic simulation method, making it much faster.

Table 4.2 Properties of selected stage-1 wells

Fracture length, ft	75
Fracture conductivity, mD.ft	100
Fracture type	Multi-layered
Minimum surface pressure, psi	200
Minimum economic surface rate, Mscf/d	900
Well type	Vertical

4.4.3 Development of the 4D linear regression equations using MWM

In this step, the MWM was applied by following the steps outlined in the previous section. A five-year production period was considered although the wells were simulated for 30 years. The reason for choosing five years was that, from a practical point of view, Stage-2 had to be initiated after observing the five-year production response of Stage-1. There was no point waiting for 10 or 20 years as the would be less area swept by Stage-1 wells because of low permeability (for TGR) and consequently, more wells would be required for increasing the recovery factor. In addition, unlike a conventional reservoir, the drainage area of a tight formation changes with time, as the pressure regime remains transient for a long period, depending on the level of permeability. The pressure regime of WR tight gas field therefore was considered to remain transient for the five-year period, which required calculating the transient drainage area (A). In this study, the transient area was calculated using Equations 4.8 and 4.9 (Stuart Alan Cox et al., 2005). The regression analysis was performed using the Statistical Package for the Social Sciences (SPSS) from IBM Corporation.

4.4.4 Creating the second set of infill wells, and predicting the corresponding Best Year (BY) rates using MWM (stage-2)

This step involved two parts: locating the wells and finding the best year rates of the new wells, outlined in the following sections.

4.4.4.1 Locating the wells
To find the location, the current reservoir model with the Stage-1 wells, as described in previous section, was simulated for 30 years, and the pressure maps obtained were analysed. After careful analysis, it was observed that some areas were not drained. So new wells were located in those areas to increase the ultimate recovery of the field. All the wells considered were fractured vertical due to the conditions of the tight gas reservoir.

4.4.4.2 Determination of the Best Year (BY) rates of the wells
Once the new wells had been located, the 4D linear regression equations developed in the previous step were used to find the corresponding Best Year (BY) rates, Virgin Best Year (VBY) rates, transient drainage area (A) and cumulative production. VBY was

122

calculated by drawing a window around each new well and performing a 2D regression analysis. The static reservoir model was used to calculate average porosity, permeability, saturation and thickness of each well.

4.5   Methodology for creating the alternative infill drilling plan

The alternative plan was created to test the effectiveness of the proposed optimum plan. The alternative method was created by placing the same number of wells as in the optimum plan, but at arbitrarily selected locations. All the wells had exactly the same properties as those in the optimum plan. This plan was created and simulated using the same simulator RUBIS from KAPPA-ECRIN. In addition, the average production rates of the wells in the optimum plan were considered as the target production rates, while simulating the alternative plan. Table 4.3 shows the model parameters used to model the alternative infill-drilling plan.

Table 4.3 Model parameters of the alternative infill drilling plan

Formation top, ft	12,137
Initial reservoir pressure, psi	6200
Gas specific gravity	0.63
Reservoir temperature, ^{o}F	210
Gas viscosity at initial conditions, cP	0.03
Gas formation volume factor, cf/scf	0.003
Number of wells	63
Fracture length, ft	75
Fracture conductivity, mD.ft	100
Fracture type	Multi-layered
Minimum surface pressure, psi	200
Minimum economic surface rate, Mscf/d	900
Well type	Vertical
Target flow rate, Mscf/d	13000

4.6   Results and discussions

The results and their detailed analysis, pertaining to both the optimisation plan and the alternative plan, have been clearly explained below. Figure 4.3 shows the history-matched 3D model created using RUBIS (KAPPA-ECRIN).
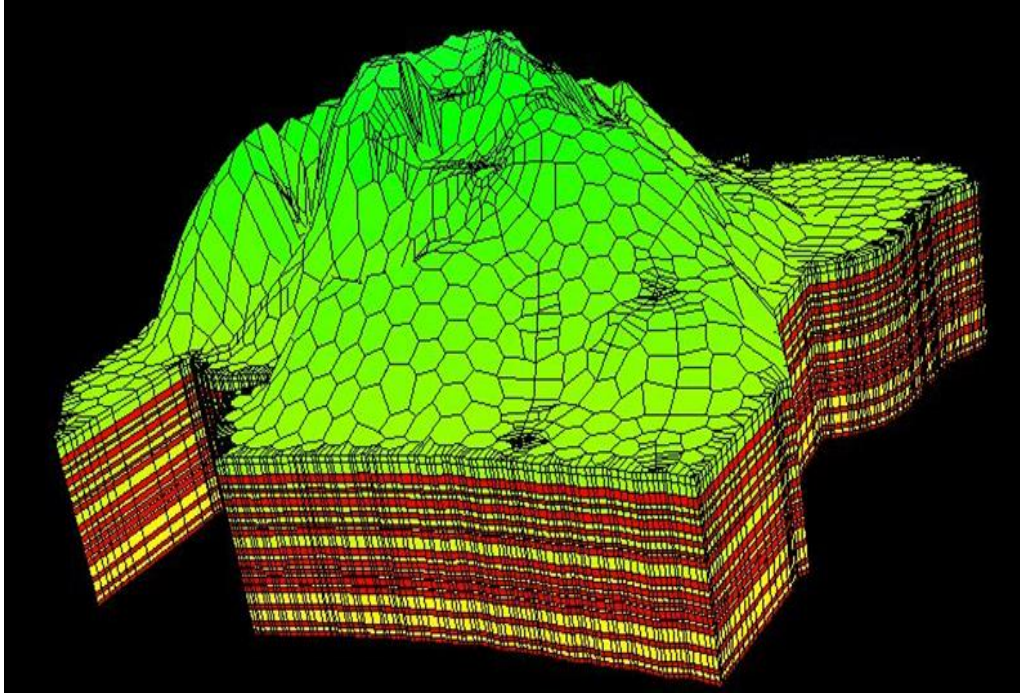
Figure 4.3 - 3D model of Whicher Range North

4.6.1   Development of optimum infill drilling plan

This plan was developed following the method outlined in the previous section.

4.6.1.1 Stage–1 of the infill drilling plan

This stage was developed using the simulator RUBIS from KAPPA-ECRIN that proposed 31 new wells to be drilled in various locations across the field.

4.6.1.1.1   Selection of well locations

In order to locate new wells, reservoir properties like porosity, permeability and saturation were studied using the property maps and the cross-sections at different locations as shown in Appendix B. Figures B.1 – B.3 in Appendix B show, respectively cross sections of porosity, permeability and gas saturation distribution, and Figure B.4 shows porosity maps of the sand layer, which were used for selecting the best locations for the new wells. Likewise, a large number of maps were analysed. The arbitrary cut-offs used are given in Table 4.1.

Apart from analysing the reservoir properties, it was also ensured that least 5 wells were within each window to aid the application of the MWM and to develop the Stage-2 wells. Through this process, 31 new wells were created, and their locations are shown in Figure 4.4. All the wells considered were vertical, and all the sand layers were hydraulically fractured.

The maximum achievable gas production rates for the 36 wells, as shown in Table B.1 in Appendix B, were determined by simulating the entire reservoir for a period of 30 years, against a minimum surface pressure of 200 psi. The manual optimisation process involved around 10 iterations for each well.
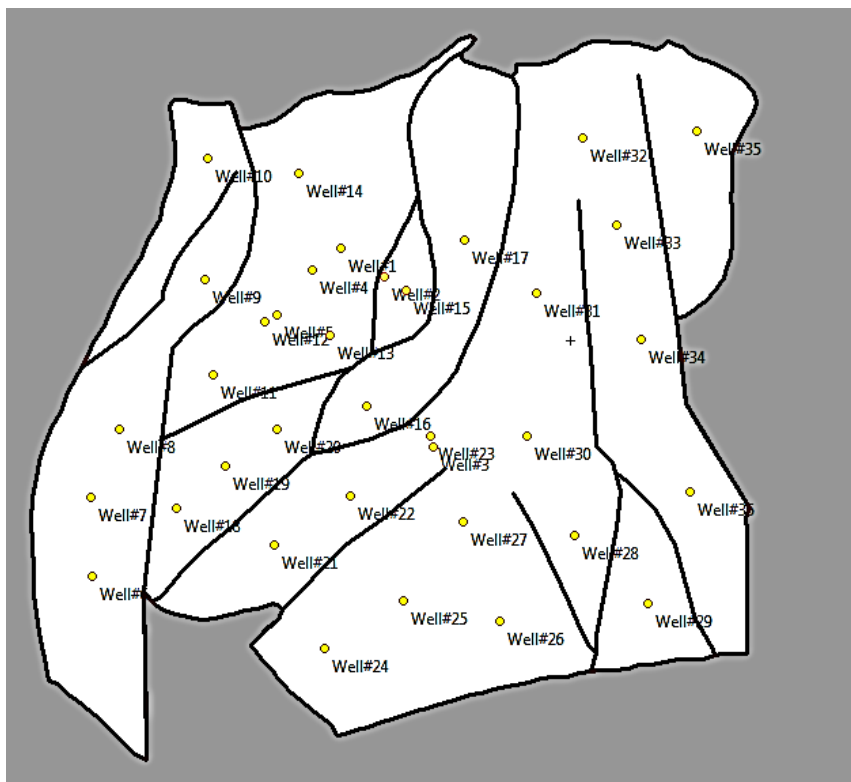
Figure 4.4 Two sample windows created around Well 4 and Well 25, which contain eight and five wells respectively. The geographic locations of the 36 wells are also shown.

4.6.1.2 Stage-2 of the infill drilling plan

After finding the production rates of all the Stage-1 wells, they were simulated for 30 years to detect undrained areas (if any). Figures B.5–B.6 in Appendix B show the pressure maps of WR, after 15 and 30 years of production, respectively. Due to the large number of wells involved, the reservoir could not be simulated as a single model due to the memory limitations of the simulator. So, it was compartmentalized into two

parts by assuming that the fault transmissibility was equal to zero (which is true for a TGR).

From Figure B.6 in Appendix B, it can be observed that there were many areas which have not been drained at all (areas indicated by red). The pressure waves did not reach these areas due to the low permeability of the reservoir. In order to improve the sweep efficiency, more infill wells need to be drilled. This will not only increase the ultimate recovery, but also accelerate the production rate, thereby recovering the maximum quantity of gas within the leasing period of the company. This led to the decision to drill Stage-2 infill wells.

4.6.1.2.1   Location of the Stage-2 infill wells

The locations for the new wells were selected with the main intention of draining the undrained areas. If new wells were not drilled, it would take much more than 30 years to drain the reservoir, and even then, some areas might still be undrained due to heterogeneity of the reservoir. Figure B.7 in Appendix B shows the pressure map of the Stage-1 reservoir after 30 years, with the proposed locations of the Stage-2 wells. In this way, 27 vertical fractured wells were proposed. Figure 4.5 shows the map of the WR field with 63 wells.
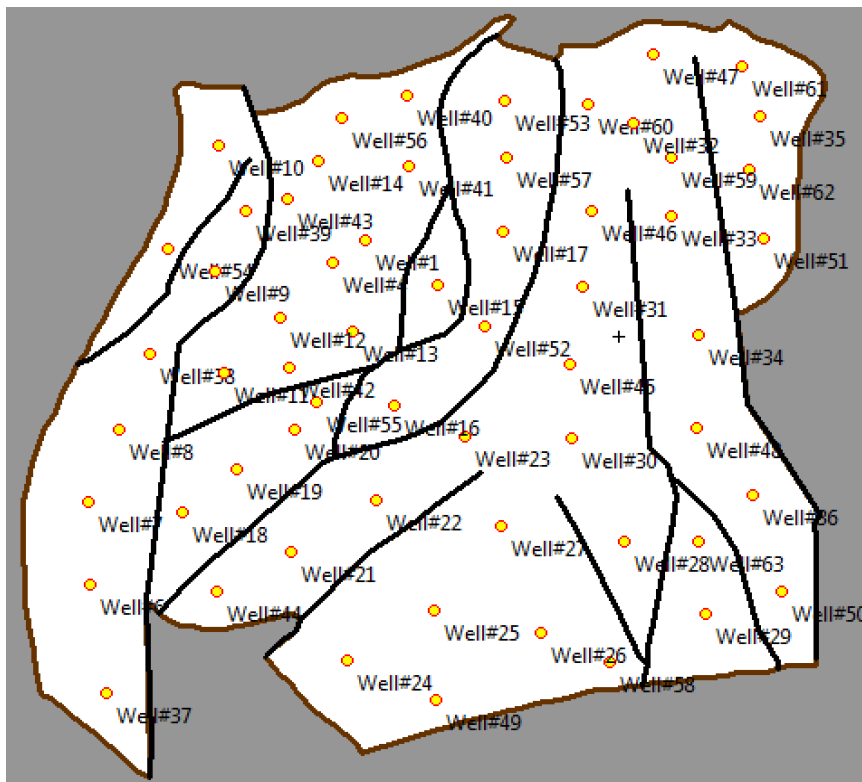
Figure 4.5 Locations of all 63 wells in the Whicher Range field

4.6.1.2.2   Best Year Rates (*BY*) of the Stage-2 wells using MWM

In order to find the Best Year rates of the new wells, first the 4D linear equations were formulated for each window. Then, by substituting the properties of the new wells into the equation, the Best Year rates of the Stage-2 wells were calculated. Table B.2 in Appendix B shows the Best Year rates of the Stage-2 wells.

4.6.1.2.3   Best Year (*BY*) rates of the Stage-2 wells from simulation

BY rates of the Stage-2 wells were also calculated using the reservoir simulator to check the accuracy of the MW method. For this, *BY* rates were calculated based upon maximizing the production rates through optimisation of the well planning process. Table B.3 in Appendix B shows the *BY* rates of Stage-2 wells determined by the simulator. Figure 4.6 shows the pressure map of the WR field after 30 years of production after placing the Stage-2 wells. Moreover, Table 4.4 shows the production data for the 30 years period.
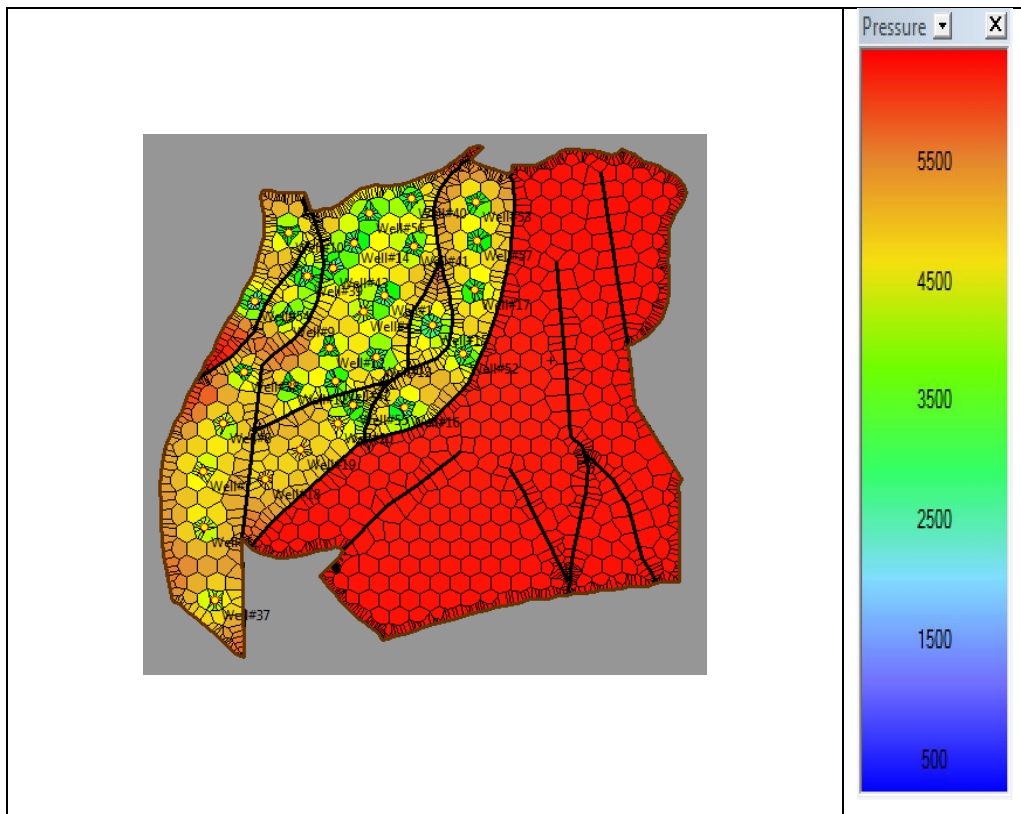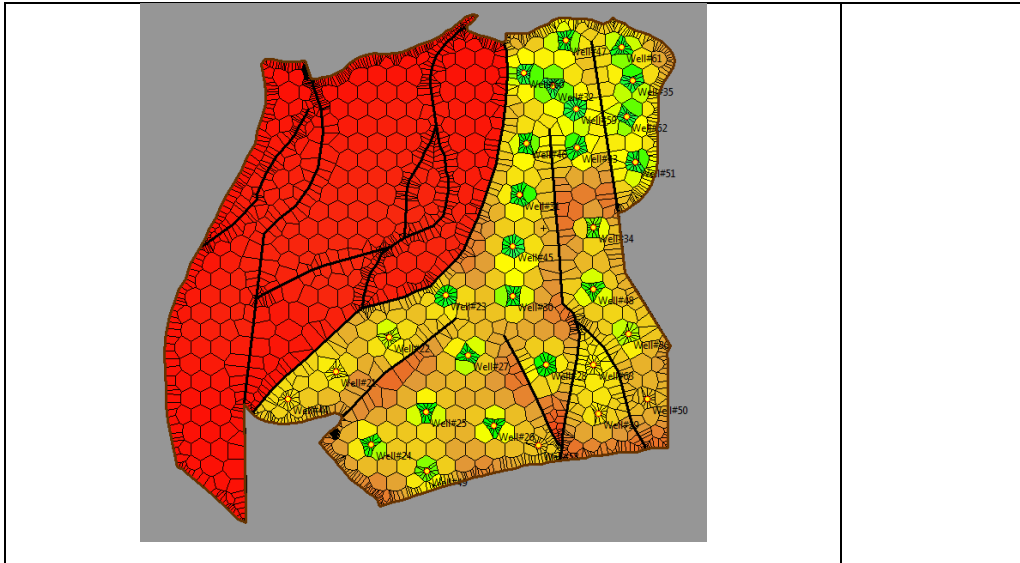
Figure 4.6 Pressure maps of the Whicher Range reservoir after 30 years (Stage-2)

From the pressure map, it can be seen that the pressure waves reached the boundaries, but the average reservoir pressure was still high enough (around 3800 psi) to support further production. Therefore, a Stage-3 program could be developed with a greater number of infill wells for better sweep efficiency and enhanced recovery of gas. Nevertheless, this depends on how much capital the company would be ready to invest. However, this discussion is beyond the scope of the focus of current study.

Table 4.4 Production data after 30 years of production for optimum plan

Parameter	Value
Cumulative production in 30 years, Bscf	1656
Number of producing wells	60
Recovery factor, %	34
GIIP, Bscf	4950

From Figure 4.7, it can be seen that the production from the optimum plan (1655 Bscf) was about 24 times that of the base model (70 Bscf). Therefore, implementation of this optimum plan could increase the recovery factor from 1.5% to 34% of the base model (initial reservoir).

128
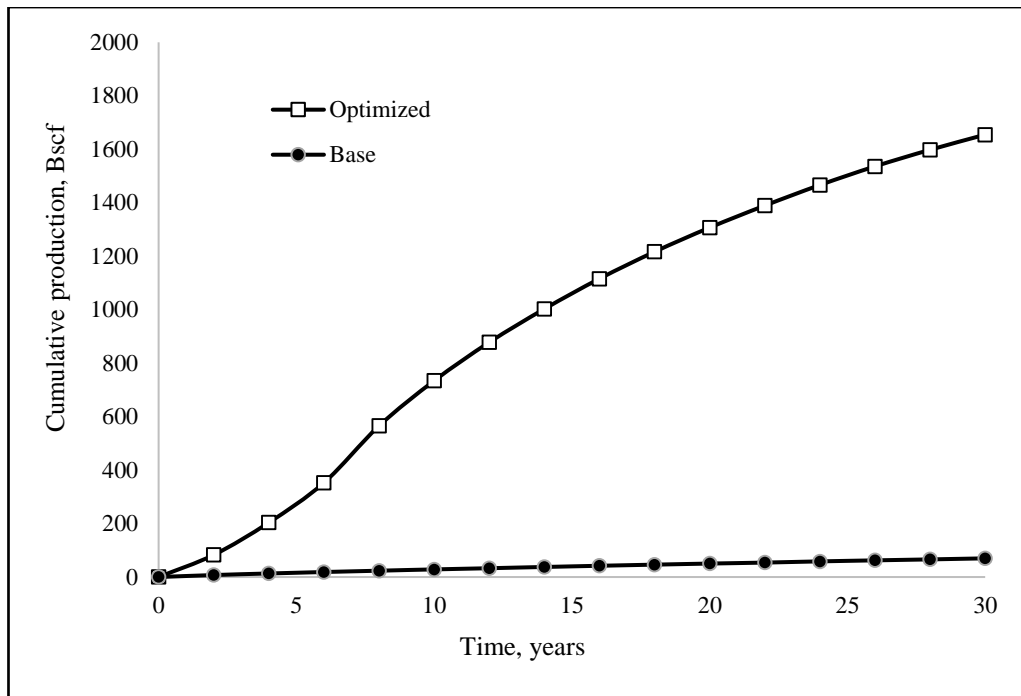
Figure 4.7 Cumulative production as a function of time for the optimised plan and base model

4.6.2 Production Performance Analysis

The analysis of predicted production performance of all the wells in the optimum plan is discussed in this section. When production history is available, it can be analysed to identify production patterns in a reservoir. But for the WR field, there was not much history available, and so the predicted performance was analysed to detect production patterns between the wells. This is helpful in identifying anomalous behaviour of wells (Bhattacharya and Nikolaou, 2013). The data inferred from this analysis can be used to predict the behaviour of new wells. Another use of this analysis is that, by looking at the predicted production rate curves, the production engineer can predict when each well has to be shut-in and opened to maintain an economic level of production.

Table 4.5 shows the observations made from the production curves (flow rate vs time plots) for each well and Table 4.6 focuses on the inferences made by analysing the observations listed in
Table 4.5.

The main reason for the above-mentioned similarities in behaviour is the similarity in reservoir properties, like porosity, permeability and gas saturation, in the well

locations.

Table 4.5 Observations made from the production curves

Behaviour	Well. No.
Well that stops production by 15 years	4
Well that stops production by 20 years	18, 19, 20, 44, 49, 58
Well that stops production by 25 years	29, 50, 63
Well that stops production by 30 years	6, 7, 8, 21, 22, 24, 28, 36, 37, 48, 55
Well that produce for 30 years and still has potential	1, 9, 10, 11, 12-17, 23, 25, 26, 27, 30-35, 38-43, 45, 46, 47, 51-54, 56, 57, 59-62
Initial flow rate <5000 Mscf/d	4
Initial flow rate 5000 - 10000 Mscf/d	6, 7, 8, 9, 18-30, 31, 34, 36, 37, 44, 45, 48, 49, 50, 51, 52, 54, 55, 58, 62
Initial flow rate 10000 - 15000 Mscf/d	1, 10, 11, 13-17, 31, 32, 33, 35, 38-43, 46, 47, 51, 52, 53, 56, 57, 59, 60, 61
Initial flow rate >15000 Mscf/d	12

Table 4.6 Inferences made by analysing the observations

Behaviour	Well. No.
Wells that have an initial rate between 5000-10000 Mscf/d and stop production by 30 years	6, 7, 8, 24, 28, 48
Wells that have an initial rate between 5000 – 10000 Mscf/d but still have potential even after 30 years	9, 23, 25, 26, 27, 30, 31, 34, 45, 51, 52, 54, 62
Wells that have an average initial rate of 10000 - 15000 Mscf/d but still have potential even after 30 years	1, 10, 11, 13-17, 31-35, 38-43, 46, 47, 51, 52, 53, 56, 57, 59, 60, 61

4.6.3   Alternative infill drilling plan

Figure 4.8 shows the location of the wells as per the alternative plan outlined earlier in the methodology section. As mentioned, the only difference between the optimum model and the alternative model was the way in which the wells were arranged in the field, while all other parameters remained the same.
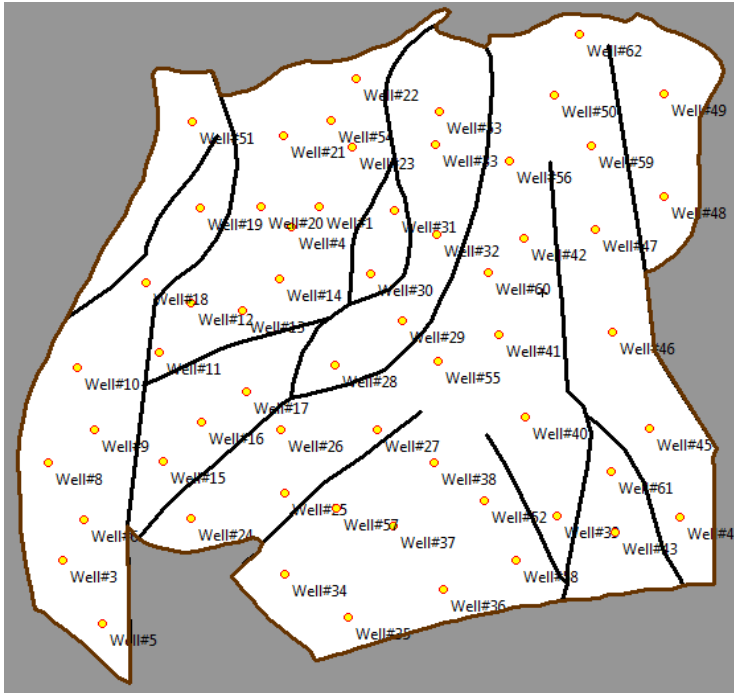
Figure 4.8 Location of wells in the alternative infill-drilling plan

Table 4.7 shows the production data after 30 years of operation. This plan was capable of producing only 1145 Bscf of gas, in 30 years, through 60 wells.

Table 4.7 Production data after 30 years of production for the alternative plan

Parameter	Value
Cumulative production in 30 years, Bscf	1145
Number of producing wells	60
Recovery factor	23
GIIP, Bscf	4950.4

From the pressure maps (Figure 4.9), it is evident that there was a lot of interference between the wells, which had led to a drop in productivity and consequently reduced the gas recovery. In addition, the average pressure of the reservoir was still high, even though 60 wells were producing. All this was because the wells were not optimally placed. So, if such a plan were to be implemented, the company would need to drill a huge number of wells to drain the reservoir, which may not be economically feasible.
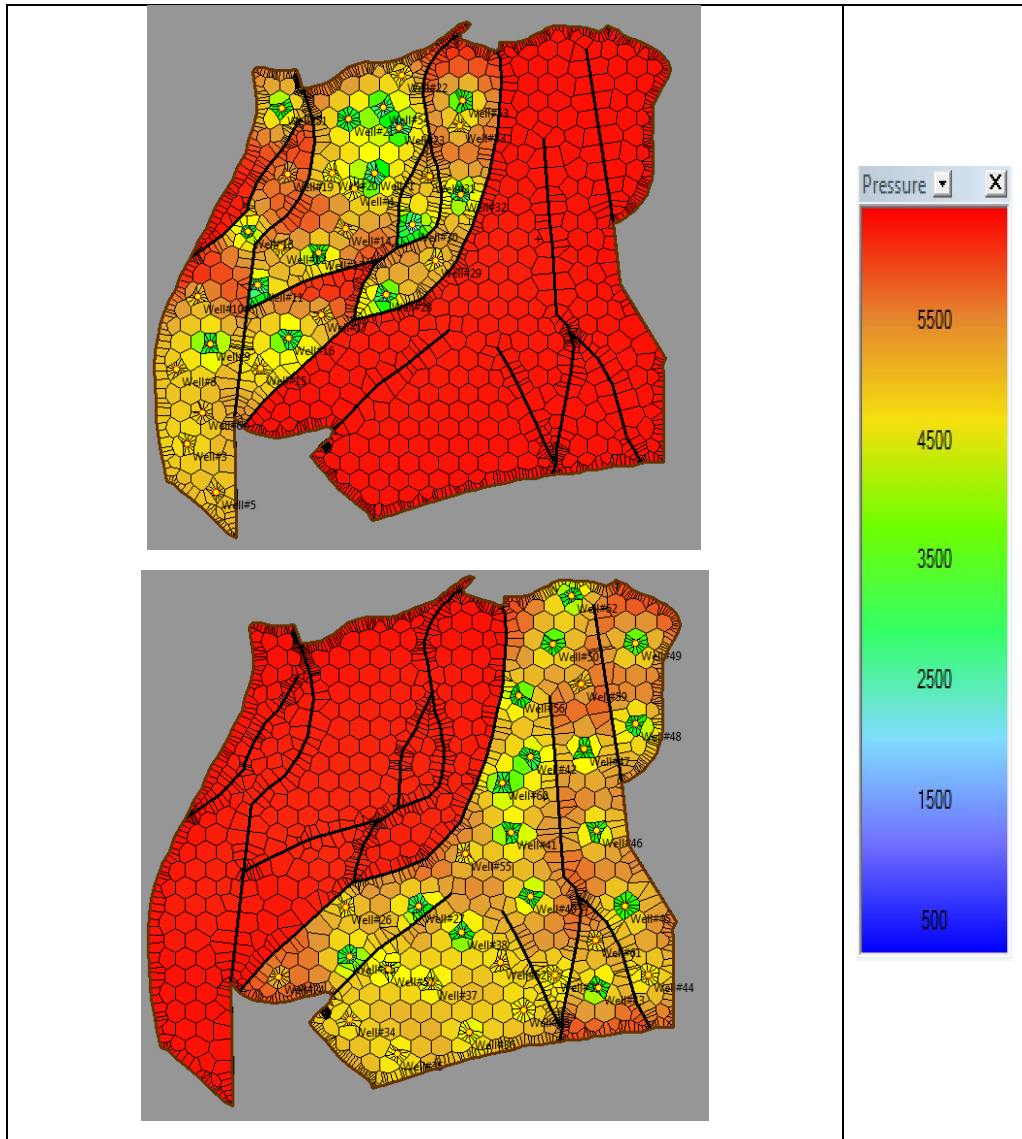
Figure 4.9 Pressure maps after a 30-year production period after implementing the alternative plan

4.6.4   Comparison of Optimum Infill Drilling Plan with Alternative Plan

Three different scenarios were considered to carry out a comparative study in order to justify the effectiveness of the proposed method as well as the developed optimum infill-drilling plan. These scenarios are:

a)   **Optimum plan,** which was developed in two stages following the method developed in this study.

b)   **Alternative plan,** which was almost similar to the developed optimum plan in all aspects except that the wells were located randomly without any logic involved; and

c) Base plan, which was based upon five exploration wells, of which only two were producing.

From Figure 4.10, it can be observed that the optimum plan, alternative plan and base plan produced 1655, 1140 and 70 Bscf, respectively. The optimised plan was capable of producing 30% more than the alternative plan and 96% more than the base plan. Hence, the optimised plan appeared to be more efficient and profitable compared to the other plans.
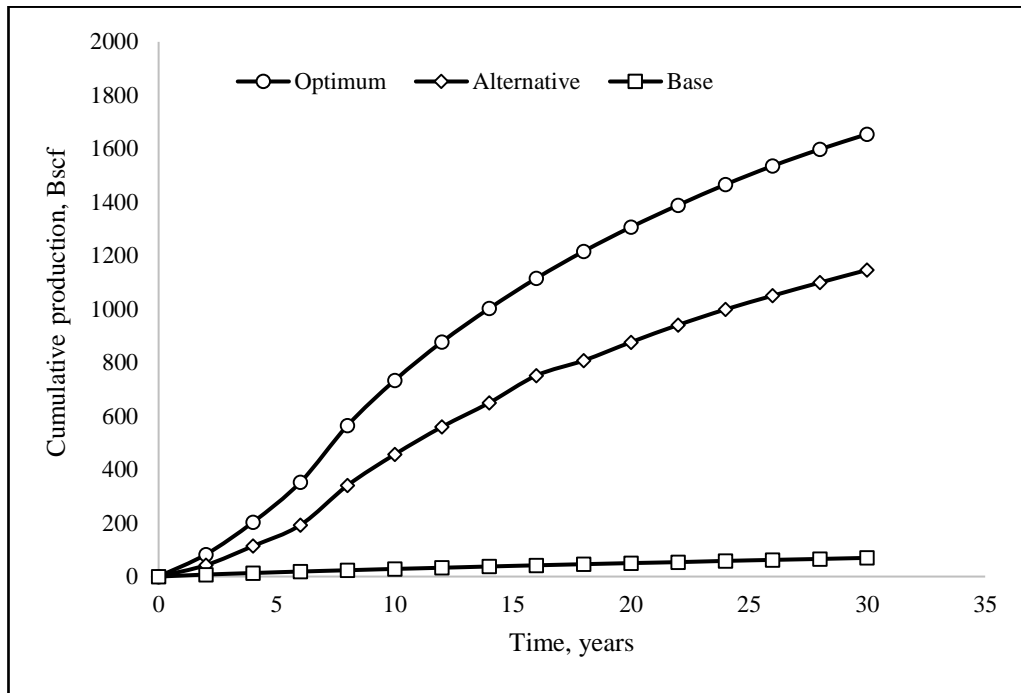
Figure 4.10 Cumulative production of optimised, alternative and base plan vs time

4.6.5 Comparison of MWM and reservoir simulation results

The Best Year (*BY*) rate predictions for Stage-2 wells from MWM were compared with that from the reservoir simulation results. In Figure 4.11, the *BY* rates from the simulation were plotted against the *BY* from MWM. From Figure 4.11, it can be prominently seen that the majority of *BY* rates predicted by MWM were very close to those predicted using the simulator. The reason for the error in some values may have been due to the use of global or regional regression in some locations due to the lack of sufficient numbers of wells within certain windows.
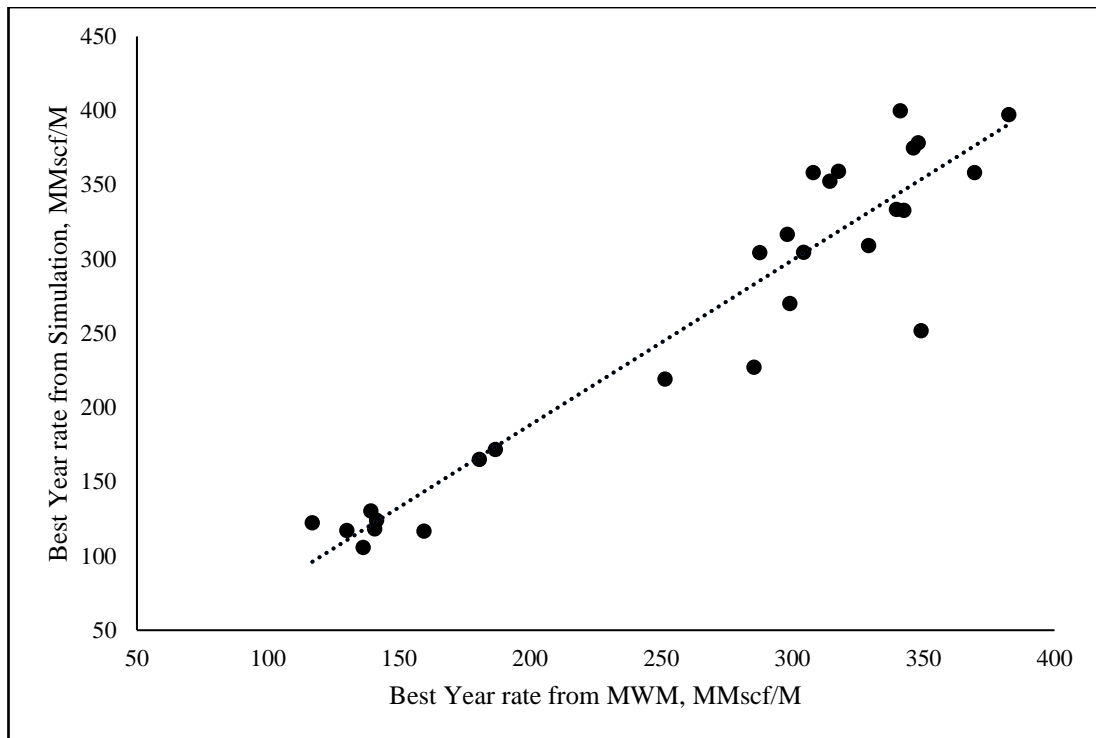
Figure 4.11 Comparison of the BY rates from MWM and reservoir simulation

A method to determine optimum infill drilling plan is proposed and presented in this chapter. The method was developed based upon reservoir simulation modelling combined with the Moving Window Method (MWM). This method was applied to develop an optimum infill-drilling plan for the Whicher Range, an Australian tight gas field.

Based on this study a 2-stage plan with 58 new infill wells is proposed. Stage-1 proposes 31 new wells at various locations, which were selected by sweet-spot analysis, and the production rates were predicted with the help of the dynamic simulation model. Stage-2 proposes 27 more wells, which were located with the sole intention of draining the undrained acreage. Moreover, MWM was applied for predicting the best year rates of these wells. The plan was compared with an alternative plan, with wells with the same properties but drilled at random locations. The results demonstrated that the proposed optimum plan for the WR tight gas field is capable of producing 30% more than the alternative plan.

The level accuracy of the proposed method is justified by comparing the results with that from the reservoir simulator. In addition, it was observed that the proposed method is capable of predicting the best year rates (*BY*) with appreciable accuracy; and it is

observed based on this study that the proposed optimum plan for the WR tight gas field should increase the ultimate recovery up to 1.7 Tscf.

Chapter 5: Hydraulic Fracture Optimization using Numerical Reservoir Simulation

The optimization process has turned out to be a central element of any decision-making process. In case of tight gas reservoir development, optimization plays a critical role. Generally, optimization has become a pivotal element in all areas of academic studies and has practical uses in real applications (Luptacik, 2010; Raju, 2014; Rao, 2009; van Ackooij et al., 2017; Vasant, 2012). In particular, petroleum engineering disciplines have been strongly developed by applying and combing simulation and optimization techniques (AL-FATLAWY, 2004; Mohammed S Al-Jawad and Hassan, 2010; Brandman et al., 2018; Hassan and Al-Jawad, 2005; Lessard, 2003; Mantica et al., 2001; Tekin and Sabuncuoglu, 2004; Viadana et al., 2012). Economic production of vertical wells in tight gas reservoirs (TGR) is definitely required, and applying hydraulic fracturing technique is the best possible completion technique for every unconventional gas reservoir (M. J. Economides and Martin, 2007). While hydraulic fracturing is the key for the economic recovery of hydrocarbon from tight gas reservoirs (TGRs), it is critical to determine the optimum fracture properties (i.e. length, width, numbers, fracture conductivity) for a given set of reservoir parameters. For instance, though a well induced with a larger hydraulic fracture half-length may provide a larger production rate (i.e. better well performance), it does not necessarily mean that a fracture length greater than an economically optimum length will generate more profit from the well.

The optimization of the production strategy of the vertical hydraulic fractured well is important to determine the optimum feasible fracture half-length which leads to calculating the maximum cumulative gas production for maximizing the net present value. The main cornerstone to design optimally hydraulic fracture wells is the estimation of the feasible cumulative gas production and the economic analysis of the production benefits. However, the design of the hydraulic fracturing includes many challenges (Al-Driweesh et al., 2014; Fallahzadeh et al., 2017; Uddameri et al., 2015). One of the main design challenges is the accurate computation of the optimum fracture half-length (Wei and Holditch, 2009; Yu et al., 2014). The optimization of the hydraulic fracturing requires a time-consuming process that needs numerous simulation runs which demand an enormous memory size and tedious simulation time. The required memory size and time is dependent on the size of the reservoir, the range

of fracture half-length, the heterogeneity of the porous media and the highly nonlinear gas flow behaviour in porous media.

This study aims to investigate different optimization techniques, including limitations to optimizing fractured vertical and multistage hydraulic fractured horizontal wells through numerical reservoir simulation models coupled with optimization techniques. The optimization technique is based on direct-search methods such as the simplex method (Chong and Zak, 2013) or random search methods such as the genetic algorithm (Arora, 2015). To perform the optimization technique, net present value (NPV) and cumulative gas production (G_p) are considered as objective functions, while fracture half-length (x_f) is set as a decision variable. Five optimization techniques are employed to assess the performances of each technique based on of two criteria: (i) the values of the objective functions; and (ii) the number of required simulation runs to reach the optimum solution. These two criteria indicate the efficiency of each optimization technique to accomplish the function evaluation in the least number of simulation runs. The chapter provides simple and efficient guidance to determine the most suitable optimization technique under different reservoir conditions and production scenarios to optimize fracture half-length for hydraulic fractured vertical wells in TGRs.

Figure 5.1 presents the workflow suggested in this chapter to identify the best optimization technique to find the optimum fracture half-length with the minimum number of simulation runs for hydraulic fracture vertical wells in TGRs. Twelve real and mechanistic reservoir simulation models are designed for competency assessment of each optimization technique under different well and reservoir conditions.
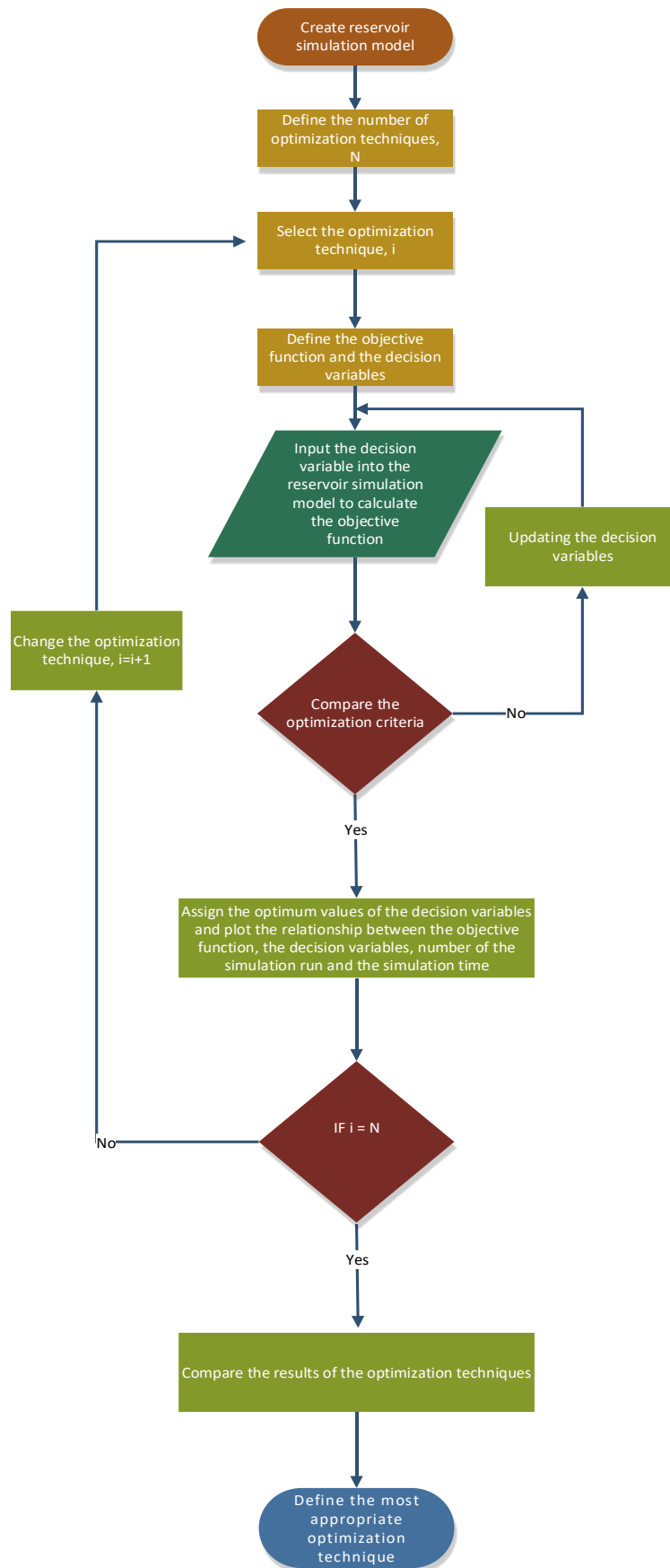
Figure 5.1 Flow chart of the study

5.1 Integrated Reservoir Simulation and Optimization techniques

The integrated reservoir simulation and optimization techniques is considered as an efficient tool to maximize the production and revenue in the oil and gas industry (Abukhamsin, 2009; Suwartadi, 2012; Temizel et al., 2017; Völcker, 2011). In this chapter, we will present a handful of the most used gas reservoir simulator, such as Petrel/Eclipse integrated with different optimization techniques. The optimization techniques include direct-search methods and random search methods to maximize the net present value (*NPV*) and cumulative gas production (G_p) with respect to hydraulic fracture parameters, for instance, fracture half-length for the hydraulic fractured vertical wells in TGRs. The chapter emphasises the investigation of the accuracy and limitations of each optimization technique integrated with reservoir simulation tasks in view of identifying the most feasible optimization techniques.

In general, the working mechanism of the integrated reservoir simulation and optimization techniques starts by the optimization engine prior to reservoir simulator. First of all, the optimization engine creates the initial values of decision variable (x_{f1}, …. , x_{fn}), and then the reservoir simulation calculates the objective function (*NPV*) based on the initial values of the decision variables. After that, if convergence criterion is met, the optimal solution is achieved. Otherwise, the decisions variables are updated by the optimization engine and pass back to the reservoir simulator to calculate the objective function using the updated variables. The optimization-reservoir simulation cycle continues until the convergence criterion is met. The process is described in Figure 5.2. The working mechanism of the integrated reservoir simulation and optimization techniques encounters many difficulties associated with the required runtime, the necessary number of simulation runs, the capacity of the computer and the number of decision variables. All of these challenges affect the performance of each optimization, and integrated with reservoir simulation, to provide an accurate and fast optimum solution.
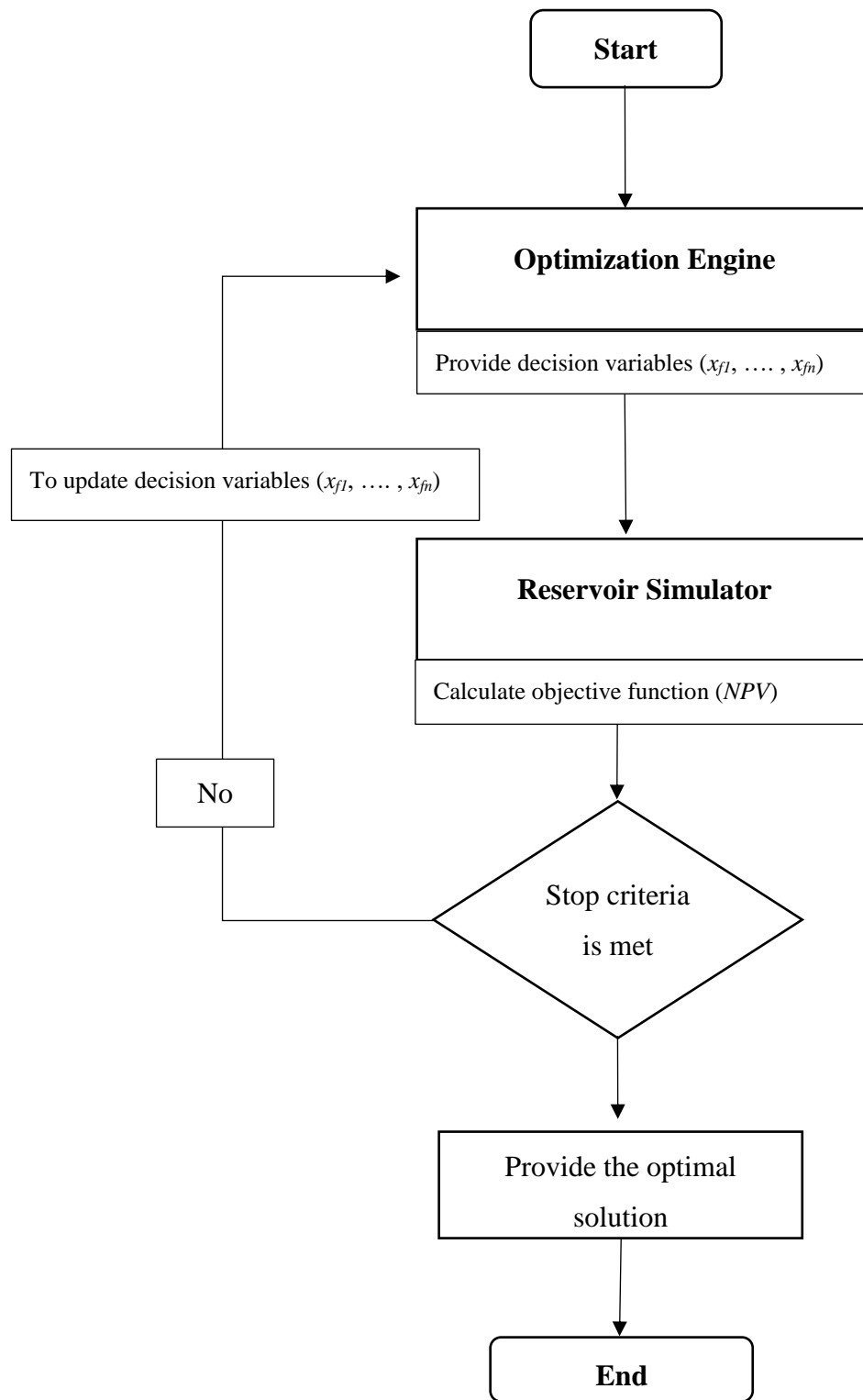
Figure 5.2 Flow diagram describing the integrated reservoir simulation and optimization process.

5.2 Objective function

The objective function in this particular study refers to what the petroleum companies intend to maximize. In this study, the objective function used for the optimization is net present value derived based on the cumulative gas production (G_p) for the period of the petroleum life cycle. This study considered 30 years as the petroleum life cycle. Therefore, two objective functions are considered: net present value (*NPV*) and cumulative gas production (G_p). The convergence threshold for the objective function, G_p or *NPV*, as a solution was assumed to be equal to 1%, below which the solution was considered as satisfactory. The convergence threshold applied in all optimization techniques used in this chapter is calculated using Equation 5.1.

$$CT = \left| \frac{NPV_{new} - NPV_{old}}{NPV_{new}} \right| \times 100\% \qquad\qquad 5.1$$

Where:

CT is the convergence threshold.

NPV_{new} is the net present value at the end of the new iteration (i+1).

NPV_{old} is the net present value at the end of the old iteration (i).

Since economy often drives any feasibility study of any prospective hydrocarbon reservoir, the net present value (*NPV*) and cumulative gas production (G_p) are considered as objective functions in this study. *NPV* mainly depends on cumulative gas production, capital costs and operating costs.

The objective of this study, as described in this chapter, is to identify the most feasible optimization technique integrated with reservoir simulation studies for the optimization of fracture half-length of fractured vertical wells in a TGR for maximization of cumulative gas production (G_p) and/or net present value (*NPV*) for a tight gas field for a 30-year production life cycle.

The cumulative gas production should as much as possible maximize *NPV*. The maximization of cumulative gas production is associated with the maximization of the gas production rate (q_t), therefore the maximum G_p can be expressed by Equation 5.2.

$$Maximum\ G_p = Maximum\ \sum_{i=1}^{m} \int_{0}^{t_p} q(t)\ \ dt \qquad\qquad 5.2$$

Where,

i is the counter of the time steps.

m is the total number of time steps.

The second objective function is net present value that is mainly the function of cumulative gas production and capital and operating expenditure (CPEX and OPEX), which are strongly a function of fracture half-length for a number of hydraulic fractured vertical wells, and can be expressed as:

$$Objective\ function = Maximum\ NPV = f\left(G_p, captial\ costs, operating\ costs\right)$$
$$= f\left(x_{f1}, x_{f2}, \ldots\ldots., x_{fn}\right)$$

Where:

n if the number of wells to be hydraulically fractured.

Therefore, NPV calculated for n number of wells can be expressed by Equation 5.3.

$$NPV = \sum_{j=1}^{n} \sum_{i=1}^{m} \left[\frac{N_{CF}}{(1-D_R)^i}\right]_i \qquad\qquad 5.3$$

Where,

N_{CF} = net cash flow = R_n - E_n

D_R = discount rate

m = the total number of time steps.

The details of the NPV model will be discussed in Chapter 6.

5.3   Decision variables

The fracture half-length (x_f) was considered the optimizing parameter for the models, with all other parameters kept constant for each optimization task. Fracture half-length

142

(x_f) for hydraulic fractured vertical wells was adopted as a decision variable because it was the main parameter controlling the extent of the flow area between the vertical well and the reservoir, and thus was the decision variable in the optimization study. The plan for the research included performing optimization on fracture half-length for single and multi-well scenarios. With multi-well scenarios, investigations were performed into performance of optimization techniques under two different assumptions: (i) x_f was assigned to be the same value for all wells as shown in Figure 5.3, and (ii) x_f was assigned to be independent for each of the three wells as shown in Figure 5.4. Therefore, each case was carried out under the second assumption, which had three decision variables, where each decision variable represented the value of fracture half-length for a fractured vertical well.
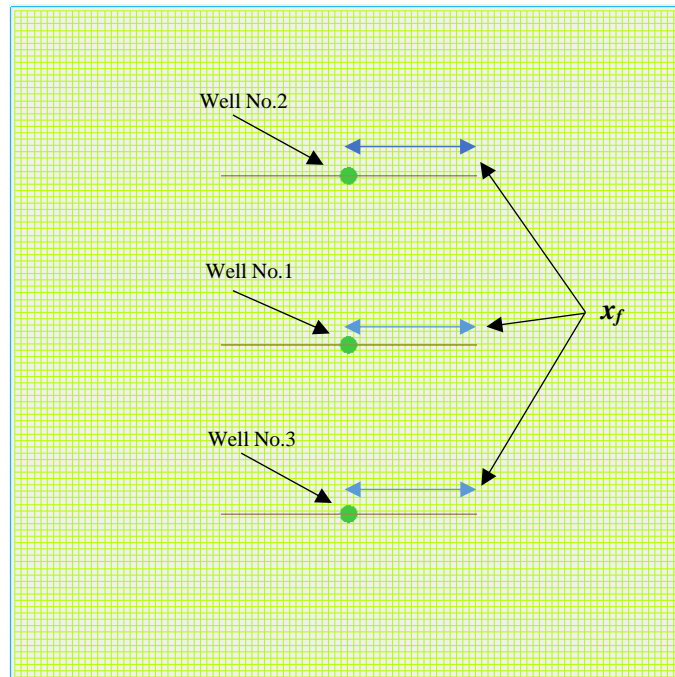
Figure 5.3 Schematic of the multi-well scenario with the same fracture half-length for all wells
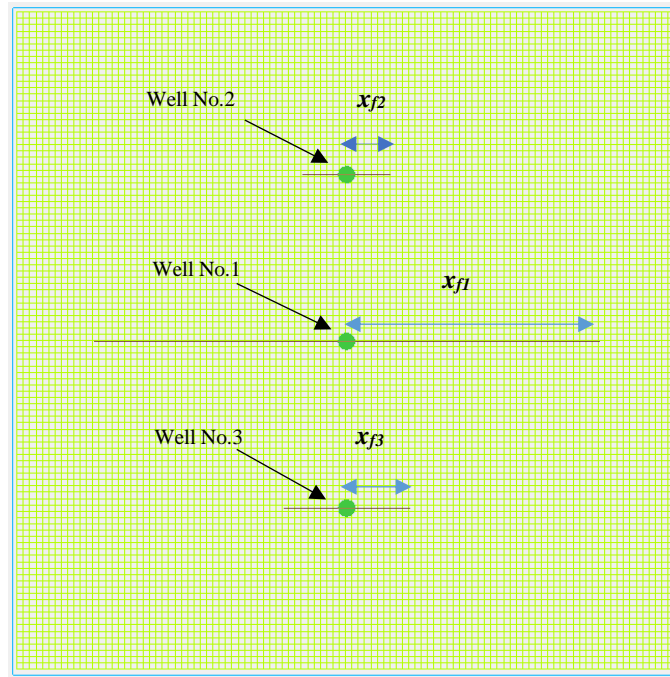
Figure 5.4 Schematic of the multi-well scenario with the independent fracture half-length for each well

5.4 Optimization techniques

There are number of optimizations techniques, including gradient-based or gradient-free methods, the downhill simplex, and genetic and neural network algorithms. The gradient-based optimization requires reliable derivatives of the objective function to achieve the optimal solution at the desired convergence threshold. The key limitation of this technique is that it can converge to unfavourable local minima/maxima rather than the global optimal solution for a complex nonlinear function that has a number of local optimal solutions. Regarding reservoir performance optimization, the importance of gradient-free optimization emerges to optimize nonlinear functions that cover most of the reservoir performance problems. Therefore, in the next sections various optimization techniques are elaborated that were used within the reservoir simulation to search for the optimal fracture half-lengths to maximize the *NPV* or G_p, objective functions.

5.4.1 Downhill simplex method

The downhill simplex method is also referred to as the Nelder-Mead method (Nelder and Mead, 1965). It simply bases on the idea of geometric simplexes where the vertices of simplex represent the decision variables that are changed to reach the optimal

solution at the optimum decision variables. This optimizer demands limited inputs which are the number and initial values of the decision variables, the upper and the lower limits of constraints, and the maximum allowed number of iterations. To avoid unfavourable termination before the convergence criteria are met, the maximum number of iterations is set to be as high as practical.

The Nelder-Mead simplex method utilizes a simplex structure to search in a n-dimensional space. A simplex is a polygon in n-dimensional space composed of *n + 1* vertices. To perform the optimization process, the Nelder-Mead method retrains the simplex with *n+1* vertices at each iteration. For the optimization problem in this research, each vertex of each simplex represented a value of fracture half-length, and *NPV* was calculated at each vertex at each iteration to evaluate the objective function.

The solution steps based on the Nelder-Mead simplex method are achieved by the following sequence. In addition, Figure 5.5 shows a simplified Flowchart of Nelder-Mead simplex algorithm used in this study.

1. Assume initial values of fracture half-length to form the initial simples.
2. The primary step to execute the optimization process is sorting. At the end of each iteration, three values of objective functions are calculated: the vertex with the highest *NPV* represents the best fracture half-length (x_{fh}), the vertex with *NPV* between the largest and the least values appears to be the next-to-worst fracture half-length (x_{fm}), and the vertex with the least *NPV* is the worst fracture half-length (x_{fl}). After completing the sorting process, the worst fracture half-length (x_{fl}) is replaced by the value derived from the average of the vertices (x_{favg}) at the next iteration using Equation 5.4 as expressed below:

$$x_{favg} = \frac{1}{n+1} \sum_{j=1}^{n+1} x_{fj} \qquad\qquad 5.4$$

3. Nelder-Mead simplex algorithm includes five search operations:

▪ Reflection: It merely reflects the worst fracture half-length (x_{fl}) on the average of the vertices (x_{favg}) to obtain a new value called the reflected fracture half-length ($x_{freflection}$), which are calculated using Equation 5.5 following the reflection search operation to calculate x_{favg}:

$$x_{frelection} = x_{favg} + a_1\left(x_{favg} - x_{fl}\right) \qquad\qquad 5.5$$

Based on the calculated *NPV* at $x_{freflection}$, the solution considers one of following search options described below:

(a) If $NPV(x_{fb}) \leq NPV(x_{freflection}) < NPV(x_{fm})$, x_{fl} is replaced by $x_{freflection}$ and the solution moves to Step 4.

(b) Expansion: if the $NPV(x_{freflection})$ is greater than $NPV(x_{fb})$, then the descending direction from x_{fl} to $x_{freflection}$ is correct, and the polygon is extended using Equation 5.6 to calculate $NPV(x_{fexpansion})$. IF $NPV(x_{fexpansion}) > NPV(x_{freflection})$, then $x_{freflection}$ is replaced by $x_{fexpansion}$ and the solution moves to Step.4; otherwise (i.e., if $NPV(x_{fexpansion}) < NPV(x_{freflection})$), then x_{fl} is replaced by $x_{freflection}$ and the solution moves to Step 4.

$$x_{fexpansion} = x_{frelection} + a_2 \left(x_{frelection} - x_{favg} \right) \qquad 5.6$$

(c) Inside contraction: If $NPV(x_{freflection})$ is less than $NPV(x_{fl})$, then a new point ($x_{fin\text{-}cont}$) is assumed in between the x_{fl} and x_{favg} using Equation 5.7, and $NPV(x_{fin\text{-}cont})$ is calculated. IF $NPV(x_{fin\text{-}cont}) > NPV(x_{fl})$, then x_{fl} is replaced by $x_{fin\text{-}cont}$ and the solution moves to Step 4. Otherwise, (i.e., IF $NPV(x_{fin\text{-}cont}) < NPV(x_{fl})$), then the solution goes to Step 3(e) (Shrinking).

$$x_{fin-cont} = x_{favg} - a_3 \left(x_{favg} - x_{fl} \right) \qquad 5.7$$

(d) Outside contraction: If $NPV(x_{fm}) > NPV(x_{freflection}) > NPV(x_{fl})$, then a new point ($x_{fout\text{-}cont}$) is assumed in between the $x_{freflection}$ and x_{favg} using Equation 5.8, and $NPV(x_{fout\text{-}cont})$ is calculated. IF $NPV(x_{fout\text{-}cont}) > NPV(x_{fl})$, then x_{fl} is replaced by $x_{fout\text{-}cont}$ and the solution moves to Step 4. Otherwise, (i.e., IF $NPV(x_{fout\text{-}cont}) < NPV(x_{fl})$), then the solution passes to Step 3(e) (Shrinking).

$$x_{fout-cont} = x_{favg} + a_3 \left(x_{favg} - x_{fl} \right) \qquad 5.8$$

(e) Shrinking: All the vertices of the simplex except x_{fb} should be shrunk using Equation 5.9:

$$x_{fi} = x_{fb} + a_4 \left(x_{fi} - x_{fb} \right) \qquad 5.9$$

Nelder and Mead (1965) recommended that the values $a_1 = 1$, $a_2 = 2$, $a_3 = 0.5$ and $a_4 = 0.5$ be employed (Gavin, 2013).

4. Termination criteria is ascertained by calculating the convergence threshold using Equation 5.1. If the convergence threshold is less than 1%, then the solution achieves the final solution. Otherwise, a new iteration should be started from Step 2 based on the updated values of x_f.

5.4.2 Simplex non-linear method

The simplex non-linear method was an improved form of the simplex optimizer (Nelder and Mead, 1965), explained above, which considers non-linear and linear constraints. Regarding the mechanism of search operations, they are the same as the operations of the downhill simplex method explained in Section 5.4.1. In terms of input, all required data are similar to the data required for downhill simplex except the constraints that could be nonlinear and linear. The convergence threshold that is calculated using Equation 5.1 was assigned below 1%.

Input initial values of x_f
(x_{fb}, x_{fb} and x_{fl})

Form initial simplex and calculate
NPV at each vertex

Sorting of values of x_f based on the *NPV*

Reflection

If $NPV(x_{fb}) \leq NPV(x_{freflection})$

$< NPV(x_{fm})$

No

Yes

Expansion, Contraction, or Shrinking

Replacement the worst values of x_f

If convergence threshold
less than 1%

No

Yes

Optimum Solution
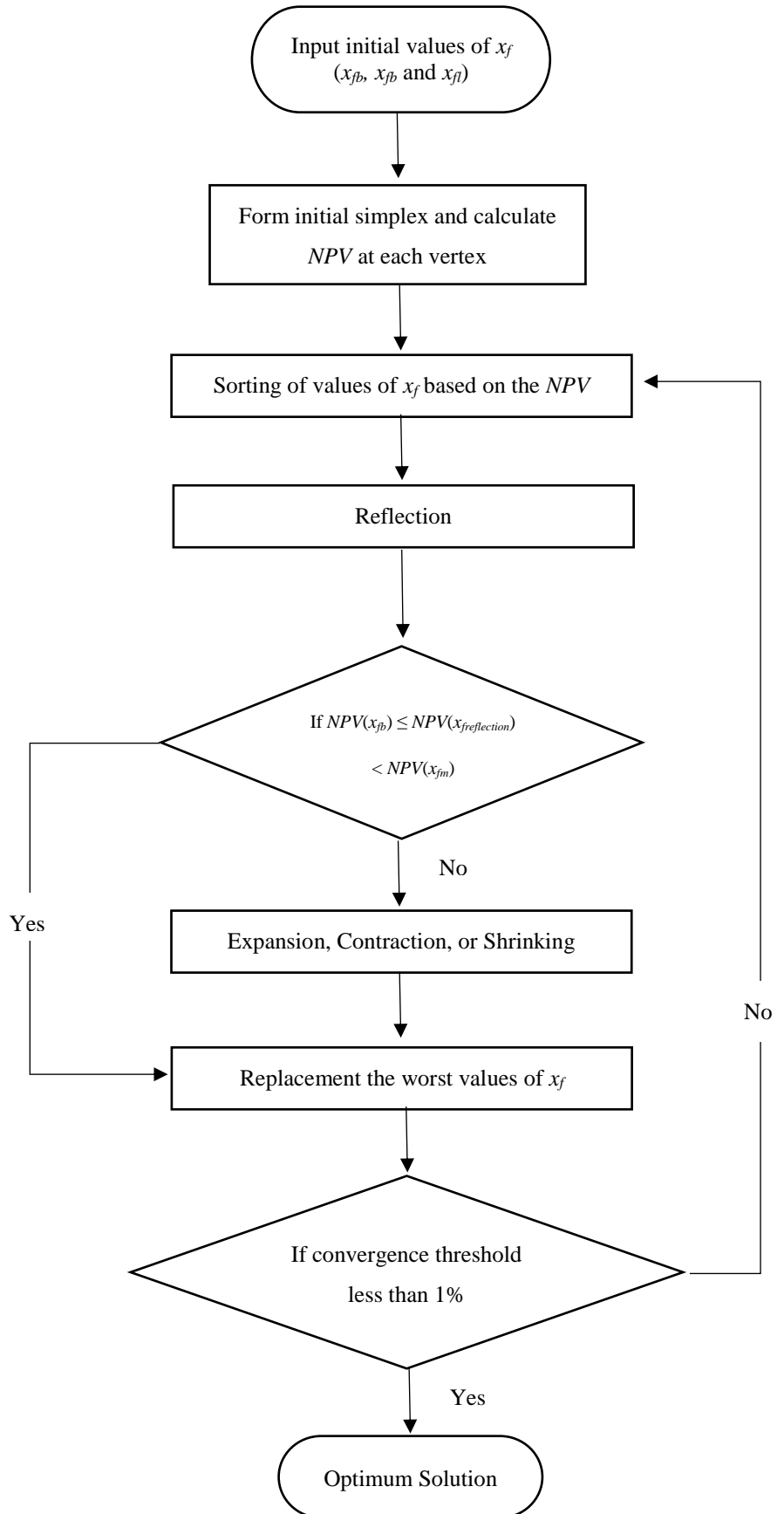
Figure 5.5 Flowchart of Nelder-Mead simplex algorithm used in this study

5.4.3 Evolutionary strategy method

Evolutionary computations have been vastly utilized to solve different kinds of optimization problems (Arnold and Beyer, 2002; Coello et al., 2007; Eiben and Smith, 2003; Kramer, 2016; Mezura-Montes and Coello, 2005). One of the most important evolutionary algorithms from the area of evolutionary computation is an evolution strategy (ES), which is considered as a global optimization algorithm (Brownlee, 2011; Hans-Paul Schwefel, 1995). ESs have been broadly employed to solve numerous optimization problems (Greenwood and Liu, 1998; Kramer, 2016; Mezura-Montes and Coello, 2005; F. Schweitzer et al., 1997), and have played a noteworthy role in optimizing the performance processes in the oil and gas industry (Bouzarkouna et al., 2012; Foroud et al., 2018; Hamdi et al., 2015).

Evolution strategies (ESs) are the algorithms which simulate on the basis of the principle of natural evolution. The strategies are based on the same main processes of natural evolution, and primarily use selection, recombination and mutation as search operators (Back et al., 1991; Kramer, 2016; Kramer et al., 2011; Michalewicz, 1996; Hans-Paul Schwefel, 1995). ESs were first recommended by H-P Schwefel (1965) and Rechenberg (1965) as a simple form known as (1+1), which operates on the grounds of two designs; a parent and a child (Beyer and Schwefel, 2002; Foroud et al., 2018; Lopes et al., 2016). The evolutionary strategy (ES) optimizer was grounded on evolutionary concepts, and has the capacity to evaluate various initial generations of cases, defined as parents. Successive generations were formed from promising parents in each prior generation applying search operations as selection, recombination and mutation. A set of strategy parameters should be stated defined, which include the mixing number (ρ), number of parents (μ), offspring (λ) per generation and others as listed in Table 5.1.

The ES mainly consists of four stages categorized into one initialization stage and three optimization mechanisms: selection, recombination, and mutation. In the initialization stage of the evolution strategy, a population consisting of a certain number of candidate solutions (x_{fi}) is generated, where the initial values of fracture half-length should be less than or equal to the upper bound and greater than the lower bound as shown below:

$$x_f^L < x_f \leq x_f^U$$

Where:

x_f^L is the lower bound of fracture half-length, ft.

x_f^U is the upper bound of fracture half-length, ft.

Then, the ES optimizer operates the selection mechanism to assess the objective function of a population of cases, so the best cases are selected to transit into the next generations. Recombination is operated to exchange the variables between the selected cases, so that the subsequent generations of cases can be formed. The recombined cases use an arithmetic average to estimate the values for the subsequent generation of cases. Finally, the mutation is run to make outliers from the present trend in the data, thus that new spaces of the problem's geometry can be investigated at the same time.

The ES has been developed since it's innovation by students at the Technical University of Berlin (Rechenberg, 1965; H-P Schwefel, 1965) until the present. The main historical development of ES focuses on the number of parents and children per generation, so the four main jumps in the trip of ES are:

1. (One parent + One child) ES with binomially distributed mutations which was founded by H-P Schwefel (1965).
2. (One parent + One child) ES with Gaussian mutations which was founded by Rechenber (Rechenber, 1971, 1973).
3. (μ+1) or steady-state ES which was developed by Rechenberg (1994). This ES is considered an important development because it changes the mechanism of the selection scheme from generation replacement of the main population, but rather replaces one individual per iteration of the main recombination-mutation-selection round of the solution (Bäck et al., 2000).

Generally, the fulfilment of the ESs mainly relies on the adjustment of the mutation strength. All of the above ESs mostly tend to decrease the impact of mutation intensity (Beyer and Schwefel, 2002). Schwefel formulated the following developed ESs in his higher degree research (Hans-Paul Schwefel, 1974, 1975).

4. (μ+λ) ES, the main development with this kind of ES is that the parents generated more than one child, and all parents and children compete directly, where the best out of the parents and children should be selected, and they will be parents of the next generation (Bäck et al., 2000).

5. (μ, λ) ES, the selection mechanism in this strategy is working to choose the best among the children only, regardless of the quality of the parents compared to the new generation.

6. $(\mu/\rho \overset{+}{,} \lambda)$ ES poses the components of the state-of-the art of evolution strategy through accomplishment of self-adaptation. A new parameter, the mixing number (ρ), is considered in this kind of ES and refers to the number of parents participating in the procreation of one child. The mixing number controls the recombination and mutation processes to accelerate the convergence towards the maximum net present value because it provides intermediate recombination and an extra heuristic for responding to convergence.

In the light of the classification of the evolution strategy, $(\mu/\rho \overset{+}{,} \lambda)$ ES was used in this study. $(\mu/\rho \overset{+}{,} \lambda)$ ES is an iterative optimization technique which can be modelled as continuous iterations of generating and assessing candidate solutions to a specific problem.

In this study, a candidate solution is considered to be a set of the fracture half-lengths (decision variables) that defines the production area in the reservoir (problem space). Assessing each value of fracture half-length (candidate solution) is achieved based on the value of *NPV* which corresponds to the candidate's decision variables. The assessing stage was achieved using the reservoir simulation model and the economic calculation. After each assessment of the *NPV*, the optimization algorithm generates new fracture half-lengths, which are evaluated based on the corresponding *NPV*. The optimization scheme consists of an optimization algorithm and reservoir simulation model, which work towards finding the optimum solution of the problem (i.e. the maximum *NPV* at the optimum fracture half-lengths) iteratively until meeting the convergence criteria. Table 5.1 presents the design parameters used in ES in this study.

Table 5.1 The design parameters used in evolution strategy

The parameter	The value
Number of parents, μ	20
Number of children, λ	10
Mixing number, ρ	2
Convergence threshold	1%
Maximum number of simulation runs	400

Figure 5.6 explains the steps and directions of the solution procedure of the evolution strategy.
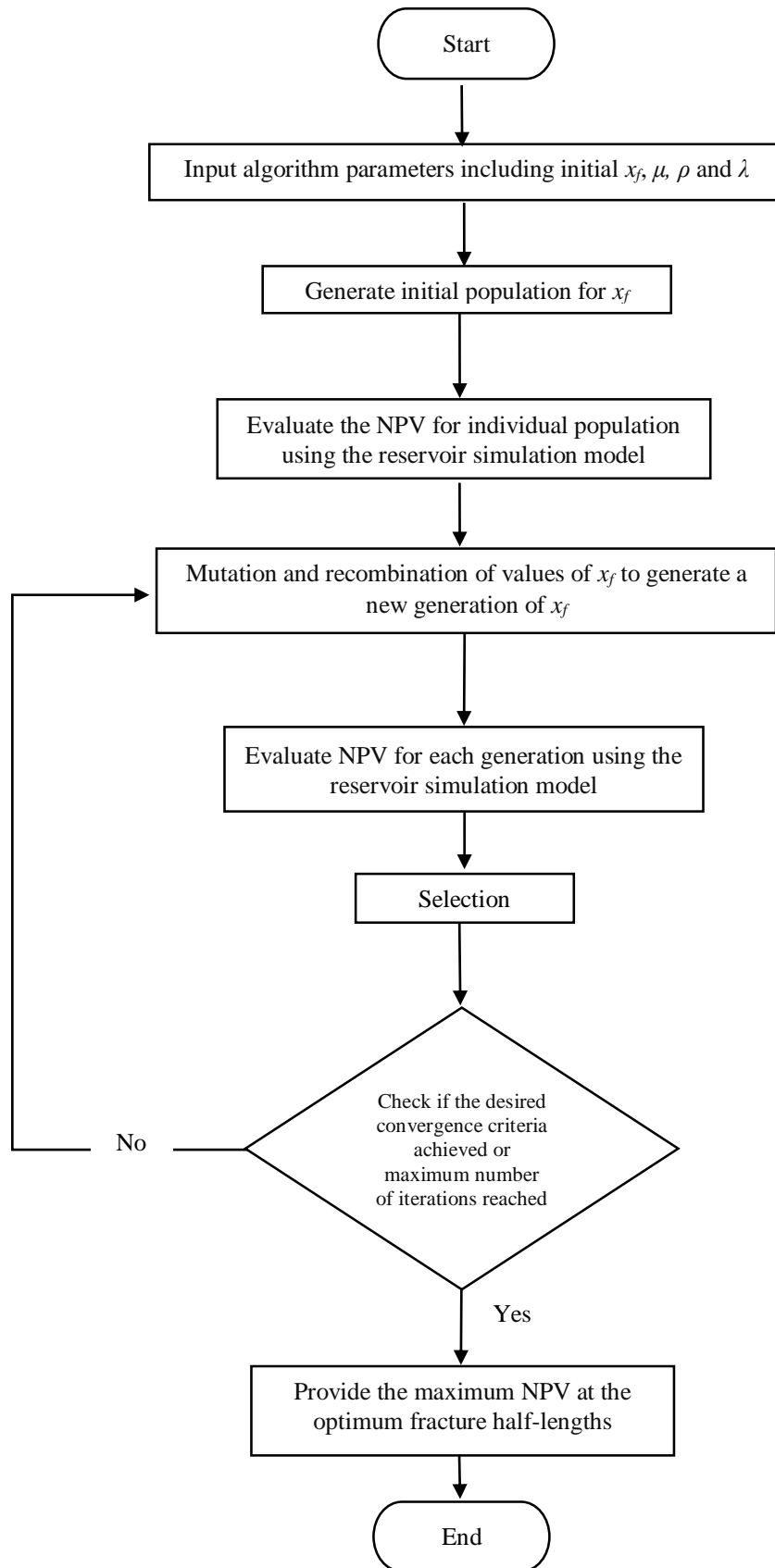
Figure 5.6 Flowchart of the evolution strategy

5.4.4 Neural net method

The neural net method was based on the simplex optimizer algorithm but applies to a black-box sigmoid-type neural net (Akram, 2011; Couet et al., 2007), although it combines neural network processing for faster execution and higher efficiency by considering cases in a parallel network. The optimizer requires limited inputs and the maximum allowed number of iterations. Similar to the other optimizers, a high maximum number of allowed iterations was assigned to avoid an unsuitable termination of the optimization operation. The optimizer employed a sigmoidal multilayer perceptron network, where data streamed from an input layer to the hidden layer nodes, and then to the output layer as a result. The number of hidden layer nodes influenced the convergence success and the complication of the network. The optimizer can adjust the number of hidden layer nodes for enabling an optimal arrangement for a solution.

This study used the neural net optimizer to find the optimum values of fracture half-length to achieve the maximum *NPV*. As mentioned above, the neural net optimizer is a combined model consisting of the downhill simplex method and neural network technique that uses sigmoid function as an activation function (Vasper et al., 2016). This optimizer trained the neural network using *n+1* simulations, where *n* is the number of decision variables. The optimizer evaluates the inputs, assumes fracture half-lengths based on the evaluation of objective functions that are calculated using the reservoir simulator. The optimizer adapted the formatted networks based on the updated values of the objective function (*NPV*) and fracture half-length (decision variables). The activation of the neural network is achieved using sigmoid function calculated for our study using Equation 5.10.

$$\sigma\left(z\right) = \frac{1}{1 + e^{-z}}$$ 5.10

Where:

z is the parameter of the sigmoid function that it is calculated using Equation 5.11.

$$z = \sum_{i=1}^{m} w_i\, x_{fi} + bias$$ 5.11

Where:

153

w_i is weight that connects between each two neurons from two different layers of the neural network. It means these weights constrain how initial values of fracture half-lengths are related to calculated values of fracture half-lengths of hidden layers after each iteration.

x_{fi} is initial values of fracture half-length that represent the inputs of the network.

Figure 5.7 explains a typical feedforward neural network consisting of the following processes: input, weighting, summation, biasing, activation, and converging.

Bias are the values which are added to the sums calculated at each x_f except the input x_f during the feedforward phase.

The training operation of the neural network requires an appropriate set of data (i.e., input (x_{fi}) and target output (NPV_f)). Throughout the training operation, the weights and biases of the network are iteratively tuned to minimize the difference between the initial calculated NPV and the final NPV (i.e., to achieve convergence threshold of less than 1%).
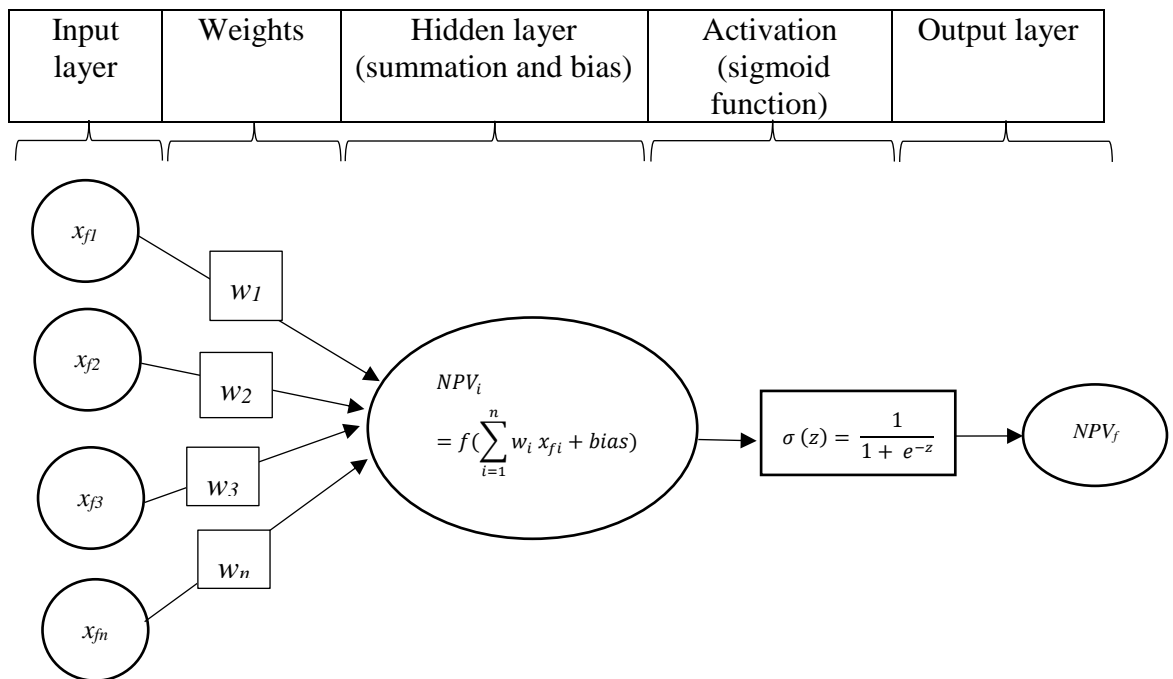
Figure 5.7 A typical feedforward neural network

5.4.5 Genetic algorithm method

The genetic algorithm(GA) can be considered an efficient tool for the optimization of many real problems (Coley, 1999; Simon, 2013; Sivanandam and Deepa, 2008). Genetic algorithms are the earliest and most vastly utilized evolutionary algorithms (Back, 1996; Bäck et al., 1997; Simon, 2013), and are considered a robust optimization technique for engineering optimization, and have been broadly applied across a wide variety of field applications (Bäck, 1997; Coello, 2000; Nelson et al., 2013; Parmee, 1998) for more than three decades. The GA, initially proposed by Holland (1975), solves both constrained and unconstrained optimization problems based on natural selection processes. The selection processes are driven by biologically motivated stochastic population-based search methods, and are modelled on the principles of natural selection and genetic recombination (Rao, 2009). The optimization technique essentially utilizes a collection of functions like genetics and evolution to determine the optimum solution of complex problems, especially where it is difficult to search all possibilities of the evaluation of function. The key functions of genetic algorithm are initialization, selection, crossover and mutation.

For a certain problem, the first step is initialization, where a population of candidate solutions (individuals), including high and low quality, are initiated. Each individual consists of variables (genes) connected to each other, as shown in Figure 5.8. The variable is coded according to a binary system. Figure 5.8 shows the construction of the population and the equivalent value of each individual as a fracture half-length.

The second step is selection in which all individuals are evaluated based on the value of the objective function (fitness) where the individuals with high fitness have a high probability to be parents to generate new children, while the individuals with low fitness have a low probability to survive. Where, the roulette wheel is considered the selection operator because it is the most appropriate, and commonly used selection scheme in genetic algorithm. The roulette wheel works to allocate probability to survive for certain fracture half-lengths (individuals), which have the highest *NPV* (fitness). This probability to survive (to be the parents of the next generation) corresponds to the ratio of individual fitness to the average population fitness.

The third step is the crossover in which each set of two good individuals who are preferred in the selection step merge together for generating new children and are

considered a new generation by exchanging part of the variables between the individuals to form new children, as shown in Figure 5.9.

The fourth step is the mutation in which part of the variables of the individuals are randomly flipped to generate new children, as shown in Figure 5.10. Mutation is relatively rare, so the mutation probability should be low. It is assumed to be 0.05 in this study, where mutation probability ranges from zero (no mutation) to one (mutate every time). Mutation is significant because it permits the genetic algorithm to explore new prospect solutions to the problem. If some spaces are missing from the population that is created in the initialization or crossover, then mutation supplies the possibility of bringing individuals from the missing spaces into the population. Therefore, mutation drives the genetic diversity in the population.

After the initialization step is done, the population replacement is performed through the cycle of selection, crossover and mutation implemented to the initial population, to generate a new population. The cycle of selection, crossover and mutation is repeated until reaching the maximum number of iterations or achieving the convergence threshold.
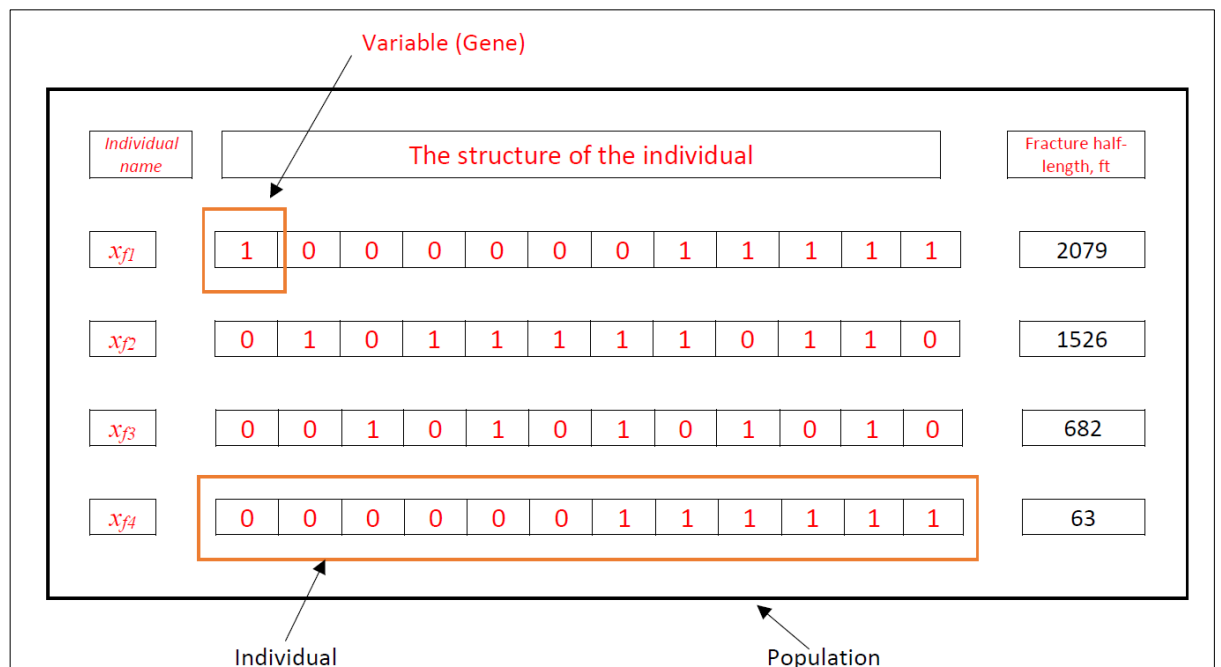
Figure 5.8 The sample of structure of population in genetic algorithm
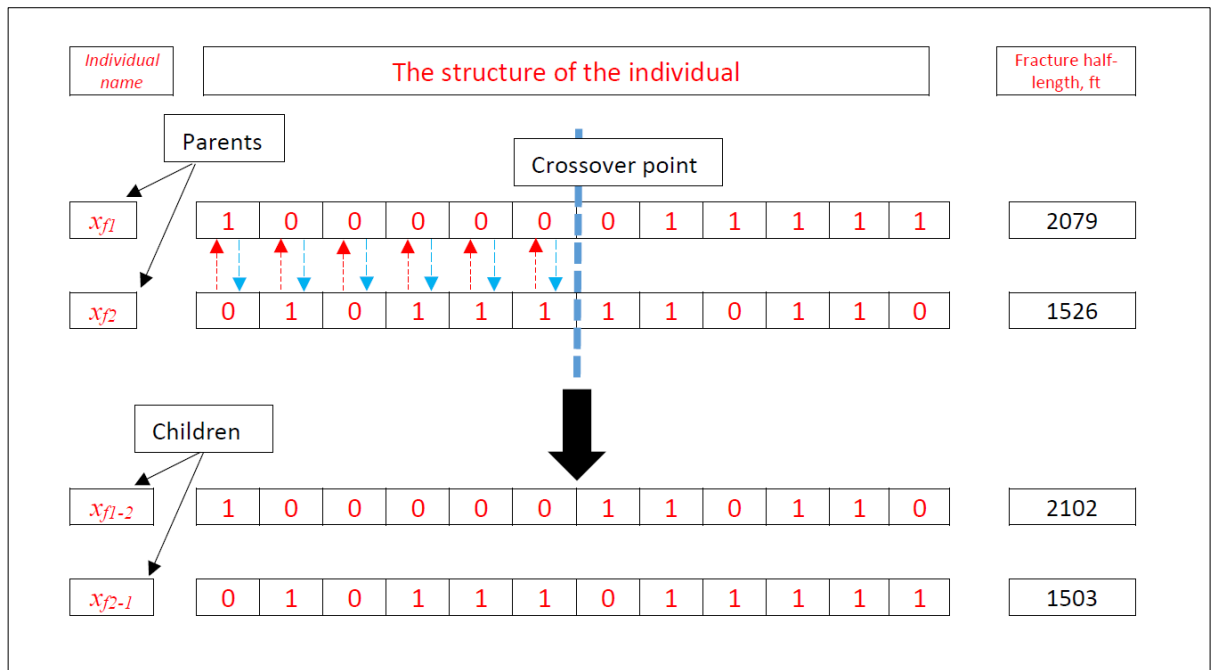
Figure 5.9 The sample mechanism of crossover in genetic algorithm
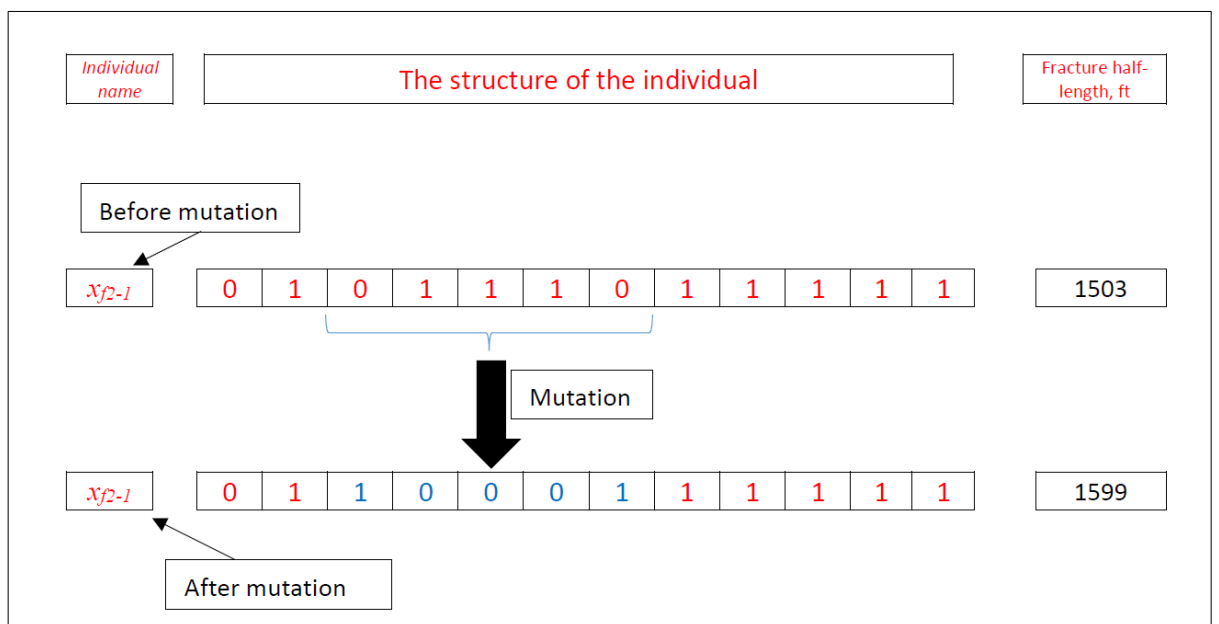
Figure 5.10 The sample mechanism of mutation in genetic algorithm

In this study, the GA technique was utilized to optimize the gas production of hydraulic fractured vertical wells in TGR, where it is used to search for the optimum fracture half-length (individuals) to maximize the objective function, *NPV*, (termed as fitness in GA technique). Table 5.2 lists the parameters used in this study to utilize the GA technique. The solution procedure of the GA is highlighted below:

157

1) Assume the initial population of fracture half-length (individuals).

2) Calculate *NPV* of each fracture half-length (individual) in that population using the reservoir simulation model.

3) Evaluate the objective function (fitness), *NPV* for each fracture half-length (individual) in that population.

4) Select the values of fracture half-length corresponding to the highest values of *NPV* (best-fit individuals) for reproduction.

5) Generate new individuals through crossover and mutation processes to generate new values of fracture half-length (children) that form a new population.

6) Calculate the *NPV* (individual fitness) of new population.

7) Check if the solution achieves the convergence threshold (1%) or reaches the maximum number of assigned iterations set as termination criteria. Meeting any of these criteria yields the optimal solution of the problem. Otherwise, the cycle of selection-crossover-mutation should be repeated from Step.3. The maximum number of iterations is considered to be 400 in our study based on experience.

Table 5.2 The properties of the parameters used in this study to utilize GA

The parameter	The value
Population size	40
Maximum number of generations	8
Mutation probability	0.05
Selection operator	Roulette wheel
Convergence threshold	1%
Maximum number of simulation runs	400

5.5   The reservoir simulation models

Twelve reservoir simulation models considered in this study include nine mechanistic models and three real models. The nine mechanistic models are developed based on three single well models and six multi-well models. The three real models are developed based upon one single well model and two multi-well models. The minimum flowing bottom-hole pressure is assumed to be100 psi. The maximum

allowable fracture half-length is limited to 2500 ft, with fracture width of 0.2 in, and fracture height is 400 ft. The simulation run time for all models is considered to be 30 years.

5.5.1 The mechanistic models

Table 5.3 shows the properties of the mechanistic models. The porosity and the thickness of all mechanistic models are assumed to be 10% and 400 ft, respectively. The base case reservoir and fracture properties are provided in Table 5.4. All reservoir models are considered to have a closed outer boundary, and its top and bottom boundaries are also considered to be sealed. All models are square with an area of 640 acres to ensure the pressure pulse reaches the boundary. Figure 5.11 depicts a sample of the mechanistic models (3D view) considered in this study. The models cover three permeabilities: 0.01, 0.05, and 0.1 mD. The well spacing between the wells is 1320 ft. Models 1, 2 and 3 are single well models, while models 4 to 9 are multi-well models. The fracture half-length is assumed to be the same for all wells in models 4 to 6, and the fracture half-length of all other wells are considered to be different.

Table 5.3 The properties of the mechanistic models

Model No.	Reservoir permeability, mD	Number of the wells	Number of decision variables
1	0.01	1	1
2	0.05	1	1
3	0.1	1	1
4	0.01	3	1
5	0.05	3	1
6	0.1	3	1
7	0.01	3	3
8	0.05	3	3
9	0.1	3	3

Table 5.4 The properties of the reservoir and fractures of the mechanistic models in this study

Reservoir pressure	6500 psi
Reservoir temperature	200°F
Reservoir area	640 acres
Porosity	0.10
Permeability in x-direction (k_x) = Permeability in y-direction (k_y)	According to the model number as explained in Table 5.3
Permeability in z-direction (k_z)	0.00001 mD
Fracture permeability	10000 mD
Fracture height	400 ft
Fracture width	0.2 inch
Fracture orientation	90°
Number of grids	10816
Grid size (x and y directions)	50 ft × 50 ft
No. of grids in x, y and z directions	104×104 ×4
Gas specific gravity	0.65
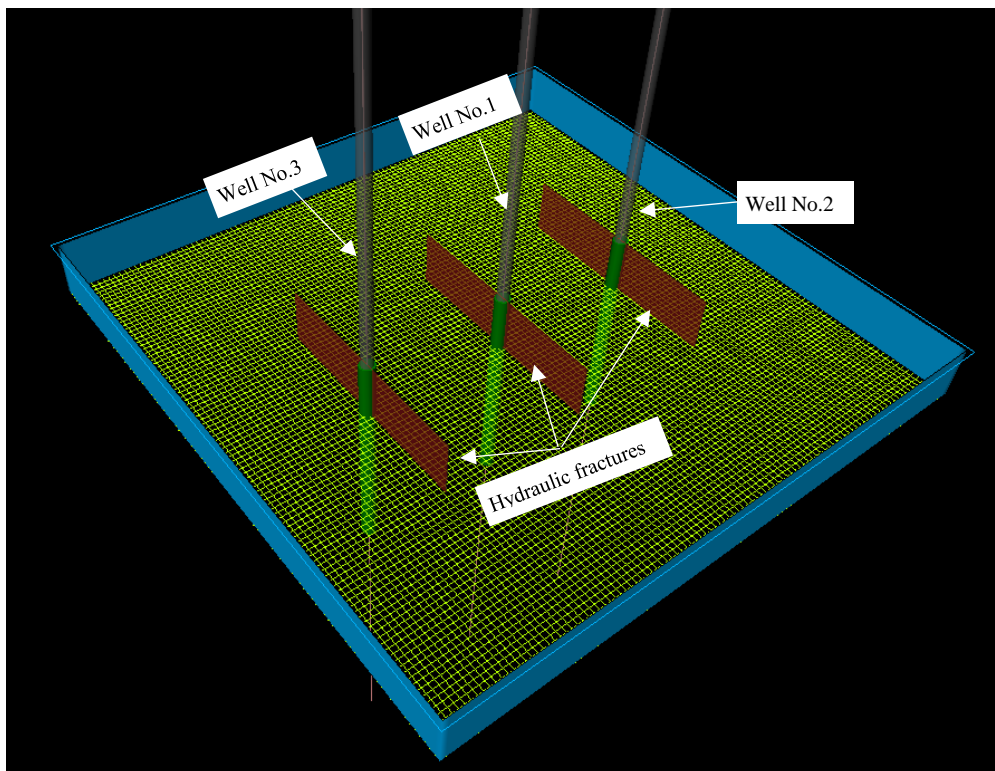
Figure 5.11 A sample of the mechanistic models (3D view)

5.5.2 The real models

Table 5.5 shows the properties of the real models. All models are based upon a real presentative reservoir formation from the Middle Eastern region. All models were developed using PETREL and Eclipse simulators. The reservoir formation includes ten wells. The reservoir formation is gas bearing and is very heterogeneous. The reservoir has a closed outer boundary and its top and bottom boundaries are also sealed. The petrophysical analysis of the reservoir formation is conducted based on the well logs and core samples of the ten wells. Figure 5.12 and Figure 5.13 present the 3D porosity and permeability maps, respectively. The top of the reservoir formation is at a depth of 11200 ft. In addition, Figure 5.14 and Figure 5.15 display frequency histograms for permeability and porosity of the data of all nine wells. Table 5.6 provides the properties of the reservoir formation and fractures for all real models. Figure 5.16 shows the locations of the three hydraulic fractured vertical wells considered in the real models. Model 10 is a single well model, while models 11 and 12 are multi-wells models. The fracture half-length is assumed to be the same for all wells in model 11. On the other hand, fracture half-length for all wells in model 12 are considered to be different. The distance between Well No 1, and each of Well No 2 and Well No.3 are 29560 ft and 26520 ft, respectively. All reservoir simulation studies for both mechanistic and real models are conducted with an objective to evaluate the performance and effectiveness of different optimization techniques discussed earlier. For instance, Figure 5.17 and Figure 5.18 explain two dimensional and three-dimensional pressures distributions for one reservoir simulation run. Figure 5.17 and Figure 5.18 illustrate the pressure distribution caused by producing from three vertical fractured wells and each well has an independent fracture half-length.

Table 5.5 The properties of the real models

Model No.	Number of the wells	Number of decision variables
10	1	1
11	3	1
12	3	3
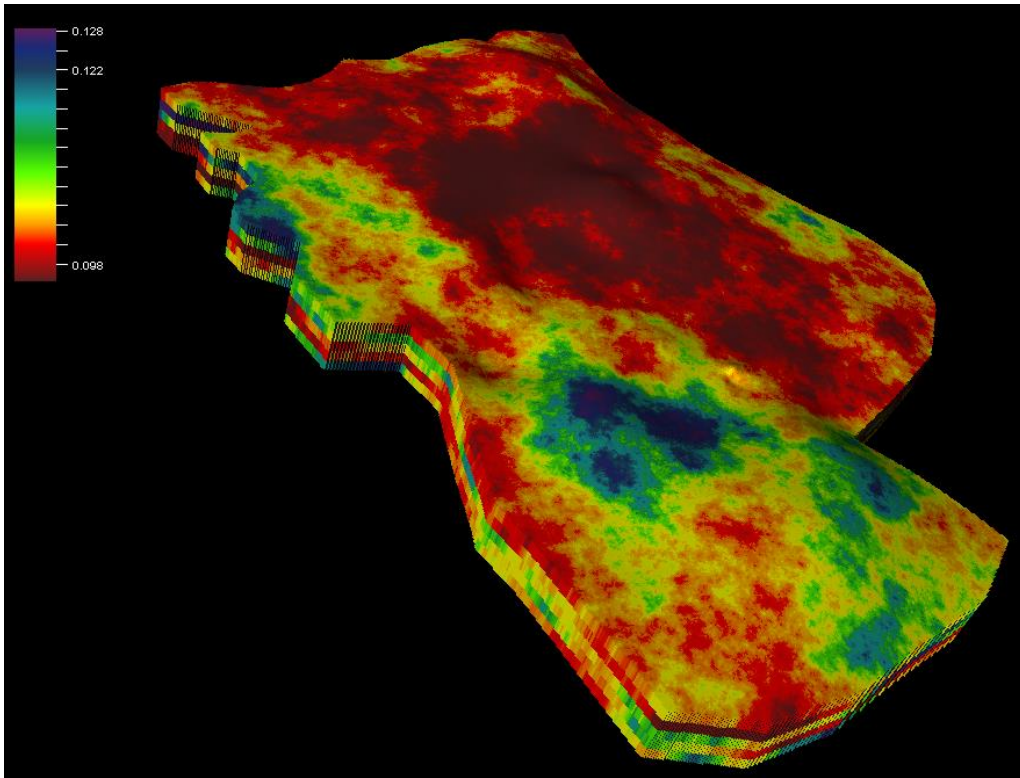
Figure 5.12 - 3D porosity maps of the real models
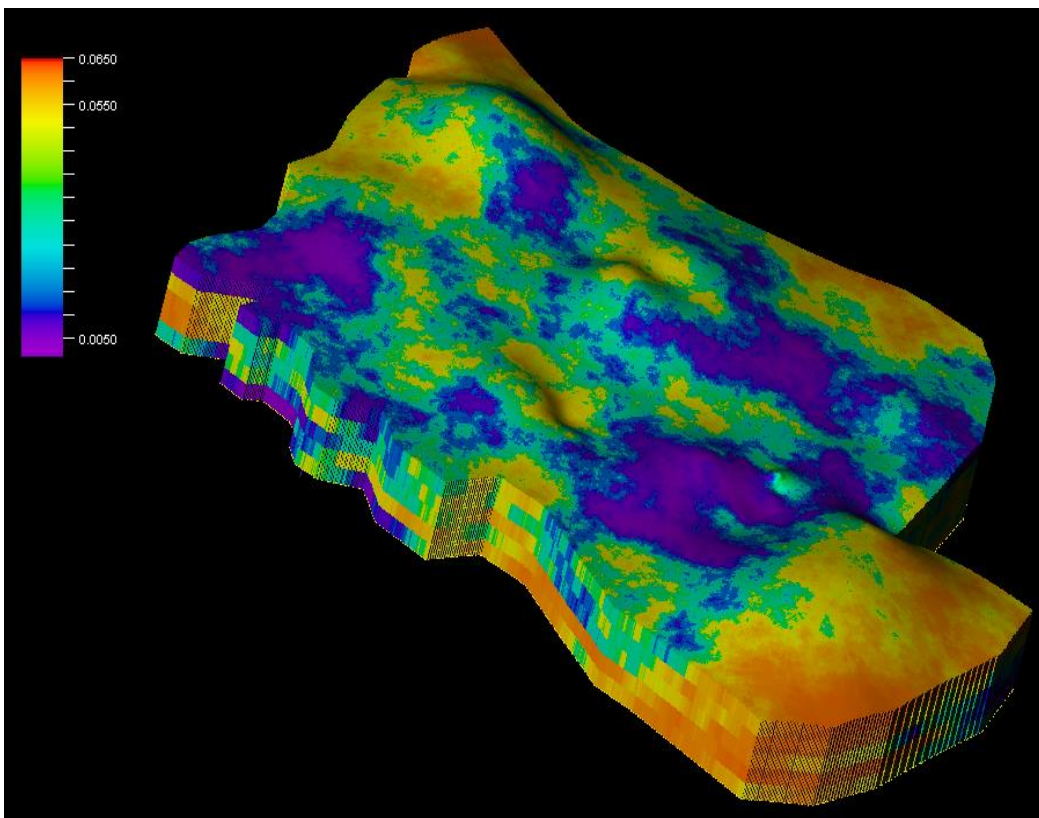
Figure 5.13 - 3D permeability maps of the real models
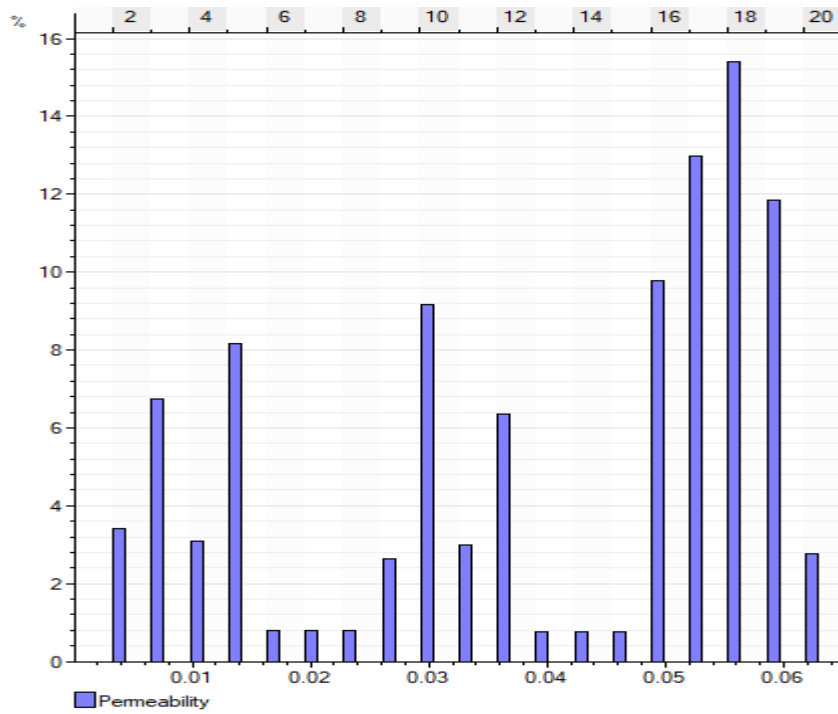
Figure 5.14 Frequency histogram of the permeability data for all wells
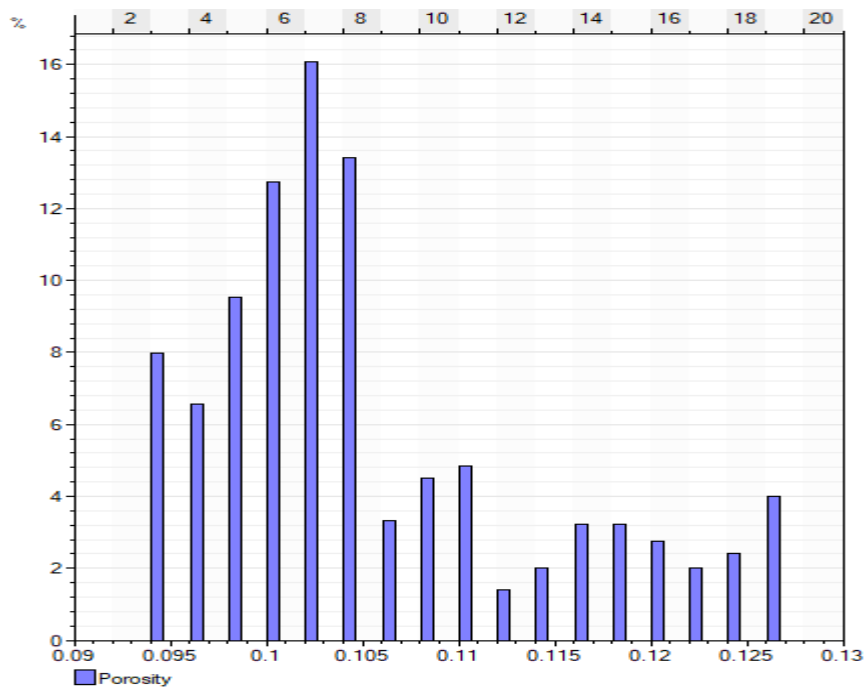
Figure 5.15 Frequency histogram of the porosity data for all wells
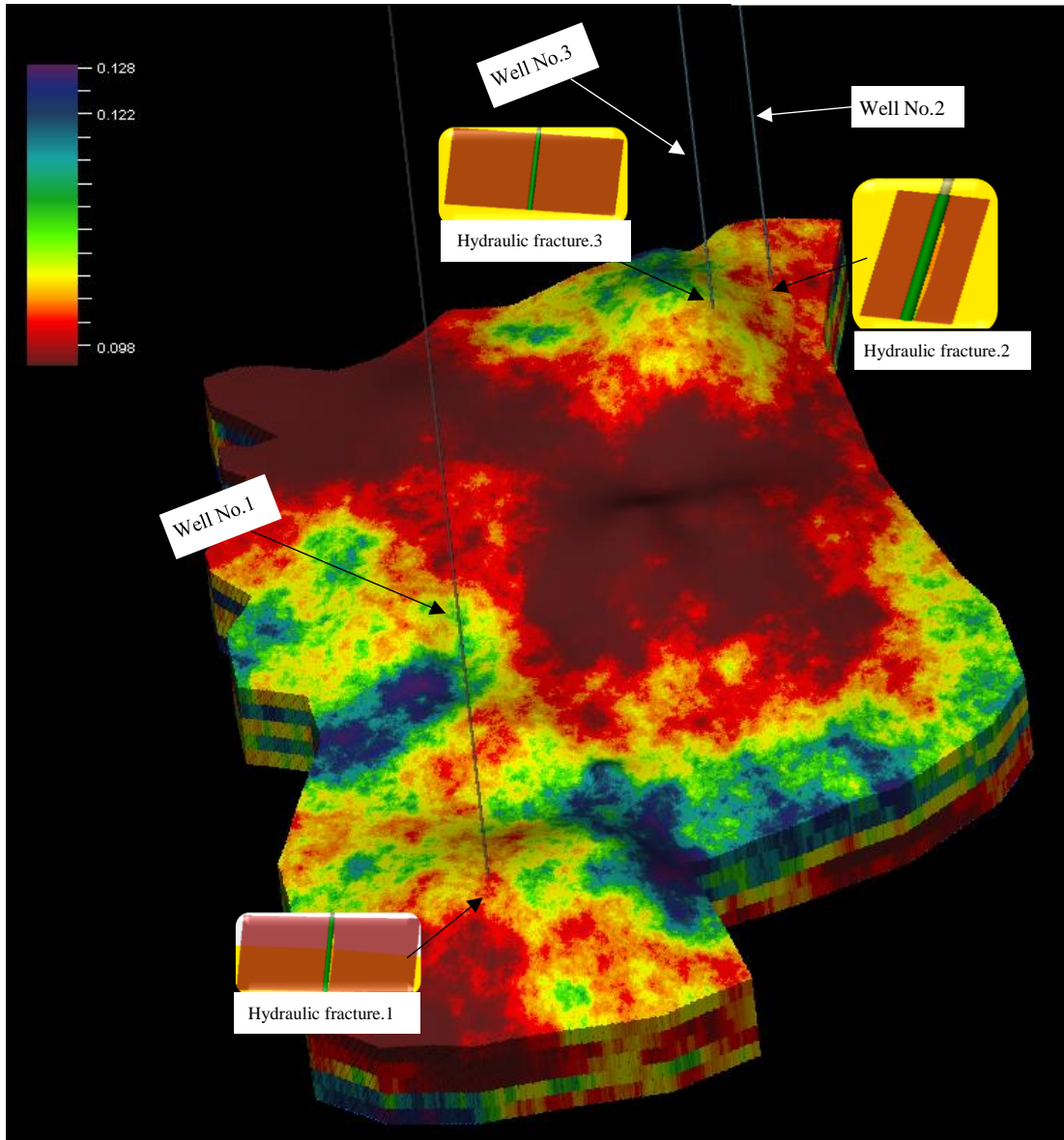
Figure 5.16 The locations of the three fracture vertical wells used in the real models

Table 5.6 The properties of the reservoir and fractures of the real models in this study

Reservoir pressure	6500 psi
Reservoir temperature	200°F
Reservoir area	18285.8 acres
Porosity	Heterogeneous - distribution is displayed in Figure 5.12 and Figure 5.15
Permeability in x-direction (k_x) = Permeability in y-direction (k_y)	Heterogenous- distribution is displayed in Figure 5.13 and Figure 5.14
Permeability in z-direction (k_z)	0.00001 mD
Fracture permeability	10000 mD
Fracture height	400 ft
Fracture width	0.2 inch
Fracture orientation	90°
Number of grids	377568
Grid size (x and y directions)	50 ft $\times$ 50 ft
No. of grids in x, y and z directions	552×684 ×4
Gas specific gravity	0.65
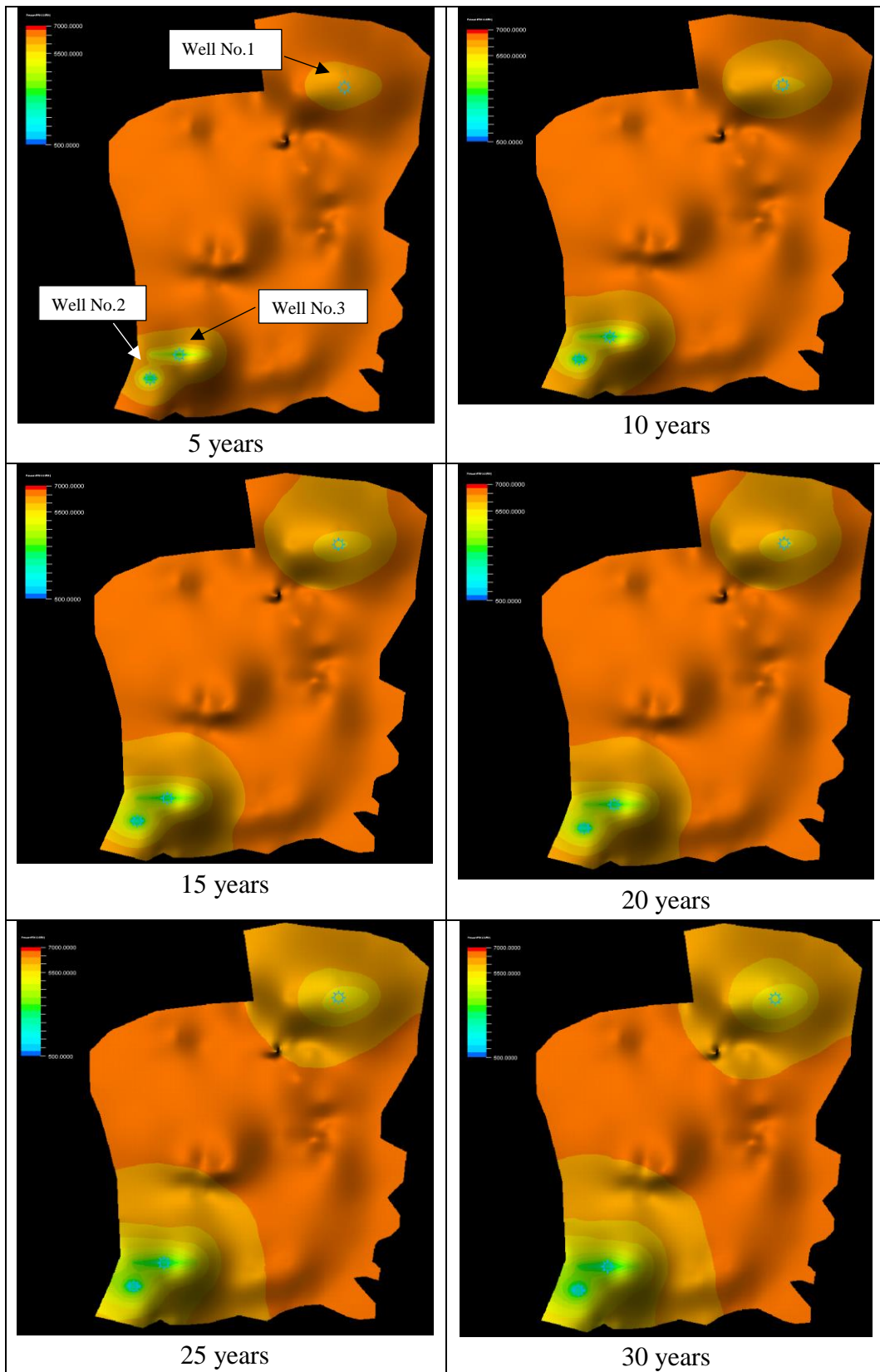
Figure 5.17 Pressure distribution in the reservoir through the production time (2D top view)
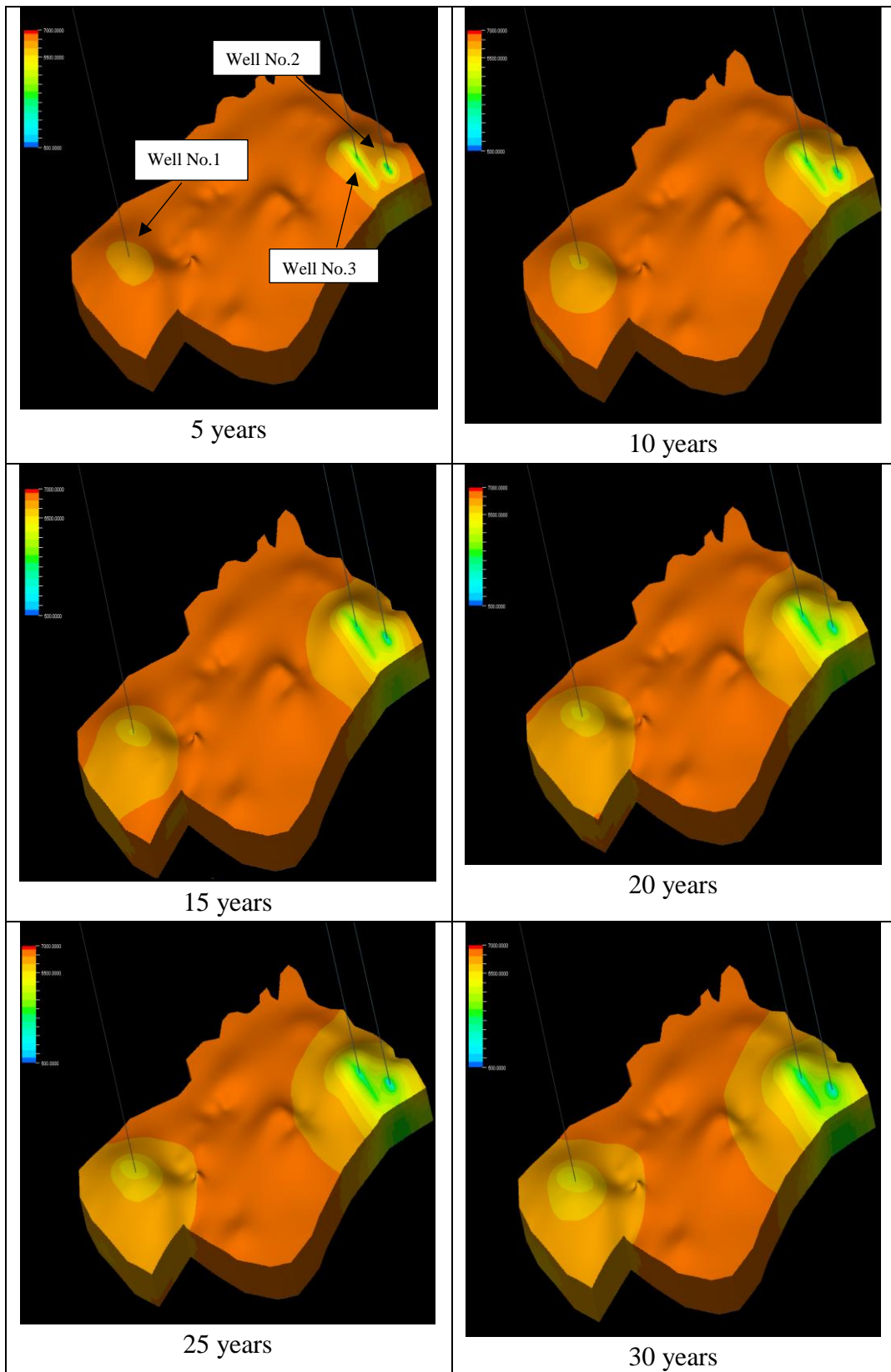
Figure 5.18 Pressure distribution in the reservoir through the production time (2D top view)

5.6 Optimization of fracture half-length

Optimization techniques are used to find the maximum net present value (*NPV*) or cumulative gas production (*G_p*) at the optimum fracture half-length for hydraulic fractured vertical wells in TGRs. The formulation for optimization of the hydraulic fracture half-length problem encounters different challenges: the high nonlinearity of pressure change with respect to time and space; the heterogeneity of the porous media, the compressibility of the gas, the complexities in well configuration and completion, reservoir size, and the number of vertical fractured wells where each x_f is a decision variable. Therefore, the decision variables in this study are fracture half-lengths for all vertical fractured wells involved in the production plan.

To setup the model, the *G_p* and *NPV* are considered as objective functions, while the fracture half-length is considered a decision variable. The fracture half-length, x_f is assumed to be bounded by $0 \leq x_f \leq 2500$ft. The maximum allowable number of reservoir simulation runs are limited to 400 to terminate the optimization process if the convergence criteria are not met. This number is set based on the researcher's experience running many simulations and the practical feasibility. Models 1, 2, 3, 4, 5, 6 and 10 represent the single decision variable optimization problem because those models are specified for single well cases, and have been formulated under the assumption that all wells inside each model have the same fracture half-length (x_f). Models 7, 8, 9, 11 and 12 are multi-decision variable optimization cases and the multiple wells are handled with different fracture half-lengths.

Five optimization techniques: genetic algorithm, evolutionary strategy, downhill simplex method, simplex non-linear method, and neural net, have been exercised in this study. These optimization techniques are selected because these are the most widely practiced derivative free optimization algorithms typically used in petroleum engineering, reservoir simulation, statistics, and sciences (Conn et al., 2009; Forouzanfar et al., 2010; Juell et al., 2010; Pham et al., 2011), and in the petroleum industries.

Each optimization technique has advantages and disadvantages (Jayanti, 2018), so it is difficult to define a unique optimization technique that has the ability to figure out all problems with the same performance (Luchian et al., 2015). In this view, this study emphasized identifying the most viably efficient optimization technique capable of

achieving relatively fast convergence (i.e., minimum number of simulation runs) towards estimating the maximum cumulative gas production or net present value at optimum fracture half-length for the hydraulic fractured vertical wells in tight gas reservoirs. The study also investigated the influence of factors associated with reservoir heterogeneity on simulation convergences.

PETREL/ECLIPSE commercial numerical reservoir simulator (Schlumberger, 2017a, 2017b) is considered the petroleum industry standard and most widely acceptable numerical simulator. This simulator is explicitly used for this study. As described earlier, 8000 numerical simulation runs on mechanistic and real models are carried out to evaluate the performance of all five optimization techniques. The cumulative gas production (G_p) as a function of fracture half-length (x_f) obtained based upon five optimization techniques are shown in Figure 5.19 to Figure 5.26, from which it can be seen that similar results in relation to cumulative gas production are achieved, regardless of the optimization techniques considered for all models. Similar results are obtained for net present value as a function of fracture half-length for all models, as stated in Figure 5.27 to Figure 5.34.

The number of reservoir simulation runs, and the corresponding simulation time required to achieve the optimum x_f based on each optimization technique is presented in Figure 5.35. The maximum G_p and NPV at optimum fracture half-length using the five optimization techniques for all reservoir models as presented in Table 5.7. demonstrates that the optimal solution based on five different optimization techniques for each model appeared to be almost the same. However, the number of reservoir simulation runs or the required reservoir simulation time to achieve the convergence to the optimum solution varied significantly in each optimization technique (Figure 5.35 and Figure 5.36). However the nonlinear simplex optimization technique provided the first convergence resulting in significant low numbers of simulation runs or simulation time compared to the four other techniques for models 1-7, 9, 10-11, while neural net provided the first convergence for models 8 and 12. The results indicate that the simplex non-linear technique appeared to be the most efficient optimization technique as it converged with very low numbers of simulation run times for all single decision variables (i.e., x_f), whether for single or multiple well models under reservoir permeability ranges from 0.01 mD to 0.1 mD. In addition, the simplex non-linear technique appeared to be the most efficient optimization technique to

determine the optimum fracture half-length for multivariable decision cases for multiple wells models for permeability of 0.01 mD and 0.1 mD. While, the neural net based optimization technique appeared to be a more efficient optimization technique for optimizing the fracture half-length of multivariable decision cases for multiple wells models with permeability 0.05 mD as shown in models 8 and 12. This study also demonstrates that the genetic algorithm and evolution strategy based optimization techniques are very time-consuming and have far longer simulation runs than the other three techniques, as shown in Figure 5.35 and Figure 5.36, which is not desirable in a routine industry environment. Such time-consuming simulation tasks can pose huge challenges with respect to achieving the project milestones, and can result in detrimental effects on decision making. For instance, the evolution strategy-based optimization technique took more than 1000 minutes to optimize the fracture half-lengths for the wells in model 12, while the neural net took only 90 minutes (i.e., 11 times faster) to accomplish the same task in the same model. For model 10, the genetic algorithm took 370 minutes to optimize the fracture half-length for a single well, while the simplex non-linear technique took 10 minutes (37 time faster) to complete the same task in the same model.
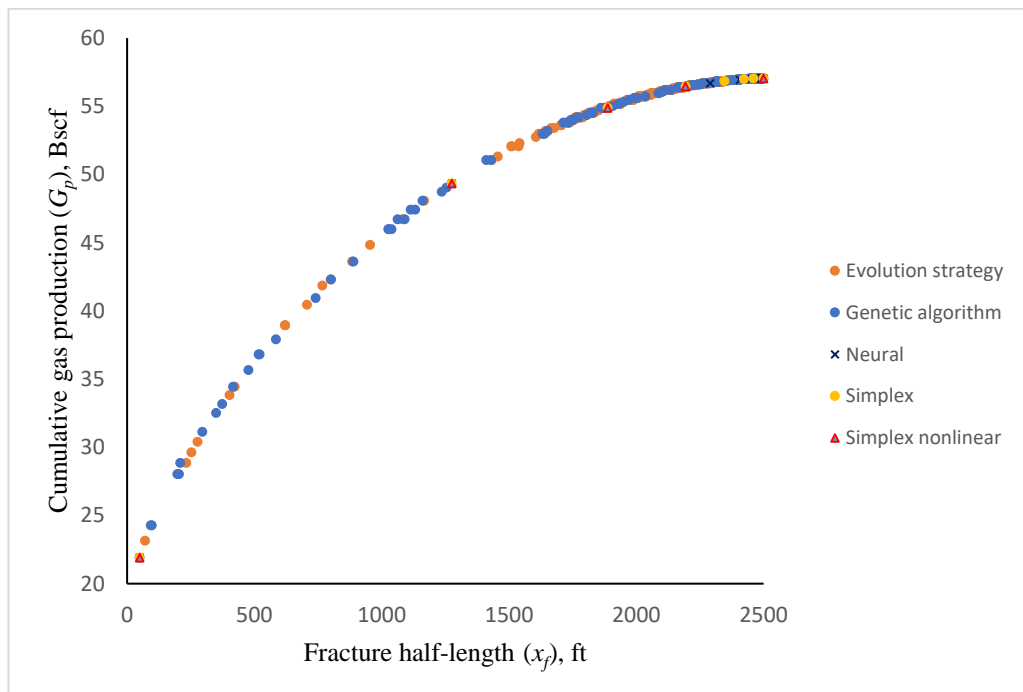
Figure 5.19 G_p vs. x_f in model 1
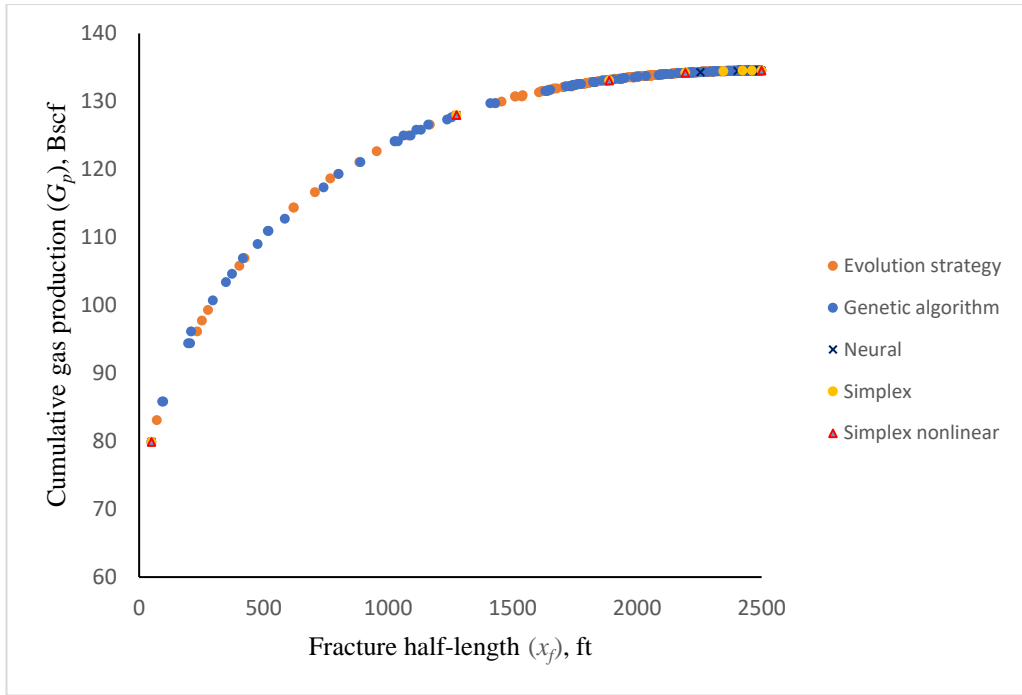
Figure 5.20 G_p vs. x_f in model 2
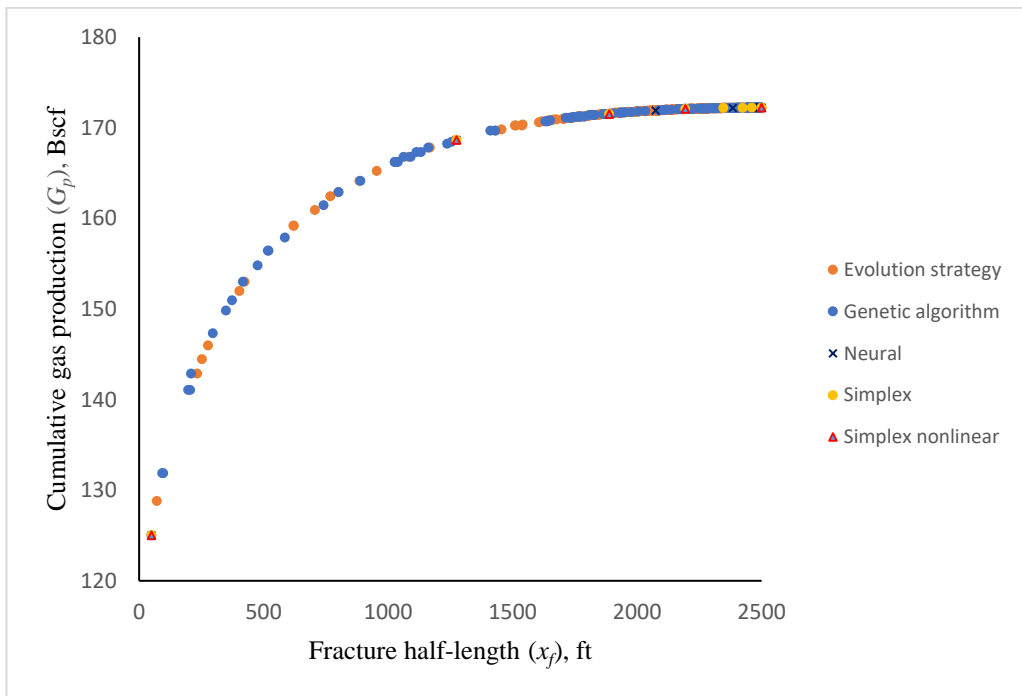
Figure 5.21 G_p vs. x_f in model 3
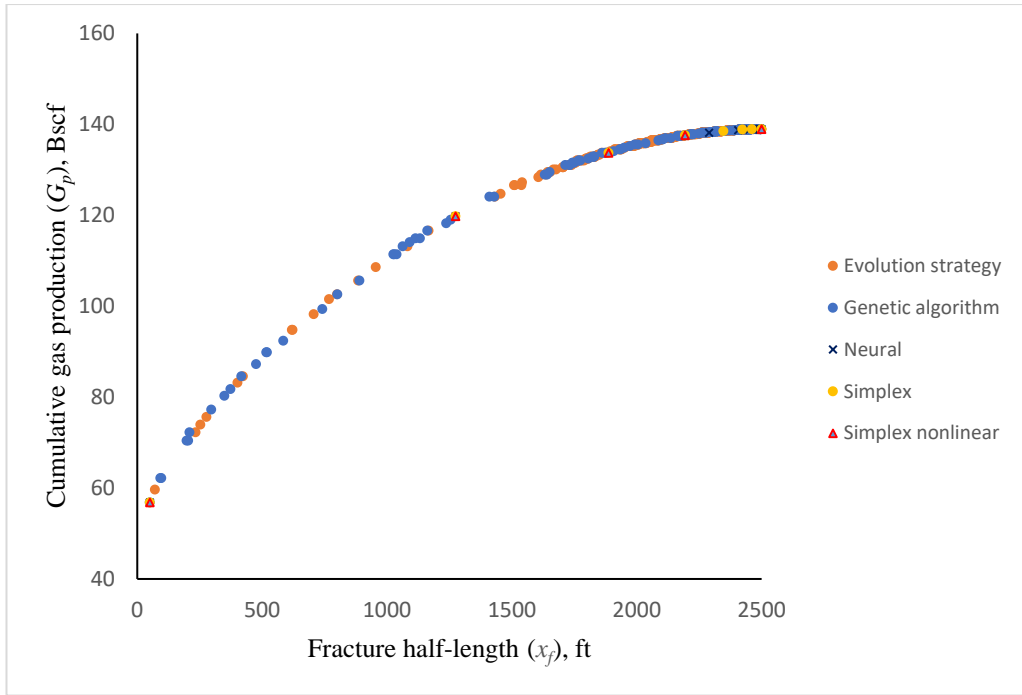
Figure 5.22 G_p vs. x_f in model 4
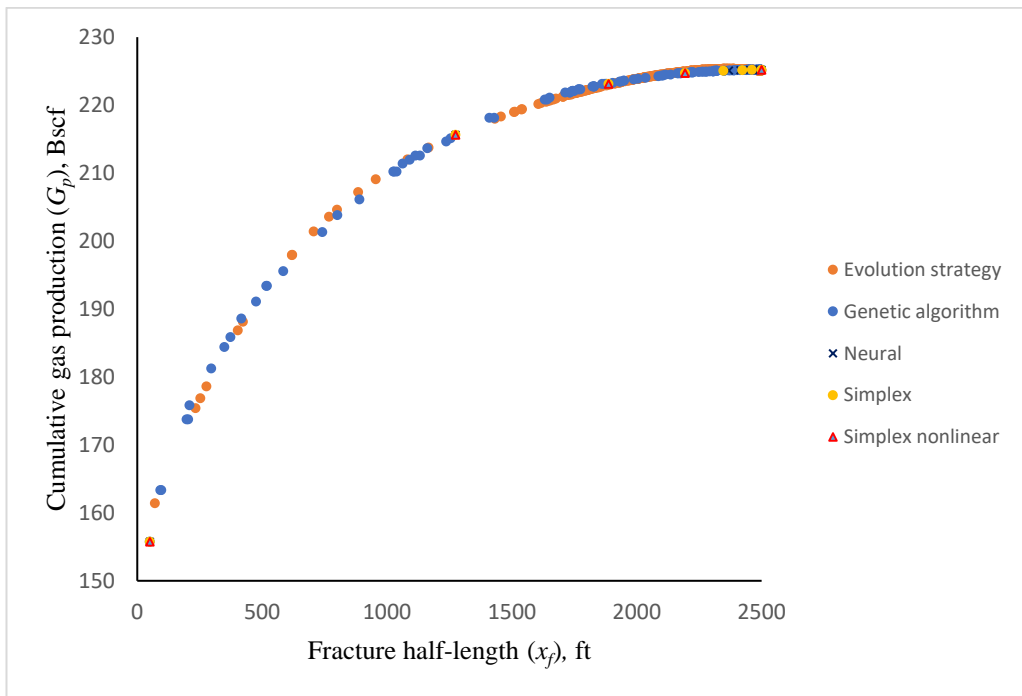
Figure 5.23 G_p vs. x_f in model 5
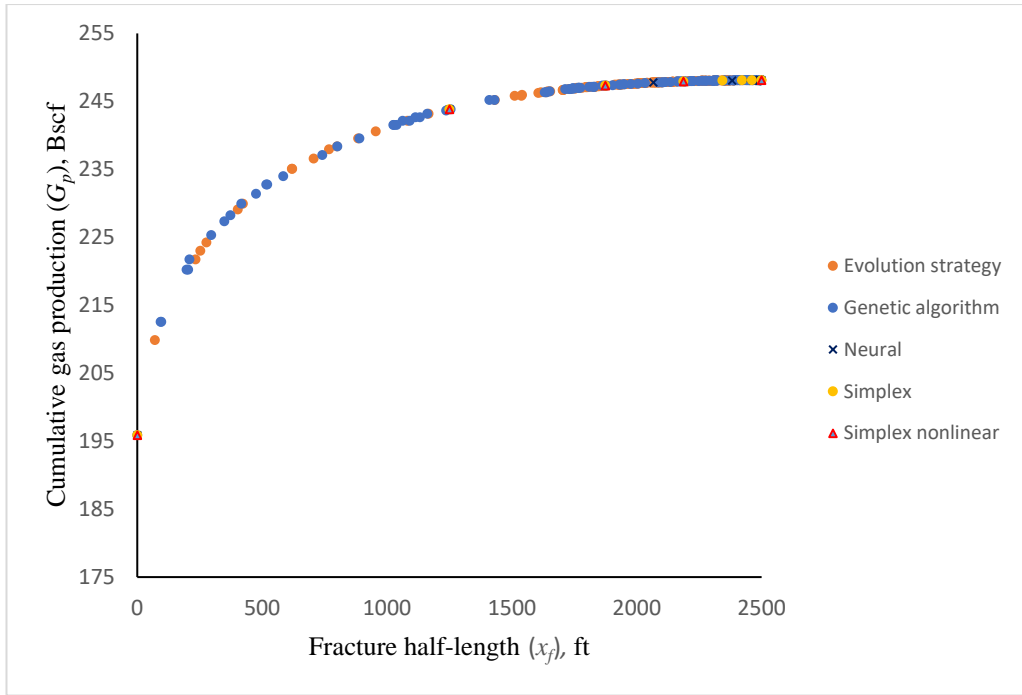
Figure 5.24 G_p vs. x_f in model 6
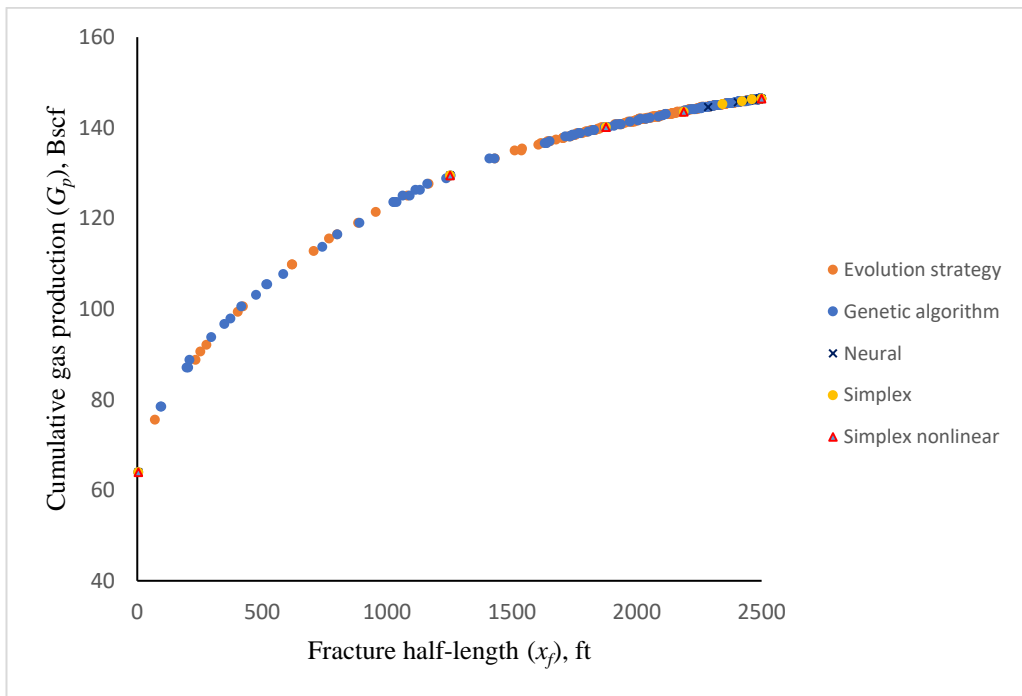
Figure 5.25 G_p vs. x_f in model 10
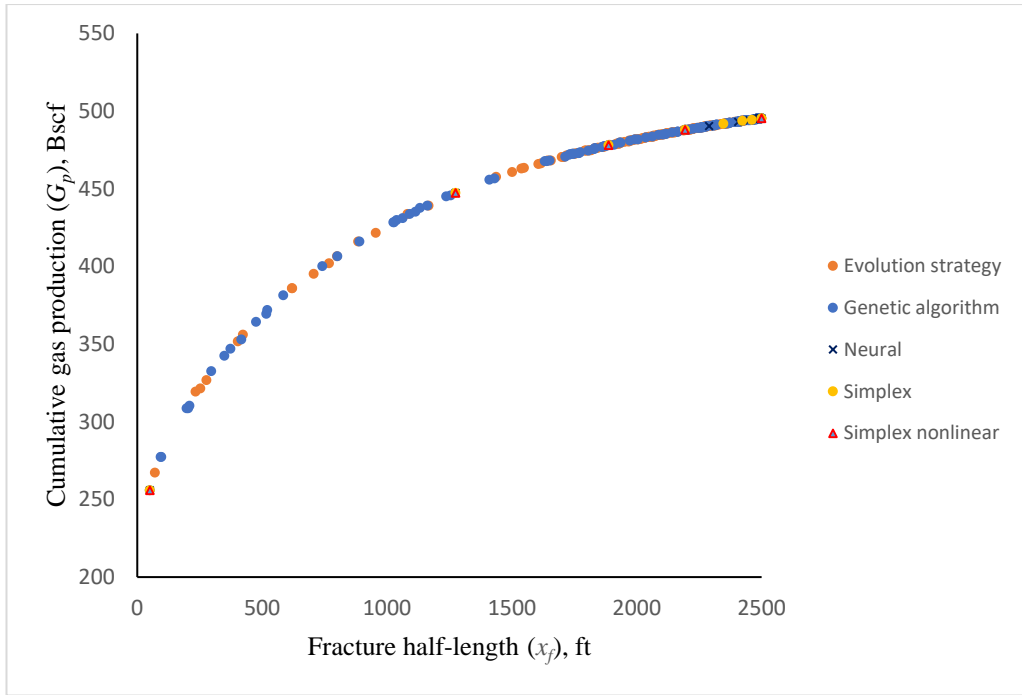
Figure 5.26 G_p vs. x_f in model 11
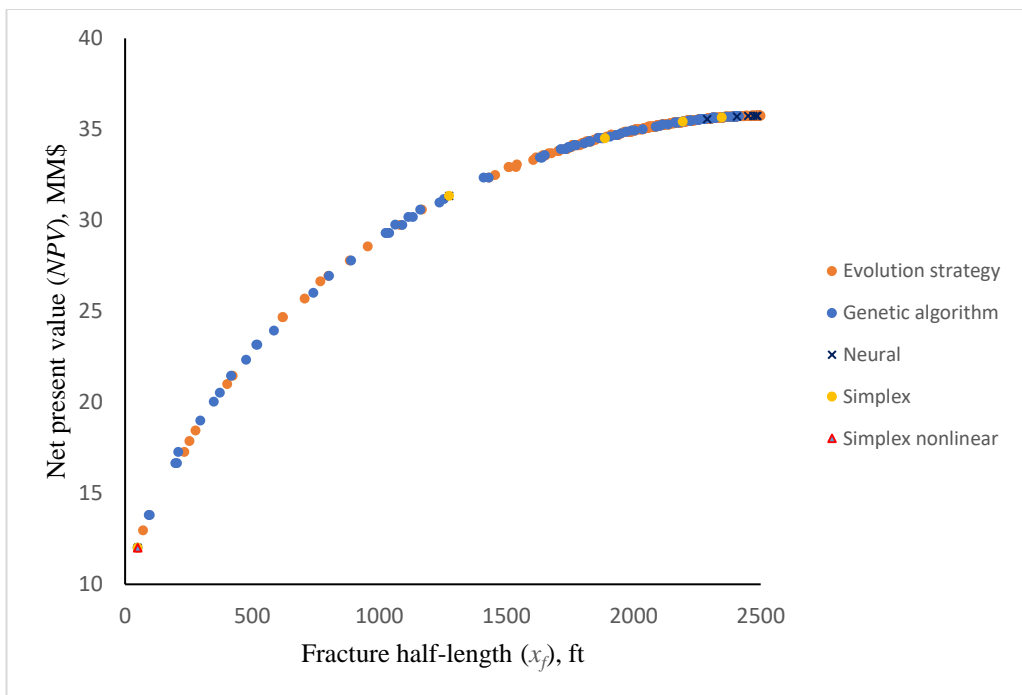
Figure 5.27 *NPV* vs. x_f in model 1
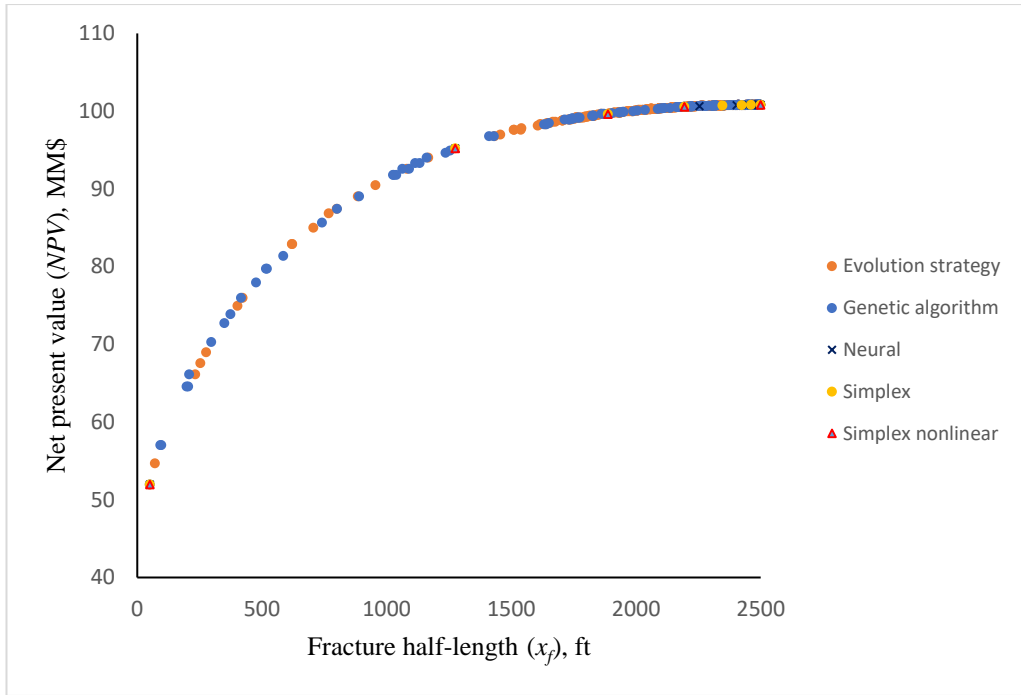
Figure 5.28 *NPV* vs. x_f in model 2
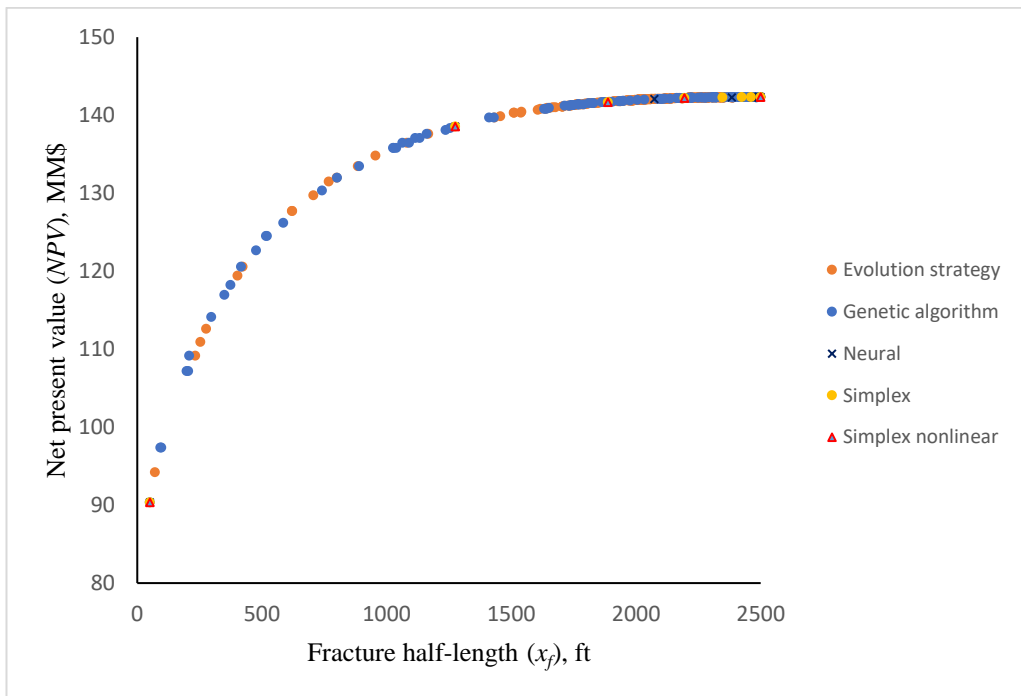
Figure 5.29 *NPV* vs. x_f in model 3
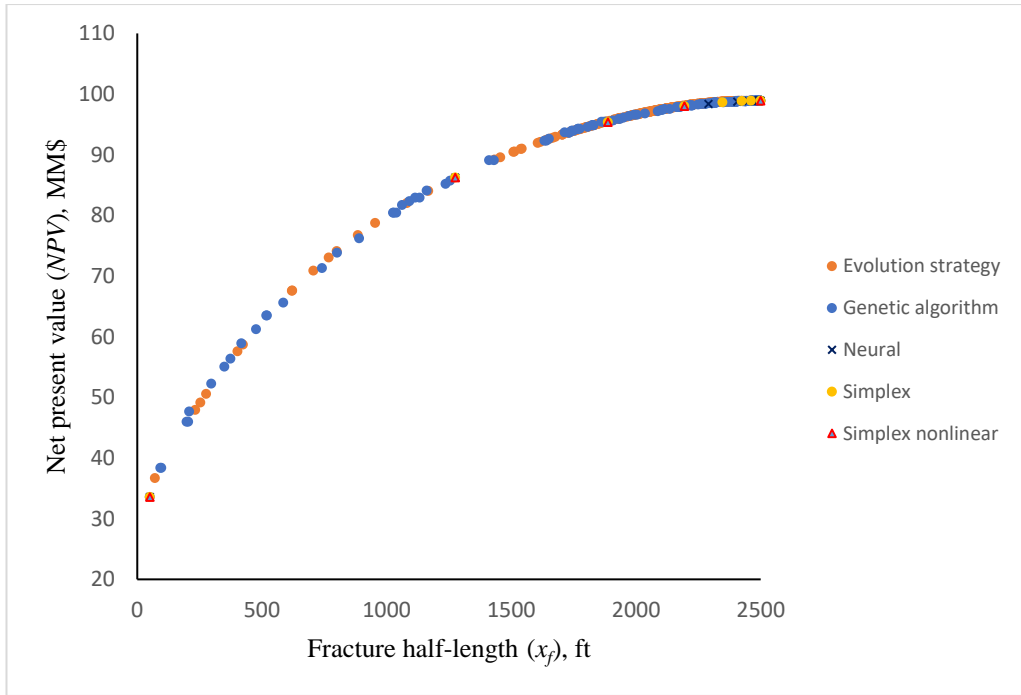
Figure 5.30 *NPV* vs. x_f in model 4
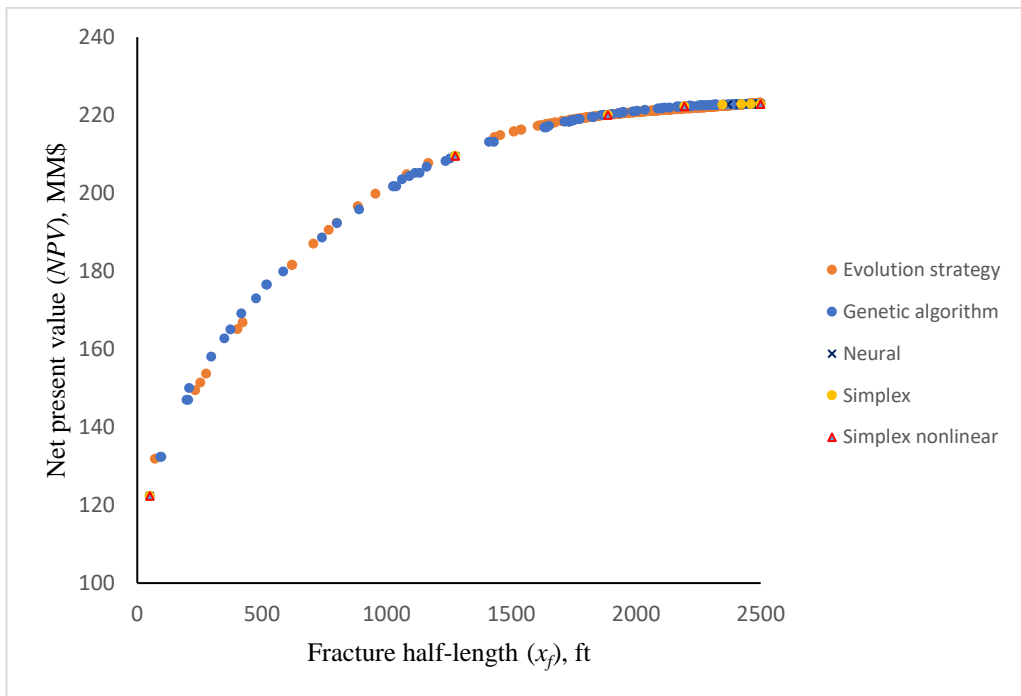
Figure 5.31 *NPV* vs. x_f in model 5
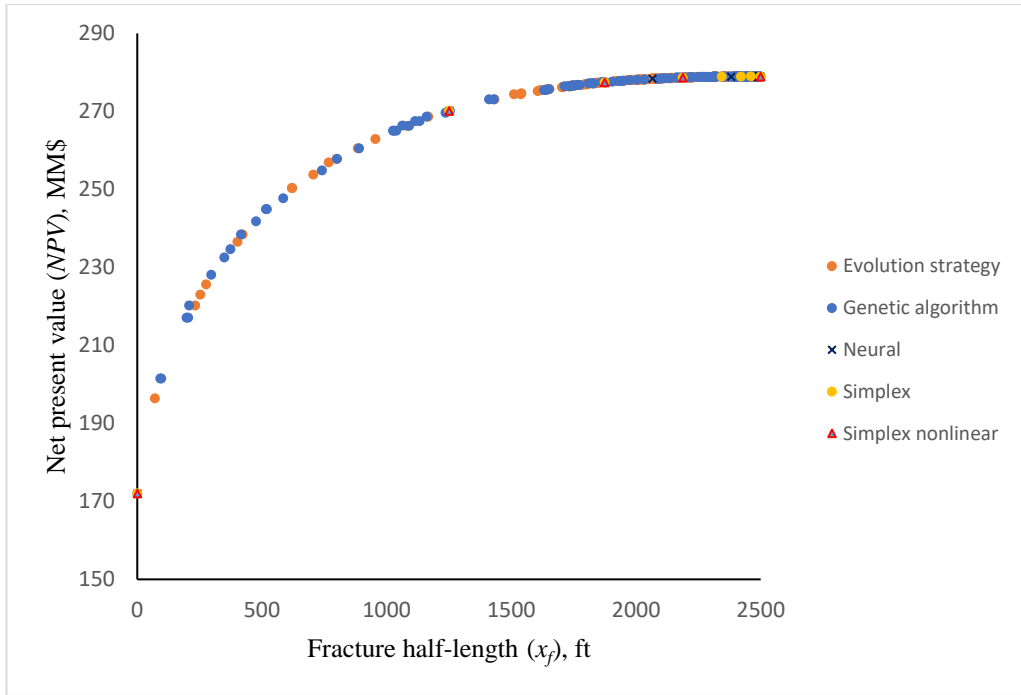
Figure 5.32 *NPV* vs. x_f in model 6
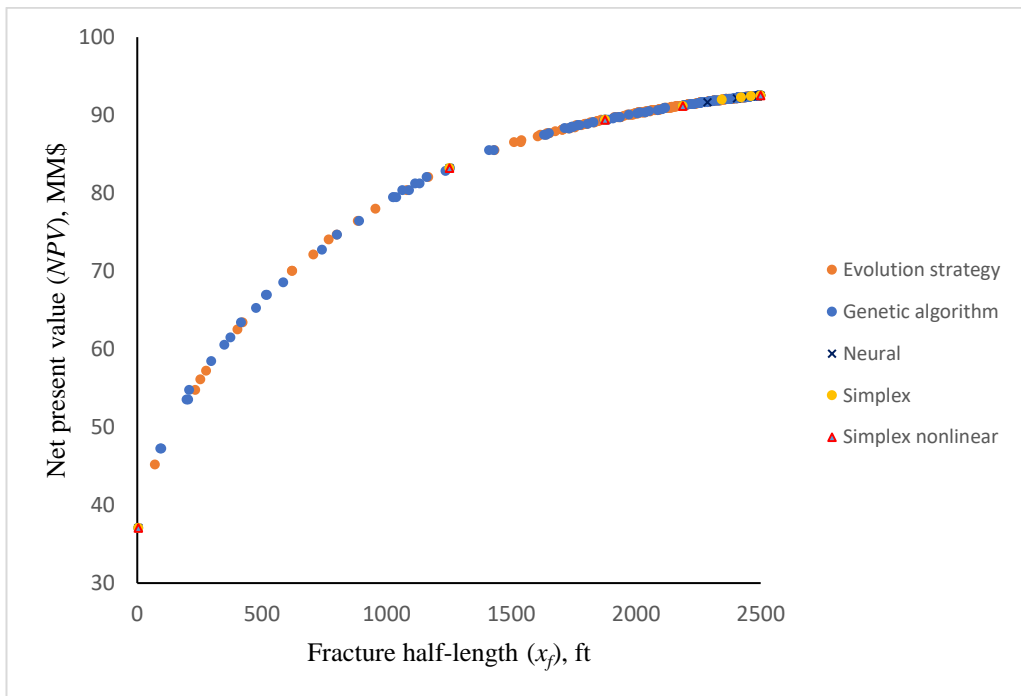
Figure 5.33 *NPV* vs. x_f in model 10
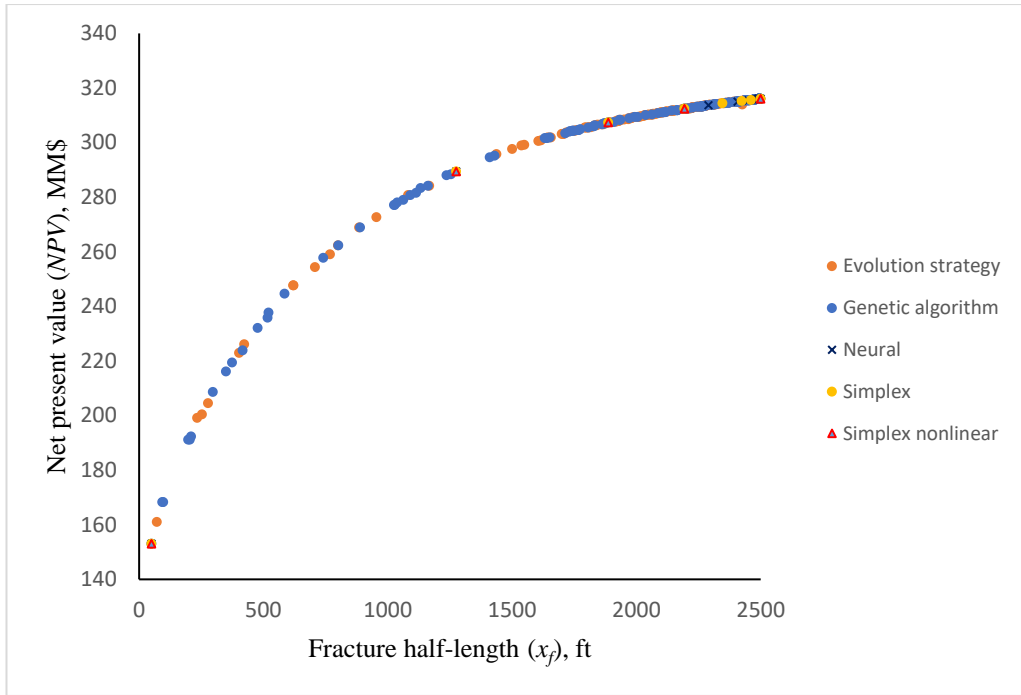
Figure 5.34 *NPV* vs. x_f in model 11
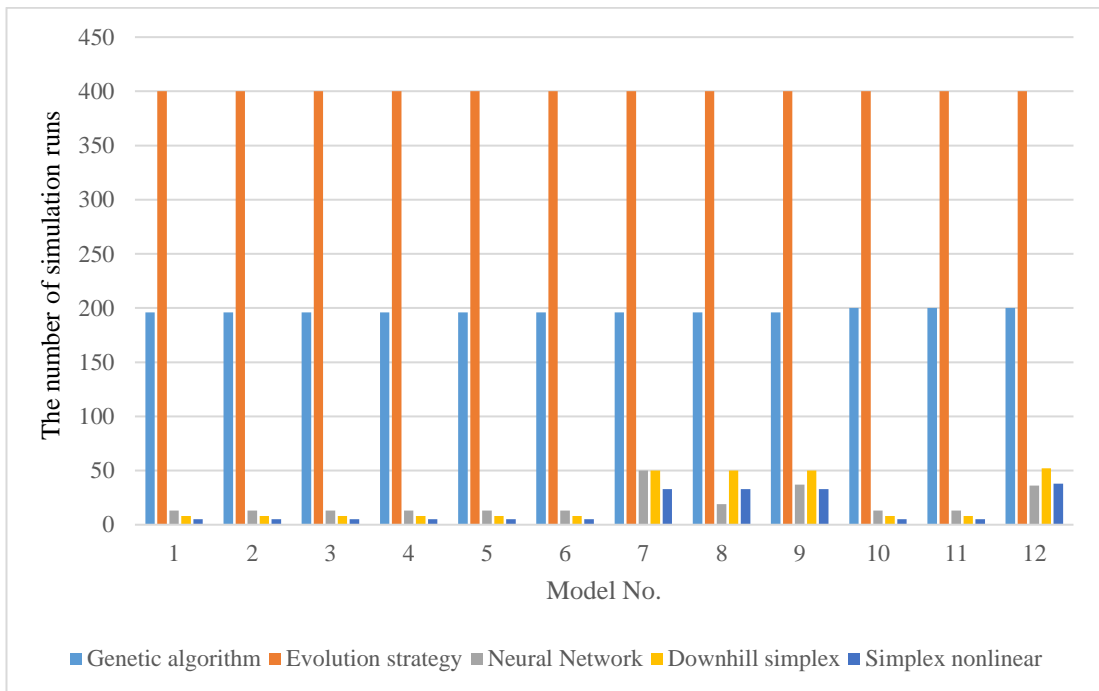
Figure 5.35 The required number of simulation runs for each optimization technique
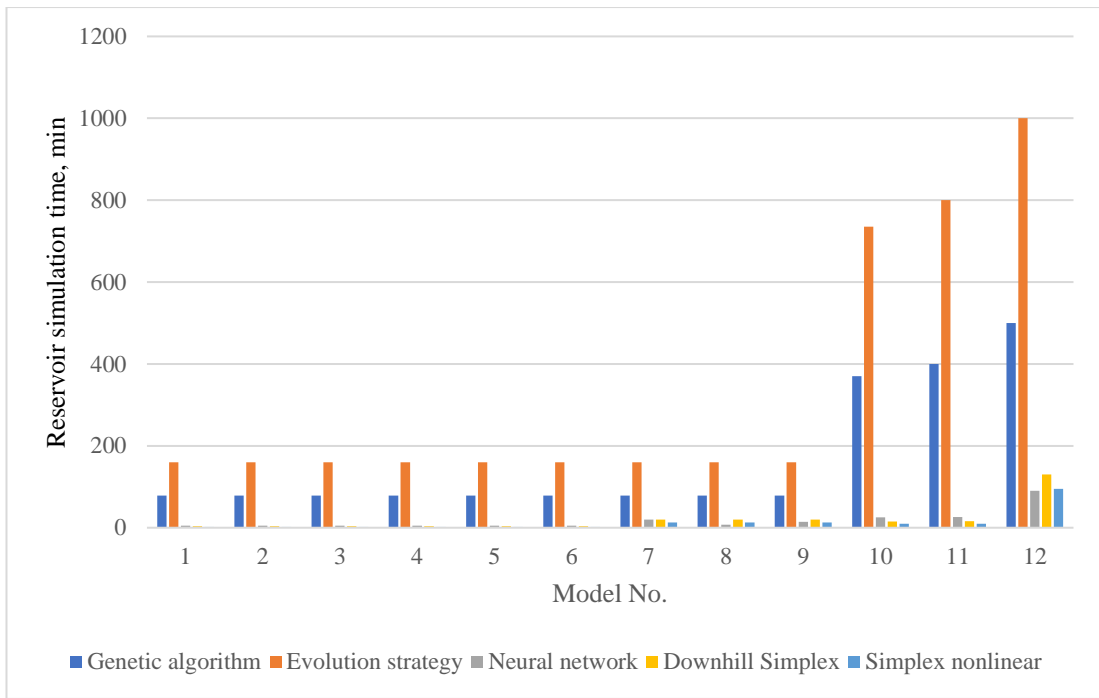
Figure 5.36 The required simulation time for each optimization technique

Table 5.7 Optimum solutions for all models

Model	Optimization technique	Objective function 1 (maximum cumulative gas production, Bscf)	Optimum fracture half-length for objective function 1, ft			Objective function 2 (maximum net present value, MM$)	Optimum fracture half-length for objective function 2, ft		
1	Genetic algorithm	57.044	2500			35.746	2491.5		
	Evolution strategy	57.044	2500			35.746	2494.5		
	Neural net	57.044	2500			35.746	2492		
	Downhill simplex	57.044	2500			35.745	2461.5		
	Simplex non-linear	57.044	2500			35.745	2500		
2	Genetic algorithm	134.537	2500			100.797	2459		
	Evolution strategy	134.537	2500			100.796	2464.5		
	Neural net	134.537	2500			100.796	2461		
	Downhill simplex	134.537	2500			100.796	2461.5		
	Simplex non-linear	134.537	2500			100.794	2500		
3	Genetic algorithm	172.226	2500			142.326	2459		
	Evolution strategy	172.226	2500			142.326	2463.5		
	Neural net	172.226	2500			142.325	2467		
	Simplex	172.226	2500			142.326	2461.5		
	Simplex non-linear	172.226	2500			142.321	2500		
4	Genetic algorithm	138.954	2500			98.896	2491.5		
	Evolution strategy	138.954	2500			98.863	2450		
	Neural net	138.954	2500			98.896	2492		
	Downhill simplex	138.954	2500			98.895	2461.5		
	Simplex non-linear	138.954	2500			98.891	2500		
5	Genetic algorithm	225.217	2500			222.877	2459		
	Evolution strategy	225.217	2500			222.866	2500		
	Neural net	225.217	2500			222.870	2492		
	Simplex	225.217	2500			222.876	2461.5		
	Simplex non-linear	225.217	2500			222.866	2500		
6	Genetic algorithm	248.112	2500			278.940	2459		
	Evolution strategy	248.112	2500			278.937	2464.5		
	Neural net	248.112	2500			278.936	2466.5		
	Downhill simplex	248.112	2500			278.939	2461		
	Simplex non-linear	248.112	2500			278.923	2500		
7	Genetic algorithm	138.018	2445.5	2166	2221	98.282	2445.5	2166	2221

Model	Optimization technique	Objective function 1 (maximum cumulative gas production, Bscf)	Optimum fracture half-length for objective function 1, ft			Objective function 2 (maximum net present value, MM$)	Optimum fracture half-length for objective function 2, ft		
	Evolution strategy	138.954	2500	2500	2500	98.892	2500	2500	2500
	Neural net	138.954	2500	2500	2500	98.896	2492.5	2492.5	2492
	Downhill simplex	138.954	2500	2500	2500	98.893	2500	2492	2499.5
	Simplex non-linear	138.954	2500	2500	2500	98.892	2500	2464.5	2500
8	Genetic algorithm	224.931	2445.5	2274	2187	222.541	2445.5	2274	2187
	Evolution strategy	225.217	2500	2500	2500	222.869	2463	2500	2500
	Neural net	225.217	2500	2500	2500	222.871	2470.5	2471	2468.5
	Downhill simplex	225.217	2500	2500	2500	222.869	2500	2464.5	2500
	Simplex non-linear	225.217	2500	2500	2500	222.869	2500	2464.5	2500
9	Genetic algorithm	247.840	2011.5	2445.5	2075	278.488	2011.5	2445.5	2075
	Evolution strategy	248.112	2500	2500	2500	278.927	2470	2500	2500
	Neural net	248.112	2500	2500	2500	278.931	2495.5	2464.5	2477
	Simplex	248.112	2500	2500	2500	278.928	2500	2464.5	2500
	Simplex non-linear	248.112	2500	2500	2500	278.928	2500	2464.5	2500
10	Genetic algorithm	146.445	2500			92.547	2491.5		
	Evolution strategy	146.445	2500			92.547	2494.5		
	Neural net	146.445	2500			92.547	2492		
	Downhill simplex	146.445	2500			92.546	2500		
	Simplex non-linear	146.445	2500			92.546	2500		
11	Genetic algorithm	495.289	2500			315.996	2492		
	Evolution strategy	495.289	2500			315.996	2492		
	Neural net	495.289	2500			315.997	2491.5		
	Downhill simplex	495.289	2500			315.992	2500		
	Simplex non-linear	495.289	2500			315.992	2500		
12	Genetic algorithm	489.835	2445.5	2279	2082.5	313.379	2445.5	2279	2082.5
	Evolution strategy	495.289	2500	2500	2500	315.992	2500	2500	2500
	Neural net	495.289	2500	2500	2500	315.996	2493.5	2500	2487.5
	Downhill simplex	495.289	2500	2500	2500	315.996	2482	2495	2500
	Simplex non-linear	495.289	2500	2500	2500	315.995	2500	2500	2484

5.6.1 Effect of number of wells on the optimization

The influence of the number of wells on the performance of the optimization technique has been studied under two assumptions. The first assumption is that all wells in the model have the same fracture half-length, while the second assumption states that each well could have a particular fracture half-length. It means that any reservoir model designed under the first assumption is a single decision variable case, while any reservoir model worked under the second hypothesis is a multi-decision variable case. Figure 5.35 shows that the GA and ES based optimization technique are not influenced by the number of decision variables because the same number of reservoir simulation runs are required under both assumptions, while the rest of the optimization techniques state a relationship between the number of decision variables and the required number of simulation runs. The downhill simplex method remains unaffected by the number of wells in the single decision variable cases. For instance, model 10 which includes a single well and model 11 which includes three wells, produce from the same reservoir, and both models require the same number of simulation runs because they are both considered under the first assumption. On the other hand, the required simulation runs to optimize fracture half-length using the downhill simplex method increases with the number of decision variables. For instance, model 11 includes three wells with the same fracture half-length achieved with an optimum solution by eight reservoir simulation runs, while model 12 includes three wells with various fracture half-lengths and was completed by 52 reservoir simulation runs. Similarly, the number of reservoir simulation runs required for the neural net and simplex non-linear optimization techniques increases when the number of decision variables are also increased, as shown in Figure 5.35.

5.6.2 Effect of permeability on the optimization

In the mechanistic models, three values of reservoir permeability: 0.01, 0.05, and 0.1 mD are considered. With a reservoir permeability of 0.01 mD, the optimum x_f is clearly close to 2500 ft, and it appears to be determined very easily from the plot of cumulative gas production with respect to fracture half-length, as shown in Figure 5.19 and Figure 5.22. For a reservoir permeability of 0.05 mD, the optimum x_f is difficult to determine from the plot because the cumulative gas production is approximately the same from the range of fracture half-length ranges from 2000 ft to 2500 ft, as shown in Figure 5.20 and Figure 5.23. For a reservoir permeability of 0.1 mD, G_p does not increase

significantly for the range of fracture half-length between 1500 ft and 2500 ft as shown in Figure 5.21 and Figure 5.24. The difficulty in finding the optimum x_f from the plot for the reservoir permeability ranges of 0.05 to 0.1 mD confirms the necessity of employing the optimization technique for achieving the optimal solution. Simplex non-linear appears to be the most suitable optimization technique for these particular multi-decision variables cases with permeability of 0.01 mD and 0.1 mD, while the neural network is found to be a relatively superior optimization technique for the multi-decision variable cases with permeability of 0.05 mD, as shown in Figure 5.35. Model 12 is a real model which includes three wells with a given fracture half-length. In this model, the permeability around Well No.1 and Well No.3 is about 0.05 mD, so the similarity between model 8 and model 12 is that both have three wells with different fracture half-lengths and the same permeability of 0.05 mD.

5.6.3   Effect of reservoir area on the optimization

Reservoir area does not affect performance for all optimization techniques in terms of the number of required reservoir simulation runs in all mechanistic and real models regardless of whether the model could represent single or multi-decision variables. For example, each applied optimization technique required the same number of simulation runs in model 1 with a reservoir area of 640 acres and model 10 with a reservoir area of 18285.8 acres. On the other hand, the simulation for real models with reservoir area of 18285.8 acres takes longer than the mechanistic model with reservoir area of 640 acres as shown in Figure 5.36.

Based on this simulation studies, the Table 5.8 provides a summary of the most effective optimization technique (with respect to the number of numerical simulation runs and their time) for different cases, and are summarized in Table 5.8. This table may be used as a guide for selecting the most effective optimization techniques in reservoir simulation to optimize the fracture half-length of hydraulic fractured vertical wells for different models and permeability.

Table 5.8 The optimization technique is effective for different cases

Case	Reservoir permeability, mD		
	0.01	0.05	0.1
Single well	Simplex non-linear	Simplex non-linear	Simplex non-linear
Multiple wells - single fracture half-length	Simplex non-linear	Simplex non-linear	Simplex non-linear
Multiple wells - multiple fracture half-length	Simplex non-linear	Neural net	Simplex non-linear

In summary, this simulation study warrants that the simplex non-linear optimization technique appears to be the most efficient with respect to obtaining the first optimum solution for the half-length of hydraulic fractured vertical wells in a tight gas reservoir for all well models with permeability ranges from 0.01 mD to 0.1 mD except the case of multiple wells - multiple fracture half-length with permeability of 0.05 mD. The neural net based optimization technique was found to be superior (with respect to simulation run time) for the multiple wells model with any fracture half-length (variable) for the reservoir permeability of 0.05 mD.

Chapter 6: Optimization of Multiple Hydraulically Fractured Horizontal Wells in Tight Gas Reservoirs

Chapter 5 described the optimization of hydraulic fractured vertical wells in tight gas reservoirs (TGRs) using integrated reservoir simulation, optimization techniques and sensitivity studies. The emphases were placed on the identification of efficient optimization approaches that can provide fast convergence with minimum simulation time without compromising the accuracy of the solution. Different types of optimization techniques were highlighted and exercised with integrated numerical simulation models using single and multiple decision variables. It was seen as possible to make significant simulation time savings on optimization without compromising the accuracy, which can lead to better management in the industry, especially in complex simulation projects. It was also demonstrated, in particular, optimization of fracture half-lengths for hydraulic fractured vertical wells in TGRs with permeability ranges from 0.01 to 0.1 mD, and that the non-linear simplex optimization technique offer significant simulation time savings for most of the cases (models) considered in this study. However, the use of non-linear simplex or any other techniques discussed in Chapter 5, integrated with numerical reservoir simulation, requires not only expert knowledge but also very comprehensive reservoir information/data for accurate optimization, which may be impossible to obtain in most cases, especially at the initial stages of a development project. In addition, it requires special skills and expertise, as well as expensive resources. Consequently, a simple yet reliable optimization technique that can optimize the hydraulic fracturing parameters without needing comprehensive reservoir data is desirable. In this view, this PhD study focuses on the development of simple yet reliable practical tools to optimize the hydraulic fracture parameters of TGRs. This chapter covers comprehensive discussion on this proposed development tool with case studies, validation, and justification. While the developed model is expected to be applicable for any type of hydraulic fractured wells (e.g. fractured vertical or multistage fractured horizontal), case studies presented in this chapter consider the multistage hydraulic fractured well, since: (i) Chapter 5 already covered discussion on a hydraulic fractured vertical well case; (ii) the problem of multistage hydraulic fractured horizontal wells (MFHWs) is relatively complex, and (iii) the MFHW technology is currently used as the most viable means of exploiting tight, ultra-tight and shale gas reservoirs.

6.1   Introduction

The exploitation and development of unconventional gas reservoirs, especially for tight sands, have grown over the last decade and the multistage hydraulic fractured horizontal well technique has verified to be the most feasible for the commercially viable production from these TGRs. However, flow and production processes and modelling for optimizing the production performance of these reservoirs are not well understood. In practice, the design and planning of the production plan for TGRs to achieve an economic rate is still a challenging task due to the complexity of optimization of MFHWs.

The determination of optimum fracture half-length, and number of fractures of MFHW in TGRs is essential to boost recovery, although the optimization of these two parameters entails many difficulties such as the complexity of designing reservoir simulation models and the formulation of optimization technique such as the genetic algorithm that are sometimes very difficult to handle for routine industry tasks. Other challenges include the need for long simulation run times or long computation times, the huge amount of data required to capture the actual reservoir scenario, and the limitations of reservoir simulators, especially with respect to handling and managing a large and complex full-scale reservoir simulation model, not to mention the hefty associated expenses. Moreover, the employment of the nonlinear optimization techniques requires a high level of programming skills, expensive commercial optimization software, and expert technical knowledge to define and solve the objective function. To simplify the optimization of hydraulic fracture length and number of fractures of MFHW in TGRs, a new practical tool is developed in this study based upon the dimensionless derivative of net present value (*NPV*). The proposed technique is capable of determining the optimum fracture half-length and number of fractures of MFHW in TGRs at dimensionless derivatives of net present value equalling zero. In addition, the correlation between the dimensionless derivative of net present value and each fracture half-length, and the number of fractures for given scenarios is proposed, and can ease the difficulty in determining the optimum fracture half-length and number of fractures in a limiting case with few reservoir simulation runs, especially when adequate data are not available. The proposed technique is validated by comparing the results with the results obtained from standard reservoir simulation studies. The results showed excellent matching between the proposed

technique and the reservoir simulation studies. The details of the model, including validation and case study results, are comprehensively discussed in this chapter.

6.2 Optimization of multistage hydraulic fracture parameters

Although earlier MFHW was considered unfavourable to develop, it is extensively used as the most viable technique nowadays to produce from TGRs (M. M. Hossain and Rahman, 2008; Li et al., 2015; F. Wang and Zhang, 2014), since the emergence of technology has made it feasible to enhance the productivity of TGRs, and compensate for the capital investments necessary for the recovery and production of commercial quantities of natural gas. Although MFHW is still a very expensive endeavour, and the physical and economic optimization is vital to maximize the gas production at lower capital costs. The physical aspects of the optimization, especially from the field development point of view, can be divided into three categories: well (well placement, number of wells, well geometry), fracture (fracture geometry, placement and fracture orientation) and reservoir. Reservoir here reflects the differences in optimum parameters corresponding to the differences in reservoir characteristics and properties. For instance, higher permeability reservoirs need shorter or no fractures in comparison with low permeability reservoirs, which provide maximum productivity when wells are completed with more extended fractures (M. Economides et al., 1991). Nevertheless, keeping the fracture geometry constant, higher permeability reservoirs will provide high productivity. This is because, considering the characteristics of tight reservoirs, fractures in tight reservoirs can drain only from the inter-reservoir regions (Ozkan et al., 2011).

Mathematical models for optimization could incur extremely laborious tasks. Further, the risk of human error always exists. However, incorporating the same concepts and the flow/production mechanisms, and modifying the reservoir simulation algorithms could enhance the accuracy of results. Nevertheless, apart from the complexities, the cost incurred while using reservoir simulation models would be an add-on to the existing high cost of development. Therefore, simple yet reliable tools available at lower costs but that generate reliable results/outcomes for optimization are desirable.

In order to overcome these shortcomings, this study proposes a simplified optimization model developed on the basis of dimensionless derivatives of net present value of the project, details of which will be discussed in the following section.

6.3   Mathematical model

As the net present value is a function of the cumulative gas production which depends on fracture half-length and the number of fractures of MFHW, the derivatives of the net present value with respect to fracture half-length and number of fractures should provide an optimum value for which there is a maximum net present value achievable. This can thus be described theoretically by Equations 6.1–6.6.

$$NPV = f(G_p, CAPEX, OPEX)$$
6.1

Where:

NPV   Net present value, $

CAPEX   Capital expenditures, $

OPEX   Operating expenses, $

For a given *CAPEX* and *OPEX*, the *NPV* can be considered as:

$$NPV = f(G_p)$$
6.2

Where,

$$G_p = f(N_f, x_f)$$
6.3

Thus,

$$NPV = f(N_f, x_f)$$
6.4

$$\frac{\partial NPV}{\partial N_f} = f'(N_f) = \frac{[NPV_{i+1} - NPV_i]}{N_{f_{i+1}} - N_{f_i}}$$
6.5

$$\frac{\partial NPV}{\partial x_f} = f'(x_f) = \frac{[NPV_{i+1} - NPV_i]}{x_{f_{i+1}} - x_{f_i}}$$
6.6

In Equations 6.1-6.6, G_p denotes cumulative gas production of wells in Mscf, x_f is the fracture half-length in feet, N_f is the number of fractures and *NPV* is the net present value in dollars, *OPEX* is the operating expenditure and *CAPEX* is the capital expenditure. The derivative of the net present value (*NPV*) plotted as a function of fracture parameters (i.e., x_f, and N_f) portrays the variation in *NPV* with respect to x_f and N_f. The G_p can be readily available from production history data of existing or offset wells from a similar field. In the case when this data is not available, it can be easily predicted from the reservoir simulation or other predictive tools (e.g., Material Balance, Decline Curve). For the purpose of this study, G_p is determined through the numerical reservoir simulation studies for a single well mechanistic model generated after undergoing extensive research using a representative tight gas field. For every other fracture parameter, x_f *and* N_f, were considered for sensitivity studies based on typical data generally found in the literature as well as from industry practices.

NPV was calculated using Equations 6.7-6.13 given below. Gas price was considered to be \$4/Mscf, calculated on the basis of the average price over the last ten years (Macrotrends, 2018). The drilling and completion costs used for the economic evaluation in this study are stated in Table 6.1 (Bagherian et al., 2010; R. Schweitzer and Bilgesu, 2009). The discount rate and income tax rate were assumed to be 0.1 and 0.2, respectively.

$$FV \ = \ PV \ (1 + DR)^n \qquad\qquad 6.7$$

$$CAPEX \ = DRC + \left(FRCS \times N_f\right) \qquad\qquad 6.8$$

$$OPEX \ = NOD \ \times DOC \qquad\qquad 6.9$$

$$TC = CAPEX \ + \ OPEX \qquad\qquad 6.10$$

$$GREV = \ G_p \ \times GPR \qquad\qquad 6.11$$

$$NCF = (1 - ITR) \times GREV - TC \qquad 6.12$$

$$NPV = \sum_{i=1}^{n} \left[\frac{NCF}{(1 - DR)^i} \right]_i \qquad 6.13$$

Where,

DRC is drilling cost.

FRCS is fracturing cost per each stage, $.

NOD is number of operation days.

DOC is daily operation cost, $.

TC is total cost, $.

GREV is gross revenue, $.

GPR is gas price, $/Mscf.

ITR is income tax rate.

FV is future value.

PV is present value.

DR is discount rate.

NCF is the net cash flow, $.

n is the number of years.

Table 6.1 Drilling and completion costs used for the economic evaluation (Bagherian et al., 2010; R. Schweitzer and Bilgesu, 2009)

Well Design – Drilling and Completion	Cost, MM$
Horizontal well drilling with 4100 ft lateral	2.74
500 ft fracture half-length per stage	0.15
1000 ft fracture half-length per stage	0.21
Daily operating cost	37.75×10^{-6}

The derivatives illustrated by Equations 6.5-6.6 can be expressed in the following dimensionless forms as shown in Equations 6.14-6.15.

$$\left(\frac{\partial NPV}{\partial N_f}\right)_{N_f} = \frac{\partial NPV}{\partial N_f} \times \frac{N_f}{NPV} \qquad\qquad 6.14$$

$$\left(\frac{\partial NPV}{\partial x_f}\right)_{x_f} = \frac{\partial NPV}{\partial x_f} \times \frac{x_f}{NPV} \qquad\qquad 6.15$$

Where:

$\left(\frac{\partial NPV}{\partial N_f}\right)_{N_f}$ is the dimensionless derivative of *NPV*, with respect to number of fractures= $(DDNPV)_{N_f}$.

$\left(\frac{\partial NPV}{\partial x_f}\right)_{x_f}$ is the dimensionless derivative of *NPV* with respect to fracture half-length = $(DDNPV)_{x_f}$.

The optimum parameters are determined at the point where the productivity increase is at a maximum, i.e., where the dimensionless derivative of net present value (*DDNPV*) with respect to optimized parameter is zero. This is where a maximum profit can be achieved. Thus, the trend of *DDNPV* with respect to optimized parameter can be employed as a tool to forecast the maximum possible production against the most optimum physical characteristics of reservoir and fracture. The mathematical model described above can be easily adopted to optimize the number of fractures (N_f) and fracture half-length (x_f) by following a graphical approach or statistical approach as described in section 6.3.1.

6.3.1 Graphical approach:

The steps to be followed to calculate the optimum N_f and x_f graphically are explained below:

1. Obtain production or history data from a considered field for certain scenario. Alternatively, this data can be obtained from a numerical simulation when the production history data is not available.

2. Calculate the derivatives of *NPV* (*DNPV*) with respect to the parameter being optimized using Equations 6.5 and 6.6. These derivatives can be determined numerically (Equations 6.5 and 6.6) or graphically based on production data from an existing analogous well or based upon numerical reservoir simulation results.

3. Calculate the $(DDNPV)_{N_f}$ and $(DDNPV)_{x_f}$ from respective *DNPV* as calculated in Step 2 using Equations 6.14-6.15.

4. Plot the *DDNPV* as a function of the considered parameter being optimized (e.g., fracture half-length, or number of fractures).

5. Using regression analysis, obtain the correlation (i.e. trend line) of the functions, $(DDNPV)_{N_f}$ and $(DDNPV)_{x_f}$.

6. Extrapolate the trend line of *DDNPV*, until it intersects the axis of respective parameters being optimized (i.e., the x-axis). The corresponding value obtained at the intersection of x-axis is the optimum value of the parameter, since the optimum value of the parameter of interest can be obtained when the value of the dimensionless derivative of net present value ≈ zero.

6.3.2 Statistical approach:

6.3.2.1 Determination of optimum number of fractures, $\left(N_f\right)_{opt}$

On the basis of a rigorous sensitivity study, it is observed that the least square method provides the best fit when *DNPV* is plotted as a function of the number of fractures, *N$_f$*, and the relationship between *DNPV* and the number of fractures appears to be semi-logarithmic (i.e., liner in semi-log plot). The function $(DDNPV)_{N_f}$ can be expressed as:

$$(DDNPV)_{N_f} = m \, ln[N_f] + c \qquad\qquad 6.16$$

Where:

m is the slope of the function $(DDNPV)_{N_f}$ and c is intercept at the y-axis. The slope, m, and intercept, c, can be calculated using the least squares regression line, and can be expressed by Equations 6.17 and 6.186.17, respectively.

$$m = \frac{\sum_{i=1}^{n} \left(\left(ln[N_f]\right)_i - \overline{ln[N_f]} \right) \left(\left[(DDNPV)_{N_f}\right]_i - \overline{(DDNPV)_{N_f}} \right)}{\sum_{i=1}^{n} \left(\left(ln[N_f]\right)_i - \overline{ln[N_f]} \right)^2}$$

6.17

$$c = \overline{(DDNPV)_{N_f}} - m \left(\overline{ln[N_f]} \right)$$

6.18

The optimum number of fractures can now readily be determined when the $(DDNPV)_{Nf}$ is equal to zero. Thus, the optimum number of fractures can be mathematically expressed by Equation 6.19.

$$\left(N_f\right)_{opt} = e^{-\frac{c}{m}}$$

6.19

Where, $i = 1,2,3\ldots.n,$ and n is the number of data points.

The mean of $(DDNPV)_{N_f}$, $\overline{(DDNPV)_{N_f}} = \sum_{i}^{n} \frac{\left((DDNPV)_{N_f}\right)_i}{n}$, and

The mean of $ln[N_f]$, $\overline{ln[N_f]} = \sum_{i}^{n} \frac{(ln[N_f])_i}{n}$

6.3.2.2 Determination of optimum fracture half-length, $\left(x_f\right)_{opt}$

On the basis of a rigorous sensitivity study, it is recognized that the quadratic least square or 2nd order polynomial function provides the best fit, when $DNPV$ is plotted as a function of fracture half-length, x_f, and the relationship between $DDNPV$ and x_f appears to be a 2nd order polynomial, and hence the function $(DDNPV)_{X_f}$ can be expressed as

$$(DDNPV)_{X_f} = a\, x_f + b{x_f}^2 + c$$

6.20

Where, $y = (DDNPV)_{X_f}$, and $x = x_f$, and a, b, c are the 2nd order polynomial coefficients, which can be determined statistically using quadratic least square approach, given by:

$$a = \frac{\{[\sum(x^2y) \times (xx)] - [\sum(xy) \times \sum(xx^2)]\}}{\{[\sum(xx) \times \sum(x^2x^2)] - [\sum(xx^2)]^2\}} \qquad 6.21$$

$$b = \frac{\{[\sum(xy) \times (x^2x^2)] - [\sum(x^2y) \times \sum(x\ x^2)]\}}{\{[\sum(xx) \times \sum(x^2x^2)] - [\sum(xx^2)]^2\}} \qquad 6.22$$

$$c = [(Sy_i)/n] - \{b \times [(Sx_i)/n]\} - \{a \times [(S(x_i{}^2))/n]\} \qquad 6.23$$

Note:

$$Sy_i = \sum y_i \qquad 6.24$$

$$Sx_i = \sum x_i \qquad 6.25$$

Where:

$$\sum(xx) = \left(\sum x_i^2\right) - \left[\left(\sum x_i\right)^2 /2\right] \qquad 6.26$$

$$\sum(xy) = \left(\sum x_i y_i\right) - \left[\left(\sum x_i\right) \times \left(\sum y_i\right)/n\right] \qquad 6.27$$

$$\sum(xx^2) = \left(\sum x_i^3\right) - \left[\left(\sum x_i\right) \times \left(\sum x_i^2\right)/n\right] \qquad 6.28$$

194

$$\sum (x^2 y) = \left(\sum x_i^2\, y_i \right) - \left[\left(\sum x_i^2 \right) \times \left(\sum y_i \right) / n \right] \qquad 6.29$$

$$\sum (x^2 x^2) = \left(\sum x_i^4 \right) - \left[\left(\sum x_i^2 \right)^2 / n \right] \qquad 6.30$$

The correlation coefficient of this relationship can be calculated using Equation 6.31.

$$r^2 = \frac{[\sum(y_i - y_{ave})^2] - \{[(n-1)/(n-p)] \times [\sum(y_i - Y_i)^2]\}}{\sum(y_i - y_{ave})^2} \qquad 6.31$$

Where:

$$Y_i = \{[2\,a\,x^2] - b^2 + b + (4\,a\,c)\}/(4\,a) \qquad 6.32$$

Finally, Equation 6.33 can be applied to find the optimum fracture half-length.

$$\left(x_f \right)_{opt} = \frac{-b \mp \sqrt{b^2 - 4\,a\,c}}{2\,a} \qquad 6.33$$

The proposed technique is validated through numerical reservoir simulation using industry standards and the widely acceptable and most reliable commercial numerical reservoir simulator, PETREL/ECLIPSE, which will be discussed in the following section.

6.4   Model validation and sensitivity studies

The proposed technique is validated by comparing the results obtained using the proposed technique with those obtained from numerical reservoir simulation studies for the same conditions using widely acceptable and reliable commercial simulator PETREL/ECLIPSE. The sensitivity studies are conducted to demonstrate the potential application of the proposed technique for optimizing the production performance of TGRs, and to study the factors affecting the performance. Due to the scarcity of enough production history data, and for demonstration purposes, the production data used in this study are based upon synthetic production data generated from the mechanistic

numerical simulation model. The range of the N_f and x_f that was used for all cases considered in this sensitivity studies is presented in Table 6.2. Each of the cases was analysed for a range of N_f and x_f for a given reservoir permeability.

Table 6.2 Cases and data considered in this study

Case No.	k (mD)	N_f		x_f (ft)	
		Min.	Max	Min	Max
1	0.01				
2	0.05	1	50	50	1600
3	0.1				

6.4.1 Mechanistic numerical model

The optimization for fracture geometry can be carried out using cumulative gas production plots. Alternatively, the proposed dimensionless derivative of *NPV* (*DDNPV*) plots can be used as they describe the change in cumulative gas production rates per unit change in interested parameters. The optimum parameters are obtained at the point where the dimensionless derivative of the net present value (*DDNPV*) function becomes zero. The sensitivity analysis and optimization of the fracture half-length, and number of fractures were first achieved for the permeability of 0.01, 0.05 and 0.1 mD. The permeability range (0.01~0.1 mD) is considered as it typically falls within the range of most of the worldwide tight gas reservoirs. The base case reservoir and fracture properties provided in Table 6.3 are also obtained from tight gas fields typically observed in Australia (H. Bahrami et al., 2012b; Crosby et al., 1998; MK Rahman et al., 2007).

Table 6.3 The properties of the reservoir and fractures considered for base case simulation

Reservoir pressure	4560 psi
Reservoir temperature	275°F
True vertical depth (TVD)	10000 ft
Measured depth (MD)	14100 ft
Horizontal well length	4100 ft
Reservoir area	320 acres
Porosity	0.05
Permeability in y-direction (k_y) = Permeability in x-direction (k_x)	0.01, 0.05, or 0.1 md
Permeability in z-direction (k_z)	0.00001 mD
Fracture half-length	500 ft
Fracture width	0.2 inch
Fracture permeability	10000 mD
Fracture height	100 ft
Fracture orientation	90°
Number of grids	22244
Grid size (x and y directions)	50 ft × 50 ft
No. of grids in x, y and z directions	84×67 ×4
Gas specific gravity	0.65

Figure 6.1 and Figure 6.2 explain the 3D view of permeability and porosity distribution, respectively, in a mechanistic reservoir model. Moreover, Figure 6.1 and Figure 6.2 show the hydraulic fractures of the horizontal well. Figure 6.3 displays the schematic 3D view of a sample model of a horizontal well with five hydraulic fractures in a mechanistic model considered in this study. The mechanistic reservoir models the permeability of 0.01, 0.05 and 0.1 mD with a range of fracture half-length from 50 ft to 1600 ft. A number of fractures ranging from 1 to 50 were considered to generate production data to validate the proposed technique. Figure 6.4 and Figure 6.5 show the pressure distribution for a case with a reservoir permeability of 0.01 mD producing by a horizontal well with five hydraulic fractures.
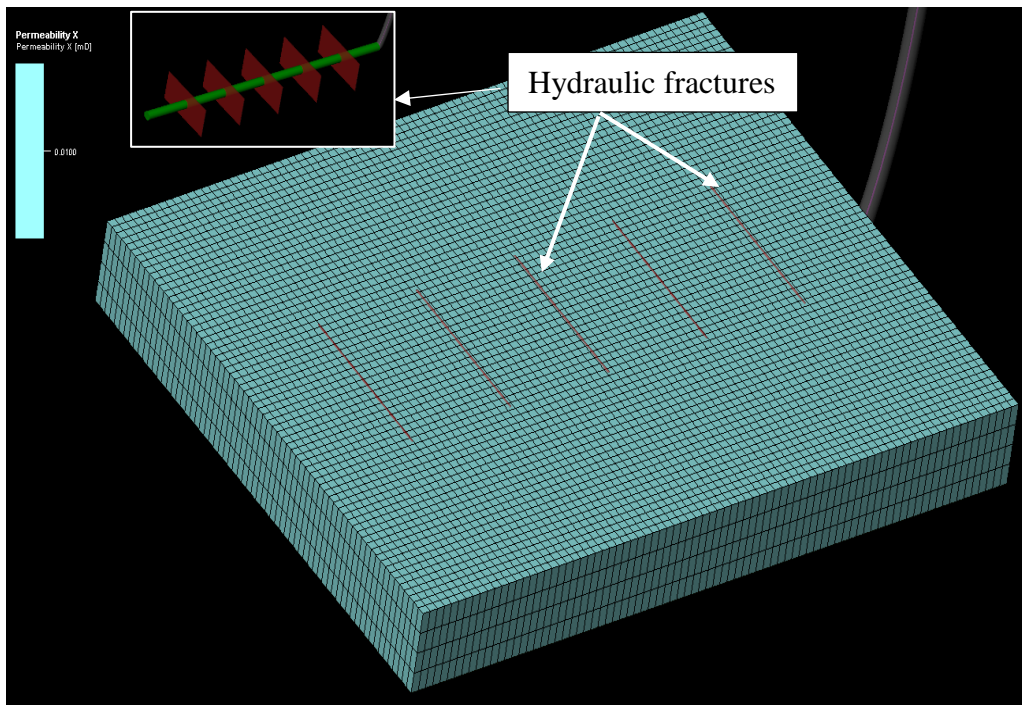
Figure 6.1 - 3D permeability map of a mechanistic model
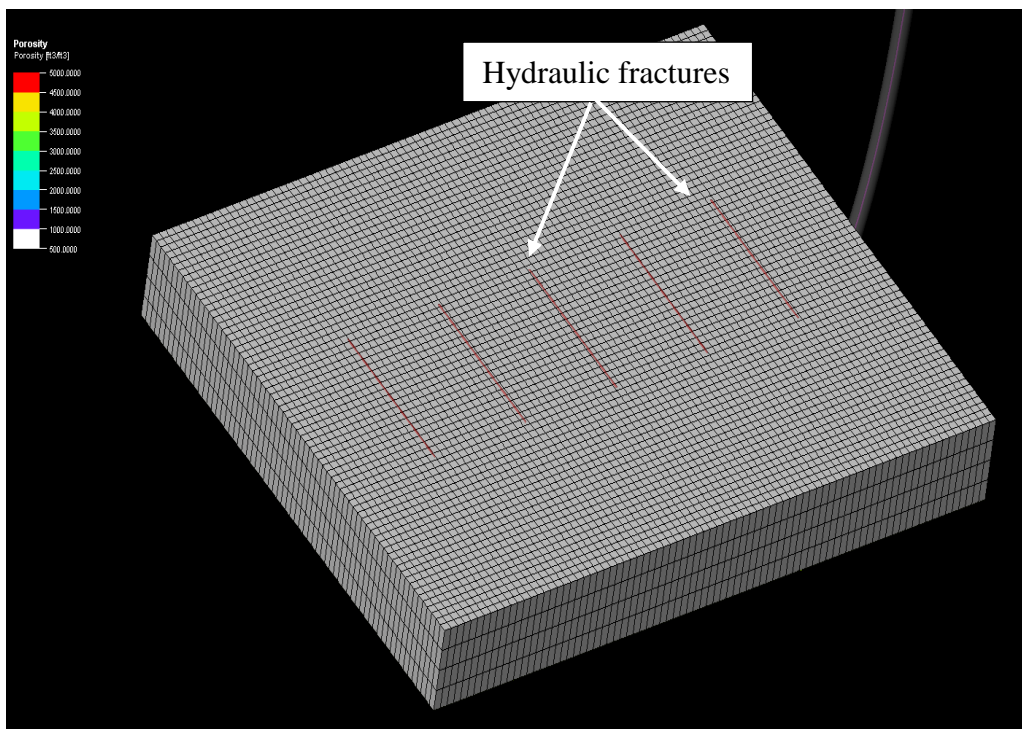
Figure 6.2- 3D porosity map of a mechanistic model
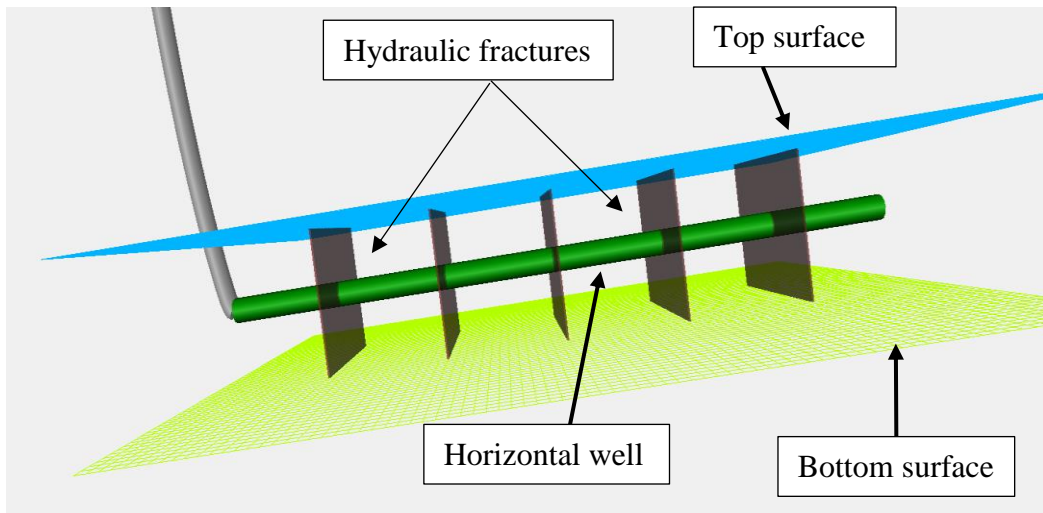
Figure 6.3 Schematic of a sample reservoir model with number of fractures (3D view)
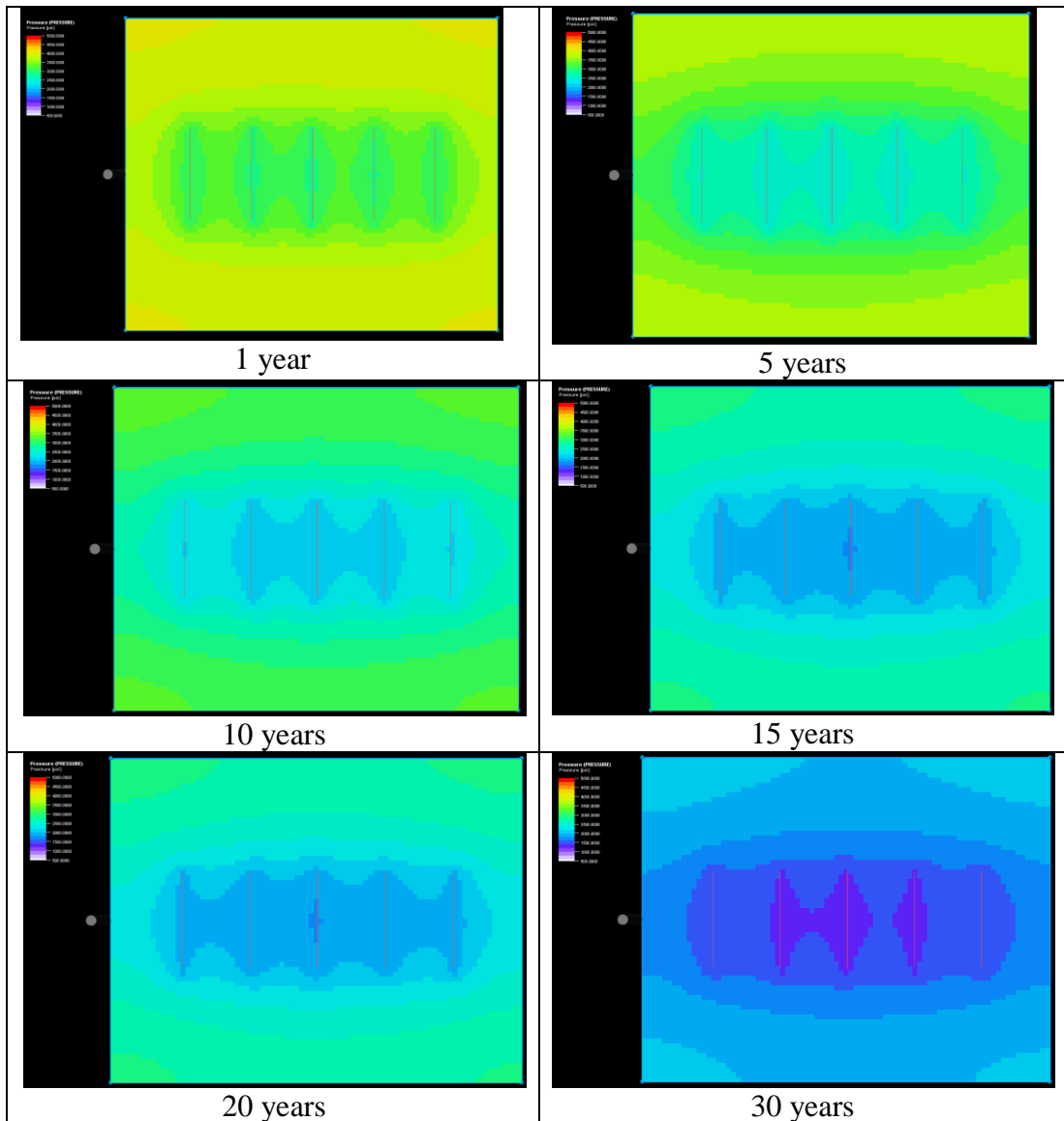
Figure 6.4 pressure distribution in the reservoir through the production time (2D top view)

199
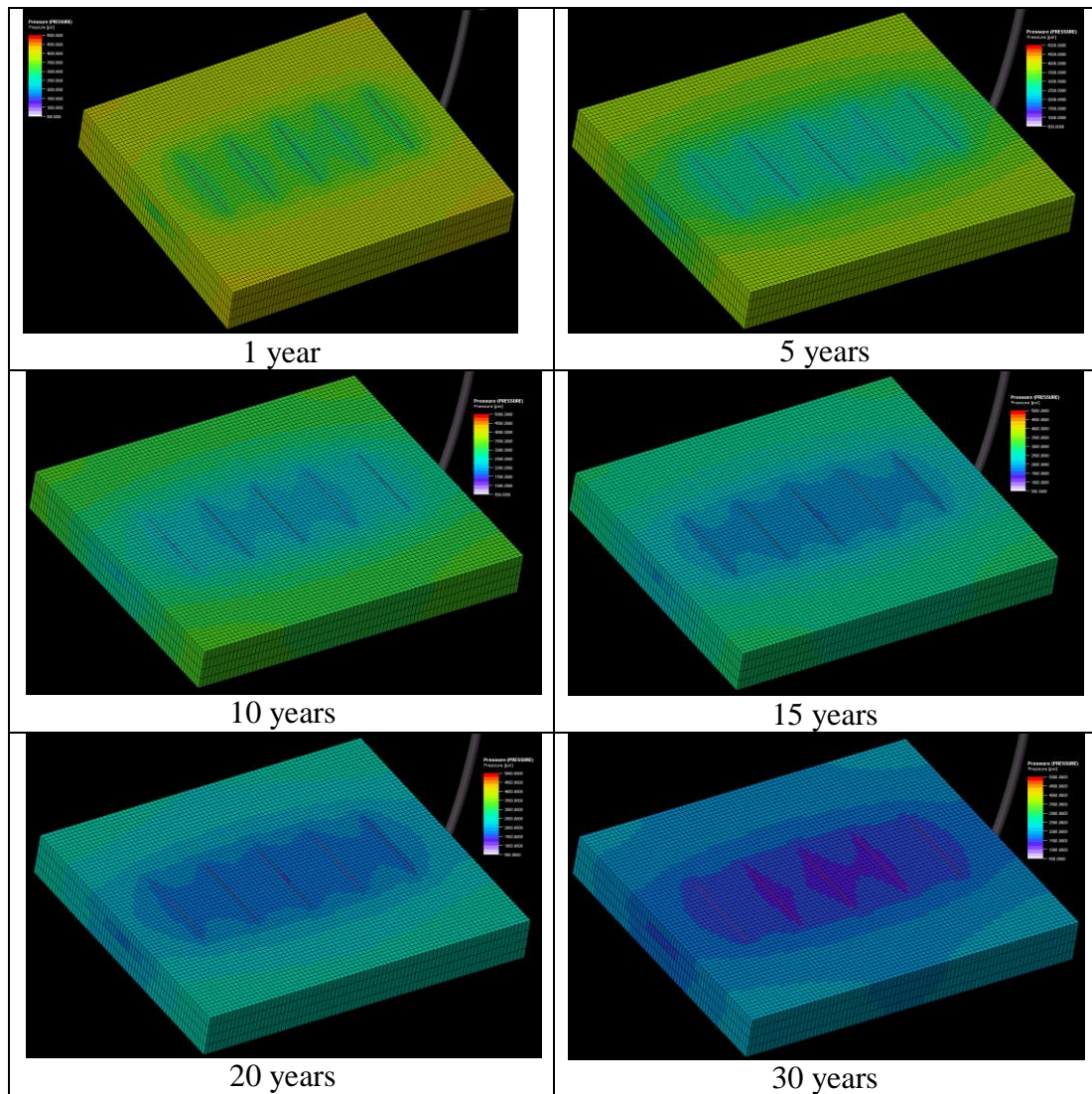
Figure 6.5 pressure distribution in the reservoir through the production time (3D view)

6.4.2   Number of fractures

Optimization of the number of fractures holds remarkable significance in the completion of designs for MFHWs, since each incremental fracture is associated with considerable capital investments, technical complexities, and a high level of uncertainty from a technical, financial and practical perspective. For instance, increasing the number of fractures may generally appear to increase the production, and thus the recovery. Such increments for numbers of fractures more than the optimum number may not be economically viable. Unnecessarily excessive numbers of fractures may also cause complexities associated with completion as well as the execution of a fracturing job.

Figures 6.6-6.8 explain the influence of N_f on gas flow rate (q_g) for different permeabilities varying from 0.01 mD to 0.1 mD. Figures 6.9-6.11 show the effect of the number of fractures on the cumulative gas production for 30 years for permeabilities varying from 0.01 mD to 0.1 mD. As can be observed from Figures 6.6-6.11, maintaining the higher gas production rate and thus the cumulative gas production, requires the number of fractures to increase as the reservoir permeability decreases. This is because the resistance to flow increases as permeability decreases, so the contact flow area between the well and the reservoir should be extended to minimize the loss due to the resistance to flow resulting from the low permeability. For horizontal wells in tight reservoirs, the most effective way to increase the contact flow area is to add more hydraulic fractures to expand the drainage area. Therefore, the less permeability the formation requires, the higher the number of hydraulic fractures.
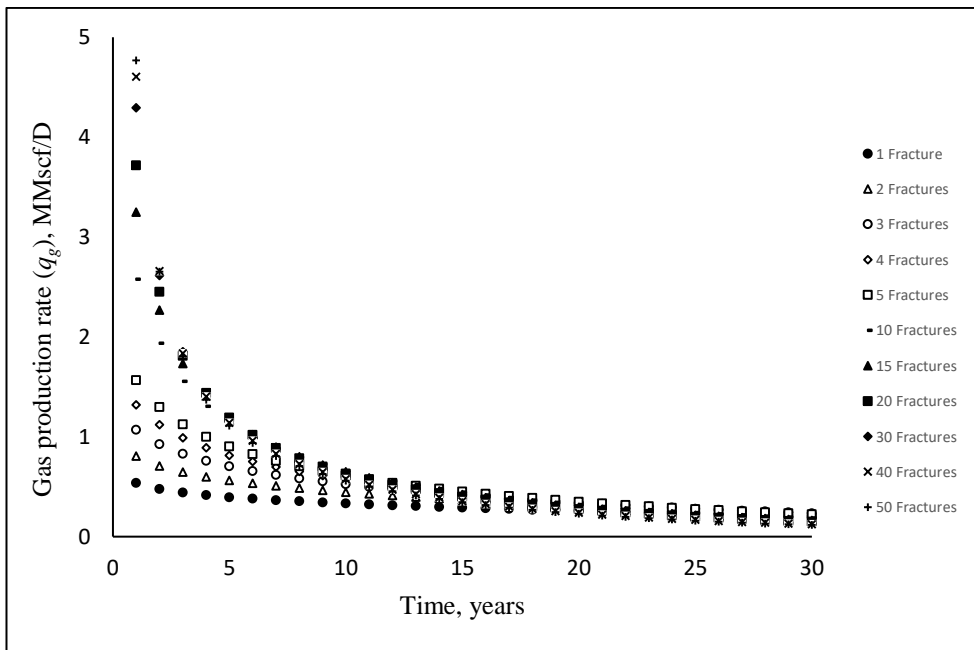
Figure 6.6 Effects of N_f on q_g for reservoir permeability of 0.01 mD over 30 years
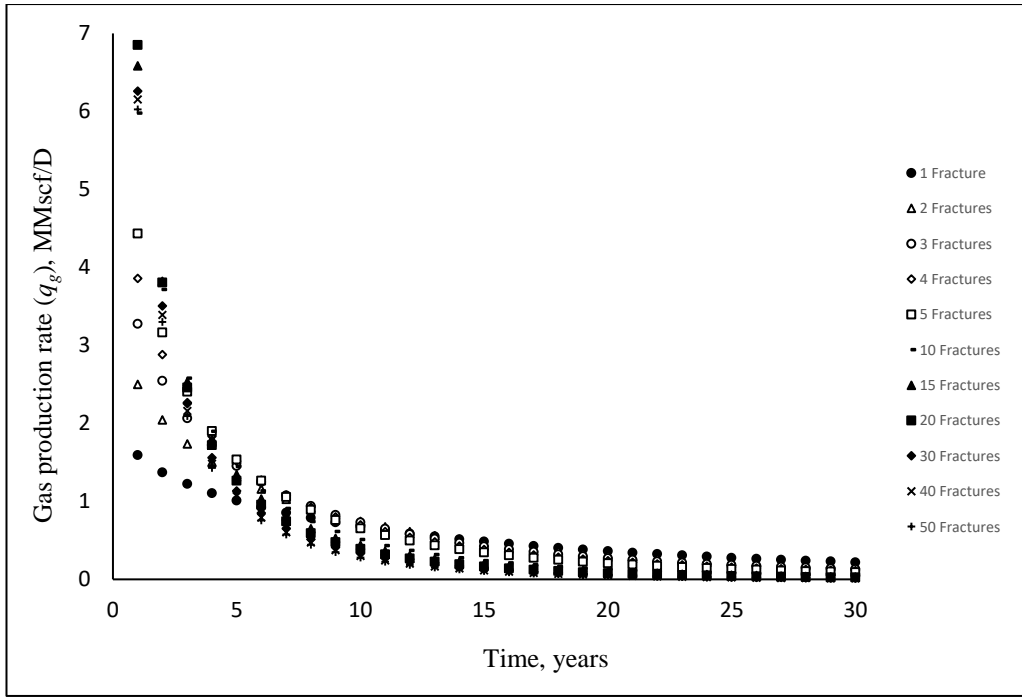
Figure 6.7 Effects of N_f on q_g for reservoir permeability of 0.05 mD over 30 years
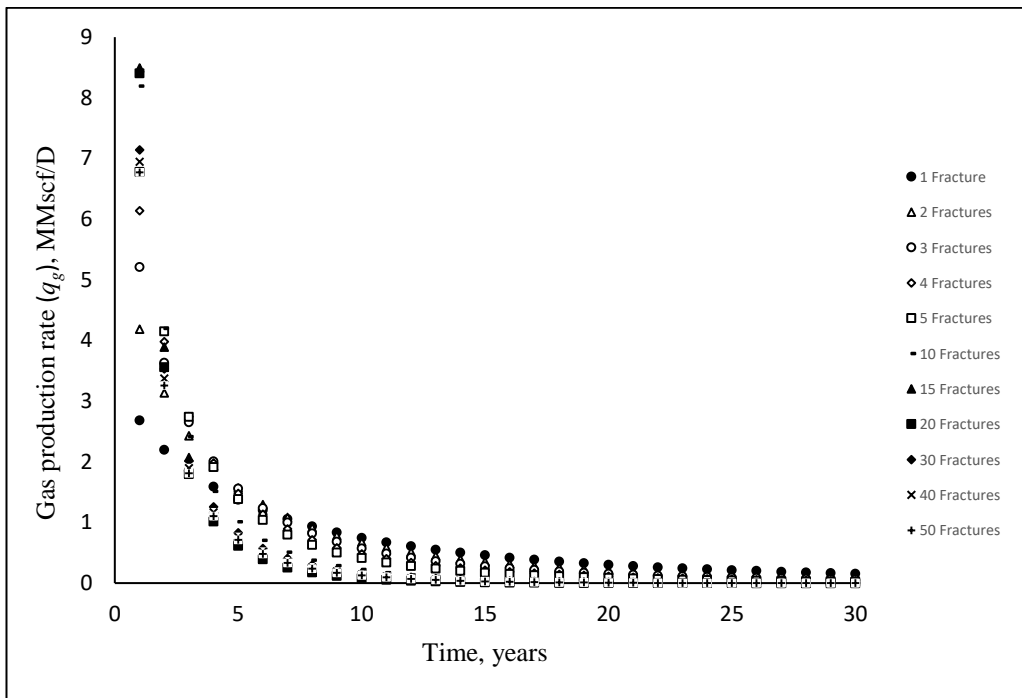
Figure 6.8 Effects of N_f on q_g for reservoir permeability of 0.1 mD over 30 years
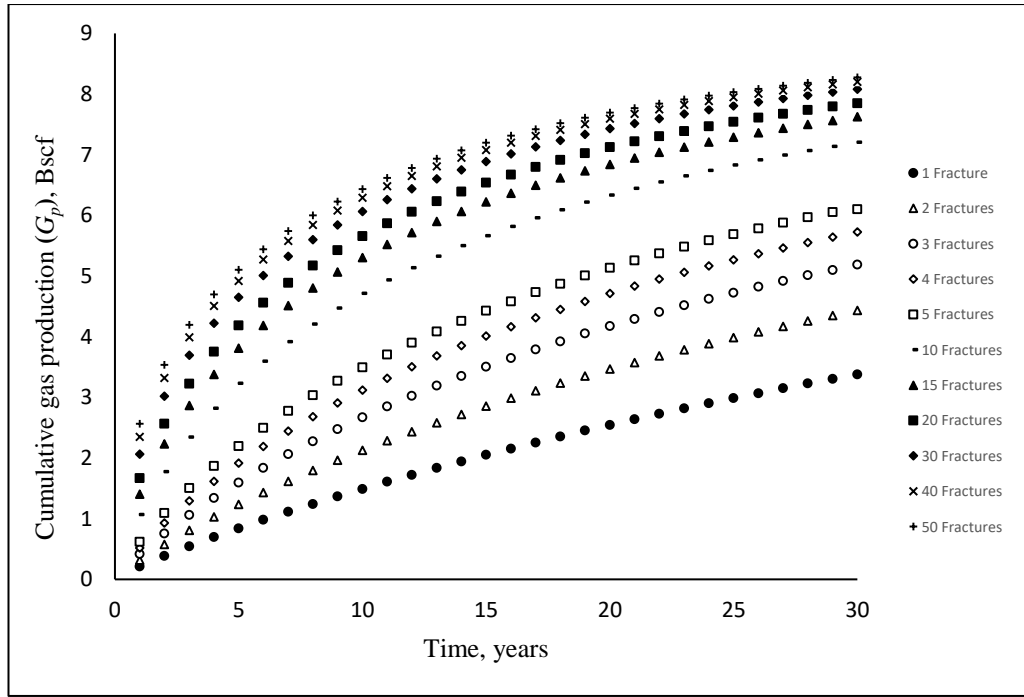
Figure 6.9 Effects of N_f on G_p for reservoir permeability of 0.01 mD over 30 years
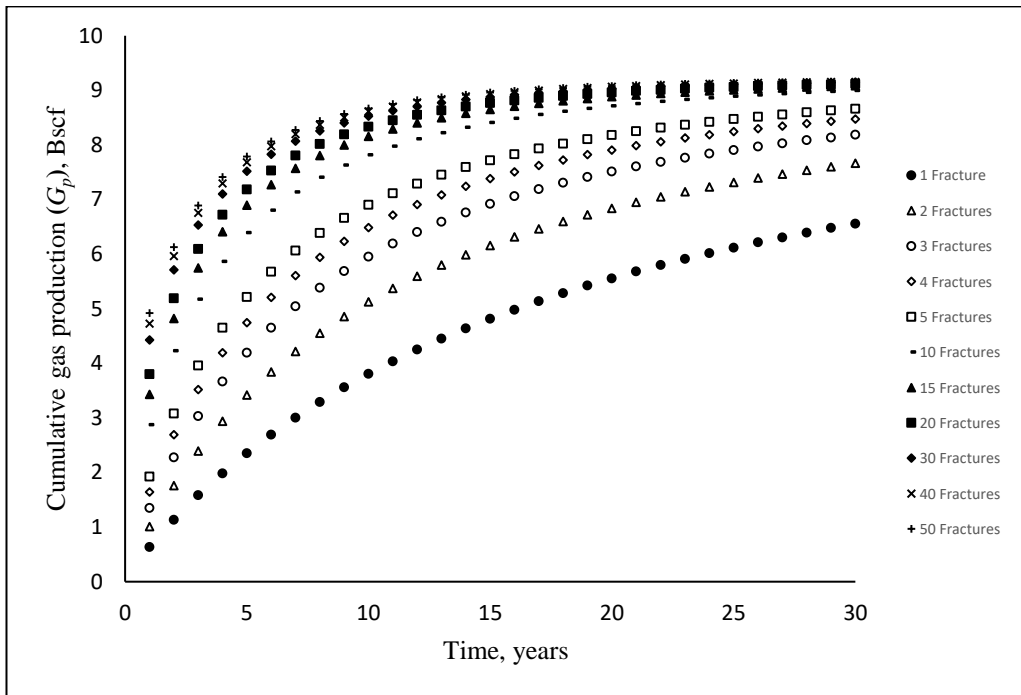
Figure 6.10 Effects of N_f on G_p for reservoir permeability of 0.05 mD over 30 years
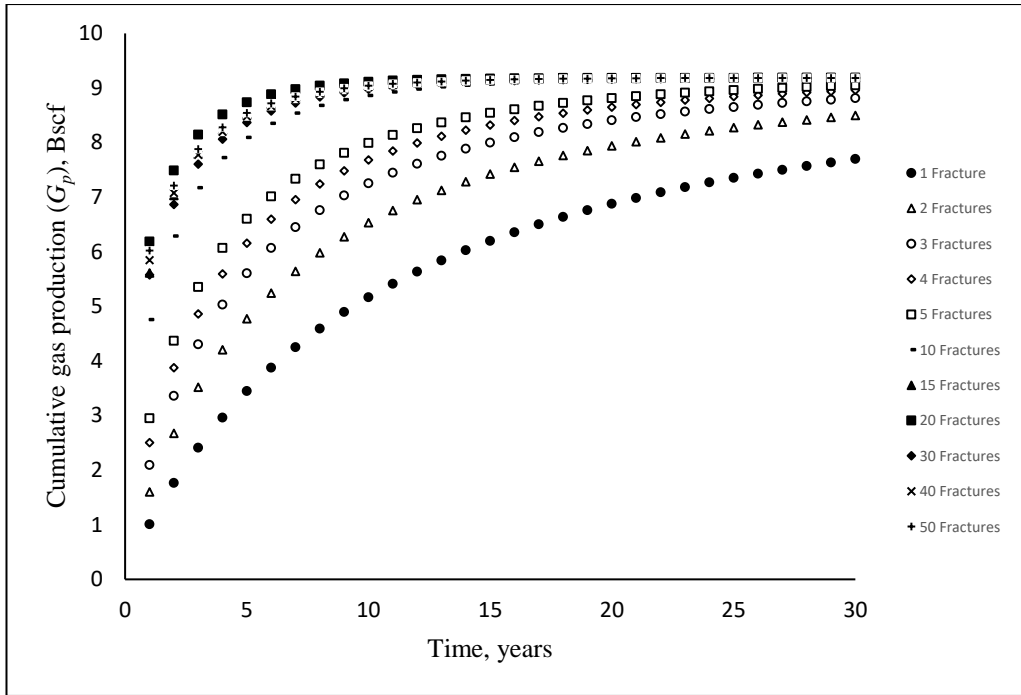
Figure 6.11 Effects of N_f on G_p for reservoir permeability of 0.1 mD over 30 years

Figure 6.12 shows that G_p increases with increasing N_f until it reaches the critical number of fractures, after which the G_p remains constant or the incremental G_p becomes insignificant. This trend appears to be sensible as cumulative gas production depends on the well drainage area, which is also a function of reservoir permeability and time. As a result, the increasing number of fractures overlaps the drainage area (interference effect), which causes decrease in the pressure drawdown and results in a decrease in the incremental rate as N_f increases beyond a specific optimum value.
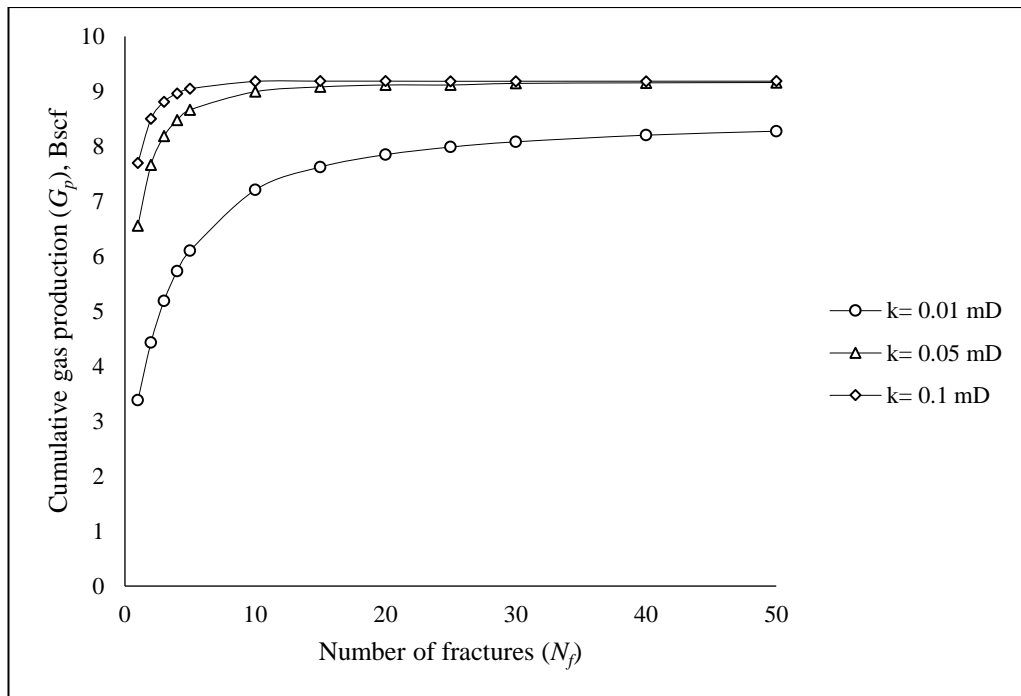
Figure 6.12 The relationship between the cumulative gas production and number of fractures for 30 years: permeability comparison

Figure 6.13 presents *NPV* at different numbers of fractures for three reservoir cases at permeabilities of 0.01, 0.05 and 0.1 mD. For the same reason as explained earlier, the *NPV* appears to increase with respect to the number of fractures up to a certain value, termed as the optimum number of fractures, after which the *NPV* decreases beyond this value. This is because the incremental rate or cumulative gas production decreases beyond the optimum value resulting in decreasing the *NPV*.

Numerical simulation of a large number of fractures towards achieving the optimum number of fractures in a horizontal well can be quite challenging since it requires a high-performance computer for such a huge computation and for the higher capacity simulator and long simulation time (in some cases it could take a week for a single run), which may not be feasible in a demanding routine industry environment, especially in a marginal case with a limited budget.

Figure 6.13 shows the net present value as a function of N_f for permeability ranges from 0.01 to 0.1 mD obtained from reservoir simulation. As expected, this figure confirms that the optimum number of fractures increases with decreasing the permeability. This corresponds with the fact that as permeability decreases, most of

the drainage takes place from the inter-reservoir region (Ozkan et al., 2011) and thus, more fractures are needed to extend the drainage footprint.

It can be recognized from Figure 6.13 that the optimum number of fractures, especially for permeability 0.05 and 0.1, lies within close proximity, which is barely possible to differentiate. This can mislead the prediction. Such difficulties can easily be overcome using the developed technique explained earlier in Section 6.3.

The $(DDNPV)_{N_f}$ is plotted as a function of the number of fractures for permeability of 0.01, 0.05 and 0.1 mD in Figure 6.14. The optimum number of fractures obtained by employing the developed technique (25, 16 and 12 for permeability 0.01, 0.05 and 0.1 mD respectively, as shown in Figure 6.14) are observed to be in good agreement with the result obtained using the numerical reservoir simulation (i.e., respectively 22, 16 and 14, as shown in Figure 6.13).

The NPVs at the optimum number of fractures for permeability 0.01~0.1 mD calculated by numerical reservoir simulation and developed technique are presented in Table 6.4. From Table 6.4, it can be clearly observed that the results obtained by both techniques are in excellent agreement, with insignificant anomalies, warranting that the developed technique can be reliably used as a good alternative tool. In addition, the developed technique is very simple, and provides fast solutions with high accuracy. The technique does not require detailed information about the reservoir, rather it requires authentic production data, and basic reservoir property data. This can be easily implemented in a routine industry environment, and can be considered as a simple tool, especially for the front-line engineer, who can perform the calculation using a simple spreadsheet-based program.
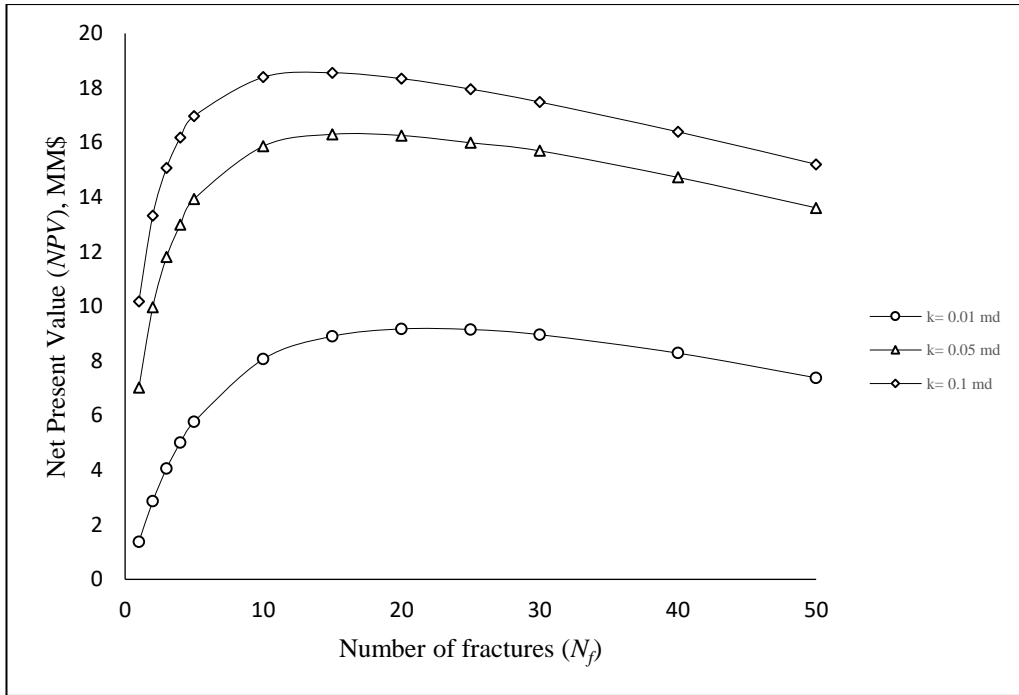
Figure 6.13 *NPV* as a function of N_f for 30 years for different permeability
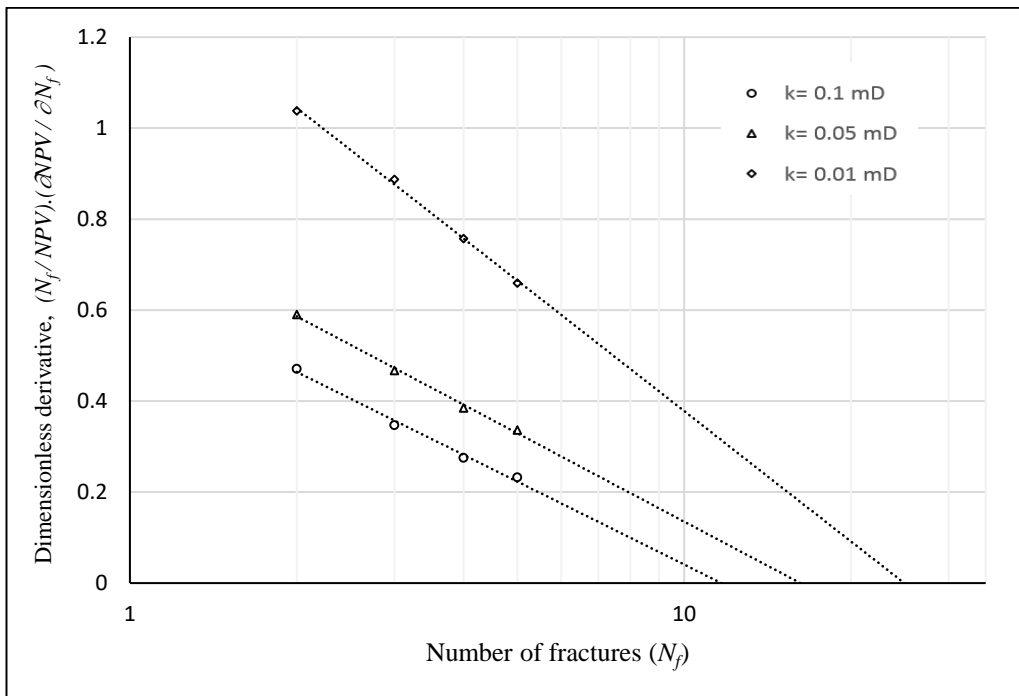
Figure 6.14 The dimensionless derivative of NPV with respect to N_f

Table 6.4 Comparison of *NPV* for optimum number of fractures

k, mD	*NPV*, MM$	
	Reservoir simulation	Proposed technique
0.01	9.193	9.152
0.05	16.322	16.322
0.1	18.569	18.535

6.4.3 Fracture length

Using the mechanistic reservoir model as explained earlier in Section 6.4.1 and using data presented in Table 6.4, a single hydraulic fracture perpendicular to the horizontal well was placed in the centre of the horizontal section of the well. The model was simulated for 30 years, and corresponding cumulative gas production (G_p) was calculated for fracture half-length ranges from 50~1600 ft for different reservoir permeability ranges from 0.01 to 0.1 mD. The calculated G_p are plotted as a function of fracture half length (x_f) in Figure 6.15 for different permeability.

It is difficult to precisely determine the optimum fracture half-length from the plot of G_p vs x_f (as shown in Figure 6.15), because in order to obtain a reasonable trends of the G_p vs x_f showing the distinct maximum point necessary to determine accurate optimum fracture half-length, huge numbers of reservoir simulation runs are needed with extremely long run times even with a high-performance computer. For instance, for this particular simulation task with a reservoir area of 320 acres, it took around 160 reservoir simulation runs over 14 hours using a high-performance computer. Hence, the same number of reservoir simulation runs for a larger reservoir area with high heterogeneity or using a computer with normal speed simulation time would take more than a week. Figure 6.15 shows that, as generally expected, the increase in permeability increases G_p with increasing x_f. Further, for the same x_f, G_p increases with increases in the permeability as a result of increasing the inter-matrix flow. Figure 6.15 illustrates that it is difficult to exactly quantify the optimum fracture half-length (x_{fopt}) for different permeability as they appear to be within very close proximity in this particular case. Although G_p increases with increasing x_f, the incremental G_p beyond $x_f = 1000$ ft, in this particular case for any permeability is observed to be insignificant (Figure 6.15). This may be because, in addition to reservoir permeability, the flow of gas also depends on well drainage area and flow regimes surrounding the wellbore. In

this particular case, the well drainage area and flow regimes seem to play a dominant role. A similar trend is also observed for *NPV* as function of x_f for different permeability as shown in Figure 6.16.

The$(DDNPV)_{X_f}$ as a function of x_f are plotted in Figure 6.17 for the reservoir permeability ranges 0.01~0.01 mD. Employing the developed technique, one can easily generate a plot of $(DDNPV)_{X_f}$ as a function of x_f for fracture half-lengths of 250, 500, and 750 ft, to obtain the trend line graphically or by regression analysis as described in Section 6.3.1, and extrapolate until the function, $(DDNPV)_{X_f} = 0$ to obtain the optimum fracture half-length, $(x_f)_{opt}$ As mentioned above, after rigorous simulation for a number of cases, the $(DDNPV)_{X_f}$ as a function of x_f is observed to follow the second order polynomial. Accordingly, the approximate equation of this function is derived following the statistical approach as discussed earlier in Section 6.3.2.2.

Figure 6.17 shows the optimum values of fracture half-length of horizontal well for different permeabilities, which are estimated employing the developed technique, and accordingly the optimum fracture half-lengths obtained are 1595, 1400 and 1265 ft for permeabilities of 0.01, 0.05 and 0.1 mD, respectively, while the optimum fracture half-lengths obtained from the reservoir simulation are 1500, 1475 and 1375 ft for permeabilities 0.01, 0.05 and 0.1 mD, respectively, as shown in Figure 6.16. The *NPV* calculated using the proposed technique and reservoir simulation are presented in Table 6.5, which shows good agreement between the two techniques, warranting that the developed technique can reliably be applied to optimize fracture half-length and can be used as an alternative to numerical reservoir simulation.
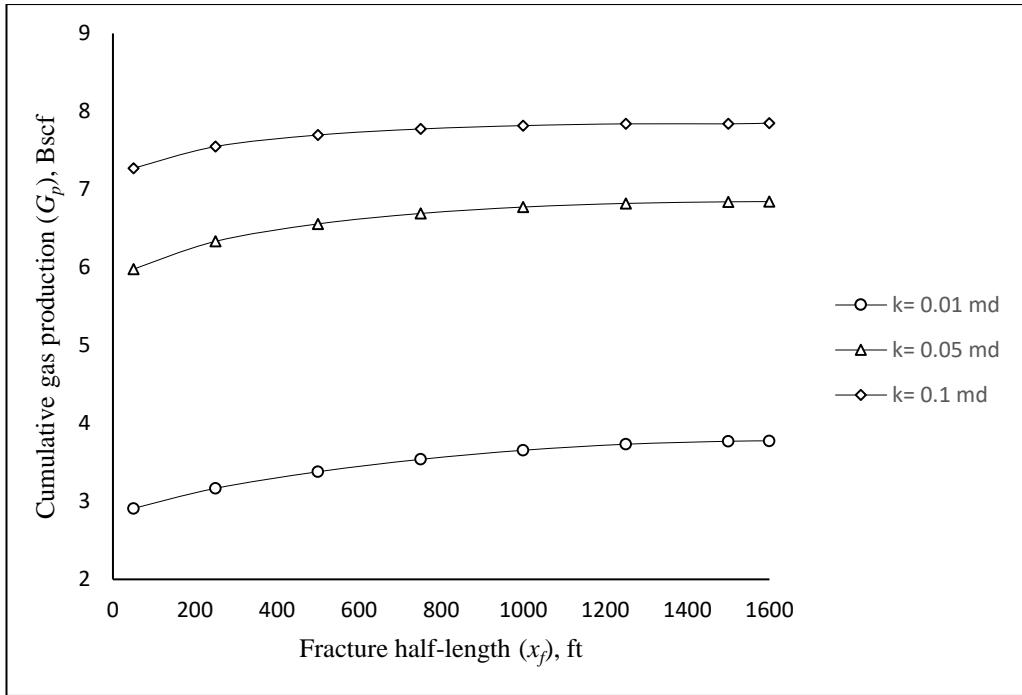
Figure 6.15 Cumulative gas production versus fracture half-length: permeability comparison
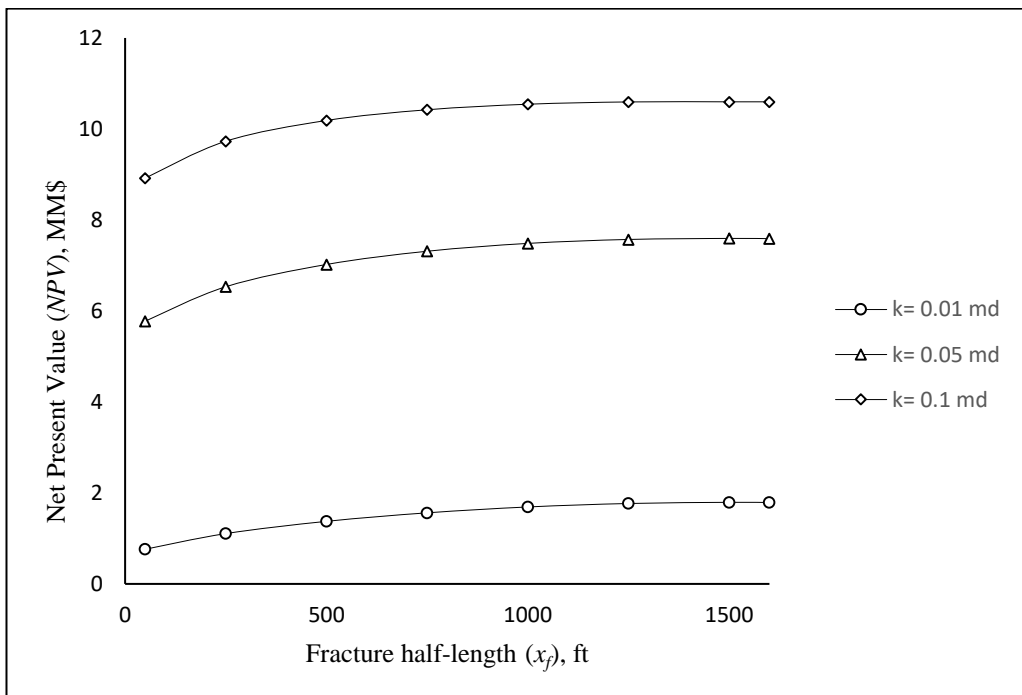
Figure 6.16 The relationship between *NPV* and fracture half-length for 30 years: permeability comparison
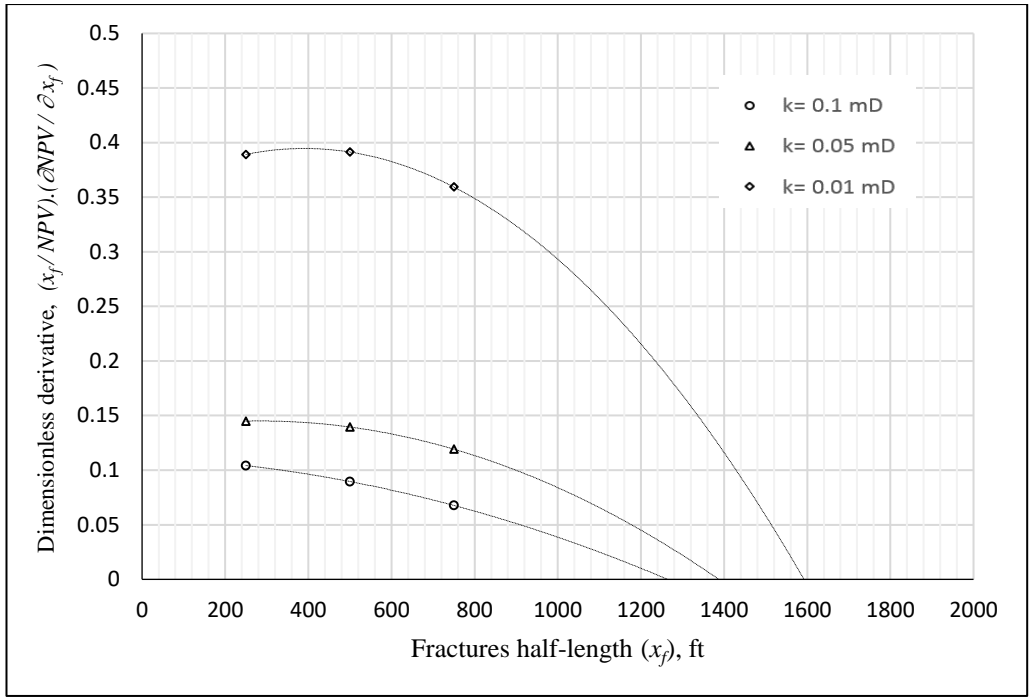
Figure 6.17 The dimensionless derivative of *NPV* with respect to fracture half-length

Table 6.5 Comparison of *NPV* calculated based on each of the suggested method and the reservoir simulation

k, mD	*NPV*, MM\$	
	Reservoir simulation	Proposed technique
0.01	1.793	1.789
0.05	7.594	7.591
0.1	10.601	10.592

As expected, lower permeability reservoir would need longer fractures to attain maximum production as a result of increased reservoir contact. This is because, as permeability decreases, the capacity of the reservoir to flow gas across the porous media also decreases, which requires a larger reservoir contact for more gas to flow in the fractures. Furthermore, increasing the fracture length increases the drainage area. This is more visible when considering lower permeability (Al-Fatlawi et al., 2017b).

211

6.4.4 Simultaneous optimization of fracture half-length and number of fractures for multistage stage fractured horizontal well

The proposed developed techniques described earlier can easily be utilized to simultaneously predict the optimum fracture half-length and number of fractures for the multistage stage fractured horizontal well (MFHW) following the steps described below:

1) Perform simulation runs to calculate the cumulative gas production for single fracture with 3~4 arbitrary fracture half-lengths (x_f), say 250, 500 and 750 ft.

2) Calculate *NPV* for each fracture half-length following the statistical approach described earlier in Section 6.3 and then calculate the *DDNPV* with respect to x_f.

3) Determine the optimum fracture half-length from the intersection between the extrapolation of the quadratic trend line of *DDNPV* and the axis of fracture half-length (x_f) following the statistical approach described in Section 6.3.2.1.

4) Using the optimum fracture half-length estimated above in Step 3, run the simulation for few numbers of fractures (say 4~5) and calculate the respective cumulative gas from the simulation.

5) Calculate *NPV* for each number of fractures using the estimate in Step 4 and then calculate the *DDNPV* with respect to N_f.

6) Determine the optimum number of fractures from the intersection between the extrapolation of the logarithmic trend line of the *DDNPV* and the axis of N_f following the statistical approach described in Section 6.3.2.1.

The above steps were utilized to optimize the fracture half-length and number of fractures for MFHW. Figure 6.18 shows the schematic of the top view of the MFHW showing that the estimated optimum number of fractures determined for an optimum half-length of 1265 ft following the above approach is 11 with a reservoir permeability 0.1 mD. This optimum fracture half-length of 1265 is determined using the approaches explained in Section 6.3.2. Similarly, the optimum number of fractures obtained are 20, 14 and 11 for the permeabilities of 0.01, 0.05 and 0.1 mD, respectively, as indicated in Figure 6.19. The optimum number of fractures obtained from the reservoir simulation studies are 19, 13 and 11 for permeabilities 0.01, 0.05 and 0.1 mD, respectively. In assessing the validity of the proposed approach, Table 6.6 presents the comparison between the *NPV* at an optimum number of fractures which was calculated

based on the proposed technique and the reservoir simulation studies. Table 6.6 confirms excellent matching between the results of the proposed technique and the reservoir simulation for the three permeabilities considered in this study. This matching confirms the credibility of the proposed approach for predicting the optimum number of fractures and fracture half-length for MFHW. The proposed optimization technique for MFHW is simple, fast and yet reliable, and can be adopted easily as a practical tool for routine industry tasks. It requires few optimum numbers of fractures grounded in 4-5 reservoir simulation runs to estimate the number of fractures with acceptable accuracy.
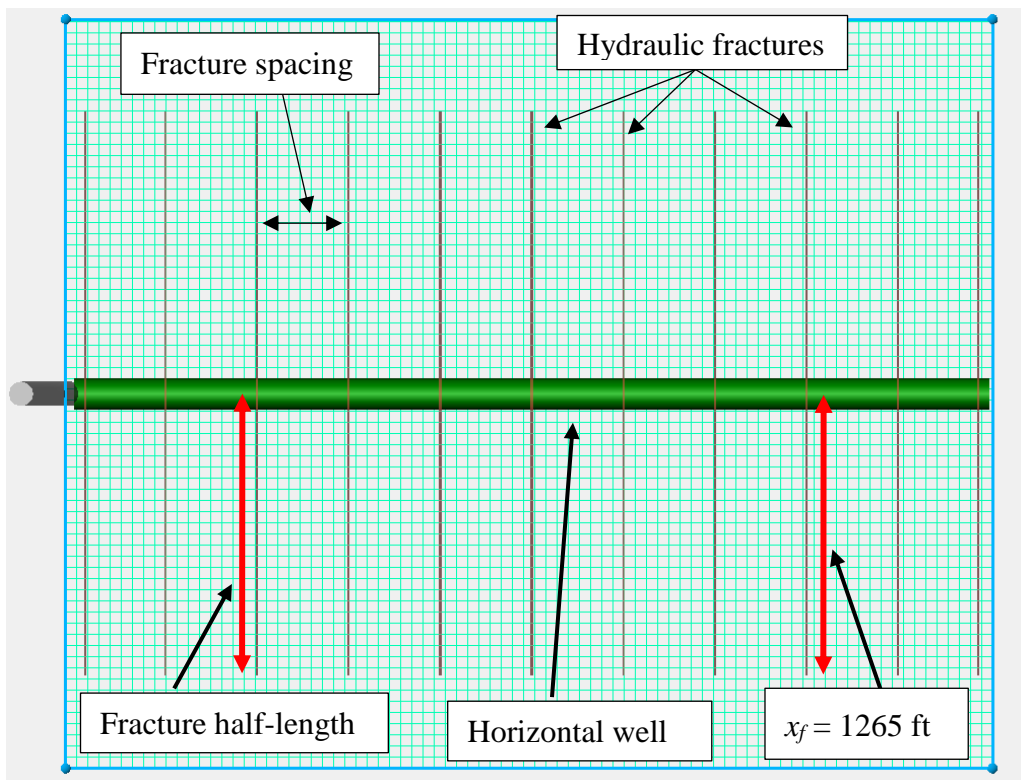
Figure 6.18 Schematic of multi stage hydraulic fractured horizontal gas well (top view)
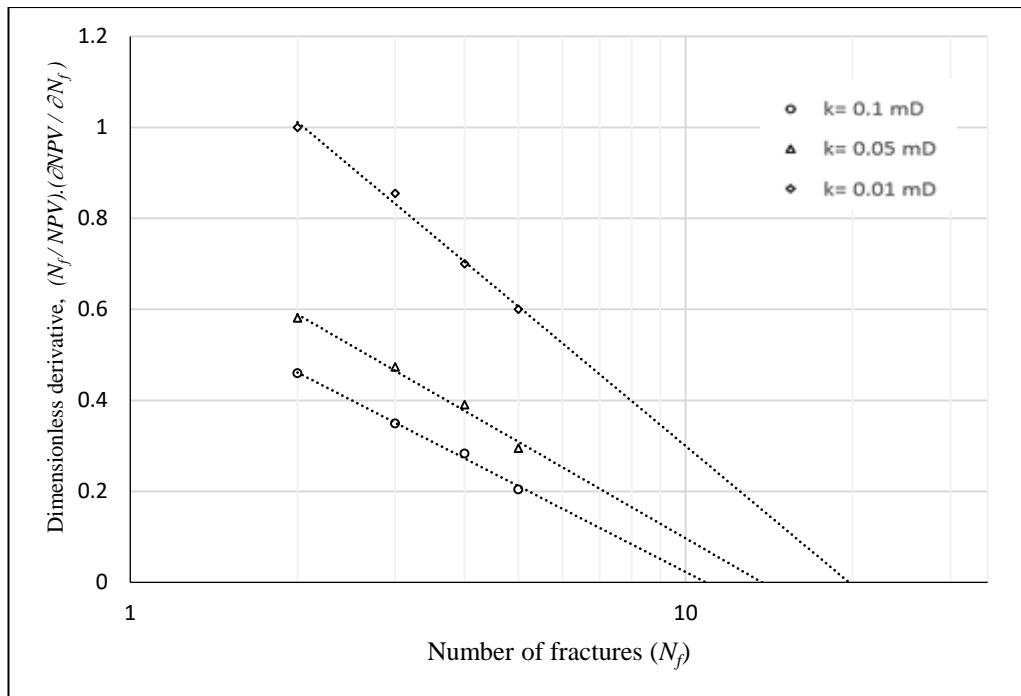
Figure 6.19 The dimensionless derivative of *NPV* with respect to number of fractures

Table 6.6 Comparison of NPV calculated based on each of the suggested method and the reservoir simulation

k, mD	*NPV*, MM$	
	Reservoir simulation	Proposed technique
0.01	10.838	10.831
0.05	16.897	16.895
0.1	18.673	18.673

Although there are many advanced techniques for the optimization of hydraulic fracture parameters to evaluate the potential development of tight gas fields, the developed simplified dimensionless *NPV* derivative based optimization technique is exercised through sensitivity studies using numerical reservoir simulation studies. It is observed that the proposed technique is simple, and provides solutions with high accuracy. In addition, the technique is fast and requires limited information. For this particular study, the production rate data is obtained from reservoir simulations studies due to unavailability of production history data covering the ranges considered in the sensitivity studies. However, it appears that the technique can be easily employed in a real field case when the production history data are available.

214

Chapter 7: Conclusions and Recommendations

The first section of the chapter introduces a summary about the achieved work in the thesis. The second section displays the full conclusions from the work illustrated in the previous chapters. The third part introduces the recommendations for future work.

7.1 Summary of achievements

The achievements of the thesis are summarized as below:

- An approach was developed to identify the most appropriate Z-factor correlation for different gas compositions under a wide range of pressures and temperatures for accurate estimation of gas initially in place (GIIP) for tight gas reservoirs.

- An advancement was made in the Material Balance Technique based on the compartmental reservoir concept for improved estimation of gas initially in place, and ultimate recovery from tight gas reservoirs (TGRs).

- A new set of type curves was created based on a new formulation of the correlation of the "pseudo-steady constant" for vertical fractured wells in TGRs is proposed to estimate gas reserve, reservoir permeability, drainage area, and fracture half-length.

- A simplified method was developed based on combined gas material balance and decline curve analysis to predict the equivalent drainage area of fractured vertical wells in TGRs.

- A numerical technique was proposed to estimate reservoir permeability and fracture half-length of vertical wells in TGRs, especially in the case of limited well test data through capturing the elliptical flow regimes.

- A method was proposed to determine an optimum infill drilling plan based on reservoir simulation modelling combined with the Moving Window Method (MWM) for drilling development of tight gas reservoirs.

- The most efficient optimization tool/technique for the optimization of fracture half-length of fractured vertical wells in tight has reservoir was identified based on integrated reservoir simulation and optimization studies.

- A technique was proposed to optimise the fracture-half-length and number of fractures for multistage hydraulic fractured horizontal wells based on the dimensionless derivative of *NPV* in tight gas reservoirs. The proposed

optimization technique is simple, yet reliable, and can easily be implemented in a routine industry environment and can easily be adopted by frontline engineers

7.2 Conclusions

1) The accuracy in estimation of gas initially in place is highly dependent on accurate determination of the gas compressibility factor (Z-factor) which is sensitive to the conditions associated with pressure, temperature and gas composition. Identification of appropriate correlation for the determination of the Z-factor satisfying the conditions is critical to accuracy of estimated reserves, production forecasting, and accuracy of reservoir simulation studies as well as for minimization of the level of uncertainty.

2) The dependency on the material balance equation, MBE (i.e. conventional MBE), based on a tank model to estimate GIIP and UR for TGRs can lead to error in estimation and increase the level of uncertainty. In general, conventional MBE underestimates the reserve estimation. The lower the reservoir permeability the greater the chance of erroneous estimates from conventional MBE.

3) The developed MBEs based on the compartmental reservoir concept estimates the GIIP and UR factor with higher accuracy for tight gas reservoirs compared to conventional technique, warranting that the compartment reservoir concept should be better exercised for such estimation.

4) The proposed approach of type curves based on modified correlation for the pseudo-steady constant is superior to the decline curve analysis and similar existing type curves, which can easily be used as a viable alternative to reservoir simulation studies for TGRs, especially in the case of limited data availability.

5) The drainage areas of the wells in TGRs no longer have fixed boundaries, which vary with production time because of low permeability.

6) Propagation of planned equivalent drainage area as a function of production time is significantly affected by the fracture half-length and reservoir permeability.

216

7) Fracture half-length and permeability have strong correlation with the planned equivalent drainage area, and reservoir shape appears to have a minor impact on the planned equivalent drainage area for TGRs.

8) A limited dataset of elliptical flow regime can be employed to perform pressure transient analysis to obtain fracture half-length and reservoir permeability in a fractured vertical well in a TGR. The proposed technique can easily be employed in a routine industry environment, and used as an effective tool, especially by young engineers who do not have extensive experience in pressure transient analysis. The workflow of this tool is simple, easy to implement and can work with limited data.

9) The Moving Window Method (MWM) for infill drilling was found to be an efficient approach for the development of optimum drilling planning for TGRs.

10) The proposed infill drilling technique developed based on the MWM approach was applied to the Whicher Range tight gas field as an example case study. The result of the case study warrants that the production from this field can potentially be increased by 30% more than can be offered by other alternative planning option for the same number of wells.

11) There are several optimization techniques that can be employed to optimize hydraulic fractured wells (both horizontal and vertical wells). The identification of the most efficient optimization technique is critical, especially from economic, resource and time constraint viewpoints.

12) The Simplex non-linear optimization technique was generally found to be more efficient from the above viewpoints to optimize hydraulic fractured vertical wells for low permeability tight gas reservoirs. However, the neural network-based optimization technique appears to work better for multi-well models for very low permeability (~0.05 mD) tight reservoirs.

13) The proposed optimization technique developed based on dimensionless derivative NPV was found to be a simple yet very reliable tool to optimize multistage fractured horizontal well for a range of tight gas reservoir permeabilities (moderately low to extremely low permeability), especially in the case when only production history data or limited reservoir data (mechanistic model) are available.

14) The sensitivity study revealed that increasing the number of fractures beyond a threshold would decrease the chance of incremental productivity, mainly due to the interference of the drainage area.

7.3 Recommendations

Tight gas reservoirs will continue to be the focus of academic and industrial research. Most of the techniques and/or tools for the analysis of TGRs from prospect evaluation to development of the tight gas field are not adequate to capture the true conditions and mechanisms, especially accurately modelling the TGRs. In particular, the prospect valuation and optimization of the production performance of TGRS is challenging, and needs continuous research and development (R&D) to fulfill many rooms. The main challenge faced in this thesis was the required length of time to run the reservoir simulation and optimization. In addition, this study purely focused from reservoir engineering and practical field development viewpoints. The geomechanics plays a significant role on efficient development of tight gas fields, especially when hydraulic fracture stimulation is a must. For instance, in addition to basic fracture parameters (e.g. fracture length, width, conductivity, and reservoir permeability), the performance of hydraulic fractured wells (vertical or horizontal well) also depends on fracture geometry (size, and shape,) propagation behavior, nature of fracture geometry, etc. To account for the influence of these issues, it is essential to include the rock mechanical model and prevailing in-situ stress condition. The coupled geomechanical and numerical reservoir may capture some of these critical aspects which are key to minimize associated uncertainties. These aspects were beyond the scope of this thesis, however. Further research is essential to advance all the models and techniques developed in this study and to take these aspects into consideration for further improvement. However, the following recommendations are made, particularly in the context of the improvement of current work through research:

- Further study may be extended to take into account geomechanical aspects for further advancement of all prosed developed models.
- All the models proposed are focused on tight gas reservoir (i.e. tight sand) with permeabilities from 0.01 to 0.1. Further study may be carried out for shale gas, shale oil and/or tight carbonate reservoirs.

- It is well known that in the process of the propagation of hydraulic fracture non-planar fractures may be developed, which in turn can interact with pre-existing natural fractures in tight gas reservoirs resulting in the development of a double porosity system in a region around wellbore. This aspect is not considered in current study as it is beyond the scope of the work, and recommended further study in this aspects, especially for naturally fractured tight formation.

- The case studies were performed to evaluate the effectiveness of various optimization techniques using integrated reservoir simulation coupled with optimization engines for hydraulic fractured vertical wells. Further work may be extended for the optimization of multistage fractured horizontal wells.

- The numerical simulation related to in-fill drilling using the Moving Window Method were performed for hydraulic fractured vertical wells. This study may be extended for multistage fractured horizontal wells.

- Further study may be extended to evaluate the effectiveness of proposed new sets of type curves for the analysis of production data for multistage fractured horizontal wells.

- The proposed optimization technique developed based on dimensionless derivative of NPV for MFHW may be further investigated for multi-well cases and for hydraulic fractured vertical wells.

References

Abass, H., Sierra, L., & Tahini, A. (2009). *Optimizing proppant conductivity and number of hydraulic fractures in tight gas sand wells.* Paper presented at the SPE Saudi Arabia Section Technical Symposium, Khobar, Saudi Arabia.

Abdi, H. (2007). The method of least squares. *Encyclopedia of Measurement and Statistics. CA, USA: Thousand Oaks*.

Abdullah, S. M. (2017). Smart Energy Consumption could Preserve Natural Resources. *Islam and Civilisational Renewal (ICR), 8*(3), 420-422.

Abukhamsin, A. Y. (2009). *OPTIMIZATION OF WELL DESIGN AND LOCATION IN A REAL FIELD.* STANFORD UNIVERSITY,

Agarwal, R. G., Gardner, D. C., Kleinsteiber, S. W., & Fussell, D. D. (1998). *Analyzing Well Production Data Using Combined Type Curve and Decline Curve Analysis Concepts*. Paper presented at the SPE Annual Technical Conference and Exhibition, New Orleans, Louisiana.

Aguilera, R. F., Harding, T., & Krause, F. (2008). *Natural Gas Production From Tight Gas Formations: A Global Perspective*. Paper presented at the 19th World Petroleum Congress, Madrid, Spain.

Ahmed, T. (2006). *Reservoir engineering handbook* (Third Edition ed.). Burlington, MA, USA: Gulf Professional Publishing.

Ahmed, U., & Meehan, D. N. (2016). *Unconventional oil and gas resources: exploitation and development*: CRC Press.

Akram, F. (2011). *Multi-Million Cell SAGD Models-Opportunity For Detailed Field Analysis.* Paper presented at the SPE Reservoir Characterisation and Simulation Conference and Exhibition.

Al-Driweesh, S. M., Dashash, A. A., Malik, A. R., Leal, J., Soriano, E., & Lopez, A. (2014). *Overcoming Hydraulic Fracturing Challenges in High Temperature and Tight Gas Reservoirs of Saudi Arabia with an Enhanced Fracturing Fluids System.* Paper presented at the IPTC 2014: International Petroleum Technology Conference, Doha, Qatar.

Al-Fatlawi, O., Hossain, M. M., & Osborne, J. (2017a). Determination of best possible correlation for gas compressibility factor to accurately predict the initial gas reserves in gas-hydrocarbon reservoirs. *International Journal of Hydrogen Energy, 42*(40), 25492-25508. doi:https://doi.org/10.1016/j.ijhydene.2017.08.030

Al-Fatlawi, O., Hossain, M. M., & Saeedi, A. (2017b). *A New Practical Method for Predicting Equivalent Drainage Area of Well in Tight Gas Reservoirs*. Paper presented at the SPE Europec featured at 79th EAGE Conference and Exhibition, Paris, France.

Al-Fatlawi, O., Mofazzal, M. H., Hicks, S., & Saeedi, A. (2016). *Developed material balance approach for estimating gas initially in place and ultimate recovery for tight gas reservoirs*. Paper presented at the Abu Dhabi International Petroleum Exhibition & Conference.

Al-Fatlawi, O., Vimal Roy, A. R., Hossain, M. M., & Kabir, A. H. (2017c). *Optimization of Infill Drilling in Whicher Range Field in Australia*. Paper presented at the SPE Kingdom of Saudi Arabia Annual Technical Symposium and Exhibition, Dammam, Saudi Arabia.

AL-FATLAWY, O. F. H. (2004). *Prediction of Optimum Separation Conditions for Sequential Field Separation System.* M. Sc. Thesis, University of Baghdad,

Al-Jawad, M. S., & Hassan, O. F. (2010). Correlating optimum stage pressure for sequential separator systems. *SPE Projects, Facilities & Construction, 5*(01), 13-16.

Al-Jawad, M. S., & Hassan, O. F. (2012). *Comprehensive Model for Flash Calculations of Heavy Oils Using the Soave-Redlich-Kwong Equation of State.* Paper presented at the North Africa Technical Conference and Exhibition.

Al Marri, H., & Kabir, A. (2015). *PVT characterization of a wet gas reservoir and its impact on reserves estimate*. Paper presented at the SPE Saudi Arabia Section Annual Technical Symposium and Exhibition, Al-Khobar, Saudi Arabia.

Aly, A., Bukhamseen, R., Ramsey, L., & Mesdour, R. (2009). *Applications of a Multidomain, Integrated Tight Gas Field Development Process in North America and How To Adapt It to the Middle East*. Paper presented at the SPE Saudi Arabia Section Technical Symposium, Al-Khobar, Saudi Arabia.

Aly, A. M., Ramsey, L., & Shehata, A. M. (2010). *Overview of Tight Gas Field Development in the Middle East and North Africa Region.* Paper presented at the North Africa Technical Conference and Exhibition, Cairo, Egypt.

Alzate, G. A., Chen, H.-Y., & Teufel, L. W. (2001). *Drainage Shape and Size of a Vertically-Fractured Tight-Gas Well*. Paper presented at the SPE Rocky Mountain Petroleum Technology Conference, Keystone, Colorado.

Anderson, J. S. (1991). *Pressure Mapping as an Aid To Understanding Reservoir Drainage*. Paper presented at the SPE Asia-Pacific Conference, Perth. Australia.

Araya, A., & Ozkan, E. (2002). *An Account of Decline-Type-Curve Analysis of Vertical, Fractured, and Horizontal Well Production Data*. Paper presented at the SPE Annual Technical Conference and Exhibition, San Antonio, Texas.

Arnold, D. V., & Beyer, H.-G. (2002). *Noisy optimization with evolution strategies* (Vol. 8): Springer Science & Business Media.

Arora, R. K. (2015). *Optimization: algorithms and applications*. New York: Chapman and Hall/CRC.

Arps, J. J. (1945). Analysis of Decline Curves. *Transactions of the AIME, 160*(01). doi:10.2118/945228-G

Back, T. (1996). *Evolutionary algorithms in theory and practice: evolution strategies, evolutionary programming, genetic algorithms*: Oxford university press.

Bäck, T. (1997). *Proceedings of the Seventh International Conference on Genetic Algorithms.* Paper presented at the International Conference on Genetic Algorithms 1997: East Lansing, Mich.).

Bäck, T., Fogel, D. B., & Michalewicz, Z. (2000). *Evolutionary computation 1: Basic algorithms and operators* (Vol. 1): CRC press.

Bäck, T., Hammel, U., & Schwefel, H.-P. (1997). Evolutionary computation: Comments on the history and current state. *IEEE transactions on Evolutionary Computation, 1*(1), 3-17.

Back, T., Hoffmeister, F., & Schwefel, H.-P. (1991). *A survey of evolution strategies.* Paper presented at the Proceedings of the fourth international conference on genetic algorithms.

Badazhkov, D., Dmitry, O., & Kovalenko, A. (2008). *Analysis of production data with elliptical flow regime in tight gas reservoirs.* Paper presented at the SPE Russian Oil and Gas Technical Conference and Exhibition.

Bagherian, B., Ghalambor, A., Sarmadivaleh, M., Rasouli, V., Nabipour, A., & Eshkaftaki, M. M. (2010). *Optimization of multiple-fractured horizontal tight gas well*. Paper presented at the SPE International Symposium and Exhibiton on Formation Damage Control, Lafayette, Louisiana, USA.

Bahadori, A. (2012). Analysing gas well production data using a simplified decline curve analysis method. *Chemical Engineering Research and Design, 90*(4), 541-547. doi:https://doi.org/10.1016/j.cherd.2011.08.014

Bahadori, A., Mokhatab, S., & Towler, B. F. (2007). Rapidly estimating natural gas compressibility factor. *Journal of Natural Gas Chemistry, 16*(4), 349-353.

Bahrami, H., Jayan, V., Rezaee, R., & Hossain, M. (2012a). Welltest analysis of hydraulically fractured tight gas reservoirs: a field example from Perth Basin, Western Australia. *The APPEA Journal, 52*(1), 587-594.

Bahrami, H., Rezaee, R., & Clennell, B. (2012b). Water blocking damage in hydraulically fractured tight sand gas reservoirs: An example from Perth Basin, Western Australia. *Journal of petroleum science and engineering, 88*, 100-106.

Bahrami, N. (2013). Tight Gas Reservoirs Characterisation for Dynamic Parameters. In *Evaluating Factors Controlling Damage and Productivity in Tight Gas Reservoirs* (pp. 13-20): Springer.

Barree, R. D., Miskimins, J., & Gilbert, J. (2015). Diagnostic fracture injection tests: common mistakes, misfires, and misdiagnoses. *SPE Production & Operations, 30*(02), 84-98.

Beyer, H.-G., & Schwefel, H.-P. (2002). Evolution strategies – A comprehensive introduction. *Natural Computing, 1*(1), 3-52. doi:10.1023/a:1015059928466

Bhattacharya, S., & Nikolaou, M. (2013). Analysis of production history for unconventional gas reservoirs with statistical methods. *SPE Journal, 18*(05), 878-896.

Bittencourt, A. C., & Horne, R. N. (1997). *Reservoir development and design optimization*. Paper presented at the SPE annual technical conference and exhibition, San Antonio, Texas.

Blasingame, T. A., Amini, S., & Rushing, J. (2007). *Evaluation of the Elliptical Flow Period for Hydraulically-Fractured Wells in Tight Gas Sands--Theoretical Aspects and Practical Considerations.* Paper presented at the SPE Hydraulic Fracturing Technology Conference, College Station, Texas, U.S.A.

Blasingame, T. A., McCray, T. L., & Lee, W. J. (1991). *Decline Curve Analysis for Variable Pressure Drop/Variable Flowrate Systems*. Paper presented at the SPE Gas Technology Symposium, Houston, Texas.

Borges, U., & Jamiolahmady, M. (2009). *Well Test Analysis in Tight Gas Reservoirs*. Paper presented at the EUROPEC/EAGE Conference and Exhibition, Amsterdam, The Netherlands.

Bouzarkouna, Z., Ding, D. Y., & Auger, A. (2012). Well placement optimization with the covariance matrix adaptation evolution strategy and meta-models. *Computational Geosciences, 16*(1), 75-92. doi:10.1007/s10596-011-9254-2

BP. (2017). *Unconventional gas and hydraulic fracturing Issue briefing*. Retrieved from

BP. (2018). *BP Statistical Review of World Energy June*. Retrieved from

Branagan, P., & Cotner, G. (1982). *A Competent and Practical Approach to Well Testing and Analysis in Tight Gas Reservoirs*. Paper presented at the SPE Unconventional Gas Recovery Symposium, Pittsburgh, Pennsylvania.

Brandman, J., Denli, H., & Trenev, D. (2018). Introduction to PDE-Constrained Optimization in the Oil and Gas Industry. In H. Antil, D. P. Kouri, M.-D. Lacasse, & D. Ridzal (Eds.), *Frontiers in PDE-Constrained Optimization* (pp. 171-203). New York, NY: Springer New York.

Brownlee, J. (2011). *Clever algorithms: nature-inspired programming recipes*: Jason Brownlee.

Cellek, M. S., & Pınarbaşı, A. (2017). Investigations on performance and emission characteristics of an industrial low swirl burner while burning natural gas, methane, hydrogen-enriched natural gas and hydrogen as fuels. *International Journal of Hydrogen Energy*.

Chacon, A., Djebrouni, A., & Tiab, D. (2004). *Determining the average reservoir pressure from vertical and horizontal well test analysis using the Tiab's Direct Synthesis technique.* Paper presented at the SPE Asia Pacific Oil and Gas Conference and Exhibition.

Chamkalani, A., Zendehboudi, S., Chamkalani, R., Lohi, A., Elkamel, A., & Chatzis, I. (2013). Utilization of support vector machine to calculate gas compressibility factor. *Fluid Phase Equilibria, 358*, 189-202.

Chen, H.-Y., & Teufel, L. W. (2000). *A new rate-time type curve for analysis of tight-gas linear and radial flows.* Paper presented at the SPE Annual Technical Conference and Exhibition, Dallas, Texas.

Cheng, Y., Lee, W. J., & McVay, D. A. (2007). *A new approach for reliable estimation of hydraulic fracture properties in tight gas wells.* Paper presented at the SPE Hydraulic Fracturing Technology Conference, College Station, Texas, U.S.A.

Cheng, Y., Lee, W. J., & McVay, D. A. (2009a). A New Approach for Reliable Estimation of Hydraulic Fracture Properties Using Elliptical Flow Data in Tight Gas Wells. *SPE Reservoir Evaluation & Engineering, 12*(02), 254-262.

Cheng, Y., McVay, D. A., & Lee, J. W. (2006). *Optimal infill drilling design for marginal gas reservoirs using a simulation-based inversion approach.* Paper presented at the SPE Eastern Regional Meeting, Canton, Ohio, USA.

Cheng, Y., McVay, D. A., & Lee, W. J. (2009b). A practical approach for optimization of infill well placement in tight gas reservoirs. *Journal of Natural Gas Science and Engineering, 1*(6), 165-176.

Chengzao, J. (2017). Breakthrough and significance of unconventional oil and gas to classical petroleum geology theory. *Petroleum Exploration and Development, 44*(1), 1-10.

Chong, E. K., & Zak, S. H. (2013). *An introduction to optimization* (Vol. 76): John Wiley & Sons.

Cinco-Ley, H., & Samaniego-V, F. (1981). Transient Pressure Analysis for Fractured Wells. *Journal of Petroleum Technology, 33*(09). doi:10.2118/7490-PA

Cipolla, C. L., & Wood, M. C. (1996). A statistical approach to infill-drilling studies: Case history of the Ozona Canyon sands. *SPE Reservoir Engineering, 11*(03), 196-202.

Coello, C. A. C. (2000). Use of a self-adaptive penalty approach for engineering optimization problems. *Computers in Industry, 41*(2), 113-127.

Coello, C. A. C., Lamont, G. B., & Van Veldhuizen, D. A. (2007). *Evolutionary algorithms for solving multi-objective problems* (Vol. 5): Springer.

Coley, D. A. (1999). *An introduction to genetic algorithms for scientists and engineers*: World Scientific Publishing Company.

Conn, A. R., Scheinberg, K., & Vicente, L. N. (2009). *Introduction to derivative-free optimization* (Vol. 8): Siam.

Couet, B., Prange, M., Bailey, W., Djikpesse, H., & Druskin, V. (2007). Method for optimal gridding in reservoir simulation. In: Google Patents.

Cox, D., Kuuskraa, V., & Hansen, J. (1996). *Advanced type curve analysis for low permeability gas reservoirs.* Paper presented at the SPE Gas Technology Symposium, Calgary, Alberta, Canada.

Cox, S. A., Gilbert, J. V., Sutton, R. P., & Stoltz, R. P. (2002, 23-26 October). *Reserve analysis for tight gas.* Paper presented at the SPE Eastern Regional Meeting, Lexington, Kentucky.

Cox, S. A., Sutton, R. P., Stoltz, R. P., & Knobloch, T. S. (2005). *Determination of Effective Drainage Area for Tight Gas Wells*. Paper presented at the SPE Eastern Regional Meeting, Morgantown, West Virginia.

Crosby, D., Yang, Z., & Rahman, S. (1998). *Transversely fractured horizontal wells: A technical appraisal of gas production in Australia.* Paper presented at the SPE Asia Pacific Oil and Gas Conference and Exhibition.

Dahroug, A. (2015). Analytical and numerical investigation of transient behaviour in hydraulically fractured tight gas reservoirs.

Dmitrievsky, A. (2005). *Meeting Natural Gas Demand: Global and Regional Challenges*. Paper presented at the 18th World Petroleum Congress, Johannesburg, South Africa.

Dong, Z., Holditch, S., McVay, D., & Ayers, W. B. (2012). Global Unconventional Gas Resource Assessment. *SPE Economics & Management, 4*(04). doi:10.2118/148365-PA

Du, K. (2008). *The Determination of Tested Drainage Area and Reservoir Characterisation from Entire Well-Test History by Deconvolution and Conventional Pressure-Transient Analysis Techniques*. Paper presented at the SPE Annual Technical Conference and Exhibition, Denver, Colorado, USA.

Dudley, B. (2013). Statistical review of world energy. *BP plc, London*.

Economides, M., Deimbachor, F. X., Brand, C. W., & Heinemann, Z. E. (1991). Comprehensive-simulation of horizontal-well performance. *SPE Formation Evaluation, 6*(04), 418-426.

Economides, M. J., & Martin, T. (2007). *Modern fracturing: Enhancing natural gas production*: ET Publishing Houston.

EIA. (2018). *Annual Energy Outlook 2018 with Projections to 2050*. Retrieved from

Eiben, A. E., & Smith, J. E. (2003). *Introduction to evolutionary computing* (Vol. 53): Springer.

El-Banbi, A. H., & Wattenbarger, R. A. (1997). *Analysis of Commingled Gas Reservoirs With Variable Bottom-Hole Flowing Pressure and Non-Darcy Flow*. Paper presented at the SPE Annual Technical Conference and Exhibition, San Antonio, Texas.

Elsharkawy, A. M. (2002). *EOS's calculations of volumetric and transport properties of sour gases and gas condensates*. Paper presented at the The 6th Saudi Engineering Conference, KFUPM, Dhahran; .

Emerick, A. A., Silva, E., Messer, B., Almeida, L. F., Szwarcman, D., Pacheco, M. A. C., & Vellasco, M. M. B. R. (2009). *Well placement optimization using a genetic algorithm with nonlinear constraints*. Paper presented at the SPE reservoir simulation symposium, Woodlands, Texas.

Engler, T. W. (2000). *A new approach to gas material balance in tight gas reservoirs.* Paper presented at the SPE Annual Technical Conference and Exhibition.

Escobar, F.-H., López, A.-M., & Cantillo, J.-H. (2007). Effect of the pseudotime function on gas reservoir drainage area determination. *CT&F-Ciencia, Tecnología y Futuro, 3*(3), 113-124.

Esfahani, S., Baselizadeh, S., & Hemmati-Sarapardeh, A. (2015). On determination of natural gas density: least square support vector machine modeling approach. *Journal of Natural Gas Science and Engineering, 22*, 348-358.

Fallahzadeh, S. H., Hossain, M. M., James Cornwell, A., & Rasouli, V. (2017). Near wellbore hydraulic fracture propagation from perforations in tight rocks: The roles of fracturing fluid viscosity and injection rate. *Energies, 10*(3), 359.

Fayazi, A., Arabloo, M., & Mohammadi, A. H. (2014). Efficient estimation of natural gas compressibility factor using a rigorous method. *Journal of Natural Gas Science and Engineering, 16*, 8-17.

Fetkovich, M. J. (1980). Decline curve analysis using type curves. *Journal of Petroleum Technology, 32*(06), 1,065-061,077.

Foroud, T., Baradaran, A., & Seifi, A. (2018). A comparative evaluation of global search algorithms in black box optimization of oil production: A case study on Brugge field. *Journal of Petroleum Science and Engineering, 167*, 131-151.

Forouzanfar, F., Li, G., & Reynolds, A. C. (2010). *A two-stage well placement optimization method based on adjoint gradient.* Paper presented at the SPE annual technical conference and exhibition.

Forsyth, D., Al Musharfi, N. M., & Al Marzooq, A. M. (2011). *Tight Gas Petrophysical Challenges in Saudi Aramco*. Paper presented at the SPE/DGS Saudi Arabia Section Technical Symposium and Exhibition, Al-Khobar, Saudi Arabia.

Fraim, M., & Wattenbarger, R. (1987). Gas Reservoir Decline-Curve Analysis Using Type Curves With Real Gas Pseudopressure and Normalized Time. *SPE Formation Evaluation, 2*(04).

French, R., Brimhall, R., & Wu, C. (1991). *A statistical and economic analysis of incremental waterflood infill drilling recoveries in West Texas carbonate reservoirs*. Paper presented at the SPE Annual Technical Conference and Exhibition, Dallas, Texas.

Gao, H., & McVay, D. (2004). *Gas infill well selection using rapid inversion methods*. Paper presented at the SPE Annual Technical Conference and Exhibition, Houston, Texas.

Garcia, J. P., Pooladi-Darvish, M., Brunner, F., Santo, M., & Mattar, L. (2006). *Well Testing of Tight Gas Reservoirs*. Paper presented at the SPE Gas Technology Symposium, Calgary, Alberta, Canada.

Gaskari, R., Mohaghegh, S. D., & Jalali, J. (2007). An integrated technique for production data analysis with application to mature fields. *SPE Production & Operations, 22*(04), 403-416.

Gavin, H. P. (2013). The Nelder-Mead algorithm in two dimensions. *CEE 201L. Duke U*.

Geertsma, J., & De Klerk, F. (1969). A Rapid Method of Predicting Width and Extent of Hydraulically Induced Fractures. *Journal of Petroleum Technology, 21*(12). doi:10.2118/2458-PA

Gentry, R. W. (1972). Decline-curve analysis. *Journal of Petroleum Technology, 24*(01), 38-41.

Gerhard, L. C., Yannacone, V. J., & Smith, C. J. (2005). *Energy and Environment: a Partnership that Works: The Actual Impacts of Oil and Gas Exploration and Development on Our Environment*: American Association of Petroleum Geologists.

Gochnour, J. R., & Slater, G. E. (1977). *Well Test Analysis In Tight Gas Reservoirs*. Paper presented at the SPE Annual Fall Technical Conference and Exhibition, Denver, Colorado.

Greenwood, G. W., & Liu, Y.-P. (1998). *Finding low energy conformations of atomic clusters using evolution strategies.* Paper presented at the International Conference on Evolutionary Programming.

Gringarten, A. C., Ramey Jr, H. J., & Raghavan, R. (1974). Unsteady-state pressure distributions created by a well with a single infinite-conductivity vertical fracture. *Society of Petroleum Engineers Journal, 14*(04), 347-360.

Guan, L. (2004). *Evaluation of a statistical infill candidate selection technique.* Texas A&M University,

Guan, L., & Du, Y. (2004). *Fast Method Finds Infill Drilling Potentials in Mature-Tight Reservoirs*. Paper presented at the SPE International Petroleum Conference in Mexico, Puebla Pue., Mexico.

Guan, L., McVay, D., Jensen, J., & Voneiff, G. (2004). Evaluation of a Statistical Method for Assessing Infill Production Potential in Mature, Low-Permeability Gas Reservoirs. *Journal of energy resources technology, 126*(3), 241-245.

Guo, G., & Evans, R. (1993). *Inflow performance and production forecasting of horizontal wells with multiple hydraulic fractures in low-permeability gas reservoirs.* Paper presented at the SPE Gas Technology Symposium, Calgary, Alberta, Canada.

Hagoort, J. (1988). *Fundamentals of gas reservoir engineering* (Vol. 23): Elsevier.

Hagoort, J. (2003). Automatic Decline-Curve Analysis of Wells in Gas Reservoirs. *SPE Reservoir Evaluation & Engineering, 6*(06). doi:10.2118/77187-PA

Hagoort, J., & Hoogstra, R. (1999). Numerical solution of the material balance equations of compartmented gas reservoirs. *SPE Reservoir Evaluation & Engineering, 2*(04), 385-392.

Hale, B. W., & Evers, J. F. (1981). Elliptical Flow Equations for Vertically Fractured Gas Wells. *Journal of Petroleum Technology, 33*(12). doi:10.2118/8943-PA

Hamdi, H., Hajizadeh, Y., & Sousa, M. C. (2015). *Gaussian Process for Uncertainty Quantification of Reservoir Models.* Paper presented at the SPE/IATMI Asia Pacific Oil & Gas Conference and Exhibition.

Han, X. L., Zhou, F. J., Xiong, C. M., Liu, X. F., & Yang, X. Y. (2013). *A New Method of Optimization Design of Hydraulic Fracture Parameters in Low Porosity and Fractured Gas Reservoir*. Paper presented at the Applied Mechanics and Materials.

Hassan, O. F., & Al-Jawad, M. S. (2005). Prediction of Optimum Separation Conditions for Sequential Field Separation System. *Journal of Engineering, 11*(3), 541-552.

Holditch, S. A. (2006). Tight gas sands. *Journal of Petroleum Technology, 58*(06), 86-93.

Holditch, S. A. (2013). Unconventional oil and gas resource development–Let's do it right. *Journal of Unconventional Oil and Gas Resources, 1*, 2-8.

Holditch, S. A., Jennings, J. W., Neuse, S. H., & Wyman, R. E. (1978). *The optimization of well spacing and fracture length in low permeability gas reservoirs.* Paper presented at the SPE Annual Fall Technical Conference and Exhibition.

Holditch, S. A., & Lee, J. (2007). Topic paper# 29: unconventional gas. *National Petroleum Council*.

Holditch, S. A., Lee, W. J., Lancaster, D. E., & Davis, T. B. (1983). Effect of Mud Filtrate Invasion on Apparent Productivity in Drillstem Tests in Low-Permeability Gas Formations. *Journal of Petroleum Technology, 35*(02). doi:10.2118/9842-PA

Holland, J. (1975). Adaptation in Natural and Artificial Systems (Ann Arbor, MI: University of Michigan).

Hongjun, W., Feng, M., Xiaoguang, T., Zuodong, L., Zhang, X., Zhenzhen, W., . . . Liuyan, Y. (2016). Assessment of global unconventional oil and gas resources. *Petroleum Exploration and Development, 43*(6), 925-940.

Hossain, M., Rahman, M., & Rahman, S. (2000). Hydraulic fracture initiation and propagation: roles of wellbore trajectory, perforation and stress regimes. *Journal of Petroleum Science and Engineering, 27*(3-4), 129-149.

Hossain, M. M., Al-Fatlawi, O., Brown, D., & Ajeel, M. (2018). *Numerical Approach for the Prediction of Formation and Hydraulic Fracture Properties Considering Elliptical Flow Regime in Tight Gas Reservoirs*. Paper presented at the Offshore Technology Conference Asia, Kuala Lumpur, Malaysia.

Hossain, M. M., & Rahman, M. (2008). Numerical simulation of complex fracture growth during tight reservoir stimulation by hydraulic fracturing. *Journal of Petroleum Science and Engineering, 60*(2), 86-104.

Huang, Q.-H., Chen, C., Yin, L., Liu, T., & Fang, T. (2015). Application of Material Balance Equations of Multicompartment Gas Reservoirs in YC Gas Reservoir.

Huang, Q., Arii, H., Sadok, A. A. B., Baslaib, M. A., & Sasaki, A. (2016). *A New Approach of Infill Drilling Optimization for Efficient Transition to Future Pattern Flood Development*. Paper presented at the Abu Dhabi International Petroleum Exhibition & Conference, Abu Dhabi, UAE.

Hurst, W. (1987). Drainage And In-Fill Drilling. In: Society of Petroleum Engineers.

Ilk, D., Anderson, D. M., Stotts, G. W. J., Mattar, L., & Blasingame, T. (2010). Production Data Analysis--Challenges, Pitfalls, Diagnostics. *SPE Reservoir Evaluation & Engineering, 13*(03). doi:10.2118/102048-PA

Ilk, D., Rushing, J., & Blasingame, T. (2008). Estimating Reserves Using the Arps Hyperbolic Rate-Time Relation—Theory, Practice and Pitfalls. Paper CIM 2008-108 presented at the 59th Annual Technical Meeting of the Petroleum Society, Calgary, Alberta, Canada, 17-19 June. In: preparation.

Ilk, D., Rushing, J. A., Perego, A. D., & Blasingame, T. A. (2008). *Exponential vs. hyperbolic decline in tight gas sands: understanding the origin and implications for reserve estimates using Arps' decline curves.* Paper presented at the SPE annual technical conference and exhibition, Denver, Colorado, USA.

International Energy Agency. (2013). *World Energy Outlook*. Retrieved from France:

Islam, M. R. (2014). *Unconventional gas reservoirs: evaluation, appraisal, and development*: Elsevier.

Ismadi, D., Kabir, C. S., & Hasan, R. (2012). The use of combined static-and dynamic-material-balance methods with real-time surveillance data in volumetric gas reservoirs. *SPE Reservoir Evaluation & Engineering, 15*(03), 351-360.

Jahabani, A., & Aguilera, R. (2009). Well Testing of Tight Gas Reservoirs. *Journal of Canadian Petroleum Technology, 48*(10). doi:10.2118/130066-PA

Jayanti, S. (2018). *Computational Fluid Dynamics for Engineers and Scientists*: Springer.

Jiang, Z.-X., Li, Z., Li, F., Pang, X.-Q., Yang, W., Liu, L.-F., & Jiang, F.-J. (2015). Tight sandstone gas accumulation mechanism and development models. *Petroleum Science, 12*(4), 587-605. doi:10.1007/s12182-015-0061-6

Jianyi, L., Shilun, L., Ping, G., Zhen, Z., Xiaofeng, Z., & Jianfen, D. (2002). Measurement of gas deviation factor. *Natural Gas Industry, 22*(2), 63-65.

Jikich, S. A., & Popa, A. S. (2000). *Hyperbolic Decline Parameter Identification Using Optimization Procedures*. Paper presented at the SPE Eastern Regional Meeting, Morgantown, West Virginia.

Jiménez, E., Cervantes, R., Magnelli, D., & Dabrowski, A. (2017). *Probabilistic Approach of Advanced Decline Curve Analysis for Tight Gas Reserves Estimation Obtained from Public Data Base.* Paper presented at the SPE Latin America and Caribbean Petroleum Engineering Conference, Buenos Aires, Argentina.

Jimenez, E., Cervantes, R., Magnelli, D., & Huerta, V. (2017). *Estimation of Tight Gas Reserves During the Transient Flow Using a Modified GPA Method.* Paper presented at the SPE Latin America and Caribbean Petroleum Engineering Conference, Buenos Aires, Argentina.

Jones, L. (1963). Reservoir Reserve Tests. *Journal of Petroleum Technology, 15*(03), 333-337.

Juell, A., Whitson, C. H., & Hoda, M. F. (2010). Model-Based Integration and Optimization--Gas-Cycling Benchmark. *SPE Journal, 15*(02), 646-657.

Kamari, A., Hemmati-Sarapardeh, A., Mirabbasi, S.-M., Nikookar, M., & Mohammadi, A. H. (2013). Prediction of sour gas compressibility factor using an intelligent approach. *Fuel Processing Technology, 116*, 209-216.

Kamari, A., Mohammadi, A. H., Lee, M., & Bahadori, A. (2017). Decline curve based models for predicting natural gas well performance. *Petroleum, 3*(2), 242-248. doi:https://doi.org/10.1016/j.petlm.2016.06.006

Kazemi, H. (1982). Low-Permeability Gas Sands. *Journal of Petroleum Technology, 34*(10). doi:10.2118/11330-PA

Khan, W. A., Rehman, S. A., Akram, A. H., & Ahmad, A. (2011). *Factors affecting production behavior in tight gas reservoirs.* Paper presented at the SPE/DGS Saudi Arabia Section Technical Symposium and Exhibition, Al-Khobar, Saudi Arabia.

Khanamiri, H. H. (2010). A non-iterative method of decline curve analysis. *Journal of Petroleum Science and Engineering, 73*(1), 59-66. doi:https://doi.org/10.1016/j.petrol.2010.05.007

Kramer, O. (2016). *Machine learning for evolution strategies* (Vol. 20): Springer.

Kramer, O., Ciaurri, D. E., & Koziel, S. (2011). Derivative-free optimization. In *Computational optimization, methods and algorithms* (pp. 61-83): Springer.

Kuchuk, F. J. (2009). *Radius of Investigation for Reserve Estimation From Pressure Transient Well Tests*. Paper presented at the SPE Middle East Oil and Gas Show and Conference, Manama, Bahrain.

Kucuk, F., & Brigham, W. E. (1979). Transient Flow in Elliptical Systems. *Society of Petroleum Engineers Journal, 19*(06). doi:10.2118/7488-PA

Kupchenko, C. L., Gault, B. W., & Mattar, L. (2008). *Tight gas production performance using decline curves.* Paper presented at the CIPC/SPE Gas Technology Symposium 2008 Joint Conference, Calgary, Alberta, Canada.

Kuppe, F., Chugh, S., & Connell, P. (2000). *Material balance for multi-layered, commingled, tight gas reservoirs.* Paper presented at the SPE/CERI Gas Technology Symposium.

Lee, A. L., Gonzalez, M. H., & Eakin, B. E. (1966). The viscosity of natural gases. *Journal of Petroleum Technology, 18*(08), 997-1000.

Lee, W. J., & Wattenbarger, R. A. (1996). *Gas reservoir engineering*. Richardson, Texas: Society of Petroleum Engineers.

Lessard, R. W. (2003). *Portfolio Optimization Techniques for the Energy Industry.* Paper presented at the SPE Hydrocarbon Economics and Evaluation Symposium, Dallas, Texas.

Li, Q., Xing, H., Liu, J., & Liu, X. (2015). A review on hydraulic fracturing of unconventional reservoir. *Petroleum, 1*(1), 8-15.

Long, D. R., & Davis, M. J. (1988). A New Approach to the Hyperbolic Curve (includes associated papers 18728 and 18942). *Journal of Petroleum Technology, 40*(07). doi:10.2118/16237-PA

Lopes, R. L., Nikhalat-Jahromi, H., & Jorge, A. M. (2016). *An Overview of Evolutionary Computing for Interpretation in the Oil and Gas Industry.* Paper presented at the Proceedings of the Ninth International C* Conference on Computer Science & Software Engineering.

Lord, M., & Collins, R. (1991). *Detecting compartmented gas reservoirs through production performance.* Paper presented at the SPE Annual Technical Conference and Exhibition.

Luchian, H., Breaban, M. E., & Bautu, A. (2015). On meta-heuristics in optimization and data analysis. Application to geosciences. In *Artificial Intelligent Approaches in Petroleum Geosciences* (pp. 53-100): Springer.

Luo, S., & Kelkar, M. G. (2010). *Infill Drilling Potential in Tight Gas Reservoirs*. Paper presented at the SPE Annual Technical Conference and Exhibition, Florence, Italy.

Luptacik, M. (2010). *Mathematical optimization and economic analysis*: Springer.

Macrotrends. (2018). Natural Gas Prices - Historical Chart.

Mahadik, M. K. H., Bahrami, H., Hossain, M., & Mitchel, T. (2012). Production decline analysis and forecasting in tight-gas reservoirs. *The APPEA Journal, 52*(1), 573-580.

Maley, S. (1985). *The Use of Conventional Decline Curve Analysis in Tight Gas Well Applications*. Paper presented at the SPE/DOE Low Permeability Gas Reservoirs Symposium, Denver, Colorado.

Mantica, S., Cominelli, A., & Mantica, G. (2001). *Combining global and local optimization techniques for automatic history matching production and seismic data.* Paper presented at the SPE Reservoir Simulation Symposium.

Mattar, L., & Moghadam, S. (2009). *Modified Power Law Exponential Decline for Tight Gas*. Paper presented at the Canadian International Petroleum Conference, Calgary, Alberta.

McCain, W., Voneiff, G., Hunt, E., & Semmelbeck, M. (1993). *A Tight Gas Field Study: Carthage (Cotton Valley) Field*. Paper presented at the SPE Gas Technology Symposium, Calgary, Alberta, Canada.

McCray, T. L. (1990). *Reservoir analysis using production decline data and adjusted time.* Texas A&M University,

McLaughlin, J. M., & Gouge, B. A. (2006). *Uses and Misuses of Pressure Data for Reserve Estimation*. Paper presented at the SPE Annual Technical Conference and Exhibition, San Antonio, Texas, USA.

Meehan, D. N. (1989). *Hydraulically fractured wells in heterogeneous reservoirs: Interaction, interference, and optimization.* (DOCTOR OF PHILOSOPHY), Stanford Univ., CA (USA),

Mezura-Montes, E., & Coello, C. A. C. (2005). A simple multimembered evolution strategy to solve constrained optimization problems. *IEEE Transactions on Evolutionary computation, 9*(1), 1-17.

Michalewicz, Z. (1996). Evolution Strategies and Other Methods. In *Genetic Algorithms + Data Structures = Evolution Programs* (pp. 159-177). Berlin, Heidelberg: Springer Berlin Heidelberg.

Mokhatab, S., Poe, W. A., & Mak, J. Y. (2015). *Handbook of Natural Gas Transmission and Processing: Principles and Practices*: Gulf Professional Publishing.

Montes, G., Bartolome, P., & Udias, A. L. (2001). *The use of genetic algorithms in well placement optimization*. Paper presented at the SPE Latin American and Caribbean petroleum engineering conference, Buenos Aires, Argentina.

Mori, M., & Tseng, C. C. (1997). A genetic algorithm for multi-mode resource constrained project scheduling problem. *European Journal of Operational Research, 100*(1), 134-141.

Naik, G. (2003). Tight gas reservoirs–an unconventional natural energy source for the future. *Accessado em, 1*(07), 2008.

Nasrabadi, H., Morales, A., & Zhu, D. (2012). Well placement optimization: A survey with special focus on application for gas/gas-condensate reservoirs. *Journal of Natural Gas Science and Engineering, 5*, 6-16.

Neal, D. B., & Mian, M. A. (1989). Early-Time Tight Gas Production Forecasting Technique Improves Reserves and Reservoir Description. *SPE Formation Evaluation, 4*(01). doi:10.2118/15432-PA

Nelder, J. A., & Mead, R. (1965). A simplex method for function minimization. *The computer journal, 7*(4), 308-313.

Nelson, R. M., Kierczak, M., & Carlborg, Ö. (2013). Higher order interactions: detection of epistasis using machine learning and evolutionary computation. In *Genome-Wide Association Studies and Genomic Prediction* (pp. 499-518): Springer.

Obuba, J., Ikiesnkimama, S., Ubani, C., & Ekeke, I. (2013). Natural gas compressibility factor correlation evaluation for Niger delta gas fields. *IOSR Journal of Electrical and Electronics Engineering, 6*(4), 1-10.

Okouma Mangha, V., Ilk, D., Blasingame, T. A., Symmons, D., & Hosseinpour-zonoozi, N. (2012). *Practical Considerations for Decline Curve Analysis in Unconventional Reservoirs - Application of Recently Developed Rate-Time Relations*. Paper presented at the SPE Hydrocarbon Economics and Evaluation Symposium, Calgary, Alberta, Canada.

Ozkan, E., Brown, M. L., Raghavan, R., & Kazemi, H. (2011). Comparison of fractured-horizontal-well performance in tight sand and shale reservoirs. *SPE Reservoir Evaluation & Engineering, 14*(02), 248-259.

Palacio, J., & Blasingame, T. (1993). *Decline curve analysis using type curves—analysis of gas well production data*. Paper presented at the Low Permeability Reservoirs Symposium, Denver, Colorado.

Pankaj, P., & Kumar, V. (2010). *Well testing in tight gas reservoir: today.* Paper presented at the SPE Oil and Gas India Conference and Exhibition, Mumbai, India.

Parmee, I. (1998). The Integration of Evolutionary and Adaptive Computing Technologies with Product/System Design and Realisation. *Springer, Plymouth, UK, 12*, 191-197.

Payne, D. A. (1996). Material-balance calculations in tight-gas reservoirs: The pitfalls of p/z plots and a more accurate technique. *SPE Reservoir Engineering, 11*(04), 260-267.

Payne, D. A., & Cormack, D. E. (1989). Optimal Fracture Design For Tight Gas Reservoirs. *Journal of Canadian Petroleum Technology, 28*(01). doi:10.2118/89-01-12

Pham, N., Malinowski, A., & Bartczak, T. (2011). Comparative study of derivative free optimization algorithms. *IEEE Transactions on Industrial Informatics, 7*(4), 592-600.

Poston, S. W., & Poe, B. D. (2008). *Analysis of production decline curves*: Society of Petroleum Engineers Richardson, TX.

Pouladi, B., Sharifi, M., Ahmadi, M., & Kelkar, M. (2017). Fast marching method assisted sector modeling: Application to simulation of giant reservoir models. *Journal of Petroleum Science and Engineering, 149*, 707-719.

Pratikno, H., Rushing, J. A., & Blasingame, T. A. (2003). *Decline Curve Analysis Using Type Curves - Fractured Wells*. Paper presented at the SPE Annual Technical Conference and Exhibition, Denver, Colorado.

Rahman, M., & Rahman, M. (2010). A review of hydraulic fracture models and development of an improved pseudo-3D model for stimulating tight oil/gas sand. *Energy Sources, Part A: Recovery, Utilization, and Environmental Effects, 32*(15), 1416-1436.

Rahman, M., Suarez, Y., Chen, Z., & Rahman, S. (2007). Unsuccessful hydraulic fracturing cases in Australia: Investigation into causes of failures and their remedies. *Journal of petroleum science and engineering, 57*(1-2), 70-81.

Rajakumar, B., & George, A. (2012). *A new adaptive mutation technique for genetic algorithm.* Paper presented at the Computational Intelligence & Computing Research (ICCIC), 2012 IEEE International Conference on.

Raju, N. (2014). *Optimization methods for engineers*: PHI Learning Pvt. Ltd.

Rao, S. S. (2009). *Engineering optimization: theory and practice*: John Wiley & Sons.

Rechenber, I. (1971). *Evolutionsstrategie: Optimierung technischer Systeme nach Prinzipien der biologischen Evolution.* (Doctoral degree), Technical University of Berlin,

Rechenber, I. (1973). Evolutionsstrategie: Optimierung technischer Systeme nach Prinzipien der biologischen Evolution. *Frommann-Holzboog Verlag, Stuttgart*.

Rechenberg, I. (1965). Cybernetic solution path of an experimental problem. *Royal Aircraft Establishment Library Translation 1122*.

Rechenberg, I. (1994). Evolutionsstrategie'94. . *Frommann-Holzboog-Verlag, Stuttgart (Germany), 1581*.

Rezaee, R., Saeedi, A., & Clennell, B. (2012). Tight gas sands permeability estimation from mercury injection capillary pressure and nuclear magnetic resonance data. *Journal of Petroleum Science and Engineering, 88-89*, 92-99. doi:https://doi.org/10.1016/j.petrol.2011.12.014

Robertson, S. (1988). Generalized Hyperbolic Equation. In: Society of Petroleum Engineers.

Rogner, H.-H. (1997). AN ASSESSMENT OF WORLD HYDROCARBON RESOURCES. *Annual Review of Energy and the Environment, 22*(1), 217-262. doi:10.1146/annurev.energy.22.1.217

Rushing, J. A., Perego, A. D., Sullivan, R., & Blasingame, T. A. (2007). *Estimating reserves in tight gas sands at HP/HT reservoir conditions: use and misuse of an Arps decline curve methodology.* Paper presented at the SPE Annual Technical Conference and Exhibition, Anaheim, California, U.S.A.

Samaniego, F., Montiel, D., Perez, G., & Arriola, A. (1997). *[RFP] 6 New Techniques for the Assessment of Drainage Areas and Reservoir Dynamics.* Paper presented at the 15th World Petroleum Congress.

Satter, A., & Iqbal, G. M. (2015). *Reservoir Engineering: The Fundamentals, Simulation, and Management of Conventional and Unconventional Recoveries*: Gulf Professional Publishing.

Satter, A., Iqbal, G. M., & Buchwalter, J. L. (2008). *Practical enhanced reservoir engineering: assisted with simulation software*: Pennwell Books.

Schlumberger. (2017a). *ECLIPSE reservoir simulation software - Reference Manual*: Schlumberger.

Schlumberger. (2017b). *Petrel reservoir engineering*. Houston, USA: Schlumberger.

Schwefel, H.-P. (1965). Kybernetische Evolution als Strategie der experimentellen Forschung in der Stromungstechnik. *Diploma thesis, Technical Univ. of Berlin*.

Schwefel, H.-P. (1974). Adaptive Mechanismen in der biologischen Evolution und ihr Einfluss auf die Evolutionsgeschwindigkeit. *Interner Bericht der Arbeitsgruppe Bionik und Evolutionstechnik am Institut für Mess-und Regelungstechnik Re, 215*(3).

Schwefel, H.-P. (1975). Binare Optimierung durch somatische Mutation Working. *TU Berlin und Medizinische Hochschule Hannover*.

Schwefel, H.-P. (1995). *Evolution and optimum seeking* (Vol. 1515): Wiley New York.

Schweitzer, F., Ebeling, W., Rose, H., & Weiss, O. (1997). Optimization of road networks using evolutionary strategies. *Evolutionary computation, 5*(4), 419-438.

Schweitzer, R., & Bilgesu, H. I. (2009). *The role of economics on well and fracture design completions of Marcellus Shale wells.* Paper presented at the SPE Eastern Regional Meeting, Charleston, West Virginia.

Shah, Y. T. (2017). *Chemical Energy from Natural and Synthetic Gas*: CRC Press.

Shen, W., Lu, J., Li, X., & Liu, X. (2014). The calculating method optimization and influencing factor analysis of deviation factor for abnormally pressured gas reservoirs. *The Electronic Journal of Geotechnical Engineering, 19*, 1711-1719.

Shirman, E. I. (1999). Universal Approach to the Decline Curve Analysis. *Journal of Canadian Petroleum Technology, 38*(13). doi:10.2118/99-13-68

Shoaib, M., Qamar, M. S., Khan, M. R., Khan, A., Mumtaz, S., & Abbasi, A. (2015). *Tight Gas Reservoir (TGR) - In Place & Reserves Estimation and Economic Feasibility of Project*. Paper presented at the SPE Middle East Oil & Gas Show and Conference, Manama, Bahrain.

Simon, D. (2013). *Evolutionary optimization algorithms*: John Wiley & Sons.

Sivanandam, S., & Deepa, S. (2008). Genetic algorithm optimization problems. In *Introduction to Genetic Algorithms* (pp. 165-209): Springer.

Smith, T. M., Sayers, C. M., & Sondergeld, C. H. (2009). Rock properties in low-porosity/low-permeability sandstones. *The Leading Edge, 28*(1), 48-59.

Soliman, M., Venditto, J., & Slusher, G. (1984). *Evaluating Fractured Well Performance Using Type Curves.* Paper presented at the Permian Basin Oil and Gas Recovery Conference, Midland, Texas.

Soliman, M. Y., East, L. E., & Ansah, J. (2008). *Well Completion Design for Tight Gas Formations*. Paper presented at the SPE Russian Oil and Gas Technical Conference and Exhibition, Moscow, Russia.

Spivey, J. P. (1986). *A New Algorithm for Hyperbolic Decline Curve Fitting*. Paper presented at the Petroleum Industry Application of Microcomputers, Silvercreek, Colorado.

Stotts, G. W. J., Anderson, D. M., & Mattar, L. (2007). *Evaluating and Developing Tight Gas Reserves- Best Practices*. Paper presented at the Rocky Mountain Oil & Gas Technology Symposium, Denver, Colorado, U.S.A.

Suwartadi, E. (2012). *Gradient-based Methods for Production Optimization of Oil Reservoirs.* Norwegian University of Science and Technology,

Tarek, A., & Nathan, M. (2012). *Advanced Reservoir Management and Engineering* (Second edition ed.): Gulf Professional Publishing.

Tekin, E., & Sabuncuoglu, I. (2004). Simulation optimization: A comprehensive review on theory and applications. *IIE transactions, 36*(11), 1067-1081.

Temizel, C., Saputelli, L., Nabizadeh, M., Balaji, K., Suhag, A., Ranjith, R., & Wijaya, Z. (2017). *Enhancing Optimization of Reservoir Simulation Processes in Next-Generation Reservoir Simulators.* Paper presented at the SPE Reservoir Characterisation and Simulation Conference and Exhibition.

Teufel, L. W., Chen, H.-Y., Engler, T. W., & Hart, B. (2004). Optimization of Infill Drilling in Naturally-Fractured Tight-Gas Reservoirs Phase II. *Washington, DC: US Department of Energy: Socorro, New Mexico: Industry Cooperative and New Mexico Institute of Mining and Technology*.

Thompson, J. K. (1981). *Use Of Constant Pressure, Finite Capacity Type Curves For Performance Prediction Of Fractured Wells In Low-Permeability Reservoirs*. Paper presented at the SPE/DOE Low Permeability Gas Reservoirs Symposium, Denver, Colorado.

Towler, B. F., & Bansal, S. (1993). Hyperbolic decline-curve analysis using linear regression. *Journal of Petroleum Science and Engineering, 8*(4), 257-268. doi:https://doi.org/10.1016/0920-4105(93)90003-W

Travis, J., Koch, D. P., Xiao, J., & Xu, Z. (2013). Real-gas equations-of-state for the GASFLOW CFD code. *International Journal of Hydrogen Energy, 38*(19), 8132-8140.

Turkarslan, G., McVay, D. A., Bickel, J. E., Montiel, L. V., & Ortiz, R. R. (2010). *Integrated Reservoir and Decision Modeling to Optimize Spacing in Unconventional Gas Reservoirs*. Paper presented at the Canadian Unconventional Resources and International Petroleum Conference, Calgary, Alberta, Canada.

Uddameri, V., Tindle, K. J., & Morse, A. (2015). *Hydraulic fracturing impacts and technologies: A multidisciplinary perspective*: CRC Press.

Valko, P. P. (2009). *Assigning value to stimulation in the Barnett Shale: a simultaneous analysis of 7000 plus production hystories and well completion records*. Paper presented at the SPE Hydraulic Fracturing Technology Conference, The Woodlands, Texas.

van Ackooij, W., Philpott, A., Sagastizábal, C., & Zorgati, R. (2017). Editorial for the special issue: "Optimization in energy". *Energy Systems, 8*(1), 3-6. doi:10.1007/s12667-016-0216-6

Vasant, P. M. (2012). *Meta-heuristics optimization algorithms in engineering, business, economics, and finance*: IGI Global.

Vasper, A., Mjos, J. E. S., & Duong, T. T. T. (2016). *Efficient Optimization Strategies for Developing Intelligent Well Business Cases.* Paper presented at the SPE Intelligent Energy International Conference and Exhibition.

Veatch, R. W. (1983). Overview of Current Hydraulic Fracturing Design and Treatment Technology--Part 1. *Journal of Petroleum Technology, 35*(04). doi:10.2118/10039-PA

Viadana, G., Albani, D., Distaso, M. N., & Sharon, A. (2012). *Integrated production optimization and surface facilities management through advanced optimization techniques.* Paper presented at the SPE International Production and Operations Conference & Exhibition, Doha, Qatar.

Völcker, C. (2011). *Production Optimization of Oil Reservoirs*. Kgs. Lyngby, Denmark: Technical University of Denmark (DTU).

Voneiff, G., & Cipolla, C. (1996). *A new approach to large-scale infill evaluations applied to the OZONA (Canyon) gas sands*. Paper presented at the Permian Basin Oil and Gas Recovery Conference, Midland, Texas.

Wang, F., & Zhang, S. (2014). Production analysis of multi-stage hydraulically fractured horizontal wells in tight gas reservoirs. *Journal of Geography and Geology, 6*(4), 58.

Wang, X., & Economides, M. (2013). *Advanced Natural Gas Engineering*. Houston, Texas: Elsevier.

Wattenbarger, R. A., El-Banbi, A. H., Villegas, M. E., & Maggard, J. B. (1998). *Production Analysis of Linear Flow Into Fractured Tight Gas Wells*. Paper presented at the SPE Rocky Mountain Regional/Low-Permeability Reservoirs Symposium, Denver, Colorado.

Wei, Y., & Holditch, S. A. (2009). *Computing estimated values of optimal fracture half length in the tight gas sand advisor program.* Paper presented at the SPE Hydraulic Fracturing Technology Conference, The Woodlands, Texas.

West, S., & Cochrane, P. (1995). Reserves Determination Using Type-Curve Matching and EMB Methods in the Medicine Hat Shallow Gas Field. *SPE Reservoir Engineering, 10*(02), 82-87.

Wu, Y., Carroll, J. J., & Zhu, W. (2012). *Sour gas and related technologies* (Vol. 1): John Wiley & Sons.

Xu, B., Haghighi, M., Li, X., & Cooke, D. (2013). Development of new type curves for production analysis in naturally fractured shale gas/tight gas reservoirs. *Journal of Petroleum Science and Engineering, 105*, 107-115.

Yan, S., Zhuo, L., JIANG, Z., Qun, L., Dongdong, L., & Zhiye, G. (2017). Progress and development trend of unconventional oil and gas geological research. *Petroleum Exploration and Development, 44*(4), 675-685.

Yesiltepe, C. (2015). *Accessed drainage volume and recovery factors of fractured horizontal wells under transient flow*: Colorado School of Mines.

Yu, W., Luo, Z., Javadpour, F., Varavei, A., & Sepehrnoori, K. (2014). Sensitivity analysis of hydraulic fracture geometry in shale gas reservoirs. *Journal of Petroleum Science and Engineering, 113*, 1-7.

Zahid, S., Bhatti, A. A., Ahmad Khan, H., & Ahmad, T. (2007). *Development of Unconventional Gas Resources: Stimulation Perspective*. Paper presented at the Production and Operations Symposium, Oklahoma City, Oklahoma, U.S.A.

Zhou, J., Patil, P., Ejaz, S., Atilhan, M., Holste, J. C., & Hall, K. R. (2006). (p, V m, T) and phase equilibrium measurements for a natural gas-like mixture using an automated isochoric apparatus. *The Journal of Chemical Thermodynamics, 38*(11), 1489-1494.

Appendix.A: Journal Paper: Determination of Best Possible Correlation for Gas Compressibility Factor to Accurately Predict the Initial Gas Reserves in Gas-Hydrocarbon Reservoirs

Determination of best possible correlation for gas compressibility factor to accurately predict the initial gas reserves in gas-hydrocarbon reservoirs

CrossMark

Omar Al-Fatlawi [a,b,], Md Mofazzal Hossain [a], Jake Osborne [a]*

[a] *Curtin University, Department of Petroleum Engineering, 26 Dick Perry Avenue, 6151 Kensington, Australia*
[b] *University of Baghdad, College of Engineering, Department of Petroleum Engineering, Baghdad, Iraq*

ARTICLE INFO

ABSTRACT

Gas compressibility factor or z-factor plays an important role in many engineering applications related to oil and gas exploration and production, such as gas production, gas metering, pipeline design, estimation of gas initially in place (GIIP), and ultimate recovery (UR) of gas from a reservoir. There are many z-factor correlations which are either derived from Equation of State or empirically based on certain observation through regression analysis. However, the results of the z-factor obtained from different correlations have high level of variance for the same gas sample under the same pressure and temperature. It is quite challenging to determine the most accurate correlation which provides accurate estimate for a range of pressures, temperatures, and gas compositions. This paper presents a novel method to accurately estimate GIIP of an Australian tight gas field through identification of the most appropriate z-factor correlations, which can accurately determine the z-factor and other PVT properties for a wide range of gas compositions, temperatures, and pressures. The sensitivity study results demonstrated that a single correlation cannot work across the range of pressures and temperatures for a certain gas sample necessary to calculate z-factor during simulation process and/or other analysis, such as material balance and volumetric estimate.

Introduction

There has been a remarkable increase in gas demand over the last decade at a faster rate than that of oil [1—4] due to its inherent advantages of low greenhouse emission. The estimation of gas properties is considered to play a vital role in almost every section of oil and gas industries [3,5,6]. For instance, the estimation of gas initially in place (GIIP), ultimate recovery (UR) of gas from a gas-hydrocarbon reservoir, and analysis of gas well test data etc. substantially depends on how accurately the gas compressibility factor known as z-factor is calculated [7,8].

Z-factor is employed to transform the volume of ideal gas to the volume of real gas. This factor modifies the behaviour of gas from perfect trend to the real trend [9,10]. Consequently, z-factor is a principal factor considered in petroleum engineering computation [7,11—13]. However, the z-factor could be either estimated by laboratory tests or using mathematical relationships. Although the laboratory tests should lead to more accurate estimation of z-factor than the mathematical

relationships, it requires expensive laboratory facilities, which may not be feasible, especially throughout the life span of gas production processes [7,14]. As a result, laboratory tests are not appropriately fit for a routine industry analysis. In addition laboratory test requires accurate sample of gas with its compositions, which are not easily accessible. Therefore, the industry relies on mathematical relationships or empirical correlations rather than the experimental work to estimate z-factor, which poses the challenging question of which correlation should be used for the calculation of z-factor.

Many correlations for the calculation of z-factor are available [15]. Each of these correlations has various intensity and deficiency in terms of the accuracy of estimated z-factor [16]. The suitability of these correlations depends on gas compositions including relative distribution of hydrocarbon and non-hydrocarbon components which varies from the region to region [17,18], range of pressure and temperatures based upon which the correlations are developed. Frequently, the gas compositions are unknown; and the temperature and pressure vary beyond the valid range. Accordingly, the z-factor correlations formulated at the first time more than 75 years ago, no unique correlation can be used adequately for all reservoirs at any temperature and pressure because each correlation was tuned to a particular range of pressure, temperature, and chemical composition. Therefore, it is quite challenging to determine the best possible z-factor correlation. The wrong determination of z-factor correlation can lead to significant error, which in turn results in underestimate or overestimate of many other gas properties, gas initially in place (GIIP) as well as ultimate recovery of gas.

In this study however, a method has been proposed and VBA interface based Excel program was developed employing the proposed method. The method is based upon widely practiced various z-factor correlations ranging from simple explicit empirical equations to those derived from Equations of State (EOS). These correlations were used to calculate z-factor at different pressures and temperatures, and then the results of these correlations were compared with the Virial Equation of State recommended in the report number 8 of American Gas Association (AGA8) and z-factor data obtained from laboratory experiments. The program generates the data in the form of four lookup tables for a range of pressure, temperature and gas composition based on sensitivity studies. The tables highlight the best possible correlations to be used to calculate z-factor for a certain gas system within a range a pressure and temperatures. The lookup tables can also be used to benchmark and determine the most accurate correlation for certain pressure (isobar) and temperature (isotherm) conditions. Each table covered group of real natural gas systems having a range of gas compositions with varied fraction of non-hydrocarbon components.

The developed program and lookup tables are used to estimate the initial gas reserves or gas initially in place for Whicher Range tight gas field; and justify the potential application of the proposed method as well as developed lookup tables as a simple tool in real field cases. The paper also presents insightful discussions including limitations of various correlations widely used by the industry for routine analysis based upon comprehensive literature review.

Mathematical relationships

The gas mixture properties including z-factor can be calculated based on certain mixing rules and EOS. Many mathematical models and/or empirical correlations are developed on this basis, and can be found in the literature. This section provides an overview of the most commonly used mathematical models/correlations used for hydrocarbon mixtures as a routine practice by oil and gas industry.

Table 1 outlines the most used mixing rules that are classified according to the required data (i.e. exact compositions or specific gravity of gas).

As described in Table 1, some mixing rules such as Kay [19], M.B. Standing [24] cannot alone handle gas mixtures containing non-hydrocarbon components. Therefore, on the grounds that the most of natural reservoir gases includes hydrogen sulphide, nitrogen and carbon dioxide, Wichert and Aziz [29] proposed an approach to correct the pseudo critical properties of gas mixtures due to the presence of carbon dioxide and hydrogen sulphide. While the Wichert and Aziz [29] approach is valid for mixtures defined by the known gas composition, R. P. Sutton [28] correlation can correct the pseudo critical properties for the gas mixtures containing impurities and defined by the specific gravity.

The published gas z-factor correlations could be classified into two kinds. The first type is the empirically derived explicit z-factor correlations, which directly calculate z-factor, while the second type is implicit z-factor correlations are mostly derived based on equations of state solved by the trial and error or iterative techniques. Of these two methods, it has been distinguished that iterative models provide results with less error than the empirical correlations due to rigorous solution techniques to the equations of state [30]. However, explicit typed empirical correlations are much faster than iterative methods and have comparable accuracy in some specific cases [31].

Based on comprehensive literature survey, it is apparent that there are two fundamental methods which are followed to calculate z-factor. The first method of calculating the z-factor involves the use of explicit empirical correlations, which are derived based on certain observations from regression analysis and/or experiments for a set of fluid samples within a certain range of pressure and temperature conditions. The earliest work on z-factor correlations was developed by Cope, Lewis, and Weber [32] and G. G. Brown, Souders, and Smith [33]. Their work was later extended and improved by G. Brown, Katz, Oberfell, and Alden [34]. Marshall B Standing and Katz [35] developed a z-factor chart for pure natural gases, which are consisted of only hydrocarbon components; and this chart was formulated for a certain range of reduced temperatures and pressures. The chart of Marshall B Standing and Katz [35] has considered one of the most used and practical approaches of calculating z-factor in petroleum engineering [36–38]. After technological development of computers and advances in numerical techniques, many z-factor correlations have been developed on the same basis of Marshall B Standing and Katz chart [35] using numerical regression methods to get more accurate results; and to extend the range of pressure, temperature and composition

Table 1 – Existing mixing rules for pseudocritical parameters estimation.

The required data of gas mixtures	Mixing rule	Description
Exact gas composition	Kay [19]	An excellent method for the determination of pseudocritical parameter for hydrocarbon only mixtures that it depends on weighted average critical properties [20].
	Stewart, Burkhardt, and Voo [21]	A mixing rule that has been evolved to handle hydrocarbon gas mixture with percentages of heavier hydrocarbon molecules.
	Corredor, Piper, and McCain Jr [22]	A developed formula of mixing rule of Stewart et al. [21] to handle gas mixtures including heptane plus fraction, and acid gases (H_2S and CO_2) and nitrogen. They excluded the requirement to identify the heptane plus fraction by depending on molecular weight of fraction instead of critical properties.
	Piper, McCain Jr, and Corredor [23]	A mixing rule that is based on the same formula Corredor et al. [22] with different coefficients which it is formulated to be valid for gases with specific gravities, varying from 1.3 to 1.8 It was designed to cover more gases containing impurities than the gas samples studied by Corredor et al. [22].
Specific gravity when composition is unknown	M.B. Standing [24]	Two mixing rules are suggested, the first is for gas has specific gravity less than 0.75 and the second is for wet gas with specific gravity equals or greater than 0.75. The Standing mixing rules are utilized widely for hydrocarbon gas mixture in the industry [25].
	R. Sutton [26]	A developed mixing rule of Stewart et al. [21] to minimize the deviation resulted due to C_{7+} fraction presence. This correlation improved the accuracy of the calculated z-factor of mixtures including C_{7+} fraction [27]. In addition, it can be used with gas condensates.
	R. P. Sutton [28]	Developed mixing rules that can be used for pure hydrocarbon mixtures and hydrocarbon gas mixtures including impurities such as H_2S, CO_2 and N_2. These correlations are employed for associated and condensate gas mixtures.

than that considered in Marshall B Standing and Katz chart [35]. Following the similar basis, many empirical correlations namely Papay (PAP) [39], Beggs and Brill (B&B) [40], Bahadori, Mokhatab, and Towler (BAH) [41], Azizi, Behbahani, and Isazadeh (AZI) [42], Heidaryan, Salarabadi, and Moghadasi (HEID) [43], Sanjari and Lay (SNL) [44], Shokir, El-Awad, Al-Quraishi, and Al-Mahdy (SHO) [45], and Mahmoud (MAH) [46] have been reported in the literature. The accuracy of these correlations widely varied and depends on the nature of the compositions of fluid sample (e.g. percentage of different hydrocarbon and non-hydrocarbon components, and other impurities), pressures and temperatures. Although these correlations are frequently used as standard practical tool, it is very challenging to select a single correlation that can cover entire range of reservoir fluid compositions, pressures and temperatures. Consequently, inappropriate selection of correlation can develop erroneous results with high level of uncertainties, and mislead the interpretation of associated analysis, which can cause detrimental effects on decision making especially if these results are used in petroleum field development planning.

The second approach involves the use of EOS, which are the mathematical relationships to be used to identify properties of hydrocarbons with respect to temperature, pressure, and fluid composition [47]. In practice, most of the EOS based correlations for z-factor calculation are implicit in nature and requires solving iteratively. On the other hand, the main difficulty to employ a cubic EOS for calculating z-factor can encourage huge uncertainties in estimating the properties of reservoir fluids, especially for heavy components [48]. Table 2 highlights widely used z-factor correlations which were formulated by modifying the coefficients of EOS using numerical regression analysis; and each correlation was derived based upon a particular set of data sets. The correlations presented in Table 2 are also implicit in nature and required to solve iteratively.

Limitations of correlations

Each of the correlations presented earlier has its own limitations. Some correlations were designed to be used as a quick

Table 2 – Iterative z-factor correlations.

The z-correlation	Equation of state	Database
Hall and Yarborough (H&Y) [49]	Carnahan and Starling [50]	Marshall B Standing and Katz [35] and 12 natural gas mixtures.
P. M. Dranchuk et al. (DPR) [37]	Benedict, Webb, and Rubin [51]	Marshall B Standing and Katz [35] and G. Brown et al. [34]
P. M. Dranchuk and H. Abou-Kassem (DAK) [52]	K.E. Starling [53]	Marshall B Standing and Katz [35]

Table 3 – Recommended reduced pressure and reduced temperature ranges for each correlation.

Correlation	Reduced Pressure Range	Reduced Temperature Range
Azizi et al. (AZI) [42]	$0.2 \leq P_{pr} \leq 11$	$1.1 \leq T_{pr} \leq 2$
Bahadori et al. (BAH) [41]	$0.2 < P_{pr} < 16$	$1.05 < T_{pr} < 2.4$
Beggs and Brill (B&B) [40]	$0 < P_{pr} < 8$	$1.2 < T_{pr}$
P. M. Dranchuk and H. Abou-Kassem (DAK) [52]	$0.2 < P_{pr} < 30$	$1 < T_{pr} < 3$
P. M. Dranchuk et al. (DPR) [37]	$0.2 < P_{pr} < 30$	$1 < T_{pr} < 3$
Hall and Yarborough (H&Y) [49]	$0.8 > P_{pr} < 4$	$1.2 < T_{pr}$
Heidaryan, Salarabadi, et al. (HEID) [43]	$0.2 < P_{pr} < 17$	$1.2 < T_{pr}$
Mahmoud (MAH) [46]	$0.1 < P_{pr} < 20$	$2.2 < T_{pr} < 4$
Papay (PAP) [39]	$P_{pr} < 8$	$T_{pr} < 2$
Sanjari and Lay (SNL) [44]	$0.01 < P_{pr} < 15$	$1.01 \leq T_{pr} \leq 3$
Shokir et al. (SHO) [45]	$0.01 < P_{pr} < 15$	$1.01 \leq T_{pr} \leq 3$

estimation tool, whilst others were designed for accuracy within wide ranges of pressure and temperature for certain samples. The correlations can also be influenced by the composition of gas sample, non-hydrocarbon components, range of pressures and temperatures and size of data sample used in its creation. Correlations are also tuned to fit only the data used for the creation of the correlation, which can present further limitations when other gas compositions are used, and consequently encourages significant error with huge uncertainties.

Table 3 provides recommended range of pseudo reduced pressure and temperature considered in different correlations in order to have a reasonable accurate estimation of z-factor.

From Table 3, it can be observed that each of the correlations mentioned above are based on a bounded range of pressure and temperature. The accuracy of estimated results using these correlations depends on how accurately each of the correlations matches with the nature of gas mixture, and range of pressures and temperatures. It becomes utterly challenging to determine a single correlation that can provide accurate estimation of z-factor for a given gas mixture within the interesting range of reservoir pressures and temperatures. Sensitivity study may help to determine which correlation would provide the estimate with the highest degree of accuracy, despite the original author's guidelines. However, this discussion warrants that a method or framework needs to be in place, which eases the process and minimize the errors as well as uncertainties.

Method of determining best possible Z-factor

In this study, both explicit and implicit correlations discussed above are rigorously tested for a range of representative gas mixtures typically exist in tight gas-hydrocarbon reservoir for a wide range of pressures and temperatures. The degree of accuracy of these correlations is evaluated through rigorous sensitivity studies and error analysis. The best possible z-factor correlation offering most accurate value of z-factor for a

certain gas sample at various pressure and temperature conditions are then developed in the form of lookup tables. Using this lookup tables, one can easily identify which correlation should offer most accurate results for a certain gas sample within expected range of pressure and temperatures. The steps of calculation followed in this study are described in a flow chart presented in Fig. 1.

As described in Fig. 1, the method involves following basic steps:
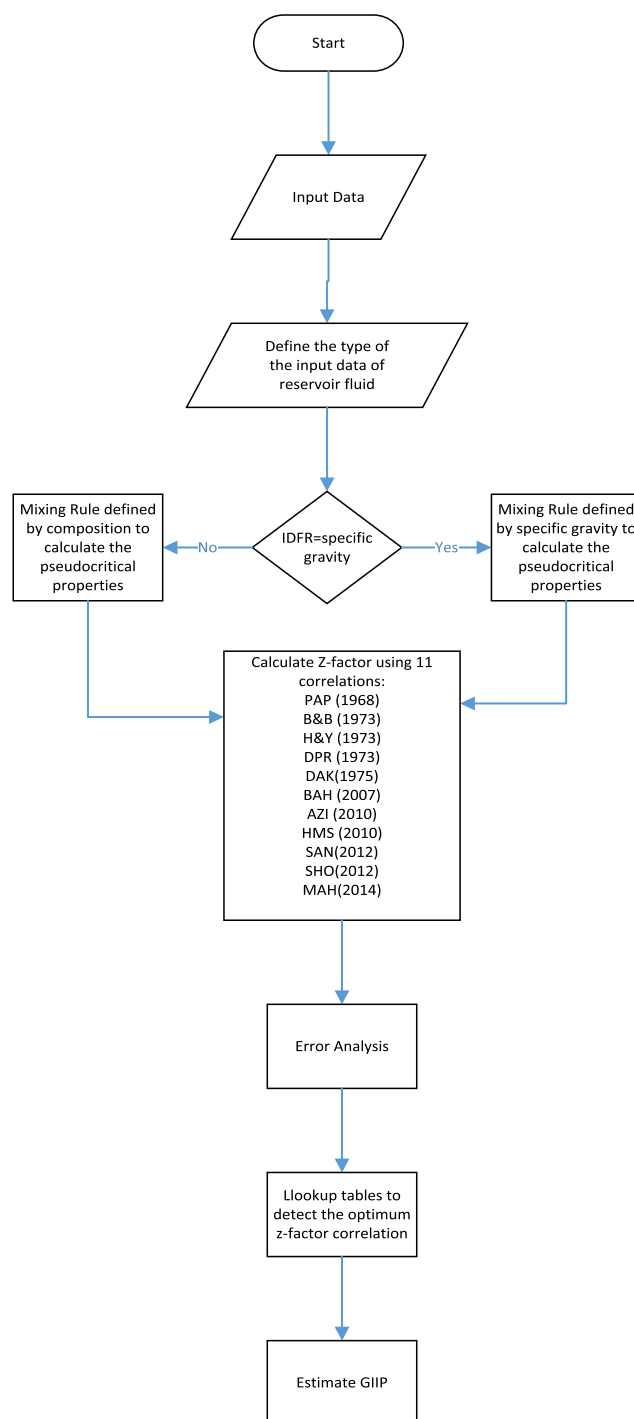
Fig. 1 – Flow chart showing the step of calculation followed in proposed method.

- Step 1: This step involves in the calculation of pseudocritical properties of reservoir fluid.
- Step 2: This step involves in the calculation of z-factor using 11 most known empirical correlations (which include both implicit and explicit typed correlations), which are widely used in the industry as a standard tool for routine practices.
- Step 3. This step is associated with error analysis using various fluid compositions, pressures and temperatures to define the most accurate or optimum z-factor correlation for a particular fluid and range of pressures and temperatures.
- Step 4: This step involves the identification of the best possible z-factor correlation which offers the minimum error, and the development of lookup tables based upon error analysis and sensitivity studies.
- Step 5: Using the developed lookup table as obtained in step 4, this step involves the determination of the best possible z-factor correlation(s) that should be considered for accurate estimation of z-factor as well as subsequent calculations.

The estimated z-factor obtained from this selected correlation is considered to be an optimum correlation, which eventually provides with the most accurate z-factor that can be used for reservoir simulation or any other relevant computation. Particularly in this study, this approach is used for the simulation of Whicher Range field, an Australian Tight Gas field in order to accurately estimate the Gas Initially in Place (GIIP).

A Visual Basic Application (VBA) interface based Excel program has been developed by employing above discussed method, which can be used to estimate z-factor of any given gas mixture or gas system for pressure ranges from 500 psi to 12000 psi, and temperature ranges from 100 °F to 400 °F. The details feature of this developed program has been elaborated in a later section below.

Development of VBA interface based excel program

The calculation of z-factor can be conducted by two methods: numerical or graphical. The graphical calculation delivers one value from one direct correlation with truncation error that differs from one user to another. The process is tedious, time-consuming, and not suitable for routine industry standard analysis. On the other hand, the numerical method can deliver many values of z-factor based on different direct and iterative correlations with better accuracy within manageable time frame. Accordingly, a computational program is

Fig. 2 — Z-factor calculation user form for considered in the developed program.

Table 4 — Natural gas compositions used for correlations analysis.

Component	Representative gas types and X_i (%)			
	Type 1	Type 2	Type 3	Type 4
C_1	94.0	87.0	79.9	65.8
C_2	4.0	3.7	3.4	2.8
C_3	2.0	1.8	1.7	1.4
CO_2	0	2.5	5.0	10.0
N_2	0	2.5	5.0	10.0
H_2S	0	2.5	5.0	10.0

developed based on numerical method to estimate z-factor using Excel spreadsheet with VBA.

The program includes both explicit (direct) method, and implicit (iterative) depending on the nature of the correlations. The direct method is applied to the empirical z-factor correlations. The correlation based on an EOS, where z-factor appears on the both sides of the correlation, are solved iteratively using combined Newton-Raphson, and the false position approaches [54]. Although the Newton-Raphson method is relatively fast approach, the accuracy of the solution solely depends on initial guess. Wrong initial guess often leads to erroneous as well as misleading results. To overcome this, the false position method was employed to solve z-factor initially to determine good initial guess for Newton-Raphson.

The program allows quick and accurate calculations of z-factor using all the correlations discussed in previous sections. It was coded in VBA, which is the native coding platform for Excel. By creating an easy to use form, users can simply enter relevant gas, pressure and temperature properties and select, which correlation they wish to calculate the z-factor. The spreadsheet has the capability to generate results for an array of pressures designated by the user. The user form for z-factor calculations is shown in Fig. 2. This user form can determine the z-factor from 11 different correlations individually, or all of them at once. Users have to simply provide the pressure and temperature at which they wish to calculate the z-factor, other relevant data and select a method for calculation of pseudocritical parameters. The user can then calculate the z-factor based upon the interested correlations by selecting corresponding correlation from drop down menu. The program populated cells in the worksheet in an array, allowing for multiple pressures to be used at once if so desired. This program can provide results from all 11 correlations calculation within 1 s up to 10 decimal places, making it an accurate and fast method to determine the z-factor using different correlations. Although the current program uses most known and widely acceptable 11 correlations considered as standard for oil and gas industry, any number of correlations can easily be incorporated into the program.

The z-factor correlations included in the program are mostly used correlations: Azizi et al. (AZI) [42], Bahadori et al. (BAH) [41], Beggs and Brill (B&B) [40], P. M. Dranchuk and H. Abou-Kassem (DAK) [52], P. M. Dranchuk et al. (DPR) [37], Hall and Yarborough (H&Y) [49], Heidaryan, Salarabadi, et al. (HEID) [43], Mahmoud (MAH) [46], Papay (PAP) [39], Sanjari and Lay (SNL) [44] and Shokir et al. (SHO) [45]. Four mixing rules for pseudocritical parameters that based on gas composition

considered in the program are: Kay [19], Stewart et al. [21], Corredor et al. [22] and Piper et al. [23]. While, two mixing rules for pseudocritical parameters that based on gas specific gravity considered are: R. Sutton [26] and M.B. Standing [24]. In addition, Wichert and Aziz's correlation [29] is employed to handle the presence of non-hydrocarbon components. All of the correlations are presented in Appendix (A).

Sensitivity studies

The sensitivity studies were carried out to evaluate the degree of accuracy of the reviewed correlations in this study to formulate lookup tables of z-factor correlations, and justify the potential application of the developed program and these lookup tables as a practical and simple tool to determine the most accurate z-factor correlation at each pressure and temperature for a given gas mixture to be used across a broad range of conditions. The evaluation criteria for the accuracy of the eleven selected correlations are based upon average absolute relative error (AARE%) and coefficient of determination (R^2) in comparison with AGA8 Equation and experimental results. The calculated results are compared with experimental data for 20 real gas samples, which added extra pressure and temperature ranges along with increasing amount of non-hydrocarbon presence.

AGA8 equation of state is a standard that was developed by the American Gas Association on the principle of the Virial Equation of State to calculate z-factor for gas mixtures [55—59]. AGA8 equation can perform the calculation of thermodynamic properties of natural and synthetic gases mixtures consisting of up to 21 components [60]. Many researches are carried out to calculate the thermodynamic properties of gas mixtures using AGA8 equation of state, and concurred that AGA8 equation states most accurate prediction with an error ranges ±0.7% [18,61,62]. AGA8 equation of state is, is however considered as an acceptable and most broadly used industry standard to calculate z-factor for gas mixtures because of its high accuracy for wide range of gas composition, temperature and pressure [63—67]. Accordingly, this equation of state is considered as a standard basis to evaluate the accuracy of z-factor correlations in this study.

Based on this sensitivity analysis, four lookup tables are developed, which highlights the best possible correlation that provides most accurate estimation of z-factor for each pressure, temperature for a given range of gas composition considered in the study. Four different groups of natural gas systems with varying amount of non-hydrocarbon components are also considered to represent a large range of reservoir dry natural gases.

Natural gas properties considered

In order to capture a large range of possible dry natural gas compositions which are found in reservoirs, four different types of representative typical natural gas system with different compositions are considered for demonstration purpose. Composition of each type of gas system are shown in Table 4. The type 1 natural gas system consists of pure hydrocarbon based mixture whereas the others contain different

Table 5 – Natural gas composition important properties of all representative types of natural gas system.

Types of Natural Gas	Pseudocritical pressure (psia)	Pseudocritical temperature (R)	Gas specific gravity (γ)	Gas molecular weight (g/gmol)
1	674.183	342.944	0.593	17.165
2	686.521	347.727	0.639	18.516
3	699.137	352.934	0.687	19.895
4	724.940	363.156	0.781	22.626

Table 6 – AARE% and R^2 in estimated z-factor using various correlation for all representative types of natural gas system.

Correlations	Type 1 AARE%	Type 1 R^2	Type 2 AARE%	Type 2 R^2	Type 3 AARE%	Type 3 R^2	Type 4 AARE%	Type 4 R^2
AZI	1.171	0.992	1.38	0.992	1.441	0.993	2.201	0.994
BAH	2.677	0.949	2.304	0.961	2.396	0.966	2.815	0.974
B&B	1.831	0.972	1.721	0.978	1.739	0.981	2.569	0.984
DAK	0.598	0.9984	0.966	0.998	1.146	0.998	2.139	0.998
DPR	0.643	0.9982	1.072	0.9979	1.243	0.9981	2.236	0.9981
H&Y	0.595	0.9984	0.901	0.9979	1.078	0.9981	2.076	0.9979
HEID	0.683	0.9977	1.048	0.9969	1.2154	0.9971	2.168	0.9968
MAH	12.2	0.671	11.83	0.6776	11.495	0.6782	10.709	0.668
PAP	14.445	0.815	15.95	0.817	15.38	0.818	16.563	0.828
SNL	1.056	0.9946	1.075	0.9945	1.478	0.9946	2.532	0.9938
SHO	18.81	0.222	18.67	0.192	17.631	0.1325	16.93	0.023

amount of non-hydrocarbon components such as hydrogen sulfide (H_2S), carbon dioxide (CO_2) and nitrogen (N_2), as common impurities seen in typical natural gas system [68]. The compositions of different types of gas system used for this analysis are listed in Table 4.

As shown in Table 4, the compositions of four types of representative gas systems considered are as follows.

- Type 1 = Pure hydrocarbon case.
- Type 2 = 2.5 mol% of each three non-hydrocarbon gases (7.5% total).
- Type 3 = 5 mol% of each three non-hydrocarbon gases (15% total).
- Type 4 = 10 mol% of each three non-hydrocarbon gases (30% total).

The pseudocritical properties of components considered in four types of gas systems are determined using Piper et al. mixing rule [23]. Table 5 lists the critical properties, specific gravity and molecular weight of each of these four types of gas system.

Evaluation criteria of the z-factor correlations with AGA8 equation and the experimental data

All correlations are evaluated based on Average Absolute Relative Error (AARE%) in comparison to AGA8 Equation and the available experimental data. Average Absolute Relative Error indicates how much a calculated value can deviate from the measured value, where zero indicates an identical result. Average absolute relative error is defined in Eq (1).

$$AARE\% = \sum_{i=1}^{n}\left(\left|\frac{y_{calculated}-y_{measured}}{y_{measured}}\right|*100\right)\Big/n \quad (1)$$

Where $y_{calculated}$ represents the value of property calculated by the correlations equation and $y_{measured}$ represents the value of property calculated from the AGA8 Equation of State or the available experimental data.

The second evaluation criterion is the coefficient of determination (R^2), which is used to determine the accuracy of the results of the z-factor correlations as compared to the results of AGA8 Equation of State or the available experimental data. The R^2 or coefficient of determination indicates how well certain data will fit into statistical models or given data [69]. The R^2 is calculated using Eq (2).

$$R^2 = 1 - \frac{Residual\ sum\ of\ squares}{Explained\ sum\ of\ squares} \quad (2)$$

Results and discussion

Estimation of z-factor for representative types of typical natural gas system

Each correlation is used to calculate the z-factor for the pressure from 500 to 12000 psi, temperature from 100 to 400 °F and composition ranges as listed in Table 4. AARE% and R^2 for each correlation are calculated by equations [1] and [2],

Table 7 – Correlation accuracy ranking of types of the representative typical natural gas system considered.

Sample No.	1st	2nd	3rd
1	H&Y	DAK	DPR
2	H&Y	DAK	HEID
3	H&Y	DAK	HEID
4	H&Y	DAK	HEID

242

Table 8 — The statistical description of the data bank for the real samples used for analysis.					
Component	Minimum mole %	Maximum mole %	Mean	Variance	Standard Dev.
C_1	42.41	96	77.933	220.458	15.024
C_2	0	28.67	5.187	45.670	7.166
C_3	0	16.2	1.696	13.069	3.883
iC_4	0	5.87	0.587	2.001	1.539
nC_4	0	1.63	0.324	0.289	0.563
iC_5	0	0.91	0.204	0.103	0.339
nC_5	0	0.79	0.117	0.061	0.262
nC_6	0	1.31	0.173	0.155	0.423
C_{7+}	0	4.51	0.323	1.188	1.192
CO_2	0	20	3.990	29.261	5.505
H_2S	0	51.37	10.413	186.813	13.971
N_2	0	5.84	1.029	2.316	1.603

respectively, and then compared to each correlation as shown in Table 6.

It is important to note that these results presented in Table 6 are the averages across the entire pressure range of 500—12000 psi and temperature of 100 to 400 °F for each sample. Based on minimum AARE% and maximum R^2 (i.e. close to 1), the top three most accurate correlations of the representative typical natural gas system are selected from Table 6 and listed below in Table 7. These results are then used to develop lookup tables as explained later.

As seen in Table 7, the Hall and Yarborough correlation (H&Y) performs the best for all four gas compositions. P. M. Dranchuk and H. Abou-Kassem (DAK), P. M. Dranchuk et al. (DPR) and the Heidaryan, Salarabadi, et al. (HEID) correlations are appeared to perform well (as AARE% is low and R^2 is close to unity). This analysis helps highlight the impact of choice of correlation on the calculation of z-factor and subsequent calculations.

Estimation of z-factor for real gas samples

To quantify the results obtained above in a real world scenario, several reservoirs were considered as the representative natural gas samples to analyse using the proposed method. Use of real reservoir data would allow the analysis to identify the effect of the presence of non-hydrocarbon gas in a real reservoir gas system on pseudocritical properties and more importantly, the z-factor. The experimental results of 20 real gas samples obtained from published studies [16,18,70—72] are used in this analysis to compare with the corresponding results of the correlations, and then AARE% and R^2 are calculated to evaluate the degree of accuracy of each correlation for each gas sample through the entire range of pressures and temperatures considered in this study. The statistical description of the data bank for these 20 real samples is presented in Table 8 depending on maximum and minimum value of different components of hydrocarbon including mean, variance and standard deviation.

The results of this analysis based on AARE% and R^2 are shown in Fig. 3 and Fig. 4, respectively. Once again, the Hall and Yarborough correlation [49] provides the best match to the experimental z-factors for the real gas samples, having an average error across all points of 1.44%. The DAK, DPR, AZI and HEID correlations are also observed to be provided accurate results across all data points having average errors less than 2%.

Development of lookup tables

Based on the results determined by the sensitivity analysis, four lookup tables have been created for four groups of real samples considered in the sensitivity analysis; and presented in Tables 9—12. It is to be noted that the real samples presented in Table 8 are categorized into 4 different groups
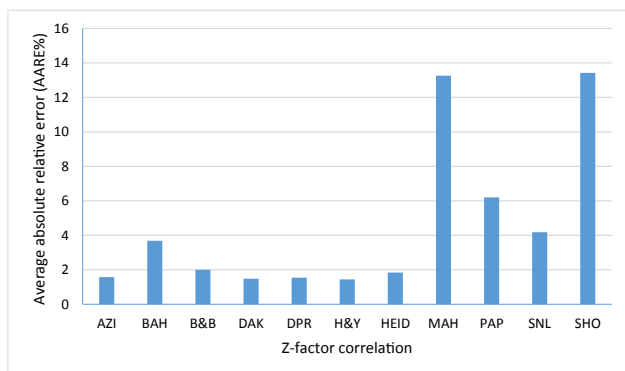
Fig. 3 — Calculated average absolute relative error for the z-factor correlations.
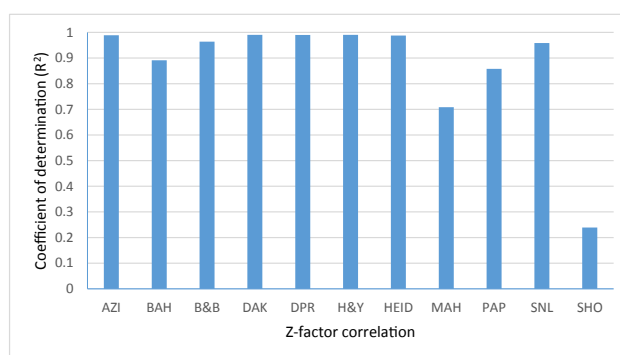
Fig. 4 — Calculated coefficient of determination for the z-factor correlations.

243

Table 9 — Recommended correlation for any temperature and pressure for Group 1 (no non-hydrocarbon gas presence).

Pressure, psi	Temperature, °F													
	0	100	125	150	175	200	225	250	275	300	325	350	375	400
500	DAK	HEID	HEID	H&Y	H&Y	B&B	B&B	B&B	B&B	B&B	MAH	AZI	SNL	SNL
1000	DPR	H&Y	H&Y	HEID	HEID	B&B	B&B	B&B	B&B	B&B	B&B	AZI	MAH	SHO
1500	B&B	DAK	HEID	PAP	B&B	B&B	B&B	B&B	B&B	B&B	B&B	B&B	B&B	SHO
2000	B&B	AZI	DPR	H&Y	PAP	PAP	B&B	B&B	B&B	B&B	B&B	B&B	B&B	AZI
2500	B&B	H&Y	DAK	DPR	DPR	PAP	PAP	SNL	B&B	B&B	B&B	B&B	SNL	SNL
3000	BAH	H&Y	HEID	DAK	DPR	DPR	PAP	PAP	B&B	B&B	B&B	B&B	SHO	SNL
3500	AZI	H&Y	AZI	DAK	DAK	DPR	DPR	PAP	B&B	B&B	B&B	B&B	B&B	SHO
4000	AZI	AZI	H&Y	AZI	DAK	DPR	DPR	BAH	BAH	B&B	B&B	B&B	DPR	DPR
4500	AZI	AZI	AZI	AZI	DAK	HEID	SHO	DPR	DPR	DPR	DPR	DPR	DPR	DPR
5000	AZI	AZI	AZI	H&Y	AZI	DAK	DAK	DPR	DPR	DPR	DPR	DPR	DPR	DPR
5500	DAK	SNL	DAK	H&Y	H&Y	DAK	HEID	DAK	SHO	PAP	DPR	DPR	DPR	DPR
6000	DAK	DAK	DAK	DAK	SNL	H&Y	DAK	DAK	DAK	B&B	B&B	DPR	DPR	DPR
6500	DAK	DAK	DAK	DAK	DAK	H&Y	H&Y	HEID	DAK	DAK	DAK	DAK	DAK	DAK
7000	DAK	DAK	DAK	DAK	DAK	DAK	H&Y	HEID	SNL	DAK	DAK	DAK	DAK	DAK
7500	DAK	DPR	DAK	DAK	DAK	HEID	HEID	HEID	H&Y	SNL	DAK	B&B	DAK	DAK
8000	DAK	DAK	DAK	DAK	DAK	HEID	HEID	AZI	H&Y	H&Y	SNL	HEID	HEID	HEID
8500	DAK	DAK	DAK	DAK	HEID	HEID	HEID	HEID	H&Y	H&Y	SNL	HEID	HEID	HEID
9000	DAK	DAK	DPR	DAK	HEID	HEID	HEID	HEID	HEID	H&Y	H&Y	HEID	HEID	HEID
9500	DPR	DPR	DPR	DPR	HEID	HEID	HEID	HEID	HEID	HEID	HEID	HEID	HEID	HEID
10000	SNL	DPR	DPR	DPR	HEID	HEID	HEID	HEID	HEID	HEID	H&Y	H&Y	H&Y	H&Y
10500	DPR	DPR	DPR	DPR	DPR	HEID	HEID	HEID	HEID	H&Y	H&Y	H&Y	H&Y	H&Y
11000	DPR	DPR	DPR	B&B	DPR	H&Y	H&Y	H&Y	H&Y	H&Y	H&Y	H&Y	H&Y	H&Y
11500	DPR	DPR	DPR	DPR	DPR	H&Y	H&Y	H&Y	H&Y	AZI	H&Y	H&Y	H&Y	B&B
12000	DPR	DPR	DPR	DPR	DPR	H&Y	H&Y	BAH	H&Y	H&Y	H&Y	H&Y	H&Y	H&Y

depending on the percentage of non-hydrocarbon components present in the real gas mixture, which are defined as:

- Group 1 — pure hydrocarbon case (i.e. non-hydrocarbon component = 0)

- Group 2 — hydrocarbons with mole percentage of non-hydrocarbon component is 0 < non-hydrocarbon ≤ 7.5
- Group 3 — hydrocarbons with mole percentage of non-hydrocarbon component is 7.5 < non-hydrocarbon ≤ 15

Table 10 — Recommended correlation for any temperature and pressure for Group 2 (0—7.5% non-hydrocarbon gas presence).

Pressure, psi	Temperature, °F												
	100	125	150	175	200	225	250	275	300	325	350	375	400
500	DAK	HEID	HEID	B&B	B&B	B&B	B&B	B&B	B&B	B&B	MAH	SNL	SNL
1000	AZI	BAH	B&B	B&B	B&B	B&B	B&B	B&B	B&B	B&B	B&B	AZI	MAH
1500	B&B	H&Y	HEID	PAP	PAP	B&B	B&B	B&B	B&B	B&B	B&B	B&B	AZI
2000	B&B	H&Y	DPR	PAP	PAP	PAP	B&B	B&B	B&B	SHO	B&B	B&B	B&B
2500	B&B	HEID	DAK	DPR	DPR	PAP	PAP	SNL	SNL	B&B	SNL	SNL	SNL
3000	BAH	BAH	AZI	DAK	DPR	DPR	PAP	PAP	B&B	B&B	B&B	B&B	SNL
3500	BAH	AZI	H&Y	AZI	DAK	DPR	DPR	PAP	DPR	B&B	BAH	B&B	SHO
4000	B&B	AZI	AZI	H&Y	AZI	DAK	BAH	BAH	BAH	BAH	B&B	B&B	DPR
4500	B&B	AZI	AZI	H&Y	H&Y	AZI	DAK	DAK	DPR	DPR	B&B	DPR	DPR
5000	B&B	AZI	AZI	H&Y	H&Y	H&Y	H&Y	DAK	DAK	PAP	DPR	DPR	DPR
5500	B&B	SNL	DAK	DAK	H&Y	H&Y	AZI	H&Y	HEID	DAK	DAK	DPR	DPR
6000	BAH	SNL	SNL	SNL	SNL	H&Y	AZI	AZI	H&Y	HEID	DAK	DAK	DAK
6500	B&B	BAH	SNL	SNL	SNL	SNL	SNL	AZI	H&Y	H&Y	H&Y	H&Y	DAK
7000	B&B	B&B	BAH	SNL	SNL	SNL	B&B	SNL	AZI	HEID	HEID	H&Y	HEID
7500	B&B	B&B	BAH	B&B	B&B	B&B	SNL	SNL	AZI	SNL	HEID	H&Y	H&Y
8000	B&B	B&B	BAH	B&B	B&B	B&B	HEID	SNL	SNL	SNL	HEID	H&Y	H&Y
8500	SNL	B&B	B&B	B&B	B&B	HEID	HEID	HEID	SNL	SNL	SNL	H&Y	B&B
9000	SNL	B&B	B&B	B&B	B&B	HEID	HEID	HEID	SNL	SNL	SNL	H&Y	H&Y
9500	SNL	SNL	B&B	B&B	HEID	HEID	HEID	HEID	SNL	SNL	SNL	H&Y	H&Y
10000	DPR	SNL	B&B	B&B	HEID	HEID	HEID	HEID	SNL	SNL	SNL	H&Y	H&Y
10500	DPR	SNL	BAH	B&B	DPR	HEID	HEID	SNL	SNL	SNL	AZI	H&Y	H&Y
11000	BAH	BAH	SNL	SNL	SNL	SNL	SNL	SNL	SNL	SNL	AZI	H&Y	H&Y
11500	DPR	B&B	B&B	SNL	SNL	SNL	SNL	SNL	SNL	SNL	AZI	H&Y	H&Y
12000	DPR	B&B	B&B	SNL	SNL	SNL	SNL	BAH	SNL	H&Y	AZI	H&Y	H&Y

Table 11 — Recommended correlation for certain temperature and pressure for Group 3 (7.5–15% non-hydrocarbon gas presence).

Pressure, psi	Temperature, °F												
	100	125	150	175	200	225	250	275	300	325	350	375	400
500	AZI	DPR	HEID	H&Y	H&Y	SHO	AZI	B&B	B&B	B&B	MAH	SNL	SNL
1000	PAP	PAP	H&Y	H&Y	HEID	HEID	B&B	B&B	B&B	B&B	B&B	B&B	MAH
1500	BAH	B&B	DPR	B&B	PAP	B&B	B&B	B&B	B&B	B&B	B&B	B&B	B&B
2000	HEID	B&B	HEID	H&Y	H&Y	PAP	PAP	B&B	B&B	SHO	B&B	B&B	B&B
2500	B&B	B&B	AZI	H&Y	DPR	DPR	PAP	SNL	B&B	SNL	SHO	B&B	SNL
3000	B&B	SHO	H&Y	H&Y	DAK	DPR	DPR	PAP	B&B	B&B	B&B	B&B	SNL
3500	BAH	BAH	BAH	H&Y	HEID	DAK	DPR	PAP	PAP	B&B	B&B	B&B	SHO
4000	B&B	AZI	AZI	H&Y	AZI	DAK	DPR	DPR	PAP	BAH	B&B	B&B	DPR
4500	B&B	AZI	AZI	H&Y	H&Y	AZI	DAK	DPR	DPR	DPR	B&B	B&B	DPR
5000	B&B	AZI	AZI	H&Y	H&Y	H&Y	DAK	DAK	SHO	DPR	DPR	DPR	DPR
5500	SNL	DAK	DAK	DAK	H&Y	H&Y	H&Y	HEID	DAK	DPR	DPR	DPR	DPR
6000	BAH	SNL	SNL	SNL	DAK	H&Y	AZI	H&Y	DAK	DAK	B&B	DPR	DPR
6500	DPR	BAH	DAK	DAK	SNL	SNL	SNL	H&Y	HEID	DAK	DAK	DAK	BAH
7000	DPR	BAH	DAK	DAK	DAK	DAK	H&Y	AZI	HEID	HEID	DAK	DAK	DAK
7500	DPR	DPR	BAH	DAK	DAK	DAK	B&B	AZI	HEID	H&Y	H&Y	DAK	DAK
8000	DPR	DPR	BAH	DAK	DAK	B&B	HEID	HEID	HEID	H&Y	SNL	H&Y	HEID
8500	DPR	DPR	DPR	SHO	DAK	B&B	HEID	HEID	AZI	HEID	H&Y	H&Y	HEID
9000	DPR	DPR	DPR	DAK	B&B	HEID	HEID	HEID	HEID	HEID	HEID	HEID	HEID
9500	SNL	DPR	DPR	DPR	B&B	HEID	HEID	HEID	HEID	HEID	HEID	H&Y	HEID
10000	DPR	DPR	DPR	DPR	B&B	HEID	HEID	HEID	HEID	HEID	HEID	H&Y	H&Y
10500	DPR	SNL	MAH	DPR	DPR	HEID	HEID	HEID	HEID	AZI	H&Y	H&Y	H&Y
11000	BAH	DPR	DPR	B&B	DPR	H&Y	HEID	HEID	HEID	H&Y	SNL	H&Y	H&Y
11500	DPR	DPR	SNL	B&B	DPR	H&Y	H&Y	H&Y	H&Y	H&Y	H&Y	H&Y	H&Y
12000	DPR	DPR	DPR	B&B	DPR	H&Y	H&Y	H&Y	H&Y	SNL	H&Y	H&Y	H&Y

- Group 4 — hydrocarbons with mole percentage of non-hydrocarbon component is 15 < non-hydrocarbon ≤ 30

The lookup table for each group of gas samples highlights the correlation which achieves the highest accuracy of z-factor calculation for a given group of gas samples at a certain pressure and temperature domain. For instance from Table 9, it can be seen that the DAK correlation can provide better estimation of z-factor for Group 1, when reservoir pressure varies from 6500 to 7000 psi within temperature range is 0 to

Table 12 — Recommended correlation for certain temperature and pressure for Group 4 (15–30% non-hydrocarbon gas presence).

Pressure, psi	Temperature, °F													
	0	100	125	150	175	200	225	250	275	300	325	350	375	400
500	AZI	H&Y	DAK	HEID	H&Y	H&Y	B&B	AZI	B&B	B&B	B&B	B&B	MAH	SNL
1000	PAP	PAP	H&Y	H&Y	HEID	B&B	B&B	B&B	B&B	B&B	B&B	B&B	AZI	AZI
1500	DPR	DPR	DAK	PAP	HEID	B&B	B&B	B&B	B&B	B&B	B&B	B&B	B&B	B&B
2000	BAH	B&B	AZI	DPR	PAP	PAP	PAP	B&B	B&B	B&B	B&B	B&B	B&B	B&B
2500	B&B	B&B	AZI	DPR	DPR	SNL	PAP	SNL	SNL	SNL	B&B	B&B	SHO	B&B
3000	B&B	SHO	H&Y	DAK	DPR	DPR	PAP	PAP	PAP	SNL	B&B	B&B	B&B	SNL
3500	B&B	H&Y	H&Y	BAH	DAK	DPR	DPR	PAP	PAP	B&B	B&B	B&B	BAH	B&B
4000	B&B	AZI	AZI	AZI	DAK	DPR	BAH	BAH	PAP	BAH	BAH	B&B	B&B	B&B
4500	B&B	AZI	AZI	AZI	DAK	DAK	SHO	DPR	DPR	PAP	DPR	B&B	B&B	B&B
5000	B&B	AZI	AZI	AZI	AZI	DAK	HEID	DPR	DPR	DPR	DPR	DPR	DPR	DPR
5500	B&B	AZI	AZI	DAK	H&Y	AZI	DAK	HEID	DPR	SHO	PAP	DPR	DPR	DPR
6000	B&B	SNL	SNL	SNL	DAK	H&Y	DAK	HEID	DPR	DPR	DPR	DPR	DPR	DPR
6500	B&B	BAH	DAK	DAK	SNL	SNL	H&Y	DAK	DAK	SHO	DPR	DPR	DPR	DPR
7000	B&B	DPR	BAH	DAK	DAK	DAK	DAK	H&Y	DAK	SNL	SNL	DPR	DPR	DPR
7500	B&B	DPR	BAH	DAK	DAK	DAK	DAK	H&Y	HEID	DAK	DAK	SNL	DAK	DAK
8000	DPR	DPR	DPR	DAK	DAK	DAK	DAK	B&B	HEID	H&Y	DAK	DAK	DAK	DAK
8500	SNL	DPR	DPR	BAH	DAK	DAK	B&B	HEID	HEID	H&Y	H&Y	DAK	DAK	SNL
9000	SNL	DPR	DPR	BAH	DAK	B&B	HEID	HEID	HEID	HEID	H&Y	H&Y	H&Y	SNL
9500	DPR	DPR	DPR	BAH	B&B	B&B	HEID	HEID	HEID	HEID	H&Y	H&Y	H&Y	SNL
10000	DPR	SNL	DPR	BAH	B&B	HEID	HEID	HEID	HEID	HEID	HEID	HEID	H&Y	SNL
10500	DPR	SNL	DPR	BAH	B&B	HEID	HEID	HEID	HEID	HEID	HEID	HEID	HEID	HEID
11000	DPR	DPR	SNL	BAH	B&B	DPR	HEID	HEID	HEID	HEID	HEID	BAH	H&Y	H&Y
11500	BAH	BAH	SNL	DPR	B&B	DPR	H&Y	HEID	HEID	HEID	HEID	H&Y	SNL	H&Y
12000	DPR	DPR	DPR	SNL	MAH	DPR	H&Y	H&Y	H&Y	BAH	H&Y	H&Y	H&Y	H&Y

Table 12a — Color code and description of different correlations abbreviated in Tables 9–12

Correlation	Azizi et al. [42]	Bahadori et al. [41]	Beggs and Brill [40]	P. M. Dranchuk and H. Abou-Kassem [52]	P. M. Dranchuk et al. [37]	Heidaryan, Salarabadi, et al. [43]	Hall and Yarborough [49]	Mahmoud [46]	Papay [39]	Sanjari and Lay [44]	Shokir et al. [45]
Legend	AZI	BAH	B&B	DAK	DPR	HEID	H&Y	MAH	PAP	SNL	SHO

Table 13 — Molar gas composition of Whicher Range Reservoir.

Component	Mole %
Methane	91.17
Ethane	4.96
Propane	1.37
IsoButane	0.22
N-Butane	0.32
Iso-Pentane	0.09
N-Pentane	0.09
Hexanes	0.09
Heptanes +	0.43
Hydrogen Sulfide	0.00
Carbon Dioxide	0.88
Nitrogen	0.38

Table 14 — The petrophysical properties of Whicher Range Reservoir.

Property	Range
Porosity, %	5—15
Water saturation, %	20—60
Permeability, md	0.1 md to less than 0.01 md
H_{net}/H_{Gross}	0.22

200 °F. DAK correlation also performs well in case the reservoir is limited to 6500—7000 psi for a temperature more than 300 °F. For z-factor calculations at certain pressures and temperatures in between each isotherm and isobar, it can be assumed that both the adjoining correlations can be used with high accuracy. Tables 9—12 represent the recommended correlation to be used for any pressure and temperature for Groups 1 to 4, respectively.

The color code and full description of correlations shown in Tables 9—12 are provided in Table 12a.

When compared to the lookup Tables 9—12, it is clear that there is no single correlation which can predict accurately for the entire range of pressure, temperature and composition. For instance, AZI correlation is appeared to work for very low reservoir pressure (up to 1000 psi), when temperature is 350 °F for Group 1. Obviously this correlation provides with erroneous result at higher pressure and at temperature of 350 °F for Group 1 (Table 9), if AZI correlation is used. It can be observed from Tables 9—12 that the B&B correlation almost appears to be best choice when reservoir pressure varies from 0 to 4000 psi for a temperature range of 300 to 375 °F for all four groups. Similarly, it is possible to determine the most appropriate correlation that should be considered for a range of pressure and temperature for a given gas sample using any of the lookup tables generated using the developed excel based computation program. The proposed method can easily be adopted to develop computation program, which can be used as a tool for any number of gas sample for a range of pressure and temperature, and generate respective lookup tables which can then be used to determine the most accurate correlation to be used for the estimation of z-factor for any subsequent calculation or analysis (e.g. reservoir simulation, well test data analysis, PVT properties). Determination of accurate correlation for a given sample within the range of pressure

| Table 15 – AARE% of z-factor correlations for Australian Tight Gas-Hydrocarbon Reservoir.												
Pressure	AZI	BAH	B&B	DAK	DPR	H&Y	HEID	MAH	PAP	SNL	SHO	Minimum AARE%	The best correlation
500	0.131	8.033	0.081	0.383	0.421	0.207	0.283	0.768	0.395	0.456	0.232	8.033	B&B
1000	0.521	6.726	0.126	0.628	0.678	0.352	0.223	1.369	0.474	0.843	2.643	6.726	B&B
1500	0.675	5.563	0.053	0.751	0.780	0.478	0.400	2.193	0.373	1.131	1.049	5.563	B&B
2000	0.310	4.851	0.008	0.351	0.329	0.170	0.512	2.930	0.230	1.735	1.265	4.851	B&B
2500	0.685	3.249	0.878	0.669	0.574	0.628	1.717	4.778	0.074	0.456	2.760	4.778	PAP
3000	0.761	1.890	1.493	0.672	0.499	0.763	1.422	6.634	0.256	1.116	3.192	6.634	PAP
3500	0.325	1.045	1.539	0.166	0.078	0.348	0.582	8.191	1.072	1.873	2.175	8.191	DPR
4000	0.129	0.016	1.697	0.076	0.376	0.143	0.069	10.023	1.850	2.036	0.736	10.023	BAH
4500	0.227	1.182	1.988	0.011	0.324	0.223	0.024	12.050	2.605	1.639	0.670	12.050	DAK
5000	0.020	1.916	1.828	0.168	0.521	0.007	0.301	13.647	4.002	1.380	2.278	13.647	H&Y
5500	0.031	2.684	1.758	0.093	0.447	0.032	0.258	15.210	5.535	0.800	3.253	15.210	AZI
6000	0.003	3.235	1.558	0.025	0.367	0.048	0.178	16.479	7.483	0.218	3.596	16.479	AZI
6500	0.454	3.208	0.875	0.361	0.682	0.334	0.473	17.113	10.278	0.063	3.482	17.113	SNL

and temperatures can help achieve quick history matching, especially in case of complex reservoir simulation studies in routine industry environment; and significantly reduce the level of uncertainty as well as unproductive time.

Application of developed method and lookup tables

In order to investigate the potential application of developed method and lookup tables in real case, the method was employed to estimate the gas initially in place (GIIP) for the Whicher Range Tight Gas field using reservoir simulation. Whicher Range Tight gas-hydrocarbon reservoir, is located about 280 km south of Perth in the Bunbury trough of the southern Perth Basin, which contains mostly natural gas with the total mole percentage of non-hydrocarbon components is of 1.26% as shown in Table 13 [73]. The reservoir pressure changes over a large range for the production time and the reservoir temperature remains relatively constant. This temperature is about 250 °F while the pressure ranges between 0 and 6500 psi. The data presented in Table 10 are found to be close match with Whicher Range tight gas-hydrocarbon reservoir fluid data, and hence used to determine the most appropriate correlation to be recommended for the simulation. It can be observed from Table 10 that at constant temperature of 250 °F, the Beggs and Brill [40], and Papay [39] correlations are appeared to provide with most accurate estimate of z-factor when pressure is below 3000 psi. However, for pressures above 3000 psi, P. M. Dranchuk et al. [37], Bahadori et al. [41], Hall and Yarborough [49], P. M. Dranchuk and H. Abou-Kassem [52], Azizi et al. [42] and Sanjari and Lay [44] correlations are considered best possible z-factor correlations as highlighted the range with dotted box in Table 10. In particular for Whicher Range reservoir at initial reservoir pressure of 5500 psi and initial reservoir temperature 250 °F, Azizi et al. (AZI) correlation [42] is appeared to be the best possible z-factor correlation for the prediction of gas initially in place.

The gas initially in place was calculated using 3D reservoir simulation model which was built based on core, logs data, and well tests data collected from five wells, PVT data and field data. PETREL simulator is employed to create the 3D model of 69 layers consisting of 5820840 grids (nx = 285, ny = 296, and nz = 69). The petro-physical properties of the reservoir are showed in Table 14.

Table 15 shows the comparison between the experimental data and the calculated z-factor obtained from each correlation at temperature of 250 °F, and pressure ranges from 500 psi to 6500 psi. The comparison is made based on the minimum average absolute relative error (AARE%) presented in Table 15. AARE% is calculated using Eq (1). Based on minimum AARE% it can be observed from Table 15 that the most accurate z-factor correlation for this gas sample at a constant temperature significantly depends on the pressure. Table 15 also indicates that the AARE% calculated at the initial pressure is the highest comparing with the rest of the pressures, so the calculation of gas initially in place that should be calculated at initial pressure will encourage the highest degree of uncertainty comparing to other reservoir calculation that is performed at pressures below the initial reservoir pressure. However z-factor correlations that have the minimum AARE% at each pressure, and the z-factor correlations recommended by the lookup tables developed in this study are in good agreement, which warrant that the lookup tables as well as developed spreadsheet program can be used as an efficient tool to determine the most appropriate correlation to be used for the calculation of z-factor with high level of accuracy. By using
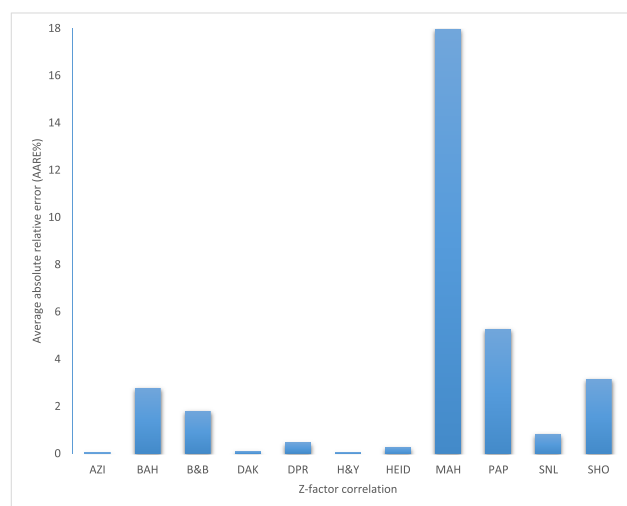
Fig. 5 – ARE% occur during estimation of GIIP.

reservoir simulation model, the gas initially in place was calculated using different z-factor correlations to identify the impact of z-factor correlation on the estimation of gas initially in place and to justify the feasibility of the developed lookup tables. Fig. 5 presents the percentage of relative error in estimated gas initially in place occurred for reservoir pressure of 5500 psi and temperature of 250 °F using different correlation as shown in Table 15. ARE% in Fig. 5 was calculated using Eq (3).

$$ARE\% = \left| \frac{GIIP_{z-correlation} - GIIP_{z-experimental}}{GIIP_{z-experimental}} \right| *100 \tag{3}$$

where $GIIP_{z\text{-correlation}}$ represents the value of GIIP calculated based on z-factor correlations and $GIIP_{z\text{-experimental}}$ represents the value of GIIP calculated based on the experimental data.

Fig. 5 shows that the random selection of z-factor could lead to overestimate the volume about 18% such as gas initially in place when it is calculated using Mahmoud correlation [46] and this error has caused a high impact on a field development plan. Fig. 5 also displays that Azizi et al. correlation [42] is the most accurate z-factor correlation because it provides with the closest estimate of gas initially in place depending on the experimental z-factor. As a result, the correlations that have the highest accuracy to estimate gas initially in place are the same correlations that can be selected from the lookup tables developed in this study.

Conclusions

This paper proposed a practical method, which can be considered as a simple, robust, and feasible approach to determine most appropriate correlation for a certain reservoir condition in order to estimate the z-factor with better accuracy; and minimize the level of uncertainties for a range of natural gas system typically produced from petroleum reservoir under different pressure and temperature conditions.

Based on this study z-factor lookup tables are created for a range of gas systems as a function of pressure and temperature, which can be used as an accurate and practical guide in order to determine or recommend the best possible z-factor correlation under a range of pressure, and temperature conditions for various gas systems. The recommended correlation then can be used to more accurately estimate other reservoir parameters, such PVT properties, gas initially in places and ultimate recovery factor. This exercise also helps achieve a quick history matching required for many petroleum engineering related computations, such well test analysis, production performance analysis, as well as complex reservoir simulation studies and minimize the level of uncertainties.

The proposed method is tested based on estimated z-factor obtained from experimental measurements; and using the AGA8 equation of state for a range of pressure, temperature and gas compositions (system), which warranted that the proposed method and created lookup tables can be successfully employed to determine most appropriate correlation for a certain condition. In particular, the method is applied to estimate gas initially in place for Whicher Range tight gas-

hydrocarbon reservoir. The estimated gas initially in place shows a good agreement with that predicted value obtained from complex reservoir simulation studies.

The proposed method is also found to be simple and practical, which can be used by inexperienced frontline engineers for decision making, especially to determine best possible z-factor correlation for any pressure ranges between 0 and 12000 psi; and temperature ranges between 100 and 400 °F for a range of gas system.

Nomenclature

AZI	Azizi et al.(42)
BAH	Bahadori et al.(41)
B&B	Beggs and Brill(40)
DAK	P. M. Dranchuk and H. Abou-Kassem(52)
DPR	P. M. Dranchuk et al.(37)
HEID	Heidaryan, Salarabadi, et al.(43)
H&Y	Hall and Yarborough(49)
MAH	Mahmoud(46)
PAP	Papay(39)
SNL	Sanjari and Lay(44)
SHO	Shokir et al.(45)
Z	Gas compressibility factor
x	Mole fraction

Greek Letter

γ	Gas specific gravity
ε	Wichert & Aziz correction factor
ρ	Density

Subscripts

i	ith component
j	jth component
pc	pseudocritical
pr	pseudoreduced
r	reduced
c	critical
g	gas

Appendix. A. Empirical and Iterative z-factor correlations

1. Papay (PAP) correlation [39].

$$Z = 1 - \frac{3.52p_{pr}}{10^{0.9813T_{pr}}} + \frac{0.274p_{pr}^2}{10^{0.8157T_{pr}}} \tag{A.1}$$

2. Beggs and Brill (BB) correlation [40].

$$Z = A + (1-A)\exp^{-B} + Cp_{pr}^{D} \tag{A.2}$$

Where the Beggs & Brill coefficients are defined in Eq. (A.2.1) to Eq. (A.2.4).

$$A = 1.39(T_{pr} - 0.92)^{0.5} - 0.36T_{pr} - 0.101 \tag{A.2.1}$$

$$B = (0.62 - 0.23T_{pr})p_{pr} + \left(\frac{0.066}{T_{pr} - 0.86} - 0.037\right)p_{pr}^2$$
$$+ \left(\frac{0.32}{10^{9(T_{pr}-1)}}\right)p_{pr}^6 \tag{A.2.2}$$

$$C = 0.132 - 0.32\log(T_{pr}) \tag{A.2.3}$$

$$D = 10^{(0.3106 - 0.49T_{pr} + 0.1824T_{pr}^2)} \tag{A.2.4}$$

3. Bahadori et al. (BAH) correlation [41].

$$Z = a + bP_{pr} + cP_{pr}^2 + dP_{pr}^3 \tag{A.3}$$

Where the Bahadori et al. coefficients are defined in Eq. (A.3.1) to Eq. (A.3.4).

$$a = A_a + B_a T_{pr} + C_a T_{pr}^2 + D_a T_{pr}^3 \tag{A.3.1}$$

$$b = A_b + B_b T_{pr} + C_b T_{pr}^2 + D_b T_{pr}^3 \tag{A.3.2}$$

$$c = A_c + B_c T_{pr} + C_c T_{pr}^2 + D_c T_{pr}^3 \tag{A.3.3}$$

$$d = A_d + B_d T_{pr} + C_d T_{pr}^2 + D_d T_{pr}^3 \tag{A.3.4}$$

Where the coefficients A_i, B_i, C_i and D_i are shown in Table A1.

Table A.1 – Tuned coefficients for Bahadori et al. correlation [41].

i	A_i	B_i	C_i	D_i
a	0.969469	−1.349238	1.443959	−0.3686
b	−0.107783	−0.127013	0.100828	−0.012319
c	0.018481	0.0523405	−0.050688	0.01087
d	−0.000584	−0.002146	0.0020961	−0.000459

4. Azizi et al. (AZI) correlation [42].

$$Z = A + \frac{B + C}{D + E}$$

Where the Azizi et al. coefficients are defined in Eq. (A.4.1) to Eq. (A.4.5).

$$A = a_0 T_{pr}^{2.16} + a_1 P_{pr}^{1.028} + a_2 P_{pr}^{1.58} T_{pr}^{-2.1} + a_3 \ln(T_{pr})^{-0.5} \tag{A.4.1}$$

$$B = a_4 + a_5 T_{pr}^{2.4} + a_6 P_{pr}^{1.56} + a_7 P_{pr}^{0.124} T_{pr}^{3.033} \tag{A.4.2}$$

$$C = a_8 \ln(T_{pr})^{-1.28} + a_9 \ln(T_{pr})^{1.37} + a_{10}\ln(P_{pr}) + a_{11}\ln(P_{pr})^2$$
$$+ a_{12}\ln(P_{pr})\ln(T_{pr}) \tag{A.4.3}$$

$$D = 1 + a_{13}T_{pr}^{5.55} + a_{14}P_{pr}^{0.68}T_{pr}^{0.33} \tag{A.4.4}$$

$$E = a_{15}\ln(T_{pr})^{1.18} + a_{16}\ln(T_{pr})^{2.1} + a_{17}\ln(P_{pr}) + a_{18}\ln(P_{pr})^2$$
$$+ a_{19}\ln(P_{pr})\ln(T_{pr}) \tag{A.4.5}$$

Where the coefficients a_1 to a_{19} are shown in Table A2.

Table A.2 – Tuned coefficients for the Azizi et al. correlation [42].

i	a_i	i	a_i
1	0.0373142485385592	11	19357955749.3274
2	−0.0140807151485369	12	−126354717916.607
3	0.0163263245387186	13	623705678.385784
4	−0.0307776478819813	14	17997651104.333
5	13843575480.9438	15	151211393445.064
6	−16799138540.7637	16	139474437997.172
7	1624178942.64976	17	−24233012984.095
8	13702270281.0869	18	18938047327.5205
9	−41645509.8964746	19	−141401620722.689
10	237249967625.013		

5. Heidaryan, Salarabadi, et al. (HEID) correlation [43].

$$Z = \frac{A_1 + A_2 \ln(P_{pr}) + A_3(lnP_{pr})^2 + A_4(lnP_{pr})^3 + \left(\frac{A_5}{T_{pr}}\right) + \left(\frac{A_6}{T_{pr}^2}\right)}{1 + A_7 \ln(P_{pr}) + A_8(lnP_{pr})^2 + \left(\frac{A_9}{T_{pr}}\right) + \left(\frac{A_{10}}{T_{pr}^2}\right)} \tag{A.5}$$

Where the coefficients A_1 to A_{10} are shown in Table A3.

Table A.3 – Tuned coefficients for the Heidaryan et al. correlation [43].

i	A_i	i	A_i
1	1.11532372699824	6	1.1575311867207
2	−0.0790395208876	7	−0.05367780720737
3	0.01588138045027	8	0.01465569989618
4	0.0088613449601	9	−1.80997374923296
5	−2.16190792611599	10	0.95486038773032

6. Mahmoud (MAH) correlation [46].

$$Z = ap_{pr}^2 + bp_{pr} + c \tag{A.6}$$

Where a, b and c are represented in Eq. (A.6.1) to Eq. (A.6.3). below;

$$a = 0.702e^{-2.5T_{pr}} \tag{A.6.1}$$

$$b = -5.524e^{-2.5T_{pr}} \tag{A.6.2}$$

$$c = 0.044T_{pr}^2 - 0.164T_{pr} + 1.15 \tag{A.6.3}$$

7. Sanjari and Lay (SNL) correlation [44].

$$Z = 1 + A_1 P_{pr} + A_2 P_{pr}^2 + \frac{A_3 P_{pr}^{A_4}}{T_{pr}^{A_5}} + \frac{A_6 P_{pr}^{(A_4+1)}}{T_{pr}^{A_7}} + \frac{A_8 P_{pr}^{(A_4+2)}}{T_{pr}^{(A_7+1)}} \qquad (A.7)$$

Sanjari and Lay [44] further increased the accuracy of this correlation by tuning the coefficients A_1 through A_8 depending on the reduced pressures. As shown in Table A4.

Table A.4 — Tuned coefficients for the Sanjiri et al. correlation [44].

A_i	$0.01 < P_{pr} < 3$	A_i	$3 < P_{pr} < 15$
1	0.007698	1	0.015642
2	0.003839	2	0.000701
3	−0.467212	3	2.341511
4	1.018801	4	−0.657903
5	3.805723	5	8.902112
6	−0.087361	6	−1.136
7	7.138305	7	3.543614
8	0.08344	8	0.134041

8. Shokir et al. (SHO) correlation [45].

$$Z = A + B + C + D + E \qquad (A.8)$$

Where the Shokir et al. coefficients are defined in Eq. (A.8.1) to Eq. (A.8.5).

$$A = 2.679562 \frac{(2T_{pr} - P_{pr} - 1)}{\left[\frac{P_{pr}^2 + T_{pr}^3}{P_{pr}}\right]} \qquad (A.8.1)$$

$$B = -7.686825 \left[\frac{P_{pr} T_{pr} + P_{pr}^2}{T_{pr} P_{pr} + 2T_{pr}^2 + T_{pr}^3}\right] \qquad (A.8.2)$$

$$C = -0.000624\left(T_{pr}^2 P_{pr} - T_{pr} P_{pr}^2 + T_{pr} P_{pr}^3 + 2T_{pr} P_{pr} - 2P_{pr}^2 + 2P_{pr}^3\right) \qquad (A.8.3)$$

$$D = 3.067747 \frac{(T_{pr} - P_{pr})}{\left(P_{pr}^2 + T_{pr} + P_{pr}\right)} \qquad (A.8.4)$$

$$E = \left[\frac{0.068059}{T_{pr} P_{pr}}\right] + 0.139489 T_{pr}^2 + 0.081873 P_{pr}^2 - \left[\frac{0.041098 T_{pr}}{P_{pr}}\right] + \left[\frac{8.152325 P_{pr}}{T_{pr}}\right] - 1.63028 P_{pr} + 0.24287 T_{pr} - 2.64988 \qquad (A.8.5)$$

9. Hall and Yarborough (H&Y) correlation [49].

$$Z = \frac{0.06125 p_{pr} e^{-1.2\left(1-\frac{1}{T_{pr}}\right)^2}}{T_{pr} \, y} \qquad (A.9)$$

where y is defined as a pseudoreduced density parameter that calculated using Eq. (A.9.1) that was solved iteratively:

$$f(y) = \frac{-0.06125 p_{pr} e^{-1.21\left(1-\frac{1}{T_{pr}}\right)^2}}{T_{pr}} + \frac{y + y^2 + y^3 - y^4}{(1-y)^3} - \frac{14.76}{T_{pr}}$$
$$- \frac{9.76}{T_{pr}^2} + \frac{4.58}{T_{pr}^3}\right)y^2 + \frac{90.7}{T_{pr}} - \frac{242.2}{T_{pr}^2} + \frac{42.4}{T_{pr}^3}\right)y^{2.18+\frac{2.82}{T_{pr}}} \qquad (A.9.1)$$

10. P. M. Dranchuk et al. (DPR) correlation [37].

$$z = \frac{0.27 p_r}{y \, T_r} \qquad (A.10)$$

where y is defined as a pseudoreduced density parameter that calculated using Eq. (A.10.1) that was solved iteratively:

$$f(y) = 1 + A_1 + \frac{A_2}{T_{pr}} + \frac{A_3}{T_{pr}^3}\right)y + \left(A_4 + \frac{A_5}{T_{pr}}\right)y^2 + \frac{A_5 A_6}{T_{pr}}y^5$$
$$+ \frac{A_7 y^2}{T_{pr}^3}\left(1 + A_8 y^2\right)e^{-A_8 y^2} - \frac{0.27 p_r}{y \, T_r} \qquad (A.10.1)$$

Where the constants A_1 to A_8 are shown in Table A5.

Table A.5 — Correlation constants for the Dranchuk, Purvis & Robinson correlation [37].

i	A_i	i	A_i
1	0.31506237	5	−0.61232032
2	−1.0467099	6	−0.10488813
3	−0.5783272	7	0.68157001
4	0.53530771	8	0.68446549

11. P. M. Dranchuk and H. Abou-Kassem (DAK) correlation [52].

$$Z = 1 + A_1 + \frac{A_2}{T_{pr}} + \frac{A_3}{T_{pr}^3} + \frac{A_4}{T_{pr}^4} + \frac{A_5}{T_{pr}^5}\right)\rho_{pr} + A_6 + \frac{A_7}{T_{pr}} + \frac{A_8}{T_{pr}^2}\right)\rho_{pr}^2$$
$$- A_9 \frac{A_7}{T_{pr}} + \frac{A_8}{T_{pr}^2}\right)\rho_{pr}^5 + A_{10}\left(1 + A_{11}\rho_{pr}^2\right)\left(\frac{\rho_{pr}^2}{T_{pr}^3}\right)exp^{\left(-A_{11}\rho_{pr}^2\right)} \qquad (A.11)$$

where;

$$\rho_{pr} = \frac{0.27 p_{pr}}{Z T_{pr}} \qquad (A.11.1)$$

Where the constants A_1 to A_{11} are shown in Table A6.

Table A.6 — Correlation constants for the Dranchuk & Abou-Kassem (DAK) correlation [52].

i	A_i	i	A_i
1	0.3265	7	−0.7361
2	−1.07	8	0.1844
3	−0.5339	9	0.1056
4	0.01569	10	0.6134
5	−0.05165	11	0.721
6	0.5475		

REFERENCES

[1] Dmitrievsky A. Meeting natural gas demand: global and regional challenges. In: 18th world petroleum congress; Johannesburg, South Africa: world petroleum congress; 2005.

[2] Dudley B. Statistical review of world energy. London: BP plc; 2013.

[3] Esfahani S, Baselizadeh S, Hemmati-Sarapardeh A. On determination of natural gas density: least square support vector machine modeling approach. J Nat Gas Sci Eng 2015;22:348–58.

[4] Gerhard LC, Yannacone VJ, Smith CJ. Energy and environment: a partnership that works: the actual impacts of oil and gas exploration and development on our environment. American Association of Petroleum Geologists; 2005.

[5] Elsharkawy AM. EOS's calculations of volumetric and transport properties of sour gases and gas condensates. In: The 6th saudi engineering conference. Dhahran: KFUPM; 2002.

[6] Wang X, Economides M. Advanced natural gas engineering. Houston, Texas: Elsevier; 2013.

[7] Chamkalani A, Zendehboudi S, Chamkalani R, Lohi A, Elkamel A, Chatzis I. Utilization of support vector machine to calculate gas compressibility factor. Fluid Phase Equilibria 2013;358:189–202.

[8] Shen W, Lu J, Li X, Liu X. The calculating method optimization and influencing factor analysis of deviation factor for abnormally pressured gas reservoirs. Electron J Geotechnical Eng 2014;19:1711–9.

[9] Mokhatab S, Poe WA, Mak JY. Handbook of natural gas transmission and processing: principles and practices. Gulf Professional Publishing; 2015.

[10] Travis J, Koch DP, Xiao J, Xu Z. Real-gas equations-of-state for the GASFLOW CFD code. Int J Hydrogen Energy 2013;38(19):8132–40.

[11] Jianyi L, Shilun L, Ping G, Zhen Z, Xiaofeng Z, Jianfen D. Measurement of gas deviation factor. Nat Gas Ind 2002;22(2):63–5.

[12] Kamari A, Hemmati-Sarapardeh A, Mirabbasi S-M, Nikookar M, Mohammadi AH. Prediction of sour gas compressibility factor using an intelligent approach. Fuel Process Technol 2013;116:209–16.

[13] Obuba J, Ikiesnkimama S, Ubani C, Ekeke I. Natural gas compressibility factor correlation evaluation for Niger delta gas fields. IOSR J Electr Electron Eng 2013;6(4):1–10.

[14] Al Marri H, Kabir A. PVT characterization of a wet gas reservoir and its impact on reserves estimate. SPE Saudi Arabia Section Annual Technical Symposium and Exhibition; Al-Khobar. Saudi Arabia: Society of Petroleum Engineers; 2015.

[15] Wu Y, Carroll JJ, Zhu W. Sour gas and related technologies. John Wiley & Sons; 2012.

[16] Fayazi A, Arabloo M, Mohammadi AH. Efficient estimation of natural gas compressibility factor using a rigorous method. J Nat Gas Sci Eng 2014;16:8–17.

[17] Cellek MS, Pınarbaşı A. Investigations on performance and emission characteristics of an industrial low swirl burner while burning natural gas, methane, hydrogen-enriched natural gas and hydrogen as fuels. Int J Hydrogen Energy 2017 [in press, available online 9 June 2017].

[18] Zhou J, Patil P, Ejaz S, Atilhan M, Holste JC, Hall KR. (p, V m, T) and phase equilibrium measurements for a natural gas-like mixture using an automated isochoric apparatus. J Chem Thermodyn 2006;38(11):1489–94.

[19] Kay W. Density of hydrocarbon gases and vapors at high temperature and pressure. Ind Eng Chem 1936;28(9):1014–9.

[20] Elsharkawy AM, Elkamel A. The accuracy of predicting compressibility factor for sour natural gases. Petroleum Sci Technol 2001;19(5–6):711–31.

[21] Stewart W, Burkhardt S, Voo D. Prediction of pseudo-critical parameters for mixtures. Kansas City, MO: AIChE Meeting; May 1959.

[22] Corredor J, Piper L, McCain Jr W. Compressibility factors for naturally occurring petroleum gases. In: SPE annual technical conference and exhibition; Washington, D.C; 1992.

[23] Piper L, McCain Jr W, Corredor J. Compressibility factors for naturally occurring petroleum gases (1993 version). SPE Annual Technical Conference and Exhibition. Society of Petroleum Engineers; 1993.

[24] Standing MB. Volumetric and phase behavior of oil field hydrocarbon systems. Society of Petroleum Engineers of AIME; 1981.

[25] Whitson CH, Brulé MR. Phase behavior: Henry L. Doherty memorial fund of AIME. Society of Petroleum Engineers; 2000.

[26] Sutton R. Compressibility factors for high-molecular-weight reservoir gases. SPE annual technical conference and exhibition. Las Vagaa, NV: Society of Petroleum Engineers; 1985.

[27] Ahmed T. Equations of state and PVT analysis. Elsevier; 2013.

[28] Sutton RP. Fundamental PVT calculations for associated and gas-condensate natural gas systems. SPE Annual Technical Conference and Exhibition. Dallas, Texas: Society of Petroleum Engineers; 2005.

[29] Wichert E, Aziz K. Calculate Zs for sour gases. Hydrocarb Process 1972;51(5):119.

[30] Chamkalani A, Mae'soumi A, Sameni A. An intelligent approach for optimal prediction of gas deviation factor using particle swarm optimization and genetic algorithm. J Nat Gas Sci Eng 2013;14:132–43.

[31] Elsharkawy AM. Efficient methods for calculations of compressibility, density and viscosity of natural gases. Fluid Phase Equilibria 2004;218(1):1–13.

[32] Cope J, Lewis W, Weber H. Generalized thermodynamic properties of higher hydrocarbon vapors1. Industrial Eng Chem 1931;23(8):887–92.

[33] Brown GG, Souders M, Smith RI. Pressure-volume-temperature relations of paraffin hydrocarbons. Industrial Eng Chem 1932;24(5):513–5.

[34] Brown G, Katz D, Oberfell G, Alden R. Fluid densities. Nat Gasol Volatile Hydrocarbons 1948;2:24.

[35] Standing MB, Katz DL. Density of natural gases. Trans AIME 1942;146(01):140–9.

[36] Chen H, Yang S, Zhang X, Ren S, Dong K, Li Y, et al. Study of phase behavior and physical properties of a natural gas reservoir with high carbon dioxide content. Greenh Gases Sci Technol 2016;6(3).

[37] Dranchuk PM, Purvis RA, Robinson DB. Computer calculation of natural gas compressibility factors using the Standing and Katz correlation. In: Annual technical meeting. edmonton: Petroleum Society of Canada; 1973.

[38] Tarom N, Hossain M. A practical method for the evaluation of the Joule Thomson effects to predict flowing temperature profile in gas producing wells. J Nat Gas Sci Eng 2015;26:1080–90.

[39] Papay J. ATermelestechnologiai parameterek valtozasa a gazlelepk muvelese Soran. OGIL MUSZ, tud, Kuzl, Budapest. 1968. p. 267–73.

[40] Beggs DH, Brill JP. A study of two-phase flow in inclined pipes. J Petroleum Technol 1973;25(05):607–17.

[41] Bahadori A, Mokhatab S, Towler BF. Rapidly estimating natural gas compressibility factor. J Nat Gas Chem 2007;16(4):349–53.

[42] Azizi N, Behbahani R, Isazadeh M. An efficient correlation for calculating compressibility factor of natural gases. J Nat Gas Chem 2010;19(6):642–5.

[43] Heidaryan E, Salarabadi A, Moghadasi J. A novel correlation approach for prediction of natural gas compressibility factor. J Nat Gas Chem 2010;19(2):189–92.

[44] Sanjari E, Lay EN. An accurate empirical correlation for predicting natural gas compressibility factors. J Nat Gas Chem 2012;21(2):184–8.

[45] Shokir EME-M, El-Awad MN, Al-Quraishi AA, Al-Mahdy OA. Compressibility factor model of sweet, sour, and condensate gases using genetic programming. Chem Eng Res Des 2012;90(6):785–92.

[46] Mahmoud M. Development of a new correlation of gas compressibility factor (Z-factor) for high pressure gas reservoirs. J Energy Resour Technol 2014;136(1). 012903.

[47] McCain Jr W. Reservoir-fluid property correlations-state of the art (includes associated papers 23583 and 23594). SPE Reserv Eng 1991;6(02):266–72.

[48] Heidaryan E, Moghadasi J, Rahimi M. New correlations to predict natural gas viscosity and compressibility factor. J Petroleum Sci Eng 2010;73(1):67–72.

[49] Hall KR, Yarborough L. A new equation of state for Z-factor calculations. Oil Gas J 1973;71(25):82–92.

[50] Carnahan NF, Starling KE. Equation of state for nonattracting rigid spheres. J Chem Phys 1969;51(2):635–6.

[51] Benedict M, Webb GB, Rubin LC. An empirical equation for thermodynamic properties of light hydrocarbons and their mixtures I. Methane, Ethane, Propane and n-Butane. J Chem Phys 1940;8(4):334–45.

[52] Dranchuk PM, Abou-Kassem H. Calculation of Z factors for natural gases using equations of state. J Can Petroleum Technol 1975;14(3).

[53] Starling KE. Fluid thermodynamic properties for light petroleum systems. Gulf Pub. Co; 1973.

[54] Gilat A, Subramaniam V. Numerical methods for engineers and scientists. 3rd ed. Wiley; 2014.

[55] EoS A-D. Compressibility and super compressibility for natural gas and other hydrocarbon gases. Transm Meas Comm Rep 1992;8.

[56] ISO-12213-2. Compressibility and super compressibility for natural gas and other hydrocarbon gases. Transmission measurement committee report, no 8. Arlington, VA: The American Gas Association; 1997.

[57] ISO-12213–2. Natural gas-calculation of compression factor. Part 2: calculation using molar-composition analysis. ISO Copyright Office Geneva; 2005.

[58] Starling KE, Savidge JL. Compressibility factors of natural gas and other related hydrocarbon gases. AGA, American Gas Association; 1994.

[59] Čapla L, Buryan P, Jedelský J, Rottner M, Linek J. Isothermal pVTmeasurements on gas hydrocarbon mixtures using a vibrating-tube apparatus. J Chem Thermodyn 2002;34(5):657–67.

[60] Kunz O, Wagner W. The GERG-2008 wide-range equation of state for natural gases and other mixtures: an expansion of GERG-2004. J Chem Eng data 2012;57(11):3032–91.

[61] Schouten J, Michels J, Janssen-van Rosmalen R. Effect of H_2-injection on the thermodynamic and transportation properties of natural gas. Int J Hydrogen Energy 2004;29(11):1173–80.

[62] Farzaneh-Gord M, Saadat-Targhi M, Khadem J. Selecting optimal volume ratio of reservoir tanks in CNG refueling station with multi-line storage system. Int J Hydrogen Energy 2016;41(48):23109–19.

[63] de Almeida JC, Velásquez J, Barbieri R. A methodology for calculating the natural gas compressibility factor for a distribution network. Petroleum Sci Technol 2014;32(21):2616–24.

[64] Estela-Uribe J, Jaramillo J, Salazar M, Trusler J. Virial equation of state for natural gas systems. Fluid phase equilibria 2003;204(2):169–82.

[65] Farzaneh-Gord M, Arabkoohsar A, Koury RN. Novel natural gas molecular weight calculator equation as a functional of only temperature, pressure and sound speed. J Nat Gas Sci Eng 2016;30:195–204.

[66] Farzaneh-Gord M, Izadi S, Deymi-Dashtebayaz M, Pishbin SI, Sheikhani H. Optimizing natural gas reciprocating expansion engines for Town Border pressure reduction stations based on AGA8 equation of state. J Nat Gas Sci Eng 2015;26:6–17.

[67] Farzaneh-Gord M, Rahbari HR. Numerical procedures for natural gas accurate thermodynamic properties calculation. J Eng Thermophys 2012;21(4):213–34.

[68] Danesh A. PVT and phase behaviour of petroleum reservoir fluids. Elsevier; 1998.

[69] Glantz SA, Slinker BK. Primer of applied regression and analysis of variance. New York: McGraw-Hill, Health Professions Division; 1990.

[70] Kumar N. Compressibility factors for natural and sour reservoir gases by correlations and cubic equations of state. Texas Tech University; 2004.

[71] Rushing JA, Newsham KE, Van Fraassen KC, Mehta SA, Moore GR. Natural gas z-factors at HP/HT reservoir conditions: comparing laboratory measurements with industry-standard correlations for a dry gas. In: CIPC/SPE gas technology symposium 2008 joint conference. Society of Petroleum Engineers; 2008.

[72] McLeod WR. Applications of molecular refraction to the principle of corresponding states. The University of Oklahoma; 1968.

[73] Alliance WAER. Whicher Range tight gas sands study. East Perth: W.A: Geological Survey of Western Australia; 2012.

Appendix.B: Supplementary Results of Infill-Drilling Potential and Optimization in Tight Gas Reservoirs
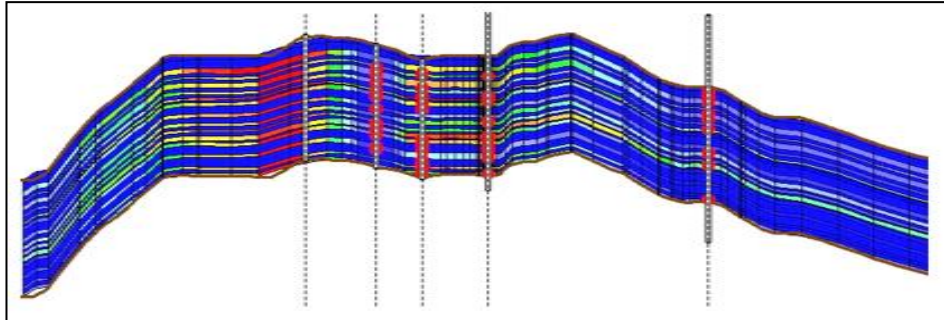
Locating stage-1 sells

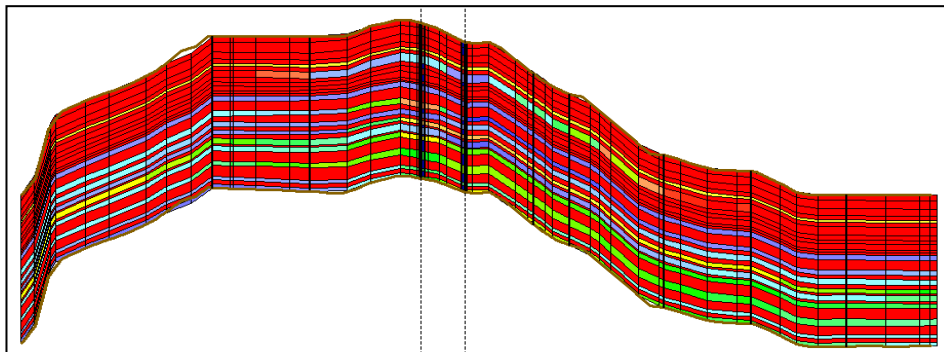Figure B.1 Porosity distribution of a cross-section of the reservoir

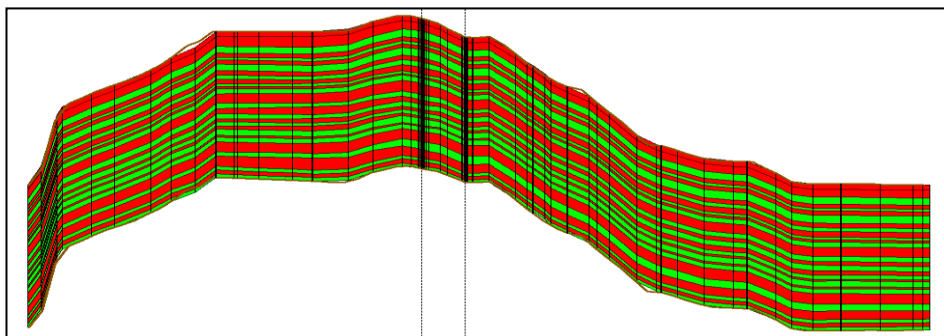Figure B.2 Permeability distribution of a cross-section of the reservoir

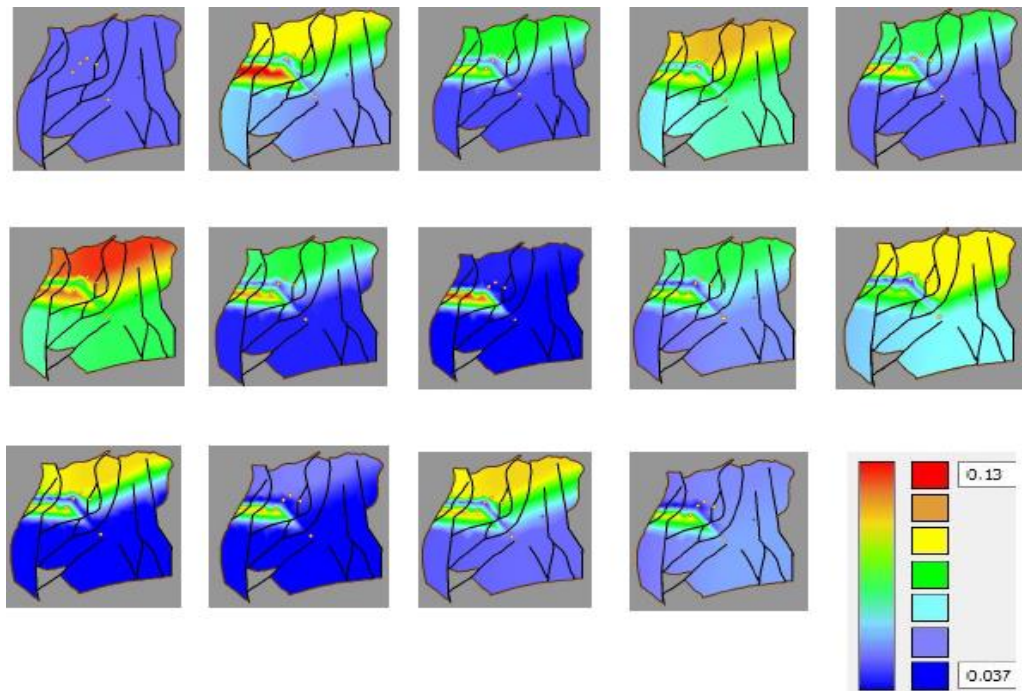Figure B.3 Gas saturation of a cross-section of the reservoir

Figure B.4 Porosity maps of sand layers

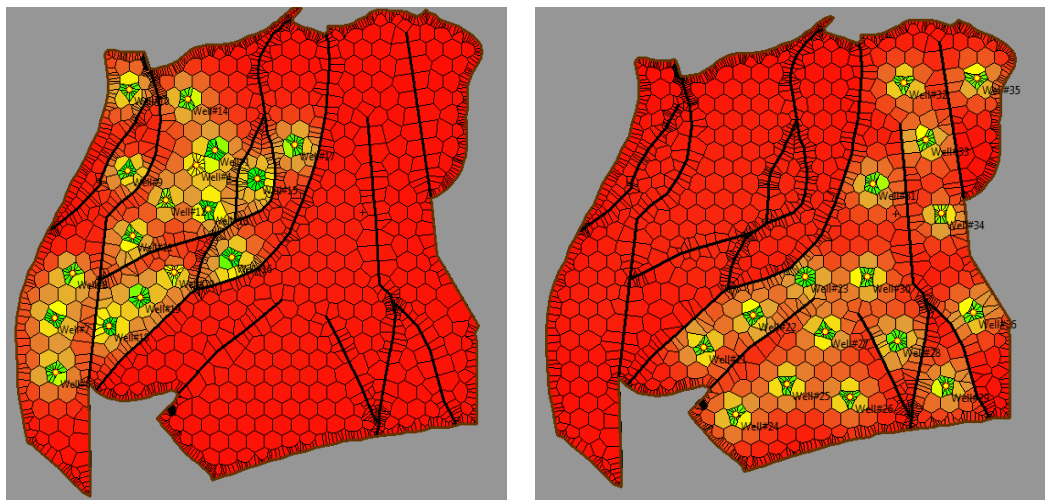## Assessment of the Effectiveness of Stage-1

Figure B.5 Pressure maps after 15 years of production, showing the two sections of the reservoir (Stage-1)
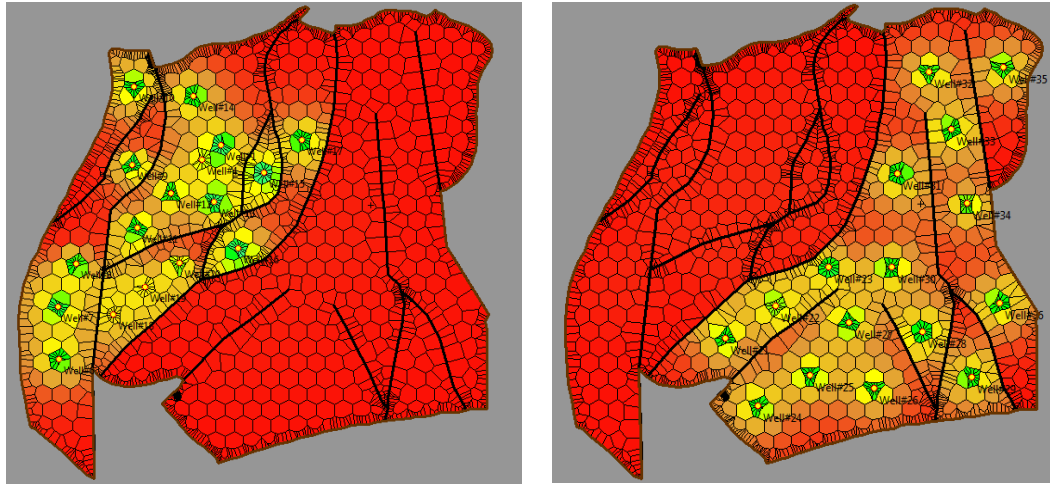
Figure B.6 Pressure map after 30 years of production, showing the two sections of the reservoir (Stage-1)

Production Rate of Stage-1 Infill Wells

Table B.1 Maximum achievable gas production rates (i.e. flow rate) for the Stage-1 infill wells

Well No.	Gas flow rate	Well No.	Gas flow rate	Well No.	Gas flow rate
i	Mscf/d	i	Mscf/d	i	Mscf/d
1	20000	16	15000	28	8200
4	4000	17	17000	29	8500
6	7000	18	6500	30	8000
7	7500	19	7500	31	14000
8	7500	20	7500	32	17000
9	7700	21	7500	33	16000
10	14500	22	9000	34	8200
11	15000	23	10000	35	16000
12	20000	24	8000	36	7500
13	16000	25	8000		
14	16000	26	8000		
15	16000	27	8000		

Figure B.7 shows the left and right half of the field with 30 producing wells each. The black circles indicate the locations of Stage-2 infill wells.
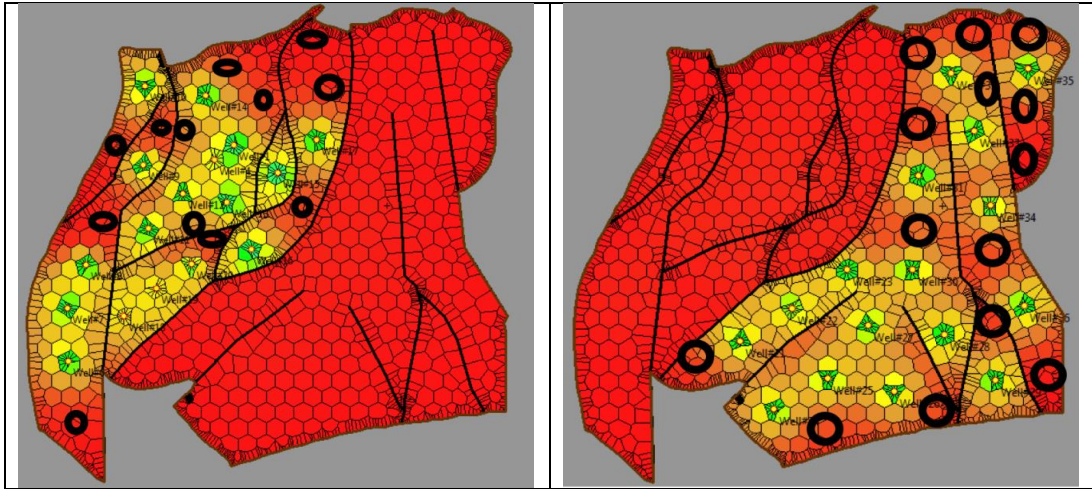

Figure B.7 Left and right sections, respectively, of the reservoir showing the locations of Stage-2 wells

Best Year Rates from MWM and Simulator

Table B.2 Best year rates of the Stage-2 wells (from MWM)

Well No:	BY	Well No:	BY
i	Mscf/month	i	Mscf/month
37	130028	51	285393
38	287609	52	349090
39	342452	53	341207
40	348003	54	251384
41	346159	55	186727
42	299062	56	308008
43	329021	57	382498
44	140626	58	136270
45	180637	59	339726
46	298009	60	314288
47	317558	61	369520
48	139252	62	304322
49	141444	63	116926
50	159489		

Table B.3 Best year rates of Stage-2 wells (from Simulator)

Well No:	BY	Well No:	BY
i	Mscf/month	i	Mscf/month
37	117083	51	227083
38	304417	52	251667
39	332833	53	399833
40	378333	54	219167
41	374917	55	171667
42	270167	56	358333
43	309167	57	397333
44	118167	58	105833
45	165083	59	333417
46	316667	60	352500
47	359167	61	358333
48	130417	62	304583
49	124167	63	122333
50	116667		

Appendix.C: Official Permissions and Copyrights

Society of Petroleum Engineers LICENSE
TERMS AND CONDITIONS

Nov 26, 2018

This is a License Agreement between Curtin University -- Omar AlFatlawi ("You") and Society of Petroleum Engineers ("Society of Petroleum Engineers") provided by Copyright Clearance Center ("CCC"). The license consists of your order details, the terms and conditions provided by Society of Petroleum Engineers, and the payment terms and conditions.

All payments must be made in full to CCC. For payment instructions, please see information listed at the bottom of this form.

License Number	4476821497771
License date	Nov 23, 2018
Licensed content publisher	Society of Petroleum Engineers
Licensed content title	Abu Dhabi International Petroleum Exhibition
Licensed content date	Jan 1, 2016
Type of Use	Thesis/Dissertation
Requestor type	Author of requested content
Format	Print, Electronic
Portion	chapter/article
Number of pages in chapter/article	12
The requesting person/organization is:	Omar Al-Fatlawi/ Curtin University
Title or numeric reference of the portion(s)	Article
Title of the article or chapter the portion is from	Developed Material Balance Approach for Estimating Gas Initially in Place and Ultimate Recovery for Tight Gas Reservoirs
Editor of portion(s)	N/Y
Author of portion(s)	Omar Al-Fatlawi
Volume of serial or monograph.	Abu Dhabi International Petroleum Exhibition & Conference, 7-10 November, Abu Dhabi, UAE
Page range of the portion	Whole article
Publication date of portion	November 2016
Rights for	Main product
Duration of use	Life of current and all future editions
Creation of copies for the disabled	no
With minor editing privileges	yes
For distribution to	Worldwide
In the following language(s)	Original language of publication
With incidental promotional use	no
The lifetime unit quantity of new product	Up to 499
Title	Mr.

259

Institution name	Curtin University
Expected presentation date	Nov 2018
Billing Type	Invoice
Billing Address	Curtin University 1/6 Lawrence Street - Como Level 6 Room no 6H19 26 Dick PERRY Ave Perth, Australia 6152 Attn: Omar Al-Fatlawi
Total (may include CCC user fee)	0.00 USD

Terms and Conditions

TERMS AND CONDITIONS
The following terms are individual to this publisher:

None

Other Terms and Conditions:
STANDARD TERMS AND CONDITIONS

1. Description of Service; Defined Terms. This Republication License enables the User to obtain licenses for republication of one or more copyrighted works as described in detail on the relevant Order Confirmation (the "Work(s)"). Copyright Clearance Center, Inc. ("CCC") grants licenses through the Service on behalf of the rightsholder identified on the Order Confirmation (the "Rightsholder"). "Republication", as used herein, generally means the inclusion of a Work, in whole or in part, in a new work or works, also as described on the Order Confirmation. "User", as used herein, means the person or entity making such republication.

2. The terms set forth in the relevant Order Confirmation, and any terms set by the Rightsholder with respect to a particular Work, govern the terms of use of Works in connection with the Service. By using the Service, the person transacting for a republication license on behalf of the User represents and warrants that he/she/it (a) has been duly authorized by the User to accept, and hereby does accept, all such terms and conditions on behalf of User, and (b) shall inform User of all such terms and conditions. In the event such person is a "freelancer" or other third party independent of User and CCC, such party shall be deemed jointly a "User" for purposes of these terms and conditions. In any event, User shall be deemed to have accepted and agreed to all such terms and conditions if User republishes the Work in any fashion.

3. Scope of License; Limitations and Obligations.

3.1 All Works and all rights therein, including copyright rights, remain the sole and exclusive property of the Rightsholder. The license created by the exchange of an Order Confirmation (and/or any invoice) and payment by User of the full amount set forth on that document includes only those rights expressly set forth in the Order Confirmation and in these terms and conditions, and conveys no other rights in the Work(s) to User. All rights not expressly granted are hereby reserved.

3.2 General Payment Terms: You may pay by credit card or through an account with us payable at the end of the month. If you and we agree that you may establish a standing account with CCC, then the following terms apply: Remit Payment to: Copyright Clearance Center, 29118 Network Place, Chicago, IL 60673-1291. Payments Due: Invoices are payable upon their delivery to you (or upon our notice to you that they are available to you for downloading). After 30 days, outstanding amounts will be subject to a service charge of 1-1/2% per month or, if less, the maximum rate allowed by applicable law. Unless otherwise specifically set forth in the Order Confirmation or in a separate written agreement signed by CCC, invoices are due and payable on "net 30" terms. While User may exercise the rights licensed immediately upon issuance of the Order Confirmation, the license is automatically revoked and is null and void, as if it had never been issued, if complete payment for the license is not received on a timely basis either from User directly or through a payment agent, such as a credit card company.

3.3 Unless otherwise provided in the Order Confirmation, any grant of rights to User (i) is "one-time" (including the editions and product family specified in the license), (ii) is non-

260

Society of Petroleum Engineers LICENSE
TERMS AND CONDITIONS

Nov 26, 2018

This is a License Agreement between Curtin University -- Omar AlFatlawi ("You") and Society of Petroleum Engineers ("Society of Petroleum Engineers") provided by Copyright Clearance Center ("CCC"). The license consists of your order details, the terms and conditions provided by Society of Petroleum Engineers, and the payment terms and conditions.

All payments must be made in full to CCC. For payment instructions, please see information listed at the bottom of this form.

License Number	4476820703112
License date	Nov 23, 2018
Licensed content publisher	Society of Petroleum Engineers
Licensed content title	SPE Europec featured at 79th EAGE Conference and Exhibition
Licensed content date	Jan 1, 2017
Type of Use	Thesis/Dissertation
Requestor type	Author of requested content
Format	Print, Electronic
Portion	chapter/article
Number of pages in chapter/article	12
The requesting person/organization is:	Omar Al-Fatlawi/ Curtin University
Title or numeric reference of the portion(s)	Article
Title of the article or chapter the portion is from	A New Practical Method for Predicting Equivalent Drainage Area of Well in Tight Gas Reservoirs
Editor of portion(s)	N/Y
Author of portion(s)	Omar Al-Fatlawi
Volume of serial or monograph.	SPE Europec featured at 79th EAGE Conference and Exhibition
Page range of the portion	Whole article
Publication date of portion	2017
Rights for	Main product
Duration of use	Life of current and all future editions
Creation of copies for the disabled	no
With minor editing privileges	yes
For distribution to	Worldwide
In the following language(s)	Original language of publication
With incidental promotional use	no
The lifetime unit quantity of new product	Up to 499
Title	Mr.

261

Institution name	Curtin University
Expected presentation date	Nov 2018
Billing Type	Invoice
Billing Address	Curtin University 1/6 Lawrence Street - Como Level 6 Room no 6H19 26 Dick PERRY Ave Perth, Australia 6152 Attn: Omar Al-Fatlawi
Total (may include CCC user fee)	0.00 USD
Terms and Conditions	

TERMS AND CONDITIONS
The following terms are individual to this publisher:

None

Other Terms and Conditions:
STANDARD TERMS AND CONDITIONS

1. Description of Service; Defined Terms. This Republication License enables the User to obtain licenses for republication of one or more copyrighted works as described in detail on the relevant Order Confirmation (the "Work(s)"). Copyright Clearance Center, Inc. ("CCC") grants licenses through the Service on behalf of the rightsholder identified on the Order Confirmation (the "Rightsholder"). "Republication", as used herein, generally means the inclusion of a Work, in whole or in part, in a new work or works, also as described on the Order Confirmation. "User", as used herein, means the person or entity making such republication.

2. The terms set forth in the relevant Order Confirmation, and any terms set by the Rightsholder with respect to a particular Work, govern the terms of use of Works in connection with the Service. By using the Service, the person transacting for a republication license on behalf of the User represents and warrants that he/she/it (a) has been duly authorized by the User to accept, and hereby does accept, all such terms and conditions on behalf of User, and (b) shall inform User of all such terms and conditions. In the event such person is a "freelancer" or other third party independent of User and CCC, such party shall be deemed jointly a "User" for purposes of these terms and conditions. In any event, User shall be deemed to have accepted and agreed to all such terms and conditions if User republishes the Work in any fashion.

3. Scope of License; Limitations and Obligations.

3.1 All Works and all rights therein, including copyright rights, remain the sole and exclusive property of the Rightsholder. The license created by the exchange of an Order Confirmation (and/or any invoice) and payment by User of the full amount set forth on that document includes only those rights expressly set forth in the Order Confirmation and in these terms and conditions, and conveys no other rights in the Work(s) to User. All rights not expressly granted are hereby reserved.

3.2 General Payment Terms: You may pay by credit card or through an account with us payable at the end of the month. If you and we agree that you may establish a standing account with CCC, then the following terms apply: Remit Payment to: Copyright Clearance Center, 29118 Network Place, Chicago, IL 60673-1291. Payments Due: Invoices are payable upon their delivery to you (or upon our notice to you that they are available to you for downloading). After 30 days, outstanding amounts will be subject to a service charge of 1-1/2% per month or, if less, the maximum rate allowed by applicable law. Unless otherwise specifically set forth in the Order Confirmation or in a separate written agreement signed by CCC, invoices are due and payable on "net 30" terms. While User may exercise the rights licensed immediately upon issuance of the Order Confirmation, the license is automatically revoked and is null and void, as if it had never been issued, if complete payment for the license is not received on a timely basis either from User directly or through a payment agent, such as a credit card company.

3.3 Unless otherwise provided in the Order Confirmation, any grant of rights to User (i) is "one-time" (including the editions and product family specified in the license), (ii) is non-

This is a License Agreement between Curtin University -- Omar AlFatlawi ("You") and Society of Petroleum Engineers ("Society of Petroleum Engineers") provided by Copyright Clearance Center ("CCC"). The license consists of your order details, the terms and conditions provided by Society of Petroleum Engineers, and the payment terms and conditions.

All payments must be made in full to CCC. For payment instructions, please see information listed at the bottom of this form.

License Number	4476821137058
License date	Nov 23, 2018
Licensed content publisher	Society of Petroleum Engineers
Licensed content title	SPE Kingdom of Saudi Arabia Annual Technical Symposium and Exhibition
Licensed content date	Jan 1, 2017
Type of Use	Thesis/Dissertation
Requestor type	Author of requested content
Format	Print, Electronic
Portion	chapter/article
Number of pages in chapter/article	23
The requesting person/organization is:	Omar Al-Fatlawi/ Curtin University
Title or numeric reference of the portion(s)	Article
Title of the article or chapter the portion is from	Optimization of Infill Drilling in Whicher Range Field in Australia
Editor of portion(s)	N/Y
Author of portion(s)	Omar Al-Fatlawi
Volume of serial or monograph.	SPE Kingdom of Saudi Arabia Annual Technical Symposium and Exhibition, 24-27 April, Dammam, Saudi Arabia
Page range of the portion	Whole article
Publication date of portion	April 2017
Rights for	Main product
Duration of use	Life of current and all future editions
Creation of copies for the disabled	no
With minor editing privileges	yes
For distribution to	Worldwide
In the following language(s)	Original language of publication
With incidental promotional use	no
The lifetime unit quantity of new product	Up to 499
Title	Mr.

263

Institution name	Curtin University
Expected presentation date	Nov 2018
Billing Type	Invoice
Billing Address	Curtin University
	1/6 Lawrence Street - Como
	Level 6 Room no 6H19
	26 Dick PERRY Ave
	Perth, Australia 6152
	Attn: Omar Al-Fatlawi
Total (may include CCC user fee)	0.00 USD
Terms and Conditions	

TERMS AND CONDITIONS
The following terms are individual to this publisher:

None

Other Terms and Conditions:
STANDARD TERMS AND CONDITIONS

1. Description of Service; Defined Terms. This Republication License enables the User to obtain licenses for republication of one or more copyrighted works as described in detail on the relevant Order Confirmation (the "Work(s)"). Copyright Clearance Center, Inc. ("CCC") grants licenses through the Service on behalf of the rightsholder identified on the Order Confirmation (the "Rightsholder"). "Republication", as used herein, generally means the inclusion of a Work, in whole or in part, in a new work or works, also as described on the Order Confirmation. "User", as used herein, means the person or entity making such republication.

2. The terms set forth in the relevant Order Confirmation, and any terms set by the Rightsholder with respect to a particular Work, govern the terms of use of Works in connection with the Service. By using the Service, the person transacting for a republication license on behalf of the User represents and warrants that he/she/it (a) has been duly authorized by the User to accept, and hereby does accept, all such terms and conditions on behalf of User, and (b) shall inform User of all such terms and conditions. In the event such person is a "freelancer" or other third party independent of User and CCC, such party shall be deemed jointly a "User" for purposes of these terms and conditions. In any event, User shall be deemed to have accepted and agreed to all such terms and conditions if User republishes the Work in any fashion.

3. Scope of License; Limitations and Obligations.

3.1 All Works and all rights therein, including copyright rights, remain the sole and exclusive property of the Rightsholder. The license created by the exchange of an Order Confirmation (and/or any invoice) and payment by User of the full amount set forth on that document includes only those rights expressly set forth in the Order Confirmation and in these terms and conditions, and conveys no other rights in the Work(s) to User. All rights not expressly granted are hereby reserved.

3.2 General Payment Terms: You may pay by credit card or through an account with us payable at the end of the month. If you and we agree that you may establish a standing account with CCC, then the following terms apply: Remit Payment to: Copyright Clearance Center, 29118 Network Place, Chicago, IL 60673-1291. Payments Due: Invoices are payable upon their delivery to you (or upon our notice to you that they are available to you for downloading). After 30 days, outstanding amounts will be subject to a service charge of 1-1/2% per month or, if less, the maximum rate allowed by applicable law. Unless otherwise specifically set forth in the Order Confirmation or in a separate written agreement signed by CCC, invoices are due and payable on "net 30" terms. While User may exercise the rights licensed immediately upon issuance of the Order Confirmation, the license is automatically revoked and is null and void, as if it had never been issued, if complete payment for the license is not received on a timely basis either from User directly or through a payment agent, such as a credit card company.

3.3 Unless otherwise provided in the Order Confirmation, any grant of rights to User (i) is "one-time" (including the editions and product family specified in the license), (ii) is non-

This is a License Agreement between Curtin University -- Omar AlFatlawi ("You") and Offshore Technology Conference ("Offshore Technology Conference") provided by Copyright Clearance Center ("CCC"). The license consists of your order details, the terms and conditions provided by Offshore Technology Conference, and the payment terms and conditions.

All payments must be made in full to CCC. For payment instructions, please see information listed at the bottom of this form.

License Number	4463401193439
License date	Oct 18, 2018
Licensed content publisher	Offshore Technology Conference
Licensed content title	Offshore Technology Conference Asia
Licensed content date	Jan 1, 2018
Type of Use	Thesis/Dissertation
Requestor type	Author of requested content
Format	Print, Electronic
Portion	chapter/article
The requesting person/organization is:	Omar Al-Fatlawi/ Curtin University
Title or numeric reference of the portion(s)	Article
Title of the article or chapter the portion is from	Numerical Approach for the Prediction of Formation and Hydraulic Fracture Properties Considering Elliptical Flow Regime in Tight Gas Reservoirs
Editor of portion(s)	N/A
Author of portion(s)	Omar Al-Fatlawi
Volume of serial or monograph.	Offshore Technology Conference Asia, 20-23 March, Kuala Lumpur, Malaysia
Page range of the portion	
Publication date of portion	March 2018
Rights for	Main product
Duration of use	Life of current and all future editions
Creation of copies for the disabled	no
With minor editing privileges	yes
For distribution to	Worldwide
In the following language(s)	Original language of publication
With incidental promotional use	no
The lifetime unit quantity of new product	Up to 499
Title	Mr.
Institution name	Curtin University

265

Expected presentation date	Nov 2018
Billing Type	Invoice
Billing Address	Curtin University 1/6 Lawrence Street - Como Level 6 Room no 6H19 26 Dick PERRY Ave Perth, Australia 6152 Attn: Omar Al-Fatlawi
Total (may include CCC user fee)	0.00 USD
Terms and Conditions	

TERMS AND CONDITIONS
The following terms are individual to this publisher:

None

Other Terms and Conditions:
STANDARD TERMS AND CONDITIONS

1. Description of Service; Defined Terms. This Republication License enables the User to obtain licenses for republication of one or more copyrighted works as described in detail on the relevant Order Confirmation (the "Work(s)"). Copyright Clearance Center, Inc. ("CCC") grants licenses through the Service on behalf of the rightsholder identified on the Order Confirmation (the "Rightsholder"). "Republication", as used herein, generally means the inclusion of a Work, in whole or in part, in a new work or works, also as described on the Order Confirmation. "User", as used herein, means the person or entity making such republication.

2. The terms set forth in the relevant Order Confirmation, and any terms set by the Rightsholder with respect to a particular Work, govern the terms of use of Works in connection with the Service. By using the Service, the person transacting for a republication license on behalf of the User represents and warrants that he/she/it (a) has been duly authorized by the User to accept, and hereby does accept, all such terms and conditions on behalf of User, and (b) shall inform User of all such terms and conditions. In the event such person is a "freelancer" or other third party independent of User and CCC, such party shall be deemed jointly a "User" for purposes of these terms and conditions. In any event, User shall be deemed to have accepted and agreed to all such terms and conditions if User republishes the Work in any fashion.

3. Scope of License; Limitations and Obligations.

3.1 All Works and all rights therein, including copyright rights, remain the sole and exclusive property of the Rightsholder. The license created by the exchange of an Order Confirmation (and/or any invoice) and payment by User of the full amount set forth on that document includes only those rights expressly set forth in the Order Confirmation and in these terms and conditions, and conveys no other rights in the Work(s) to User. All rights not expressly granted are hereby reserved.

3.2 General Payment Terms: You may pay by credit card or through an account with us payable at the end of the month. If you and we agree that you may establish a standing account with CCC, then the following terms apply: Remit Payment to: Copyright Clearance Center, 29118 Network Place, Chicago, IL 60673-1291. Payments Due: Invoices are payable upon their delivery to you (or upon our notice to you that they are available to you for downloading). After 30 days, outstanding amounts will be subject to a service charge of 1-1/2% per month or, if less, the maximum rate allowed by applicable law. Unless otherwise specifically set forth in the Order Confirmation or in a separate written agreement signed by CCC, invoices are due and payable on "net 30" terms. While User may exercise the rights licensed immediately upon issuance of the Order Confirmation, the license is automatically revoked and is null and void, as if it had never been issued, if complete payment for the license is not received on a timely basis either from User directly or through a payment agent, such as a credit card company.

3.3 Unless otherwise provided in the Order Confirmation, any grant of rights to User (i) is "one-time" (including the editions and product family specified in the license), (ii) is non-exclusive and non-transferable and (iii) is subject to any and all limitations and restrictions
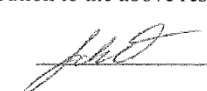
266

Attribution of Authorship

Paper: "Determination of best possible correlation for gas compressibility factor to accurately predict the initial gas reserves in gas-hydrocarbon reservoirs" International Journal of Hydrogen Energy 42.40 (2017): 25492-25508.

Authors and full affiliations: Omar Al-Fatlawi [a, b], Md Mofazzal Hossain[a], Jake Osborne[a]

[a] Curtin University, Department of Petroleum Engineering, 26 Dick Perry Avenue, 6151 Kensington, Australia.

[b] University of Baghdad, College of Engineering, Department of Petroleum Engineering, Baghdad, Iraq

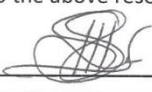|	Conception and design	Acquisition of data and method	Data conditioning and manipulation	Analysis and statistical method	Interpretation and discussion	Final approval
Dr. Md Mofazzal Hossain	×			×	×	×
I acknowledge that these represent my contribution to the above research output. Name: Mofazzl Hossain Signature: Date 03/2018						
Jake Osborne		×	×	×		
I acknowledge that these represent my contribution to the above research output. Name: JAKE OSBORNE Signature Date: 16-10-18						

Attribution of Authorship

Paper: "Developed Material Balance Approach for Estimating Gas Initially in Place and Ultimate Recovery for Tight Gas Reservoirs" Abu Dhabi International Petroleum Exhibition & Conference, 7-10 November (2016), Abu Dhabi, UAE. Society of Petroleum Engineers.

Authors and full affiliations: Omar Al-Fatlawi [a, b], Md Mofazzal Hossain[a], Steven Hicks, Ali Saeedi[a]

[a] Curtin University, Department of Petroleum Engineering, 26 Dick Perry Avenue, 6151 Kensington, Australia.

[b] University of Baghdad, College of Engineering, Department of Petroleum Engineering, Baghdad, Iraq

	Conception and design	Acquisition of data and method	Data conditioning and manipulation	Analysis and statistical method	Interpretation and discussion	Final approval
Dr. Md Mofazzal Hossain	X		X		X	X
I acknowledge that these represent my contribution to the above research output. Name: Mofazzal Hossain Signature: Date: 3/12/2018						
Steven Hicks		X		X	X	
I acknowledge that these represent my contribution to the above research output. Name: STEVEN HICKS Signature: Date 27/11/18						
Ali Saeedi						X
I acknowledge that these represent my contribution to the above research output. Name: ALI SAEEDI Signature: Date: 27/11/2018						

Attribution of Authorship

Paper: "A New Practical Method for Predicting Equivalent Drainage Area of Well in Tight Gas Reservoirs" SPE Europec featured at 79th EAGE Conference and Exhibition, 12-15 June (2017), Paris, France. Society of Petroleum Engineers.

Authors and full affiliations: Omar Al-Fatlawi [a,b], Md Mofazzal Hossain[a], Ali Saeedi[a]

[a] Curtin University, Department of Petroleum Engineering, 26 Dick Perry Avenue, 6151 Kensington, Australia.

[b] University of Baghdad, College of Engineering, Department of Petroleum Engineering, Baghdad, Iraq

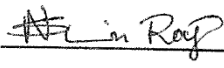|	Conception and design	Acquisition of data and method	Data conditioning and manipulation	Analysis and statistical method	Interpretation and discussion	Final approval
Dr. Md Mofazzal Hossain	x			x	x	x
I acknowledge that these represent my contribution to the above research output. Name: Mofazzal Hossain Signature: ___ Date 2/12/2018						
Ali Saeedi						X
I acknowledge that these represent my contribution to the above research output. Name: ALI SAEEDI Signature: ___ Date: 27/11/2018						

Attribution of Authorship

Paper: "Optimization of Infill Drilling in Whicher Range Field in Australia" In SPE Kingdom of Saudi Arabia Annual Technical Symposium and Exhibition. Society of Petroleum Engineers. (2017, June).

Authors and full affiliations: Omar Al-Fatlawi [a, b], Aswin R. Vimal Roy[a], Md Mofazzal Hossain[a], Akim H. Kabir[c]

[a] Curtin University, Department of Petroleum Engineering, 26 Dick Perry Avenue, 6151 Kensington, Australia.

[b] University of Baghdad, College of Engineering, Department of Petroleum Engineering, Baghdad, Iraq

[c] Saudi Aramco, Kingdom of Saudi Arabia.

	Conception and design	Acquisition of data and method	Data conditioning and manipulation	Analysis and statistical method	Interpretation and discussion	Final approval
Aswin R. Vimal Roy			X	X	X	X

I acknowledge that these represent my contribution to the above research output.

Name: _ASWIN ROY VIMAL ROY_ Signature: _____ Date _9/11/2018_

	Conception and design	Acquisition of data and method	Data conditioning and manipulation	Analysis and statistical method	Interpretation and discussion	Final approval
Dr. Md Mofazzal Hossain	X			X	X	X

I acknowledge that these represent my contribution to the above research output.

Name: _Mofazzal Hossain_ Signature: _____ Date _3/12/2018_

	Conception and design	Acquisition of data and method	Data conditioning and manipulation	Analysis and statistical method	Interpretation and discussion	Final approval
Akim H. Kabir						X

I acknowledge that these represent my contribution to the above research output.

Name: _AKIM H. KABIR_ Signature: _____ Date _15 Nov 2018_

Attribution of Authorship

Paper: "Numerical Approach for the Prediction of Formation and Hydraulic Fracture Properties Considering Elliptical Flow Regime in Tight Gas Reservoirs" Offshore Technology Conference Asia, 20-23 March (2018), Kuala Lumpur, Malaysia. Offshore Technology Conference.

Authors and full affiliations: Omar Al-Fatlawi [a, b], Md Mofazzal Hossain[a], Dominic Brown, and Mohammed Ajeel [a, b]

[a] Curtin University, Department of Petroleum Engineering, 26 Dick Perry Avenue, 6151 Kensington, Australia.

[b] University of Baghdad, College of Engineering, Department of Petroleum Engineering, Baghdad, Iraq

	Conception and design	Acquisition of data and method	Data conditioning and manipulation	Analysis and statistical method	Interpretation and discussion	Final approval
Dr. Md Mofazzal Hossain	X			X	X	X

I acknowledge that these represent my contribution to the above research output.

Name: _Mofazzal Hossain_ Signature: _____ Date: _3/12/2018_

Dominic Brown	X	X	X	X		

I acknowledge that these represent my contribution to the above research output.

Name: _DOMINIC BROWN_ Signature: _____ Date: _30/11/18_

Mohammed Ajeel		X				

I acknowledge that these represent my contribution to the above research output.

Name: Mohammed Ajel Signature: _____ Date: 19/11/2018